2018-12-20

An Analysis of North American Taeniolabidoid Multituberculate (Mammalia, Allotheria) Dentitions Using Mammalian Dietary Proxies

Robson, Selina Viktoria

UNIVERSITY OF CALGARY

An Analysis of North American Taeniolabidoid Multituberculate (Mammalia, Allotheria)

Dentitions Using Mammalian Dietary Proxies

by

Selina V. Robson

A THESIS

SUBMITTED TO THE FACULTY OF GRADUATE STUDIES

IN PARTIAL FULFILMENT OF THE REQUIREMENTS FOR THE

DEGREE OF MASTER OF SCIENCE

GRADUATE PROGRAM IN BIOLOGICAL SCIENCES

CALGARY, ALBERTA

DECEMBER, 2018

Abstract

In this thesis, a set of dietary proxies – dental microwear analysis, cusp row ratios (CRR) (similar to shearing ratios), relief index (RFI), orientation patch count rotated (OPCR), and Dirichlet normal energy (DNE) – was used to infer diets of North American taeniolabidoid multituberculates. Based on the signals recovered by these proxies, taeniolabidoid diets did not vary consistently with body size: small-bodied and large-bodied taeniolabidoids had similar dietary signals for almost all proxies, the only difference being in microwear feature dimensions. Dental microwear signals suggest that taeniolabidoids and non-taeniolabidoid cimolodontans may have had different diets, but all other proxies have recovered equivalent signals between the two groups. Dietary classifications are inconsistent among CRR, RFI, OPCR, and DNE. This suggests that these proxies are not equally good predictors and that their generalizability to non-therian mammals may need to be re-evaluated.

Preface

This thesis is original, unpublished, independent work by the author, S. V. Robson.

Acknowledgements

Table of Contents

List of Tables

List of Figures and Illustrations

11

List of Symbols, Abbreviations and Nomenclature

I#/#, C#/#, P#/#, M#/#	Incisors#/#, Canines#/#, Premolar#/#, Molars#/#. Numerical values denote the number of teeth of each type found in one side of the mouth. Upper dentition is in the numerator and lower dentition is in the denominator. For example, a formula of I2/2, C1/1, P2/2, M3/3 (human adult) indicates two upper and lower incisors, one upper and lower canine, two upper and lower premolars, and three upper and lower molars

Technical abbreviations:

A2D	Occlusal footprint area
A3D	Crown surface area
CRL	Cusp row length
CRR	Cusp row ratio
CT	Computed tomography
DFA	Discriminant Function Analysis
DNE	Dirichlet normal energy
IF	Implicit Fairing
LMM	Low magnification microwear
LS	Laplacian Smoothing
LS scans	Laplacian Smoothed scans with 0.1% outlier exclusion

OPC	Orientation patch count
OPCR	Orientation patch count rotated
OPC/R	Orientation patch count/rotated – refers to the combination of orientation patch count and orientation patch count rotated
RFI	Relief index
ROI	Region of interest
SEM	Scanning electron microscope
SQ	Shearing quotient
SRA	Shearing ratio
3D-OPCR	Three dimensional OPCR
30i scans	30-iteration smoothed scans with 5.0% outlier exclusion

Institutional abbreviations:

AMNH	American Museum of Natural and Cultural History (New York, NY, USA)
NMMNH	New Mexico Museum of Natural History and Science (Albuquerque, NM, USA)
ROM	Royal Ontario Museum (Toronto, ON, Canada)
TMP	Royal Tyrrell Museum of Palaeontology (Drumheller, AB, Canada)
UALVP	University of Alberta Laboratory for Vertebrate Paleontology (Edmonton, AB, Canada)

UCM	University of Colorado Museum of Natural History (Boulder, CO, USA)
UM	University of Michigan Museum of Paleontology (Ann Arbor, MI, USA)
UW	University of Wyoming Geological Museum (Laramie, WY, USA)

Chapter 1: Introduction

Multituberculata (Allotheria) are an extinct order of non-therian mammals from the Mesozoic and early Cenozoic (Kielan-Jaworowska et al., 2004). The order is divided into two suborders: the paraphyletic "Plagiaulacida" and the monophyletic Cimolodonta (Kielan-Jaworowska et al., 2004). Multituberculates had a geographic range that included Laurasia, Africa, Madagascar, and possibly Argentina and Australia (Sigogneau-Russell, 1991; Hahn et al., 2003; Kielan-Jaworowska et al., 2004; Krause et al., 2006; Weil and Krause, 2008; Rich et al., 2009), as well as a long temporal range, with specimens known from the Kimmeridgian (Late Jurassic) through to the Chadronian (Late Eocene) (Weil and Krause, 2008). The ancestral dental formula for multituberculates is I3/1, C0/0, P4-5/3-4, M2/2, but reduced formulae occur in derived forms, and incisor and premolar morphologies are quite variable across groups (Kielan-Jaworowska et al., 2004; Weil and Krause, 2008). Furthermore, there is cranial and postcranial evidence of terrestrial, fossorial, and scansorial/arboreal taxa, indicating that multituberculates occupied a diverse range of ecological niches (Jenkins and Krause, 1983; Krause and Jenkins, 1983; Miao, 1988; Kielan-Jaworowska and Gambaryan, 1994; Weil and Krause, 2008).

The taxonomic and ecological diversity of multituberculates has long drawn attention to the group, with inferred diet being one area of particular interest. When multituberculates were first described, a debate quickly began as to whether they were herbivorous (Falconer, 1857), frugivorous (Falconer, 1857; Gidley, 1909), carnivorous (Owen, 1871; Broom, 1910), ovivorous (Cope, 1884), or omnivorous (Hennig, 1922). Multituberculates have many superficial similarities to rodents, including a similar range of body sizes, predominantly unidirectional power strokes when chewing, gliriform incisors adapted for gnawing, and a diastema developed between the incisors and premolars (Kielan-Jaworowska et al., 2004; Weil and Krause, 2008).

1

These similarities have led researchers to suggest that multituberculates were ecologically equivalent to rodents (Weil and Krause, 2008). However, there are also many differences between multituberculates and rodents. Multituberculates were palinal chewers (backward-directed power stroke) while rodents are proal chewers (forward-directed power stroke) (Gingerich, 1977; Krause, 1982). The lower premolars of multituberculates are also dissimilar to those of rodents: multituberculate lower premolars tend to be blade-like teeth that are morphologically distinct from the molars (Kielan-Jaworowska et al., 2004). This is especially true of cimolodontan p4s, which are often modified as large, arcuate blades (Kielan-Jaworowska et al., 2004). Simpson (1926) noted that the blade-like premolars of multituberculates are most similar to those of rat-kangaroos among living mammals, and these similarities have led several researchers to suggest that multituberculates, like rat kangaroos, may have been omnivores (Clemens and Kielan-Jaworowska, 1979; Krause, 1982).

Despite these superficial similarities, the homologies of multituberculate and therian teeth are not clear (Kielan-Jaworowska et al., 2004; Weil and Krause, 2008). Multituberculate molars were initially designated as "molars" based on their morphology and their relative position in the tooth row (Simpson, 1928, 1929). In fact, the P4/4s of cimolodontan multituberculates are not definitively known to have deciduous precursors (Greenwald, 1988; Wible and Rougier, 2000), which suggests that they may be molars too (Clemens and Lillegraven, 1986; Greenwald, 1988; Luckett, 1993; Wible and Rougier, 2000; but see Xu et al., 2015). Therefore, while the cheek teeth of some therians may be analogous to the cheek teeth of multituberculates, a particular therian cheek tooth (e.g. m1) should not be considered homologous to that same multituberculate cheek tooth.

1.1 Taeniolabidoids

Taeniolabidoidea is a predominately Paleocene superfamily of cimolodontan multituberculates known from Asia and North America (see Williamson et al., 2015; Xu et al., 2015; Mao et al., 2016; Scott et al., 2018 for discussions about included taxa). Cranial and post-cranial evidence suggests that taeniolabidoids were terrestrial or fossorial (Miao, 1988; Kielan-Jaworowska and Qi, 1990; Kielan-Jaworowska and Gambaryan, 1994). Taeniolabidoids are an interesting superfamily because of their derived dentition (dental formula I2/1, C0/0, P1-2/1, M2/2) and large range of body sizes. Taeniolabidoids have chisel-shaped lower incisors, a reduced P4 and p4, and enlarged molars with many bulbous cusps (Kielan-Jaworowska et al., 2004; Weil and Krause, 2008). The gliriform incisors were self-sharpening, similar to those of rodents, and are thought to have been used for cropping and gnawing (Kielan-Jaworowska et al., 2004; Weil and Krause, 2008). The reduced p4 is triangular in lateral view and functioned as an extension of the molar row rather than as an independent shearing blade (Granger and Simpson, 1929; Miao, 1986; Kielan-Jaworowska et al., 2004). The bulbous molar cusps predominantly develop wear on their apices rather than on their lateral or medial sides (unlike in other multituberculates), indicating that they were primarily used for grinding (Granger and Simpson, 1929; Miao, 1986, 1988; Simmons, 1987; Kielan-Jaworowska et al., 2004; Weil and Krause, 2008), and cranial morphology indicates that taeniolabidoids had a very strong medial temporalis (Broom, 1914; Granger and Simpson, 1929; Miao, 1988; Gambaryan and Kielan-Jaworowska, 1995). Taken together, these features suggest that taeniolabidoids may have had a more herbivorous diet than other multituberculates (Granger and Simpson, 1929; Miao, 1988; Kielan-Jaworowska et al., 2004; Weil and Krause, 2008).

In addition to dental features, a second argument favouring taeniolabidoid herbivory relates to body size. Taeniolabidoids include the largest multituberculates currently known (Williamson et al., 2015; Mao et al., 2016; Scott et al., 2018), the largest of which, *Taeniolabis taoensis,* is estimated to have been at least the size of a modern beaver (Weil and Krause, 2008; Wilson et al., 2012; Scott et al., 2018). The large body size of taeniolabidoids is relevant in the context of Kay's Threshold, a body-size threshold established from primate data. Kay's Threshold is a "rule of thumb" that states that mammals exceeding a certain body mass threshold (~500-700 g) are capable of subsisting on a predominately folivorous diet, while those below the threshold are capable of subsisting on a predominately insectivorous diet (Kay and Hylander, 1978; Kay and Covert, 1984; Anthony and Kay, 1993). The threshold is primarily related to metabolic demands. Insects are high in protein, but they are often small and hard to capture, so an insectivorous diet (excepting myrmecophagy) is not sustainable for mammals larger than ~500 g (Kay and Covert, 1984). Conversely, leaves are easy to acquire in large quantities, but their nutrients are locked-up in structural carbohydrates that are difficult to break down (Kay and Covert, 1984). Given that small mammals must process proportionally more food per unit body mass than large mammals (Kleiber, 1961), mammals under ~700 g cannot process sufficient amounts of foliage to gain energy from the food, rendering folivory unsustainable (Kay and Covert, 1984).

Arguments have been made in favour of taeniolabidoids having foliage as a main component of their diet because the estimated body masses of all known taeniolabidoids, including the smallest, exceed Kay's Threshold (e.g., *Valenopsalis joyneri* and *Catopsalis alexanderi*, which are estimated to have had body masses of 0.77-1.37 kg and 1.35-2.61 kg,

respectively; Weil and Krause, 2008; Christensen, 2012; Scott et al., 2018). Two lines of evidence now challenge this threshold argument.

First, recent work has demonstrated that marsupials do not conform to Kay's Threshold (Hogue and ZiaShakeri, 2010). This is likely because marsupials have different metabolic demands than placentals: marsupials typically have basal metabolic rates that are ~67% that of placentals (MacMillen and Nelson, 1969; Dawson and Hulbert, 1970). If Kay's Threshold is related to metabolic demands, then it stands to reason that mammals with lower metabolic rates would not conform to the threshold. In fact, marsupials as small as 152 g (*Pseudochirulus mayeri*) have been observed to be folivorous (Gipps and Sanson, 1984). Furthermore, several insectivorous marsupials have body masses that exceed 500 g (Hogue and ZiaShakeri, 2010). Multituberculates are non-therian mammals (Janis and Weil, 2008), so there is little reason to suspect that they had the same metabolic demands as placentals, and it could be justifiably inferred that multituberculates would not conform to Kay's Threshold.

The second line of evidence comes from a recently described species of diminutive taeniolabidoid, *Catopsalis kakwa* (Scott et al., 2018). *Catopsalis kakwa* is estimated to have had a mass of 0.41-0.66 kg, approximately the size of an eastern gray squirrel (Scott et al., 2018). Even if Kay's Threshold was true for multituberculates, *C. kakwa* falls below the threshold for folivory. However, *C. kakwa* has a dental morphology similar to that of other taeniolabidoids (Scott et al., 2018). If taeniolabidoid dental morphology suggests an herbivorous diet, *C. kakwa* should have been herbivorous despite its small body size. This raises questions, two of which are: Were the diets of small-bodied taeniolabidoids, especially *C. kakwa*, demonstrably different from those of large-bodied taeniolabidoids? And, were the diets of taeniolabidoids demonstrably

different from those of non-taeniolabidoid cimolodontans, most of which are inferred to have been omnivorous?

1.2 Dietary Proxies for Extinct Mammals

Direct evidence of diet is rarely preserved in the fossil record. Rather, researchers use dietary proxies to make inferences about extinct animals. Three of the proxies used on extinct mammals are dental microwear, shearing ratios, and dental topographic analysis.

Dental microwear refers to microscopic damage done to teeth, usually during feeding (Walker et al., 1978; Ryan, 1979; Gordon and Walker, 1983; Teaford and Oyen, 1989; Ungar et al., 1995; Mainland, 2003; Sanson et al., 2007; Schulz et al., 2013; Daegling et al., 2016). Because substances with different structural properties produce microwear of characteristic shapes and sizes (Walker et al., 1978), microwear can be used to infer diet. Dental microwear has a rapid turnover rate, so it essentially captures the animal's "last meal" rather than long-term diet (Teaford and Oyen, 1989; Teaford and Glander, 1991; Teaford, 1994).

Shearing ratios (SRA) are a modification of the more familiar shearing quotient (Kay and Covert, 1984; Anthony and Kay, 1993; Strait, 1993a; Meldrum and Kay, 1997). Both proxies are two-dimensional quantifications of tooth shearing ability, which is itself correlated with diet: greater shearing ability is characteristic of mammals that consume more resistant foods (Strait, 1993a-b). The primary difference between the two is that shearing ratios are calculated using tooth area with shearing quotients are calculated using tooth length. To date, shearing quotients have only been used to infer primate diets, while shearing ratios have been expanded to other mammalian clades (Strait, 1993 a-b; Christensen, 2012, 2014).

6

Dental topographic analysis refers to a suite of three-dimensional metrics (relief index, orientation patch count, and Dirichlet normal energy being the three most common) that are used to quantify different aspects of tooth shape. Relief index (RFI) calculates the topographic relief of a tooth, orientation patch count (OPCR) counts the number of facets on a tooth, and Dirichlet normal energy (DNE) quantifies the curvature of a tooth (Evans et al., 2007; Boyer, 2008; Bunn et al., 2011). Like shearing ratios, the values produced with dental topographic analysis are characteristic of different diets (Evans et al., 2007; Boyer, 2008; Bunn et al., 2011).

All of these proxies were initially developed for therian mammals (Evans et al., 2007; Boyer, 2008; Bunn et al., 2011). Since then, the proxies have been expanded to non-therian mammals (Wilson et al., 2012) and, in the case of dental microwear analysis, non-mammals (e.g. Purnell, 1995; Rybczynski and Reisz, 2001; Purnell et al., 2006; Whitlock, 2011). Dental microwear, shearing ratios, and dental topographic analysis (specifically OPCR) were selected for this study because they have all been applied to multituberculates previously (Christensen, 2012; Wilson et al., 2012), however, none of these metrics has been used to examine differences among taeniolabidoids, or to examine differences between the smallest-bodied taeniolabidoids and non-taeniolabidoid cimolodontans.

1.3 Included Taxa

A subset of North American taeniolabidoids was included in this study. Taxa were chosen based on body size and specimen availability. The taxa include *C. kakwa* (n = 11), *V. joyneri* (n = 26), and *C. alexanderi* (n=9), the three smallest-bodied North American taeniolabidoids, and *T. taoensis* (n = 17), *Catopsalis waddleae* (n = 1), and *Catopsalis calgariensis* (n = 2, 10), three of the largest-bodied North American taeniolabidoids. *Catopsalis*

fissidens (n = 7) and *Catopsalis johnstoni* (n = 1) were included as intermediate-sized taeniolabidoids. Specimens of *C. calgariensis* (n = 2) from the type locality, and those of a *C. calgariensis*-like species from Wyoming were both included but analysed separately; several significant morphological differences suggest that the two are not conspecific. The *C. calgariensis*-like species from Wyoming is referred to as *C.* cf. *calgariensis* (n = 10) in this thesis. The dietary proxies used in this study have previously been used to infer that *T. taoensis* (see Christensen, 2012; Wilson et al., 2012) and *C. alexanderi* (see Wilson et al., 2012) were predominately herbivorous.

A sample of non-taeniolabidoid cimolodontans was included for comparative purposes. These taxa were selected based on availability, and include cimolomyids (*Cimolomys* sp. (n = 13), Cimolomyid 1 (n = 26), *Meniscoessus major* (n = 11), *Meniscoessus robustus* (n = 7)), ptilodontids (*Ptilodus* sp. (n = 8)), and neoplagiaulacids (*Mesodma* sp. (n = 14), an indeterminate neoplagiaulacid (n = 1)), as well as one eucosmodontid (*Stygimys kuszmauli* (n = 1)) and one microcosmodontid (cf. *Acheronodon vossae* (n=1)) (Kielan-Jaworowska et al., 2004; Weil and Krause, 2008). Unlike the taeniolabidoids, some non-taeniolabidoid cimolodontans (particularly eucosmodontids and ptilodontids) may have been scansorial (Simpson and Elftman, 1928; Krause and Jenkins, 1983). Most non-taeniolabidoid cimolodontans are thought to have been omnivorous based on their dental morphologies (Kielan-Jaworowska et al., 2004; Weil and Krause, 2008). Dietary proxies have been used to reconstruct many of the included non-cimolodontan taxa (*M. major*, *Mesodma* sp., *Ptilodus* sp., *Stygimys kuszmauli*) as omnivorous or insectivorous previously (Christensen, 2012; Wilson et al., 2012). It should be noted that there are some discrepancies among proxies: *M. robustus* has variably been reconstructed as a plant-dominated omnivore (Wilson et al., 2012) or an herbivore (Christensen, 2012), while *Cimolomys*

8

sp. has variable been reconstructed as an insectivore (Christensen, 2012) or an herbivore (Wilson et al., 2012).

The spatiotemporal distribution of the included taxa can be found in Appendix A.

1.4 Literature Cited

Anthony, M. R. L., and R. F. Kay. 1993. Tooth form and diet in ateline and alouattine primates: reflections on the comparative method. American Journal of Science 293A:356–382.

Boyer, D. M. 2008. Relief index of second mandibular molars is a correlate of diet among prosimian primates and other euarchontan mammals. Journal of Human Evolution 55:1118–1137.

Broom, R. 1910. On *Tritylodon*, and on the relationships of the Multituberculata. Proceeding of the Zoological Society of London 1910:760–768.

Broom, R. 1914. On the sturcture and affinities of the Multituberculata. Bulletin of The American Museum of Natural History 33:115–134.

Bunn, J. M., D. M. Boyer, Y. Lipman, E. M. St. Clair, J. Jernvall, and I. Daubechies. 2011. Comparing Dirichlet normal surface energy of tooth crowns, a new technique of molar shape quantification for dietary inference, with previous methods in isolation and in combination. American Journal of Physical Anthropology 145:247–261.

Christensen, H. B. 2012. Mammalian adaptation to herbivory in the aftermath of the KT extinction. The University of Chicago, 112 pp.

Christensen, H. B. 2014. Similar associations of tooth microwear and morphology indicate similar diet across marsupial and placental mammals. PLoS ONE 9:1–11.

Clemens, W. A., and J. A. Lillegraven. 1986. New Late Cretaceous, North American advanced therian mammals that fit neither the marsupial nor eutherian molds. Contributions to

Geology, University of Wyoming, Special Paper 3:55–85.

Clemens, W. A., and Z. Kielan-Jaworowska. 1979. Multituberculata; pp. 99–149 in J. A. Lillegraven, Z. Kielan-Jaworowska, and W. A. Clemens (eds.), Mesozoic mammals: the first two-thirds of mammalian history. University of California Press, Berkeley.

Cope, E. D. 1884. The Tertiary Marsupialia. American Naturalist 18:686–697.

Daegling, D. J., L. C. Hua, and P. S. Ungar. 2016. The role of food stiffness in dental microwear feature formation. Archives of Oral Biology 71:16–23.

Dawson, T. J., and A. J. Hulbert. 1970. Standard metabolism, body temperature, and surface areas of Australian marsupials. American Journal of Physiology 218:1233–1238.

Evans, A. R., G. P. Wilson, M. Fortelius, and J. Jernvall. 2007. High-level similarity of dentitions in carnivorans and rodents. Nature 445:78–81.

Falconer, H. 1857. Description of two species of fossil mammalian genus *Plagiaulax* from Purbeck. Quarterly Journal of the Geological Society of London 13:261–282.

Gambaryan, P. P., and Z. Kielan-Jaworowska. 1995. Masticatory musculature of Asian taeniolabidoid multituberculate mammals. Acta Palaeontol. Pol. 40:45–108.

Gidley, J. W. 1909. Notes on the fossil mammalian genus *Ptilodus*, with description of a new species. Proceeding of the United States National Museum 36:611–626.

Gingerich, P. D. 1977. Patterns of evolution in the mammalian fossil record; pp. 469–500 in A. Hallam (ed.), Patterns of Evolution, as Illustrated by the Fossil Record. Elsevier Scientific Publishing Company, New York.

Gipps, M., and G. D. Sanson. 1984. Mastication and digestion in *Pseudocheirus*; pp. 237–246 in A. P. Smith and I. D. Hume (eds.), Possums and Gliders. Surrey Beatty, Sydney.

Gordon, K. D., and A. C. Walker. 1983. Playing 'possum: a microwear experiment. American

Journal of Physical Anthropology 60:109–112.

Granger, W., and G. G. Simpson. 1929. A revision of the Tertiary Multituberculata. Bulletin of

the American Museum of Natural History 56:601–676.

Greenwald, N. S. 1988. Patterns of tooth eruption and replacement in multituberculate mammals.

Journal of Vertebrate Paleontology 8:265–277.

Hahn, G., and R. Hahn. 2003. New multituberculate teeth from the Early Cretaceous of

Morocco. Acta Palaeontologica Polonica 48:349–356.

Hennig, E. 1922. Die Säugerzähne des wüttembergischen Rhät-Lias-Bonebeds. Neues Jahrbuch

Für Mineralogie, Geologie Und Paläontologie 46:181–267.

Hogue, A. S., and S. ZiaShakeri. 2010. Molar crests and body mass as dietary indicators in

marsupials. Australian Journal of Zoology 58:56–68.

Janis, C. M., and A. Weil. 2008. Non-eutherian Mammal Summary; pp. 7–18 in C. M. Janis, G.

F. Gunnell, and M. D. Uhen (eds.), Evolution of Tertiary Mammals of North America.

Volume 2: Small Mammals, Xenarthrans, and Marine Mammals. Cambridge University

Press, New York.

Jenkins, F. A. J., and D. W. Krause. 1983. Adaptations for climbing in North American

multituberculates (Mammalia). Science, New Series 220:712–715.

Kay, R. F., and W. L. Hylander. 1978. The dental structure of mammalian folivores with special

reference to primates and Phalangeroidea (Marsupialia); pp. 173–191 in G. G. Montgomery

(ed.), The Ecology of Arboreal Folivores. Smithsonian Institution Press, Washington, D.C.

Kay, R. F., and H. H. Covert. 1984. Anatomy and behavior of extinct primates; pp. 467–508 in

D. J. Chivers, B. A. Wood, and A. Bilsborough (eds.), Food Acquisition and Processing in

Primates. Plenum Press, New York.

Kielan-Jaworowska, Z., and T. Qi. 1990. Fossorial adaptations of a taeniolabidoid

    multituberculate mammal from the Eocene of China. Vertebrata PalAsiatica 28:81–94.

Kielan-Jaworowska, Z., and P. P. Gambaryan. 1994. Postcranial anatomy and habits of Asian

    multituberculate mammals. Fossils & Strata 36:1–92.

Kielan-Jaworowska, Z., R. L. Cifelli, and Z.-X. Luo. 2004. Mammals from the Age of

    Dinosaurs: Origins, Evolution, and Structure. Columbia University Press, New York, 630

    pp.

Kleiber, M. 1961. The Fire of Life. John Wiley & Soncs, Inc., New York, 454 pp.

Krause, D. W. 1982. Jaw movement, dental function, and diet in the Paleocene multituberculate

    Ptilodus. Paleobiology 8:265–281.

Krause, D. W., and F. A. J. Jenkins. 1983. The postcranial skeleton of North American

    multituberculates. Bulletin of the Museum of Comparative Zoology 150:199–246.

Krause, D. W., P. M. O. Connor, K. C. Rogers, D. Scott, G. A. Buckley, and R. R. Rogers. 2006.

    Late Cretaceous terrestrial vertebrates from Madagascar: implications for Latin American

    biogeography. Annals of the Missouri Botanical Garden 93:178–208.

Luckett, W. P. 1993. An ontogenetic assessment of dental homologies in therian mammals; pp.

    182–204 in F. S. Szalay, M. J. Novacek, and M. C. McKenna (eds.), Mammal Phylogeny—

    Mesozoic Differentiation, Multituberculates, Monotremes, Early Therians, and Marsupials.

    Springer-Verlag, New York.

MacMillen, R. E., and J. E. Nelson. 1969. Bioenergetics and body size in dasyruid marsupials.

    American Journal of Physiology 217:1246–1251.

Mainland, I. L. 2003. Dental microwear in grazing and browsing Gotland sheep (*Ovis aries*) and

    its implications for dietary reconstruction. Journal of Archaeological Science 30:1513–

1527.

Mao, F., Y. Wang, and J. Meng. 2016. New specimens of the multituberculate mammal *Sphenopsalis* from China: implications for phylogeny and biology of taeniolabidoids. Acta Palaeontologica Polonica 61:429–454.

Meldrum, D. J., and R. F. Kay. 1997. *Nuciruptor rubricae*, a new pitheciine seed predator from the Miocene of Colombia. American Journal of Physical Anthropology 102:407–427.

Miao, D. 1986. Dental anatomy and ontogeny of *Lambdopsalis bulla* (Mammalia, Multituberculata). Contributions to Geology, University of Wyoming 24:65–76.

Miao, D. 1988. Skull morphology of *Lambdopsalis bulla* (Mammalia, Multituberculata) and its implications to mammalian evolution. Contributions to Geology, University of Wyoming, Special Paper 4:1–104.

Owen, R. 1871. Monograph of the fossil Mammalia of the Mesozoic formations. Monograph of the Palaeontological Society 24:1–115.

Purnell, M. A. 1995. Microwear on conodont elements and macrophagy in the first vertebrates. Nature 374:798–800.

Purnell, M. A., P. J. B. Hart, D. C. Baines, and M. A. Bell. 2006. Quantitative analysis of dental microwear in threespine stickleback: A new approach to analysis of trophic ecology in aquatic vertebrates. Journal of Animal Ecology 75:967–977.

Rich, T. H., P. Vickers-Rich, T. F. Flannery, B. P. Kear, D. J. Cantrill, P. Komarower, L. Kool, D. Pickering, P. Trusler, S. Morton, N. van Klaveren, and E. M. Fitzgerald. 2009. An Australian multituberculate and its palaeobiogeographic implications. Acta Palaeontologica Polonica 54:1–6.

Ryan, A. S. 1979. Wear striation direction on primate teeth: a scanning electron microscope

examination. American Journal of Physical Anthropology 50:155–168.

Rybczynski, N., and R. R. Reisz. 2001. Earliest evidence for efficient oral processing in a
terrestrial herbivore. Nature 411:684–687.

Sanson, G. D., S. A. Kerr, and K. A. Gross. 2007. Do silica phytoliths really wear mammalian
teeth? Journal of Archaeological Science 34:526–531.

Schulz, E., V. Piotrowski, M. Clauss, M. Mau, G. Merceron, and T. M. Kaiser. 2013. Dietary
abrasiveness is associated with variability of microwear and dental surface texture in
rabbits. PLoS ONE 8:1–7.

Scott, C. S., A. Weil, and J. M. Theodor. 2018. A new, diminutive species of *Catopsalis*
(Mammalia, Multituberculata, Taeniolabidoidea) from the early Paleocene of southwestern
Alberta, Canada. Journal of Paleontology 1–15.

Sigogneau-Russell, D. 1991. First evidence of Multituberculata (Mammalia) in the Mesozoic of
Africa. Neues Jahrbuch Fur Palaontologie, Monatshefte 2:119–125.

Simmons, N. B. 1987. A revision of *Taeniolabis* (Mammalia : Multituberculata), with a new
species from the Puercan of eastern Montana. Journal of Paleontology 61:794–808.

Simpson, G. G. 1926. Mesozoic Mammalia, IV; the multituberculates as living animals.
American Journal of Science 63:228–250.

Simpson, G. G. 1929. American Mesozoic Mammalia. Peabody Museum (Yale University)
Memoirs 3:1–171.

Simpson, G. G., and H. O. Elftman. 1928. Hind limb musculature and habits of a Paleocene
multituberculate. American Museum Novitates 333:1–19.

Strait, S. G. 1993a. Molar morphology and food texture among small-bodied insectivorous
mammals. American Society of Mammalogists 74:391–402.

Strait, S. G. 1993b. Differences in occlusal morphology and molar size in frugivores and

faunivores. Journal of Human Evolution 25:471–484.

Teaford, M. F. 1994. Dental microwear and dental function. Evolutionary Anthropology: Issues,

News, and Reviews 3:17–30.

Teaford, M. F., and O. J. Oyen. 1989. *In vivo* and *in vitro* turnover in dental microwear.

American Journal of Physical Anthropology 80:447–460.

Teaford, M. F., and K. E. Glander. 1991. Dental microwear in live, wild-trapped *Alouatta*

palliata from Costa Riva. American Journal of Physical Anthropology 85:313–319.

Ungar, P. S., M. F. Teaford, K. E. Glander, and R. F. Pastor. 1995. Dust accumulation in the

canopy: A potential cause of dental microwear in primates. American Journal of Physical

Anthropology 97:93–99.

Walker, A., H. N. Hoeck, and L. Perez. 1978. Microwear of mammalian teeth as an indicator of

diet. Science, New Series 201:908–910.

Weil, A., and D. W. Krause. 2008. Multituberculata; pp. 19–38 in C. M. Janis, G. F. Gunnell,

and M. D. Uhen (eds.), Evolution of Tertiary Mammals of North America. Volume 2: Small

Mammals, Xenarthrans, and Marine Mammals. Cambridge University Press, New York.

Whitlock, J. A. 2011. Inferences of diplodocoid (Sauropoda: Dinosauria) feeding behavior from

snout shape and microwear analyses. PLoS ONE 6.

Wible, J. R., and G. W. Rougier. 2000. Cranial anatomy of *Kryptobaatar dashzevegi*

(Mammalia, Multituberculata), and its bearing on the evolution of mammalian characters.

Bulletin of The American Museum of Natural History 247:1–120.

Williamson, T. E., S. L. Brusatte, R. Secord, and S. Shelley. 2015. A new taeniolabidoid

multituberculate (Mammalia) from the middle Puercan of the Nacimiento Formation, New

Mexico, and a revision of taeniolabidoid systematics and phylogeny. Zoological Journal of the Linnean Society 177:183–208.

Wilson, G. P., A. R. Evans, I. J. Corfe, P. D. Smits, M. Fortelius, and J. Jernvall. 2012. Adaptive radiation of multituberculate mammals before the extinction of dinosaurs. Nature 483:457–460.

Xu, L., X. Zhang, H. Pu, S. Jia, J. Zhang, J. Lü, and J. Meng. 2015. Largest known Mesozoic multituberculate from Eurasia and implications for multituberculate evolution and biology. Scientific Reports 5:1–11.

Chapter Two: Molar Microwear of Cimolodontan Multituberculates

2.1 Introduction

Dental microwear is often used as a proxy for diet. Microwear is produced when hard foods and/or dust and exogenous grit come into contact with teeth, leaving microscopic abrasions on the enamel and dentine (Walker et al., 1978; Ryan, 1979a; Gordon and Walker, 1983; Teaford and Oyen, 1989; Ungar et al., 1995; Mainland, 2003; Sanson et al., 2007; Schulz et al., 2013; Daegling et al., 2016). Microwear has a fast turnover rate – typically days or weeks – so the microwear preserved on a tooth provides evidence of the type of material consumed just prior to death (Teaford and Oyen, 1989; Teaford and Glander, 1991; Teaford, 1994). Feeding types (e.g. browsing versus grazing) can be distinguished based on patterns of microwear features (e.g. pits, scratches, gouges) because the quantity and composition of hard materials affects microwear formation (Walker et al., 1978; Solounias and Semprebon, 2002).

There is a large body of literature on dental microwear (see Gordon, 1988; Teaford, 1988, 1991, 1994, 2007; Walker and Teaford, 1989; Rose and Ungar, 1998; Ungar et al., 2008; Belmaker, 2018 for reviews), reflecting both its popularity and its problems. Microwear has been

16

used to infer the diets of a multitude of organisms, including conodonts (Purnell, 1995), actinopterygians (Purnell et al., 2006; Baines et al., 2014), dinosauriforms (Kubo and Kubo, 2013) and dinosaurs (Fiorillo, 1998; Whitlock, 2011), basal therapsids (Rybczynski and Reisz, 2001; Goswami et al., 2005), and many mammals (Walker et al., 1978; Rensberger, 1978; Teaford and Walker, 1984; Grine, 1986; Solounias et al., 1988; Valkenburgh et al., 1990; Solounias and Hayek, 1993; Solounias and Semprebon, 2002; Godfrey et al., 2004; Semprebon et al., 2004; Nelson et al., 2005; Townsend and Croft, 2008; Schubert et al., 2010; Green and Resar, 2012; McAfee and Green, 2015; Hedberg and DeSantis, 2017). Differences in microwear shape, size, and frequency are commonly used to distinguish among dietary categories: for example, gross differences in pit and scratch frequencies are useful for separating browsing behavior from grazing behavior in some groups, such as ungulates and primates (e.g. Solounias and Semprebon, 2002; Godfrey et al., 2004). These gross differences are less meaningful in small-bodied mammals, which tend to have subtler microwear signals and more variation within dietary categories (Strait, 1993; Townsend and Croft, 2008; Gomes Rodrigues et al., 2009; Oliver et al., 2014). For example, within caviomorph rodents, grazers have both the highest scratch frequencies (>20 per tooth) and the lowest scratch frequencies (<8 per tooth), as well as some of the highest and lowest large and small pit frequencies (Townsend and Croft, 2008). Fruit-seed and grass-leaf eating caviomorphs have scratch and pit frequencies similar to those of some grazing caviomorphs, although with less variation within each dietary group (Townsend and Croft, 2008). Researchers have found that, for small-bodied mammals, feature size needs to be used in conjunction with scratch and pit frequencies to distinguish among diets. For example, while murid rodents tend to have similar total scratch counts, grazing murids have a relatively

high frequency of fine scratches while frugivorous murids have a relatively high frequency of coarse scratches (Gomes Rodrigues et al., 2009).

To further complicate matters, the frequency of certain features may be indicative of multiple diets: a high frequency of fine scratches has been observed on grazing murid rodents, but also on lumbricophagous (earthworm-eating) moles and tenrecs (Silcox and Teaford, 2002; Gomes Rodrigues et al., 2009). Likewise, a high frequency of pits has been noted on small insectivorous mammals, but also on frugivorous murids, omnivorous ground squirrels, and fossorial caviomorphs (Strait, 1993a; Nelson et al., 2005; Townsend and Croft, 2008; Gomes Rodrigues et al., 2009). In some cases, such as grazing caviomorphs, both high scratch frequencies and high pit frequencies have been observed (Townsend and Croft, 2008). Additionally, generalist species have high intra-specific variation with respect to scratch and pit frequencies, which can make dietary categorization difficult (Gomes Rodrigues et al., 2009).

Despite these difficulties, some dietary predictions about small-bodied mammals can still be made using microwear. Within a clade, hard-object (e.g. beetles, hard fruits, seeds) eaters tend to have a higher frequency of pits and coarse features than soft-object eaters, and grazers tend to have higher fine scratch frequencies than non-grazers. This means that dietary inferences about extinct taxa can be made if the microwear signals of closely-related extant taxa are known. For the non-therian multituberculates, there are no closely-related extant taxa. Comparisons to therian microwear can be made but these comparisons should be done cautiously.

Microwear has been documented on many multituberculate specimens. Often, the microwear has been used to reconstruct jaw trajectory during the mastication cycle rather than diet (Simpson, 1926; Krause, 1982; Lazzari et al., 2010). One study used microwear to examine dietary changes within single multituberculate taxa (*Cimexomys* and *Mesodma*) across the K-Pg

boundary and found that there are distinct differences in microwear between Cretaceous and Paleocene specimens (Weil and Pignataro, 2007a-b). Christensen (2012) examined microwear in many Mesozoic and Cenozoic multituberculate taxa. She inferred that *Meniscoessus robustus* and *Taeniolabis taoensis* were herbivores based on their microwear signals. Although she also collected microwear data for some small-bodied multituberculates, these data do not appear to be included in her analysis (Christensen, 2012).

2.1.1 Microwear analysis: cautions and considerations.

2.1.1.1 Selecting an imaging method.

There are many methods for studying microwear. Most early studies used scanning electron microscopy (SEM) to capture images of either teeth or casts of teeth (see Gordon, 1988; Teaford, 1988, 1991, 1994, 2007; Walker and Teaford, 1989; Rose and Ungar, 1998). Researchers counted and categorized microwear directly from these images. SEM microwear studies are numerous, but there has been relatively little standardization of technique. Varying magnifications, resolutions, and feature categorization criteria have led to difficulties when comparing results. Furthermore, SEM usage tends to be expensive and time consuming, necessitating small sample sizes.

Light microscopy is an inexpensive and often more efficient alternative to SEM. The use of light microscopy for microwear analysis was popularized by Solounias and Semprebon (2002). Casts of specimens are made, and microwear is either counted directly from the cast while it is viewed under a microscope, or from digital photographs of the cast taken through a microscope. When taking photographs, high dynamic range imaging (HDRI, i.e. a set of photos taken at different light exposures) can be used to capture a greater range of microwear features (Fraser et al., 2009).

Light microscopy studies use lower magnifications than SEM studies. Thus, microwear imaged with a light microscope is often referred to as low-magnification microwear (LMM). The standard magnification for LMM studies is 35x (70x for small specimens), whereas SEM studies often use magnifications over 100x (Solounias and Semprebon, 2002; Nelson et al., 2005; Fraser et al., 2009; Oliver et al., 2014; Kalthoff and Green, 2017).

Both LMM and SEM studies rely on researchers to count and categorize microwear. This leads to inter-observer error (Grine et al., 2002; Galbany et al., 2005; Mihlbachler and Beatty, 2012; Mihlbachler et al., 2012). An alternative approach is dental microwear topographic analysis (DMTA), a semi-automated method that relies on tandem scanning confocal microscopy and uses scale-sensitive fractal analysis to quantify the surface topography of a tooth (Ungar et al., 2003; Scott et al., 2006). DMTA is appealing because it eliminates the subjectivity inherent in manually counting microwear. The calculation itself is automated, but a researcher is still responsible for selecting specimens and identifying taphonomic features, and there appears to be variation in DMTA results depending on the microscope used (Arman et al., 2016). Furthermore, DMTA results cannot be directly compared to LMM and SEM results because DMTA produces a set of topographic parameters rather than scratch and pit counts.

I elected to collect images with an SEM. Light microscopy was not feasible for my study because a high magnification (200x) was needed to image microwear on small specimens. Furthermore, the available light microscopes were housed in a building prone to vibrations, and the vibrations resulted in blurred photographs. DMTA was also not practical for my study because many specimens had taphonomic features and/or dirt on their cusps. Some dirt was removed during cleaning, but particulates often remained and were captured during the molding/casting process. This meant that there were few large clean areas that could be analyzed

with DMTA; the process would have included the taphonomic features and the dirt as part of the surface topography. SEM images did not have these problems – they were of sufficiently high resolution and clarity, and I was able to ignore the taphonomic features and dirt when counting the microwear.

2.1.1.2 Selecting teeth and cusps.

A majority of microwear studies have focused on cheek teeth, although incisor microwear studies are not unheard of. Microwear is preferentially collected from equivalent locations on homologous teeth for all specimens in a study. For example, most ungulate microwear studies use the lingual band of the M2 paracone (Solounias and Semprebon, 2002). This standardization is because microwear patterns change along the tooth row and among cusps of the same tooth (Gordon, 1982; Teaford and Walker, 1984; Solounias and Semprebon, 2002). These differences may be related to how each tooth and each cusp is used for food processing (Gordon, 1982). However, comparative studies have not been conducted on mammals that chew with a predominately unidirectional power stroke; microwear patterns may be distributed differently for these mammals. This is important because multituberculates were palinal chewers (Krause, 1982). In their multituberculate microwear study, Weil and Pignataro (2007a, 2007b) used a wear facet with a consistent position in the M1 cusp row. Christensen (2012) included wear facets from all upper and lower molars and she did not find any significant differences among the teeth, although her sample was quite small. Like Christensen (2012), I did not discriminate based on tooth position or cusp. This was because I had limited material. More extensive comparisons are necessary to determine if there are differences in microwear along multituberculate tooth rows.

2.1.1.3 What produces microwear?

There is an ongoing debate as to the cause of microwear. The two hypothesized primary sources are phytoliths (microscopic silica structures found inside of plants), and exogenous grit and dust. Phytoliths are an appealing explanation for microwear because they are directly linked to diet. Exogenous grit and dust are not necessarily indicators of diet, but they are indicators of aridity and feeding height. This distinction is important because it affects what dietary inferences can be made from microwear analysis.

Early studies suggested that opal phytoliths were the predominant source of microwear (Walker et al., 1978; Solounias et al., 1988; Solounias and Hayek, 1993). The premise of this argument was that phytoliths were harder than enamel (Baker et al., 1959), and it was therefore assumed that the high concentration of phytoliths in monocotyledons (mainly grasses) was responsible for causing microwear scratches. This explanation is not entirely without merit; phytoliths have been found at the ends of microwear scratches on the teeth of medieval humans (Fox et al., 1994).

Not all researchers agree with the phytolith explanation for microwear. Several lines of evidence have now arisen suggesting that exogenous grit and dust are also major components. Grit is a plausible source of microwear: mammalian grazers can acquire grit while eating low-lying plants (Solounias and Semprebon, 2002), and browsers can ingest canopy dust while feeding (Ungar et al., 1995). However, the grit hypothesis has not been universally accepted: for example, early laboratory experiments purportedly demonstrating that exogenous grit consumed during feeding can create microwear (Ryan, 1979a, 1979b; Covert and Kay, 1981; Peters, 1982) were challenged on the basis of questionable methodologies (Gordon and Walker, 1983; but see Kay and Covert, 1983 for a response; Teaford, 1988). More recently, a field study found that

sheep with higher quantities of exogenous grit in their diet had more microwear striations on their teeth (Mainland, 2003). This again suggested that grit may be responsible for microwear, but the diets of the sheep were not controlled so phytoliths could not be eliminated as a source.

A recent replication of Baker et al.'s (1959) phytolith study further called the role of phytoliths into question. Using measurement techniques that were not available to Baker et al. (1959), Sanson et al. (2007) found that grass phytoliths are much softer than mammalian enamel. Other recent experiments have also found that phytoliths are softer than enamel (Erickson, 2014; Lucas et al., 2014), although these results have been disputed (Rabenold and Pearson, 2014). Sanson et al. (2007) also noted that the typical size of microwear striations reported in the literatures matches the size of grit particles, not phytoliths. This appears to be a good argument at first, but experiments using uniformly-sized grit particles to produce microwear features have demonstrated that microwear features tend to be an order of magnitude smaller than the culpable particles (Maas, 1991, 1994).

The relative softness of phytoliths may be a compelling piece of evidence, but even so, phytoliths cannot not be entirely discounted as a microwear source. Relatively soft substances are still capable of damaging hard surfaces, including enamel (Richardson, 1968; Rabenold and Pearson, 2014; Xia et al., 2015). In these cases, wear appears to be driven by pressure and critical attack angle rather than hardness (Richardson, 1968; Rabenold and Pearson, 2014; Xia et al., 2015). Furthermore, there are still noticeable differences between monocotyledon and dicotyledon foliage signals after the foliage has been cleaned to ensure that no other substances (e.g. grit, seeds) are present (Schulz et al., 2013). These persistent differences are thought to be the result of phytoliths (Schulz et al., 2013). Recently, a study using controlled-food trials with dust-free and dust-laden conditions demonstrated that both phytoliths and dust contribute to

microwear, but that dust does not overshadow the microwear signal produced by phytoliths: grazer and browser microwear signals were distinctly different, regardless of the dust content on the food (Merceron et al., 2016).

Laboratory experiments have shown that other foodstuffs (e.g. apples, biscuits, cereal) are able to create microwear when grit is not present (Peters, 1982; Teaford and Oyen, 1986, 1989; Gügel et al., 2001; Schulz et al., 2013; Daegling et al., 2016). These foods include seeds and bones (Daegling et al., 2016), which explains microwear observed on the teeth of frugivores and carnivores. Foodstuffs with higher elastic moduli (i.e. stiffness) seem to produce more microwear, although the relationship is not entirely straightforward (Daegling et al., 2016). To complicate matters even more, a recent feeding study on rats found that quartz sand produces high amounts of microwear, but only when the rats consume soft foods (Rusnack et al., 2017). When hard foods are consumed, the addition of quartz sand does not significantly affect microwear, and the hard food microwear is indistinguishable from plain soft food microwear (Rusnack et al., 2017). It appears that there is an interaction between food type and abrasive material (Rusnack et al., 2017).

The decades-long discussion about the origin of microwear is unlikely to end soon. Recent papers continue to contradict each other and to question the findings of earlier researchers, and the addition of new research does not seem to clarify the matter. Taken together, studies indicate that many factors contribute to the production of microwear (see Belmaker (2018) for a review). Exogenous dust and grit are clearly able to (and almost certainly do) create microwear, but this does not mean that they are the only source. Phytoliths are also a likely culprit, as are hard foods such as seeds. The relative contribution of each source is still up for debate; I suspect that contributions differ depending on diet, species, and environment. If so, this

would mean that microwear does not have a one-to-one relationship with diet. This does not invalidate microwear as a gross dietary proxy. Comparisons among taxa can still reveal differences in diet and feeding location. However, researchers should use caution when making dietary inferences about extinct species. For example, a "grazing" signal could indicate consumption of monocotyledons, but it could also indicate that the animals were simply feeding close to the ground.

2.1.1.4 Effects of taphonomy on microwear.

Specimens often experience taphonomic alterations before they are collected. These alterations include damage from transport, mechanical weathering, and acid exposure (Belmaker, 2018). Microwear, which is only preserved on the outer surfaces of teeth, is readily affected by taphonomy. Experiments simulating fluvial and terrestrial transport have demonstrated that microwear features can be erased in as few as five hours (Gordon, 1984). It is also possible for pits and scratches to be added when exposed to sand abrasion (Puech et al., 1985; King et al., 1999). Acid exposure can both create and erase features, depending on acidity and exposure time (Puech et al., 1985; King et al., 1999). In general, taphonomic processes tend to erase features more than they add them, but the latter can still occur (King et al., 1999).

It is standard protocol to examine specimens for signs of taphonomy before conducting a microwear analysis (Belmaker, 2018). Any specimens that are taphonomically altered are excluded from the analysis. Identification of taphonomic effects is relatively easy when working with the teeth of large-bodied mammals, but those of small-bodied mammals do not always show signs of taphonomy at scales that are visible with an optical microscope (Belmaker, 2018). This means that researchers are more likely to accidentally include taphonomically altered teeth in

studies of small mammals. This is of particular concern to my study because many of the included specimens have been fluvially transported (Lofgren, 1995).

Preparation can also affect microwear signals. Preparation marks may be mistaken for microwear (e.g. parallel scratches) and be included in microwear counts, and protective coatings (e.g. shellac) can obscure microwear. Preparation marks can often be distinguished from microwear by their sharp edges and their superimposition over microwear – I did not include features with these characteristics in my analysis. Specimens with protective coatings did not have analyzable microwear and were excluded from the sample.

2.1.1.5 Effects of microstructure on microwear.

Surprisingly few studies have examined the relationship between dental microwear and enamel microstructure. Microstructure has been used in conjunction with microwear to make inferences about diet (Teaford et al., 1996; Tseng, 2012), but these studies did not examine whether microstructure affects microwear formation. The only studies that have examined the relationship found that nonprismatic enamel and prismatic enamels (Types I, II, and III) produce different microwear patterns in response to shearing forces (Maas, 1991) but not compressive forces (Maas, 1994). Among prismatic enamels, prism size and type do not matter per se, but the orientation of crystallites affects striation size (Maas, 1991).

The effects of microstructure on microwear are important because most of the taxa included in this study have gigantoprismatic enamel. Gigantoprismatic enamel is characterized by extremely large and widely separated prisms (Fosse et al., 1978) and is only found in some cimolodontan multituberculates (Fosse et al., 1978, 1985). For example, taeniolabidoids and cimolomyids, both cimolodontan, have gigantoprismatic enamel, but ptilodontoids (e.g. *Mesodma* and *Ptilodus*), also cimolodontan, do not (Kielan-Jaworowska et al., 2004, p. 279-

282). Experiments by Maas (1991, 1994) suggest that pits are not affected by prism configuration but that scratch widths are. This means that a "large" scratch on a taeniolabidoid or cimolomyid tooth may not be equivalent to a "large" scratch on a therian (or ptilodontoid) tooth, rendering direct comparisons tenuous.

2.1.1.6 Effects of phylogeny on microwear.

Until recently, microwear analysis was thought to be phylogenetically independent, and very few microwear studies have accounted for phylogeny (see Fraser et al., 2018a-b for discussion). Without phylogenetic corrections, false positives (type I errors; e.g. falsely detecting differences in microwear signals) are more common (Rohlf, 2006; Barr and Scott, 2014). Fraser et al. (2018) demonstrated that there may be a phylogenetic signal present in microwear and that, while DMTA exhibits greater phylogenetic signal than LMM, both signals are high. The authors posit that the lower phylogenetic signal in LMM may be a result of coarser scale, higher inter-observer error, and less influence of enamel microstructure. These results do not mean that microwear is useless as a dietary proxy – rather, they indicate that caution should be used when comparing microwear results between distantly related clades. This is particularly important when conducting microwear studies with extinct taxa. The dental microwear signals of extinct taxa are usually compared to those of extant taxa to make dietary inferences. This is often a necessary step, but the influence of phylogeny should be considered when comparisons are being made.

2.2 Methods

2.2.1 Molding and casting.

The available multituberculate teeth were examined for taphonomic alterations before molding, and altered teeth were excluded. The remaining teeth were cleaned with a cotton swab or small brush to remove dirt from the surface. When necessary and possible, acetone was also applied to the specimens. Specimens that could not be adequately cleaned were excluded from the sample.

After cleaning, molds were made of the specimens with a high precision polyvinylsiloxane (either President microSystem^{TM} Regular Body, Coltène/Whaledent$^®$, or Sinclair VPS Impression Material Medium Body, Regular Set, Sinclair Dental) (Appendix B). A preliminary comparison between the two compounds suggests that they capture similar microwear signatures (Creighton et al., 2018), so the use of both compounds should not be a confounding variable.

The occlusal surfaces of multituberculate molars are predominately on the labial and lingual sides of the cusps. This causes problems when trying to observe microwear – the areas of interest are blocked from view by a cusp row. To overcome this problem, molds of individual cusp rows (rather than whole teeth) were made. The issue was only discovered after whole-tooth molds had been made of the AMNH and some NMMNH specimens. These particular molds were cut with a scalpel to isolate the individual cusp rows for casting.

For m1s and m2s, the labial side of the lingual cusp row was molded. For M1s, the lingual side of the middle cusp row was molded. The lingual side of the labial cusp row was molded for M2s. These particular rows were chosen because they were well preserved in a large number of teeth and they were relatively easy to mold. When worn rows did not have a

28

distinctive lingual and labial side, molds were made of the flattened occlusal surface. In some cases, the preferred cusp row was damaged or did not preserve microwear. When this occurred, a different cusp row was chosen. The complete list of molded cusp rows can be found in Appendix B.

Molds were embedded in receptacles made of a two-part putty compound (Coltène/Whaledent®). Epo-Tek #301 epoxy resin was then poured into the molds to make casts. Before pouring, the epoxy was degassed using a vacuuming chamber to remove bubbles. After pouring, casts were examined under a light microscope and remaining bubbles were manually removed using a pipette tip and blunt probe. Wet casts were placed in the fume hood and left to dry for 72 hours. Once dry, the casts were examined under a light microscope again to determine if they were good candidates for microwear analysis.

2.2.2 Scanning electron microscopy.

Casts were coated with gold using a sputter coater. They were then scanned in high vacuum with secondary electron imaging using a FEI Quanta Feg 250 SEM. Secondary electron imaging was chosen over backscatter electron imaging because feature extinction is less prevalent with secondary electrons (Galbany et al., 2004). The casts were imaged at either 100x or 200x magnification, depending on the size of the tooth (Appendix B). All images were taken with a voltage of 2.50 kV and a field of view of 1.49 mm. The resultant images were all 2048 x 1887 pixels. Because the pixel density remained constant while magnification changed, the 200x images had higher resolution than the 100x images for an equivalent area of the tooth. This was necessary because of the small size of the teeth: a lower magnification (and thus resolution) would have rendered the microwear uncountable. The difficulties with resolution were discovered after the larger teeth had already been scanned at 100x magnification. Differences in

magnification and resolution can affect microwear signals (Mihlbachler and Beatty, 2012), but it has been demonstrated that differences between 100x magnification and 200x magnification are negligible (Oliver et al., 2014), and that species-level differences in microwear are detectable for a wide range of resolutions (Mihlbachler and Beatty, 2012). Therefore, differences in magnification and resolution were likely inconsequential in this study.

Most microwear studies try to select a specific homologous cusp for imaging. I was unable to do this because the homologies of multituberculate cusps are unclear, there are a variable number of cusps in the cusp row, and microwear was not consistently present on any one cusp. Therefore, I imaged cusps primarily based on the presence of microwear. When many cusps had microwear, I imaged two or three cusps: one anterior cusp, one middle cusp (when present), and one posterior cusp. The list of cusp locations used in the study can be found in Appendix B.

2.2.3 Counting microwear.

The five best representative teeth of each taxon were selected for microwear analysis. When more than five specimens had equivalent microwear, I randomly chose the five to be used. In some cases, two or more of the best representatives came from different teeth preserved on the same jaw. I treated the microwear counts of these teeth as if they were independent of each other because, after counting the microwear, I determined that the microwear counts among the associated teeth of a taxon were as variable as the microwear counts among the unassociated teeth of the same taxon. Associated teeth of *C. fissidens* and *Ptilodus* sp. were included in the analysis Appendix B.

After the five specimens were chosen, a single image of each specimen was randomly selected for counting, ensuring that no tooth or cusp position was purposefully favoured. For two

taxa (*Catopsalis calgariensis* and Cimolomyid 1), the five-specimen protocol was not followed. For *C. calgariensis*, only one specimen was available for study (additional specimens of *C. calgariensis* from the Shotgun locality in Wyoming differ from homologous teeth of *C. calgariensis* from the type locality in Alberta. The Shotgun locality specimens were analyzed separately as *C*. cf. *calgariensis*). For Cimolomyid 1, because the initial five specimens produced unusually variable microwear counts, I added two additional specimens out of concern that the initial five were not a representative sample.

The selected images were imported into Adobe Photoshop and contrast was adjusted to make the microwear more visible. The images were then imported into Fiji (available https://imagej.net/Fiji). Two 0.1 x 0.1 mm regions of interest (ROIs) were circumscribed on each cusp using the Rectangle and Paintbrush tools (Figure 2.1). This ROI size has previously been used for rodent microwear analysis (Gomes Rodrigues et al., 2009; Firmat et al., 2011; Oliver et al., 2014). Each SEM image included an embedded scale bar that was used to set the size of the ROIs.

Once the images were prepared for microwear counting, they were given random numerical identifications to ensure that the taxonomic identity of each image was obscured and that microwear counts were as objective as possible. When counting the microwear, two versions of each image were opened, one in Photoshop and one in Fiji. The Photoshop version was for reference: it remained unmarked, but the brightness and contrast were repeatedly adjusted to emphasize different features. The Fiji version was marked-up with the Paintbrush tool, following a consistent colour scheme to demarcate features (Figure 2.1; Appendix C). Images taken at 100x magnification were enlarged to 200% in Fiji to aid in identification of small features. Images taken at 200x magnification were not enlarged. The reference images in Photoshop were

31

typically kept at 100%, but I occasionally zoomed in and out during marking. After the images were marked, the Fiji Cell Counter plug-in was used to count the features. All features in the ROIs were included, as were features only partially included in the ROIs. The two ROIs were averaged together to get an average feature count for the specimen.

I followed the methods of Solounias and Semprebon (2002) in classifying features as pits, scratches, and gouges, and further categorizing them based on size. Scratches were defined as features with a width to length ratio of less than 1:4 and pits were defined as features with a width to length ratio of 1:4 or more (Grine, 1986). Typically, scratches are further categorized as either fine or coarse, and pits as either small or large (Solounias and Semprebon, 2002). I elected to separate the multituberculate microwear into three categories instead – small, medium, and large – in order to account for the large size range of the specimens.

Following Gomes Rodrigues et al. (2009), small pits had a diameter of 5 µm or less and fine scratches had a width of 5 µm or less. This distinction has previously been used when classifying rodent microwear (Gomes Rodrigues et al., 2009; Firmat et al., 2011; Oliver et al., 2014). Medium pits had a diameter between 5 µm and 10 µm (including 10 µm), and large pits had a diameter exceeding 10 µm. When measuring irregularly shaped pits, I used the average of the largest and smallest widths to make a classification. Similar to the pits, medium scratches had widths between 5 µm and 10 µm (including 10 µm), and coarse scratches had widths exceeding 10 µm.

Like Solounias and Semprebon (2002), I considered gouges to be large, irregularly shaped features that could not be classified as pits or scratches. Gouges are usually not differentiated further, but I chose to distinguish between two types of gouges: shallow and deep. Shallow gouges are features that are only present on the upper surface of the enamel. Deep gouges

32

penetrate the enamel further and tend to be as deep, if not deeper, than the large pits. The true

depth of the gouges could not be measured from the images, so the classification was purely

based on relative depth.

A.

B.

C.

det	HV	spot	WD	HFW	mag ⊞	pressure	temp	400 μm
ETD	2.50 kV	3.0	22.5 mm	1.49 mm	100 x	5.13e-4 Pa	---	

det	HV	spot	WD	HFW	mag ⊞	pressure	temp	400 μm
ETD	2.50 kV	3.0	22.5 mm	1.49 mm	100 x	5.13e-4 Pa	---	
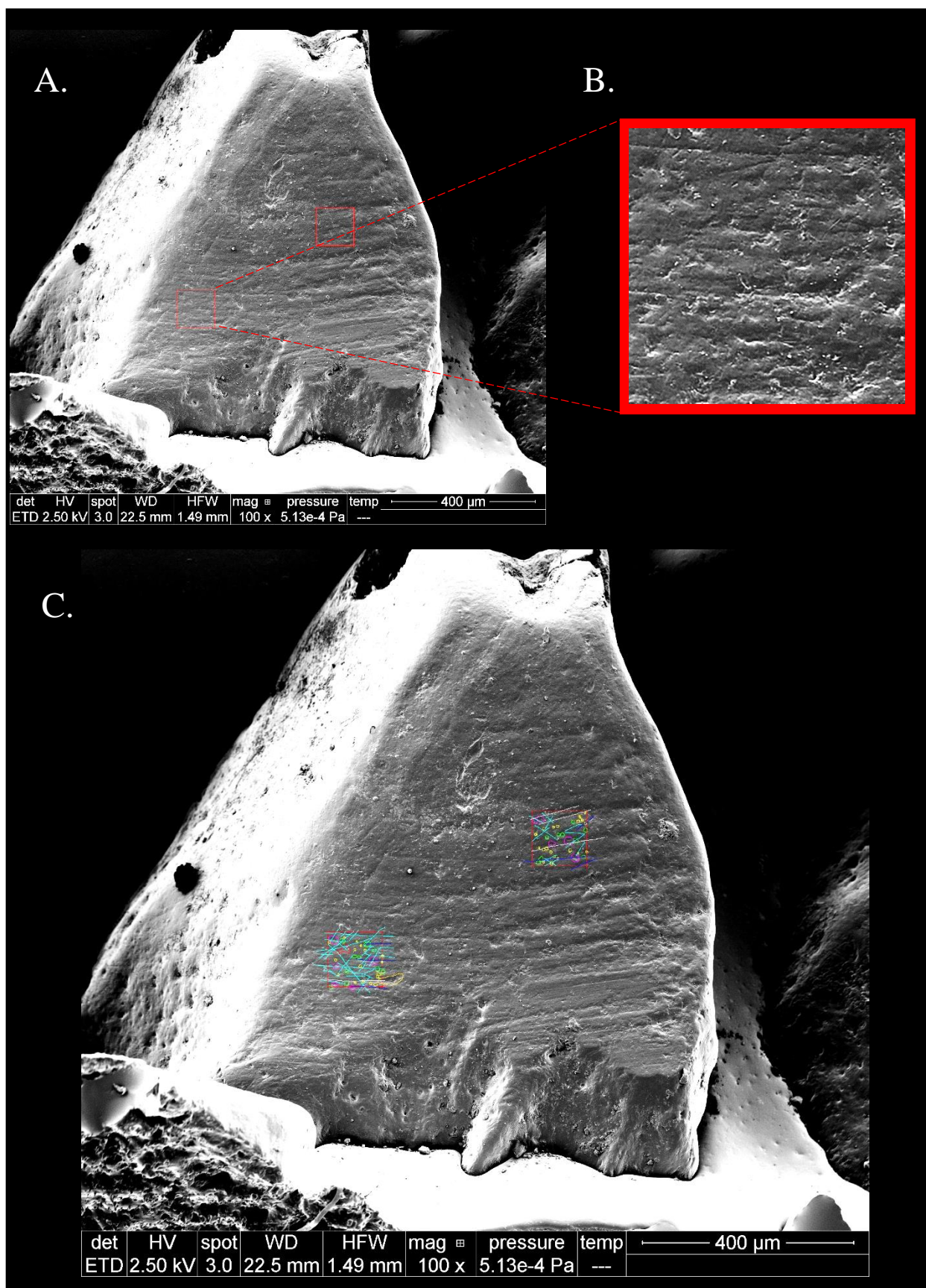
Figure 2.1 SEM image of a *V. joyneri* m1 cusp (UALVP 6596). A) SEM image prepared for counting with two 0.1 X 0.1 mm ROIs circumscribed in red B) Enlarged image of one ROI ready for counting C) Counted image with microwear features designated by colour. The colour scheme can be found in Appendix C.

2.2.4 Analyzing data.

I analyzed scratch-to-pit ratios ((fine scratches + medium scratches + large scratches) : (medium pits + large pits)) and feature-size ratios ((fine scratches) : (medium pits + large pits + medium scratches + large scratches + gouges + flakes)) to determine if there were differences in microwear among taxa. Relative numbers of scratches and pits, and relative numbers of fine and coarse features, have both been used to distinguish the diets of small-bodied mammals previously (Silcox and Teaford, 2002; Nelson et al., 2005; Townsend and Croft, 2008; Gomes Rodrigues et al., 2009). I elected to use ratios rather than feature totals because features totals are affected by ROI dimensions, which vary across studies (e.g. see Townsend and Croft, 2008 compared to Gomes Rodrigues et al., 2009). Statistics were not performed on the data because of small sample sizes. All scratch categories were all included in the analysis, but only medium and large pits were included, as previous studies have indicated that small pits ($\leq$ 5 µm) are not useful for distinguishing dietary categories (Townsend and Croft, 2008; Gomes Rodrigues et al., 2009; Oliver et al., 2014). Gouges were included in the "coarse feature" category for feature-size comparisons, but they were not included the scratch-to-pit comparisons. Microwear counts can be found in Appendix B.

2.3 Results

    2.3.1 Scratches and pits.

The average numbers of scratches and pits are similar for all taxa included in this study (Figure 2.2; Appendix B). A few specimens of *Mesodma* sp., *Cimolomys* sp., and Cimolomyid 1 have high scratch counts, as does one specimen of *Valenopsalis joyneri*, but other specimens of these taxa have low scratch and pit counts. Average scratch counts range from 11.5 (*C. calgariensis*) to 29.7 (SD = 6.02) (*Cimolomys* sp.), and average pit counts range from 4.30 (SD = 1.47) (*Mesodma* sp.) to 950 (SD = 3.29) (*V. joyneri*) (Table 2.1).

Most of the study taxa have fairly low scratch-to-pit ratios (around two to four). *Mesodma* sp. is an outlier with a scratch-to-pit ratio of 6.47 (SD = 2.71). The ratio of *Mesodma* sp. is likely elevated by the unusually high scratch-to-pit ratios on two specimens (Figure 2.3; Appendix B). The taeniolabidoids have lower average ratios than the non-taeniolabidoids – the taeniolabidoid with the highest average ratio is *Catopsalis alexanderi* (3.04, SD = 1.09), and this ratio is smaller than *Ptilodus* sp. (3.44, SD = 1.06), the non-taeniolabidoid with the lowest average ratio (Figure 2.3; Table 2.1). Even so, there is quite a bit of overlap in ratios between individual taeniolabidoid and non-taeniolabidoid specimens (Figure 2.3; Table 2.1). Differences among the taeniolabidoids are small, as are the differences among the non-taeniolabidoids excepting *Mesodma* sp. (Figure 2.3).

Table 2.1. Mean scratches, pits, fine features, and coarse features for each taxon included in the study.

Table abbreviations: **N** – number of specimens; **SD** – **s**tandard deviation.

Taxon	N	Mean scratches (SD)	Mean pits (SD)	Mean scratch: pit (SD)	Mean fine (SD)	Mean coarse (SD)	Mean fine: coarse (SD)
Taeniolabis taoensis	5	18.6 (2.99)	8.90 (1.98)	2.09 (0.57)	15.8 (2.68)	12.5 (2.10)	1.24 (0.30)
Catopsalis cf. *calgariensis*	5	16.2 (3.26)	6.40 (2.01)	2.53 (0.94)	13.2 (3.34)	10.8 (2.44)	1.22 (0.41)
Catopsalis calgariensis	1	11.5 (--)	6.50 (--)	1.77 (--)	9.50 (--)	9.50 (--)	1.00 (--)
Catopsalis fissidens	5	22.7 (4.72)	8.30 (2.18)	2.73 (0.92)	21.3 (4.74)	10.5 (2.61)	2.03 (0.67)
Catopsalis alexanderi	5	21.9 (3.56)	7.20 (2.29)	3.04 (1.09)	19.7 (3.83)	10.7 (1.75)	1.84 (0.47)
Valenopsalis joyneri	5	21.1 (2.96)	9.50 (3.29)	2.22 (0.83)	18.6 (1.80)	12.5 (5.23)	1.49 (0.64)
Catopsalis kakwa	5	14.8 (4.58)	5.60 (1.85)	2.64 (1.20)	13.9 (4.32)	7.80 (3.46)	1.78 (0.96)
Cimolomyid 1	7	28.7 (9.99)	7.00 (2.10)	4.10 (1.89)	26.9 (9.85)	9.50 (1.97)	2.83 (1.19)
Cimolomys sp.	5	29.7 (6.02)	8.20 (2.99)	3.62 (1.51)	27.6 (5.81)	10.9 (3.12)	2.53 (0.90)
Meniscoessus major	5	25.0 (3.79)	6.50 (1.64)	3.85 (1.13)	23.5 (3.45)	8.30 (2.20)	2.83 (0.86)
Meniscoessus robustus	5	18.0 (3.82)	4.70 (0.68)	3.83 (0.98)	16.3 (5.12)	7.20 (1.21)	2.26 (0.81)
Mesodma sp.	5	27.8 (6.74)	4.30 (1.47)	6.47 (2.71)	26.3 (7.33)	6.80 (1.69)	3.87 (1.44)
Ptilodus sp.	5	21.3 (4.70)	6.20 (1.33)	3.44 (1.06)	19.5 (5.39)	8.60 (0.97)	2.27 (0.68)
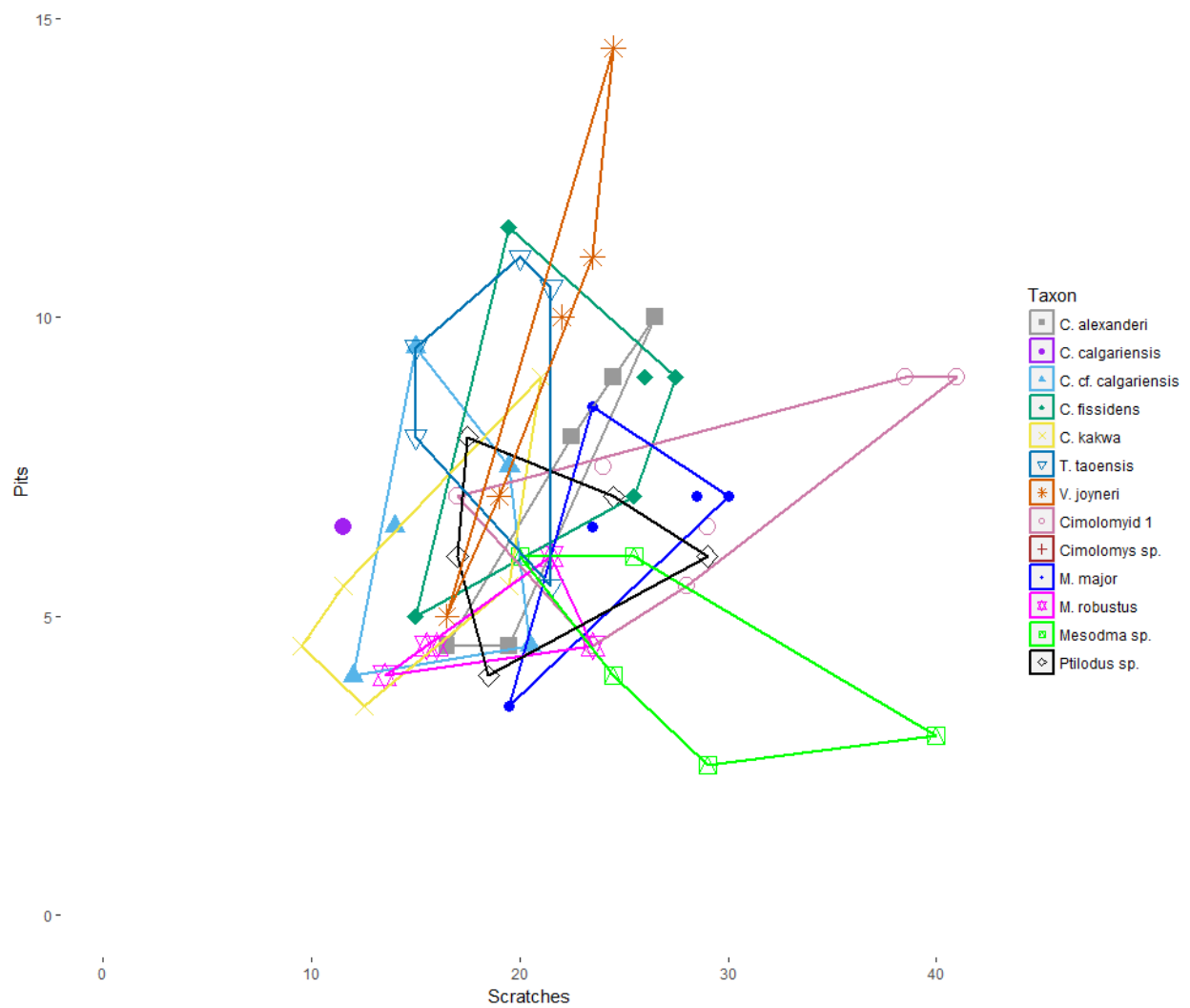
Figure 2.2. Minimum convex hull polygons of individual specimen scratch and pit counts organized by taxon.
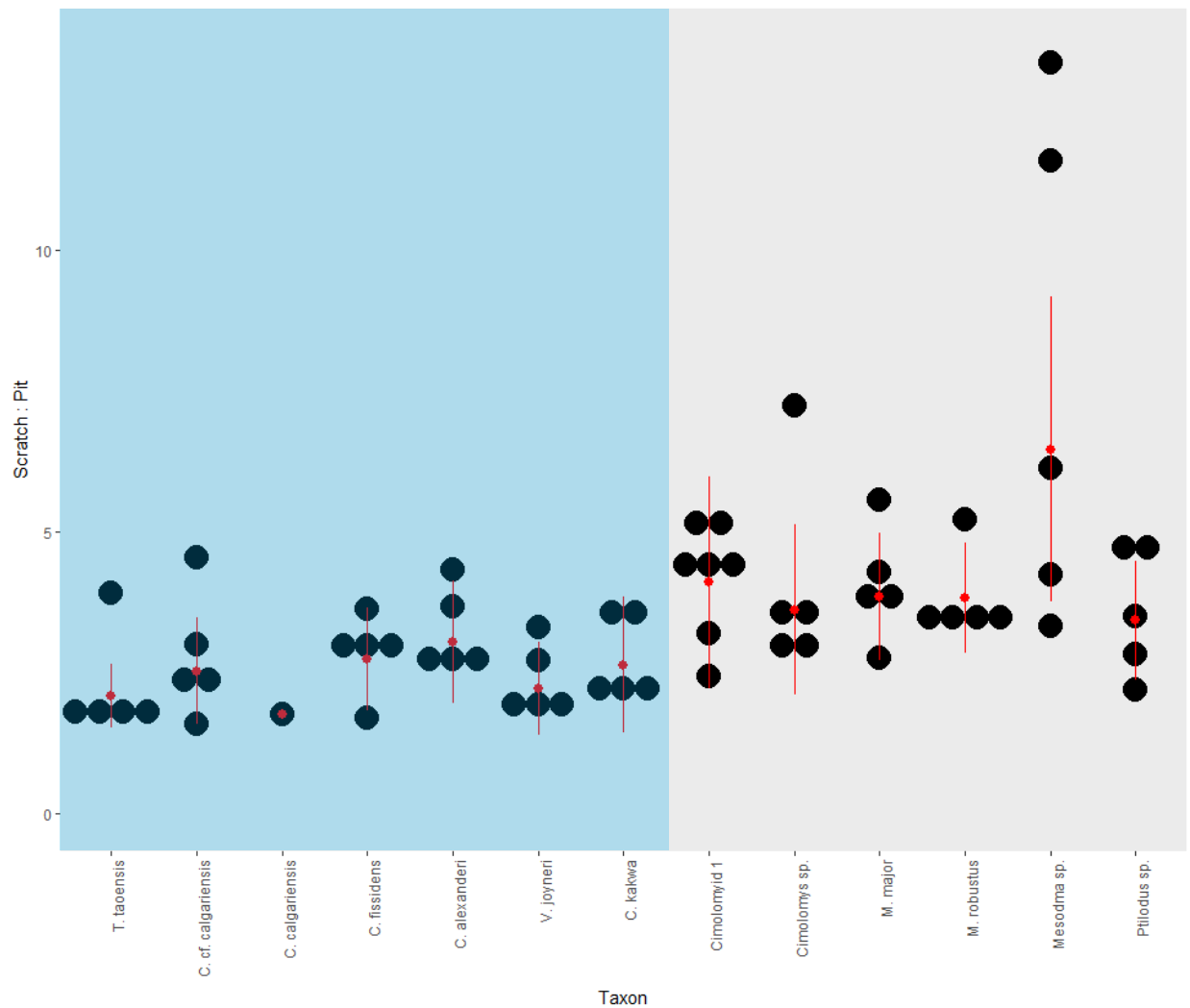
Figure 2.3. Dot plots of scratch to pit ratios by taxon. Small pits are not included in the ratios. Each specimen is represented by a solid black circle. Each taxon mean is represented by a solid red circle with the red line representing one standard deviation from the mean. Taeniolabidoids are in the shaded blue area and are organized by inferred body size, with the largest-bodied taxon (*T. taoensis*) on the left and the smallest-bodied taxon (*C. kakwa*) on the right. Non-taeniolabidoids are in the shaded grey area and are not organized by inferred body size.

2.3.2 Feature size.

The distribution of fine and coarse features for individual specimens is similar to the distribution of scratches and pits for individual specimens (Figure 2.4). Fine pits were not included in the analysis, so fine feature counts are based on fine scratches solely. As with the scratch-to-pit ratios, taeniolabidoids tend to have lower fine-to-coarse feature ratios than the non-taeniolabidoids (Figure 2.5; Table 2.1). *Catopsalis fissidens* has the greatest average fine-to-coarse feature ratio for the taeniolabidoids, with approximately twice as many fine features as coarse features (2.03, SD = 0.67). *Meniscoessus robustus* has the lowest non-taeniolabidoid ratio, with 2.26 (SD = 0.81) times as many fine features as coarse features. Even so, some taeniolabidoids and non-taeniolabidoids have overlapping ratios when individual specimens are considered. *Mesodma* sp. has the highest average fine-to-coarse ratio (Table 2.1), the value of which is elevated by one specimen (Figure 2.5).

There is a great deal of both intra- and inter-taxon variation in fine features (Appendix B). The average number of fine features ranges from 9.50 in *C. calgariensis* to 27.6 (SD = 5.81) in *Cimolomys* sp. (Table 2.1). However, there are no clear trends in the distribution of fine features Among the taxa.

Coarse features can be divided into medium features and large features. Medium features are those that fall between 5 µm and 10 µm in width, while large features have a width greater than 10 µm. Gouges are included in the large feature category. There are a greater number of medium features than large features, and most of the inter-taxon variation in coarse features is attributable to medium features (Appendix B). Large features have a relatively uniform distribution across taxa, although the taeniolabidoids tend to have a greater spread of individual values than the non-taeniolabidoids (Appendix B).
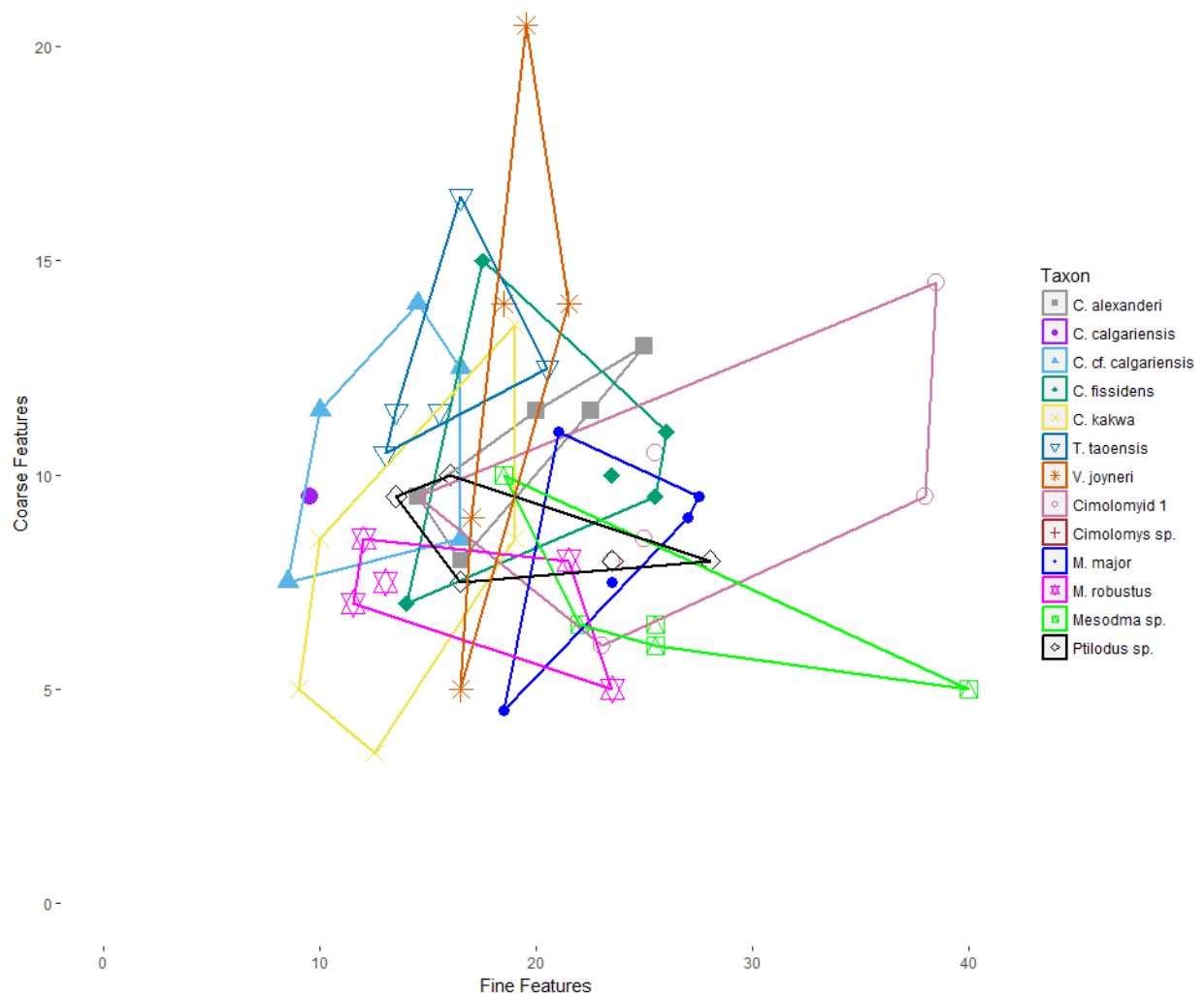
Figure 2.4. Minimum convex hull polygons of individual specimen coarse and fine feature counts organized by taxon.
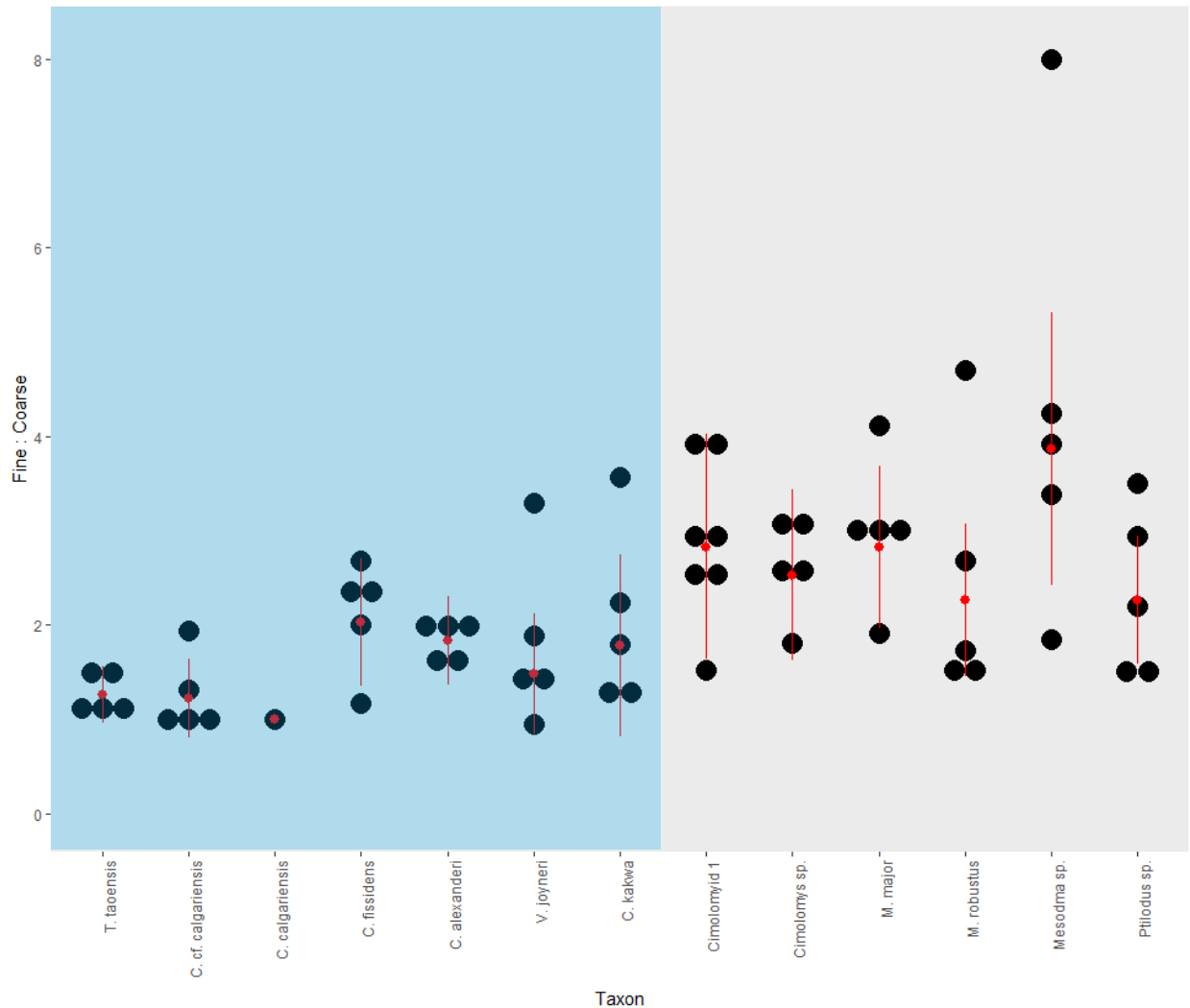
Figure 2.5. Dot plots of fine to coarse ratios by taxon. Small pits are not included in the ratios. Each specimen is represented by a solid black circle. Each taxon mean is represented by a solid red circle with the red line representing one standard deviation from the mean. Taeniolabidoids are in the shaded blue area and are organized by inferred body size, with the largest-bodied taxon (*T. taoensis*) on the left and the smallest-bodied taxon (*C. kakwa*) on the right. Non-taeniolabidoids are in the shaded grey area and are not organized by inferred body size.

2.4 Discussion

2.4.1 Comparisons within this study.

2.4.1.1 Scratches and pits.

Scratch-to-pit ratios do not vary greatly among the multituberculate taxa examined in this study. The taeniolabidoids have the lowest scratch-to-pit ratios, but these ratios are only slightly lower than those for most of the non-taeniolabidoids, and the differences between the two are within the range of variation reported for rodents of the same dietary category (Townsend and Croft, 2008; Gomes Rodrigues et al., 2009). This suggests that these multituberculates, both taeniolabidoids and non-taeniolabidoids alike, were consuming materials with similar structural properties. A larger sample is necessary to determine whether the slight differences between the two are significant.

Unlike the other taxa, *Mesodma* sp. has a very high average scratch-to-pit ratio, which is the result of two specimens having exceptionally high ratios. Previous work has found that there is a significant difference in molar microwear in specimens of *Mesodma thompsoni* across the K-Pg boundary: Cretaceous specimens tend to have a high quantity of pits while Paleocene specimens tend to have a high quantity of long, thin scratches (Weil and Pignataro, 2007a-b). The *Mesodma* sp. specimens included in this study come from the Bug Creek Anthills of northeastern Montana, which is a reworked locality that contains both Lancian (Late Cretaceous) and Puercan (early Paleocene) material (Lofgren, 1995). The large spread of *Mesodma* sp. scratch-to-pit ratios found in this study may be a result of both Lancian and Puercan specimens being included in the analysis.

2.4.1.2 Feature dimensions.

There are differences in feature size among the taxa, but these differences are difficult to interpret. Interestingly, most of the differences arise from features between 5 and 10 µm in width. Features wider than 10 µm are found almost equally among the taxa. This could indicate that feature width is not related to body size, but it could also mean that the distinction between "medium" and "large" features is unnecessary. In the future, rather than assigning the features to ordinal categories, it may be more informative to directly compare numerical values.

The large-bodied taeniolabidoids (*T. taoensis, C.* cf. *calgariensis, C. calgariensis*) have slightly lower fine-to-coarse feature ratios than the smaller taeniolabidoids. However, the present sample size is too small to determine whether the ratios are significantly different. The taeniolabidoids tend to have a greater number of coarse features than the non-taeniolabidoids, but these differences are also minor, and the values for all taxa fall within the range of values reported for single dietary categories established for murid rodents (Gomes Rodrigues et al., 2009). Many of the studied taxa had a wide spread of coarse microwear features which in rodents has been interpreted as indicating a generalist diet (Gomes Rodrigues et al., 2009). Similarly, Weil and Pignataro (2007a-b) posited that changes observed in *M. thompsoni* microwear across the K-Pg boundary indicated that the species was a generalist. This study does not have the quantity of data needed to examine intra-taxon variation across the K-Pg boundary, but the wide spread of features does generally support a generalist diet for many of the included taxa.

2.4.2 Comparisons to previous multituberculate microwear work.

Weil and Pignataro (2007a-b) studied the microwear of species of *Mesodma* and *Cimexomys* that cross the K-Pg boundary. They found that microwear signals differed between Cretaceous and Paleocene individuals, with Cretaceous specimens having more pitting and

Paleocene specimens have more fine, long scratches. However, total numbers of features and scratch-to-pit ratios were not reported, so they cannot be compared to the results of the present study.

Christensen (2012) performed microwear counts on the teeth of many multituberculate taxa, including specimens of *Cimolomys* spp., *Meniscoessus major*, *Meniscoessus robustus*, *Mesodma* spp., *Ptilodus* spp., and *T. taoensis*. Christensen consistently recorded lower microwear counts than I did, both in terms of total scratches and scratch-to-pit ratios. She and I had similar total pit counts, but not for the same species. These discrepancies likely arise from inter-observer error and differences in methodologies. Inter-observer error is common in both LMM and SEM studies, even when the same specimens are used among counters (Grine et al., 2002; Semprebon et al., 2004; Galbany et al., 2005; Purnell et al., 2006; Mihlbachler et al., 2012). These rates of inter-observer error often rise when counts are done by novice counters (Galbany et al., 2005; Mihlbachler et al., 2012). Both Christensen and I were relatively novice counters, and we did not include any of the same specimens in our analyses (Christensen, 2012). Microwear only lasts for several days to weeks, and it represents evidence of the "last meal" of the organism in question, so variation among individuals is expected. This variation is especially high for generalist species and for species with seasonal diets (Gomes Rodrigues et al., 2009). Furthermore, Christensen used LMM (70x magnification) and counted microwear directly from the casts, not photographs. This could explain why Christensen (2012) counted fewer scratches than I counted in this study.

2.4.3 Comparisons to extant small mammals.

The multituberculate teeth examined in this study have a higher frequency of small pits, fine scratches, and large pits than the teeth of extant caviomorph and murid rodents (Townsend

and Croft, 2008; Gomes Rodrigues et al., 2009). Coarse scratch averages are similar to those reported from murid rodents (Gomes Rodrigues et al., 2009), and gouge averages are similar to those reported from caviomorph rodents (Townsend and Croft, 2008).

Of the features included in the main analysis, fine scratches have the most intra- and inter-taxon variation (Appendix B). While the total numbers of fine scratches are higher than those reported from murid rodents, the intra-taxon variation is similar (Gomes Rodrigues et al., 2009). An abundance of fine scratches has been reported for grass-eating murids (Gomes Rodrigues et al., 2009). High scratch frequencies have also been reported for grazing caviomorphs, although in this case the scratches were not differentiated by size (Townsend and Croft, 2008). Grazing rodents are not the only small mammals with an abundance of scratches. For example, lumbricophagous moles and tenrecs also have many fine scratches on their teeth (Silcox and Teaford, 2002), and these are believed to be caused by the coincident ingestion of dirt along with prey items. The prevalence of scratches on cimolodontan multituberculate teeth could indicate that they were ingesting a lot of exogenous grit. However, a direct comparison between multituberculate and therian microwear ignores the likely phylogenetic-dependence of microwear (Fraser et al., 2018a) and potential differences in imaging techniques (Kalthoff and Green, 2017), so the higher number of scratches on the multituberculate teeth may not indicate greater grit ingestion.

The prevalence of large pits is interesting. Previous studies have suggested that a high prevalence of coarse microwear features, particularly large pits and gouges, is indicative of insectivory and frugivory in murid, sciurid, and caviomorph rodents (Nelson et al., 2005; Townsend and Croft, 2008; Gomes Rodrigues et al., 2009). In these cases, the insectivorous rodents were eating hard-bodied insects and the frugivorous rodents were consuming hard fruits

and engaging in some degree of granivory (Nelson et al., 2005; Townsend and Croft, 2008; Gomes Rodrigues et al., 2009). These data concur with earlier findings that small-bodied microchiropterans and primates that engage in soft-bodied insectivory and seedless, soft-fruit frugivory have lower pit counts than those taxa engaging in hard-bodied insectivory and hard-fruit frugivory (Strait, 1993). The high pit counts on the studied multituberculate teeth suggest that most of the multituberculates (possibly excepting *Mesodma* sp.) were consuming resistant items. However, as with the fine scratches, phylogenetic and methodological considerations mean that a direct comparison between therians and multituberculates is tenuous.

2.4.4 Cimolodontan dental microwear and locomotor habits.

The microwear signals recovered in this study are somewhat surprising given that taeniolabidoid multituberculates were likely terrestrial or possibly fossorial (Miao, 1988; Kielan-Jaworowska and Qi, 1990; Kielan-Jaworowska and Gambaryan, 1994), while some non-taeniolabidoid cimolodontans were likely scansorial (Simpson and Elftman, 1928; Jenkins and Krause, 1983; Krause and Jenkins, 1983). Mammals that eat foods close to ground-level (e.g. grazers) tend to ingest more exogenous grit, resulting in microwear dominated by scratches (Teaford and Walker, 1984; Solounias and Semprebon, 2002). Mammals that consume foods from trees (e.g. browsers) tend to have microwear dominated by pits (Teaford and Walker, 1984; Solounias and Semprebon, 2002). Given that taeniolabidoids were likely terrestrial, and therefore feeding close to the ground, it was expected that they would have a relatively high frequency of fine features, especially scratches, on their teeth. This result was not recovered in the present study – the taeniolabidoids had a relatively high frequency of pits and coarse features.

The prevalence of pits and coarse features on the taeniolabidoid teeth it is not without precedent. Nelson et al. (2005) found that omnivorous ground squirrels had a higher frequency of

pits and coarse features than frugivorous tree squirrels, possibly because ground squirrels consume more seeds and chitin than tree squirrels do. Furthermore, Townsend and Croft (2008) found that some grazing caviomorphs (*Ctenomys* and *Chinchilla*) had microwear signals indicative of hard-object feeding because of their burrowing habits. Based on these previous studies, the microwear signal recovered in the present study suggests that taeniolabidoids were consuming resistant items as part of their diet or through other behaviours. This concurs with the morphology of taeniolabidoid cheek teeth, which are relatively well-adapted for grinding resistant materials.

The prevalence of fine scratches on the non-taeniolabidoid cimolodontan teeth suggests that they were consuming large quantities of exogenous grit during feeding. The locomotor habits of most North American cimolodontans have not been reconstructed: it is possible that many were terrestrial taxa that fed close to the ground. Some ptilodontids were possibly scansorial (Jenkins and Krause, 1983; Krause and Jenkins, 1983), which suggests that they may have fed farther above the ground. The one ptilodontid taxon included in the microwear analysis – *Ptilodus* sp. – has the lowest scratch-to-pit ratio and the second-lowest fine-to-coarse feature ratio of the non-taeniolabidoid cimolodontans. This suggests that *Ptilodus* sp. was ingesting less exogenous grit than many of the other non-taeniolabidoid cimolodontans, possibly because *Ptilodus* sp. was feeding above ground level. However, *Ptilodus* sp. does have more fine scratches than the taeniolabidoids, indicating that *Ptilodus* sp. was consuming relatively large quantities of exogenous grit and relatively few resistant items compared to the taeniolabidoids.

2.5 Summary and Conclusions

Large- and small-bodied taeniolabidoids do not noticeably differ in their scratch-to-pit ratios. However, the taeniolabidoids do have slightly lower scratch-to-pit ratios than the included non-taeniolabidoids. In extant taxa, a high prevalence of scratches has been associated with the consumption of exogenous grit (e.g. Silcox and Teaford, 2002; Solounias and Semprebon, 2002; Townsend and Croft, 2008; Gomes Rodrigues et al., 2009; Belmaker, 2018). The relatively low scratch-to-pit ratios on the taeniolabidoids suggests that the taeniolabidoids were consuming less grit than the non-taeniolabidoids. *Mesodma* sp. has a particularly high scratch-to-pit ratio. This ratio is probably the result of some Paleocene specimens being included in the sample – Paleocene specimens of *Mesodma* have an abundance of fine scratches (Weil and Pignataro, 2007a-b), indicating the ingestion of large quantities of grit.

The large-bodied taeniolabidoids have lower fine-to-coarse feature ratios than the small-bodied taeniolabidoids, and the taeniolabidoids (including the small-bodied taxa) have slightly lower fine-to-coarse ratios than the included non-taeniolabidoids. Relatively low fine-to-coarse ratios have been observed on insectivorous and frugivorous rodents (Nelson et al., 2005; Townsend and Croft, 2008; Gomes Rodrigues et al., 2009). Thus, the low fine-to-coarse ratios of the large-bodied taeniolabidoids may be an indication that the larger taeniolabidoids were consuming more resistant substances (e.g. insect exoskeletons, hard fruits, seeds) than the smaller taeniolabidoids. Furthermore, the taeniolabidoids may have been consuming more resistant substances than the non-taeniolabidoids. The variation in feature dimensions may also indicate that the taeniolabidoids, particularly the large-bodied taeniolabidoids, were consuming larger sized items.

The scratch-to-pit ratios and fine-to-coarse feature ratios are suggestive of dietary differences among the studied multituberculates, but a cavate remains: the differences among the studied taxa are no greater than the differences observed in extant caviomorph and murid rodents within the same dietary category (e.g. grazing caviomorphs can have scratch-to-pit ratios ranging from < 2.00 to > 35.0) (Townsend and Croft, 2008; Gomes Rodrigues et al., 2009). However, the microwear observed in this study may not be directly comparable to the microwear on rodent teeth – this study employed a different imaging methodology, and a phylogenetic signal may be present in the data. A larger multituberculate sample is necessary to determine whether the differences observed among the studied taxa are significant.

2.6 Literature Cited

Arman, S. D., P. S. Ungar, C. A. Brown, L. R. G. DeSantis, C. Schmidt, and G. J. Prideaux. 2016. Minimizing inter-microscope variability in dental microwear texture analysis. Surface Topography: Metrology and Properties 4:doi: 10.1088/2051-672X/4/2/024007.

Baines, D. C., M. A. Purnell, and P. J. B. Hart. 2014. Tooth microwear formation rate in *Gasterosteus aculeatus*. Journal of Fish Biology 84:1582–1589.

Baker, G., L. H. P. Jones, and I. D. Wardrop. 1959. Cause of wear in sheep's teeth. Nature 184:1583–1584.

Barr, W. A., and R. S. Scott. 2014. Phylogenetic comparative methods complement discriminant function analysis in ecomorphology. American Journal of Physical Anthropology 153:663–674.

Belmaker, M. 2018. Dental microwear of small mammals as a high resolution paleohabitat proxy: opportunities and challenges. Journal of Archaeological Science: Reports 18:824–

838.

Berthaume, M. A., L. K. Delezene, and K. Kupczik. 2018. Dental topography and the diet of
Homo naledi. Journal of Human Evolution 118:14–26.

Broom, R. 1914. On the structure and affinities of the Multituberculata. Bulletin of The
American Museum of Natural History 33:115–134.

Buckley, G. A. 1995. The multituberculate *Catopsalis* from the early Paleocene of the Crazy
Mountains Basin in Montana. Acta Palaeontologica Polonica 40:389–398.

Christensen, H. B. 2012. Mammalian adaptation to herbivory in the aftermath of the KT
extinction. The University of Chicago, 112 pp.

Clemens, W. A., and J. A. Lillegraven. 1986. New Late Cretaceous, North American advanced
therian mammals that fit neither the marsupial nor eutherian molds. Contributions to
Geology, University of Wyoming, Special Paper 3:55–85.

Covert, H. H., and R. F. Kay. 1981. Dental microwear and diet: implications for determining the
feeding behaviors of extinct primates, with a comment on the dietary pattern of
Sivapithecus. American Journal of Physical Anthropology 55:331–336.

Creighton, J. H., S. V. Robson, and J. M. Theodor. 2018. A comparison of dental molding and
casting compounds used for microwear analysis. Journal of Vertebrate Paleontology,
Program and Abstracts 110.

Daegling, D. J., L. C. Hua, and P. S. Ungar. 2016. The role of food stiffness in dental microwear
feature formation. Archives of Oral Biology 71:16–23.

Erickson, K. L. 2014. Prairie grass phytolith hardness and the evolution of ungulate hypsodonty.
Historical Biology 26:737–744.

Fiorillo, A. R. 1998. Dental microwear patterns of the sauropod dinosaurs *Camarasaurus* and

Diplodocus: evidence for resource partitioning in the late Jurassic of North America. Historical Biology 13:1–16.

Firmat, C., H. Gomes Rodrigues, R. Hutterer, J. C. Rando, J. A. Alcover, and J. Michaux. 2011. Diet of the extinct Lava mouse *Malpaisomys insularis* from the Canary Islands: insights from dental microwear. Naturwissenschaften 98:33–37.

Fosse, G., Z. Kielan-Jaworowska, and S. G. Skaale. 1985. The microstructure of tooth enamel in multituberculate mammals. Palaeontology 28:435–449.

Fosse, G., Ø. Eskildsen, S. Risnes, and R. E. Sloan. 1978. Prism size in tooth enamel of some Late Cretaceous mammals and its value in multituberculate taxonomy. Zoologica Scripta 7:57–61.

Fox, C., A. Pérez-Pérez, and J. Juan. 1994. Dietary information through the examination of plant phytoliths on the enamel surface of human dentition. Journal of Archaeological Science 21:29–34.

Fraser, D., R. J. Haupt, and W. A. Barr. 2018a. Phylogenetic signal in tooth wear dietary niche proxies. Ecology and Evolution 1–14.

Fraser, D., R. J. Haupt, and W. A. Barr. 2018b. Phylogenetic signal in tooth wear dietary niche proxies: what it means for those in the field. Ecology and Evolution 1–5.

Fraser, D., J. C. Mallon, R. Furr, and J. M. Theodor. 2009. Improving the repeatability of low magnification microwear methods using high dynamic range imaging. Palaios 24:818–825.

Galbany, J., L. M. Martínez, and A. Pérez-Pérez. 2004. Tooth replication techniques, SEM imaging and microwear analysis in Primates: methodological obstacles. Anthropologie 41:5–12.

Galbany, J., L. M. Martinez, H. M. Lopez-Amor, V. Espurz, O. Hiraldo, A. Rombero, J. De

Juan, and A. Perez-Perez. 2005. Error rates in buccal-dental microwear quantification using scanning electron microscopy. Scanning 27:23–29.

Gambaryan, P. P., and Z. Kielan-Jaworowska. 1995. Masticatory musculature of Asian taeniolabidoid multituberculate mammals. Acta Palaeontol. Pol. 40:45–108.

Godfrey, L. R., G. M. Semprebon, W. L. Jungers, M. R. Sutherland, E. L. Simons, and N. Solouniase. 2004. Dental use wear in extinct lemurs: evidence of diet and niche differentiation. Journal of Human Evolution 47:145–169.

Gomes Rodrigues, H., G. Merceron, and L. Viriot. 2009. Dental microwear patterns of extant and extinct Muridae (Rodentia, Mammalia): ecological implications. Naturwissenschaften doi 10.1007/s00114-008-0501-x.

Gordon, K. D. 1982. A study of microwear on chimpanzee molars: implications for dental microwear analysis. American Journal of Physical Anthropology 59:195–215.

Gordon, K. D. 1984. Taphonomy of dental microwear, II. American Journal of Physical Anthropology 63:164–165.

Gordon, K. D. 1988. A review of methodology and quantification in dental microwear analysis. Scanning Microscopy 2:1139–1147.

Gordon, K. D., and A. C. Walker. 1983. Playing 'possum: a microwear experiment. American Journal of Physical Anthropology 60:109–112.

Goswami, A., J. J. Flynn, L. Ranivoharimanana, and A. R. Wyss. 2005. Dental microwear in Triassic amniotes: implications for paleoecology and masticatory mechanics. Journal of Vertebrate Paleontology 25:320–329.

Green, J. L., and N. A. Resar. 2012. The link between dental microwear and feeding ecology in tree sloths and armadillos (Mammalia: Xenarthra). Biological Journal of the Linnean

Society 107:277–294.

Grine, F. E. 1986. Dental evidence for dietary differences in *Australopithecus* and *Paranthropus*: a quantitative analysis of permanent molar microwear. Journal of Human Evolution 15:783–822.

Grine, F. E., P. S. Ungar, and M. F. Teaford. 2002. Error rates in dental microwear quantification using scanning electron microscopy. Scanning 24:144–153.

Gügel, I. L., G. Grupe, and K. Kunzelmann. 2001. Simulation of dental microwear: characteristict traces by opal phytoliths give clues to ancient human dietary behavior. American Journal of Physical Anthropology 114:124–138.

Hedberg, C., and L. R. G. DeSantis. 2017. Dental microwear texture analysis of extant koalas: clarifying causal agents of microwear. Journal of Zoology 301:206–214.

Janis, C. M., and A. Weil. 2008. Non-eutherian Mammal Summary; pp. 7–18 in C. M. Janis, G. F. Gunnell, and M. D. Uhen (eds.), Evolution of Tertiary Mammals of North America. Volume 2: Small Mammals, Xenarthrans, and Marine Mammals. Cambridge University Press, New York.

Jenkins, F. A. J., and D. W. Krause. 1983. Adaptations for climbing in North American multituberculates (Mammalia). Science, New Series 220:712–715.

Kalthoff, D. C., and J. L. Green. 2017. Feeding ecology in Oligocene mylodontoid sloths (Mammalia, Xenarthra) as revealed by orthodentine microwear analysis. Journal of Mammalian Evolution doi:10.100.

Kay, R. F., and H. H. Covert. 1983. True grit: a microwear experiment. American Journal of Physical Anthropology 61:33–38.

Kielan-Jaworowska, Z., and T. Qi. 1990. Fossorial adaptations of a taeniolabidoid

multituberculate mammal from the Eocene of China. Vertebrata PalAsiatica 28:81–94.

Kielan-Jaworowska, Z., and P. P. Gambaryan. 1994. Postcranial anatomy and habits of Asian
multituberculate mammals. Fossils & Strata 36:1–92.

Kielan-Jaworowska, Z., R. L. Cifelli, and Z.-X. Luo. 2004. Mammals from the Age of
Dinosaurs: Origins, Evolution, and Structure. Columbia University Press, New York, 630
pp.

King, T., P. Andrews, and B. Boz. 1999. Effect of taphonomic processes on dental microwear.
American Journal of Physical Anthropology 108:359–373.

Krause, D. W. 1982. Jaw movement, dental function, and diet in the Paleocene multituberculate
Ptilodus. Paleobiology 8:265–281.

Krause, D. W., and F. A. J. Jenkins. 1983. The postcranial skeleton of North American
multituberculates. Bulletin of the Museum of Comparative Zoology 150:199–246.

Kubo, T., and M. Kubo. 2013. Dental microwear of a Late Triassic dinosauriform, *Silesaurus
opolensis*. Acta Palaeontologica Polonica 59:305–312.

Lofgren, D. L. 1995. The Bug Creek problem and the Cretaceous-Tertiary Transition at McGuire
Creek, Montana. University of California Publications in Geological Sciences 140:1–185.

Lucas, P. W., A. Van Casteren, K. Al-fadhalah, A. S. Almusallam, A. G. Henry, S. Michael, J.
Watzke, D. A. Reed, T. G. H. Diekwisch, D. S. Strait, and A. G. Atkins. 2014. The role of
dust, grit and phytoliths in tooth wear. Annales Zoologici Fennici 51:143–152.

M'Kirera, F., and P. S. Ungar. 2003. Occlusal relief changes with molar wear in *Pan troglodytes
troglodytes* and *Gorilla gorilla gorilla*. American Journal of Primatology 60:31–41.

Maas, M. C. 1991. Enamel etructure and microwear: an experimental study of the response of
enamel to shearing force. American Journal of Physical Anthropology 85:31–49.

Maas, M. C. 1994. A scanning electron-microscopic study of in vitro abrasion of mammalian

    tooth enamel under compressive loads. Archives of Oral Biology 39:1–11.

Mainland, I. L. 2003. Dental microwear in grazing and browsing Gotland sheep (*Ovis aries*) and

    its implications for dietary reconstruction. Journal of Archaeological Science 30:1513–

    1527.

McAfee, R. K., and J. L. Green. 2015. The role of bite force in the formation of orthodentine

    microwear in tree sloths (Mammalia: Xenarthra: Folivora): implications for feeding

    ecology. Archives of Oral Biology 60:181–192.

Merceron, G., A. Ramdarshan, A. Francisco, D. Gautier, J. Boisserie, X. Milhet, A. Novello, and

    D. Pret. 2016. Untangling the environmental from the dietary: dust does not matter.

    Proceedings of the Royal Society B: Biological Sciences 283:20161032.

Miao, D. 1986. Dental anatomy and ontogeny of *Lambdopsalis bulla* (Mammalia,

    Multituberculata). Contributions to Geology, University of Wyoming 24:65–76.

Miao, D. 1988. Skull morphology of *Lambdopsalis bulla* (Mammalia, Multituberculata) and its

    implications to mammalian evolution. Contributions to Geology, University of Wyoming,

    Special Paper 4:1–104.

Mihlbachler, M. C., and B. L. Beatty. 2012. Magnification and resolution in dental microwear

    analysis using light microscopy. Palaeontologia Electronica 15:1–15.

Mihlbachler, M. C., B. L. Beatty, A. Caldera-siu, D. Chan, and R. Lee. 2012. Error rates and

    observer bias in dental microwear analysis using light microscopy. Palaeontologia

    Electronica 15:1–22.

Nelson, S., C. Badgley, and E. Zakem. 2005. Microwear in modern squirrels in relation to diet.

    Palaeontologia Electronica 8:1–15.

Oliver, A., V. Hernandez-Ballarin, P. Lopez-Guerrero, I. Garcia-Paredes, M. A. Alvarez-Sierra, and A. R. Gomez Cano. 2014. Dental microwear analysis in Gliridae (Rodentia): methodological issues and paleodiet inferences based on *Armantomys* from the Madrid Basin (Spain). Journal of Iberian Geology 40:157–166.

Peters, C. R. 1982. Electron-optical microscopic study of incipient dental microdamage from experimental seed and bone crushing. American Journal of Physical Anthropology 57:283–301.

Puech, P.-F., A. Prone, H. Roth, and F. Cianfarani. 1985. Reproduction experiementale de processus d'usure des surfaces dentaires des Hominides fossiles: consequences morphoscopiques et exoscopiques avec application a l'Hominide I de Grausi. Comptes Rendus de l'Académie Des Sciences III 301:59–64.

Purnell, M. A. 1995. Microwear on conodont elements and macrophagy in the first vertebrates. Nature 374:798–800.

Purnell, M. A., P. J. B. Hart, D. C. Baines, and M. A. Bell. 2006. Quantitative analysis of dental microwear in threespine stickleback: a new approach to analysis of trophic ecology in aquatic vertebrates. Journal of Animal Ecology 75:967–977.

Rabenold, D., and O. M. Pearson. 2014. Scratching the surface: A critique of Lucas et al. (2013)'s conclusion that phytoliths do not abrade enamel. Journal of Human Evolution 74:130–133.

Renaud, S., and R. Ledevin. 2017. Impact of wear and diet on molar row geometry and topography in the house mouse. Archives of Oral Biology 81:31–40.

Rensberger, J. M. 1978. Scanning Electron Microscopy of Wear and Occlusal Events in Some Small Herbivores; pp. 415–438 in P. M. Butler and K. A. Joysey (eds.), Development,

Function and Evolution of Teeth. Academic Press Inc. (London) LTD, New York.

Richardson, R. C. D. 1968. The wear of metals by relatively soft abrasives. Wear 11:245–275.

Rohlf, F. J. 2006. A comment on phylogenetic correction. Evolution 60:1509–1515.

Rose, J. C., and P. S. Ungar. 1998. Gross Dental Wear and Dental Microwear in Historical
Perspective; pp. 349–386 in Dental Anthropology. Springer-Verlag, Wien.

Rusnack, F., M. C. Mihlbachler, and B. L. Beatty. 2017. Experimental approaches to assess the
effect of food texture and grain composition of abrasives in the case of dental microwear.
Journal of Vertebrate Paleontology, Program and Abstracts 188.

Ryan, A. S. 1979a. Wear striation direction on primate teeth: a scanning electron microscope
examination. American Journal of Physical Anthropology 50:155–168.

Ryan, A. S. 1979b. A preliminary scanning electron microscope examination of wear striation
direction on primate teeth. Journal of Dental Research 58:525–530.

Rybczynski, N., and R. R. Reisz. 2001. Earliest evidence for efficient oral processing in a
terrestrial herbivore. Nature 411:684–687.

Sanson, G. D., S. A. Kerr, and K. A. Gross. 2007. Do silica phytoliths really wear mammalian
teeth? Journal of Archaeological Science 34:526–531.

Schubert, B. W., P. S. Ungar, and L. R. G. DeSantis. 2010. Carnassial microwear and dietary
behaviour in large carnivorans. Journal of Zoology 280:257–263.

Schulz, E., V. Piotrowski, M. Clauss, M. Mau, G. Merceron, and T. M. Kaiser. 2013. Dietary
abrasiveness is associated with variability of microwear and dental surface texture in
rabbits. PLoS ONE 8:1–7.

Scott, C. S., A. Weil, and J. M. Theodor. 2018. A new, diminutive species of *Catopsalis*
(Mammalia, Multituberculata, Taeniolabidoidea) from the early Paleocene of southwestern

Alberta, Canada. Journal of Paleontology 1–15.

Scott, R. S., C. A. Brown, R. S. Scott, P. S. Ungar, T. S. Bergstrom, and C. A. Brown. 2006. Dental microwear texture analysis: technical considerations. Journal of Human Evolution 51:339–349.

Semprebon, G. M., L. R. Godfrey, N. Solounias, M. R. Sutherland, and W. L. Jungers. 2004. Can low-magnification stereomicroscopy reveal diet? Journal of Human Evolution 47:115–144.

Silcox, M. T., and M. F. Teaford. 2002. The diet of worms: an analysis of mole dental microwear. Journal of Mammalogy 83:804–814.

Simpson, G. G. 1926. Mesozoic Mammalia. IV. The multituberculates as living mammals. American Journal of Science 11:228–250.

Simpson, G. G., and H. O. Elftman. 1928. Hind limb musculature and habits of a Paleocene multituberculate. American Museum Novitates 333:1–19.

Solounias, N., and L. C. Hayek. 1993. New methods of tooth microwear analysis and application to dietary determination of two extinct antelopes. Journal of Zoology 229:421–445.

Solounias, N., and G. Semprebon. 2002. Advances in the reconstruction of ungulate ecomorphology with application to early fossil equids. American Museum Novitates 3366:1–49.

Solounias, N., M. Teaford, and A. Walker. 1988. Interpreting the diet of extinct ruminants: the case of a non-browsing giraffid. Paleobiology 14:287–300.

Strait, S. G. 1993. Molar microwear in extant small-bodied faunivorous mammals: an analysis of feature density and pit frequency. American Journal of Physical Anthropology 79:63–79.

Teaford, M. F. 1988. A review of dental microwear and diet in modern mammals. Scanning Microscopy 2:1149–1166.

Teaford, M. F. 1991. Dental nicrowear: what can it tell us about diet and dental function?; pp. 341–356 in M. A. Kelley and C. S. Larsen (eds.), Advances in Dental Anthropology. Wiley-Liss, Inc., New York.

Teaford, M. F. 1994. Dental microwear and dental function. Evolutionary Anthropology: Issues, News, and Reviews 3:17–30.

Teaford, M. F. 2007. Dental microwear and paleoanthropology: cautions and considerations; pp. 345–368 in Dental Perspectives on Human Evolution: State of the Art Research in Dental Paleoanthropology.

Teaford, M. F., and A. Walker. 1984. Quantitative differences in dental microwear between primate species with different diets and a comment on the presumed diet of *Sivapithecus*. American Journal of Physical Anthropology 64:191–200.

Teaford, M. F., and O. J. Oyen. 1986. Dental microwear in vervets raised on different diets. American Journal of Physical Anthropology 69:270.

Teaford, M. F., and O. J. Oyen. 1989. *In vivo* and *in vitro* turnover in dental microwear. American Journal of Physical Anthropology 80:447–460.

Teaford, M. F., and K. E. Glander. 1991. Dental microwear in live, wild-trapped *Alouatta palliata* from Costa Riva. American Journal of Physical Anthropology 85:313–319.

Teaford, M. F., M. C. Maas, and E. L. Simons. 1996. Dental microwear and microstructure in early oligocene primates from the Fayum, Egypt: implications for diet. American Journal of Physical Anthropology 101:527–543.

Townsend, K. E. B., and D. A. Croft. 2008. Enamel microwear in caviomorph rodents. Journal of Mammalogy 89:730–743.

Tseng, Z. J. 2012. Connecting Hunter-Schreger band microstructure to enamel microwear

features: new insights from durophagous carnivores. Acta Palaeontologica Polonica 57:473–484.

Ungar, P. S., M. F. Teaford, K. E. Glander, and R. F. Pastor. 1995. Dust accumulation in the canopy: A potential cause of dental microwear in primates. American Journal of Physical Anthropology 97:93–99.

Ungar, P. S., C. A. Brown, T. S. Bergstrom, and A. Walker. 2003. Quantification of dental microwear by tandem scanning confocal microscopy and scale-sensitive fractal analyses. Scanning 25:185–193.

Ungar, P. S., R. S. Scott, J. R. Scott, and M. F. Teaford. 2008. Dental microwear analysis: Historical perspectives and new approaches; pp. 389–425 in J. D. Irish and G. C. Nelson (eds.), Techniques and Application in Dental Anthropology. Cambridge University Press.

Valkenburgh, B. Van, M. F. Teaford, and A. Walker. 1990. Molar microwear and diet in large carnivores: inferences concerning diet in the sabretooth cat, *Smilodon fatalis*. Journal of Zoology 222:319–340.

Walker, A., and M. Teaford. 1989. Inferences from quantitative analysis of dental microwear. Folia Primatol 53:177–189.

Walker, A., H. N. Hoeck, and L. Perez. 1978. Microwear of mammalian teeth as an indicator of diet. Science, New Series 201:908–910.

Weil, A., and F. Pignataro. 2007a. Dental microwear in multituberculate mammals and dietary change across the K/T boundary in Eastern Montana. Journal of Morphology 268:1148A.

Weil, A., and F. Pignataro. 2007b. Dietary inferences from dental microwear in multituberculate mammals from the Hell Creek and Tullock formations of Eastern Montana. Journal of Vertebrate Paleontology 27:163A–164A.

Weil, A., and D. W. Krause. 2008. Multituberculata; pp. 19–38 in C. M. Janis, G. F. Gunnell, and M. D. Uhen (eds.), Evolution of Tertiary Mammals of North America. Volume 2: Small Mammals, Xenarthrans, and Marine Mammals. Cambridge University Press, New York.

Whitlock, J. A. 2011. Inferences of diplodocoid (Sauropoda: Dinosauria) feeding behavior from snout shape and microwear analyses. PLoS ONE 6.

Xia, J., J. Zheng, D. Huang, Z. R. Tian, L. Chen, Z. Zhou, P. S. Ungar, and L. Qian. 2015. New model to explain tooth wear with implications for microwear formation and diet reconstruction. Proceedings of the National Academy of Sciences 112:10669–10672

Chapter Three: Cusp Row Ratios of Cimolodontan Lower Molars

3.1 Two-Dimensional Quantifications of Tooth Shape

Many animals use teeth to mechanically acquire and process foods. Food items vary in their material properties, and tooth shapes vary in kind. The relationship between dental form and function has been recognized for centuries, and paleontologists have long used tooth shape to infer the diets of extinct animals (e.g. Hunter, 1778; Cuvier, 1833; Owen, 1840; Cope, 1883; Osborn, 1907).

More recently, efforts have been made to quantify tooth shape. Kay (1978) showed that the crest lengths of primate molars can be used to distinguish between dietary categories. When the lengths of shearing crests (usually on the m2) are regressed on tooth length, frugivorous primates have distinctly shorter crests than those of insectivorous and folivorous primates (Kay, 1975). The residual from the regression line of crest length over tooth length (in log space) is the shearing quotient (SQ). SQ has been used for decades to distinguish diets in primates (e.g. Kay and Covert, 1984; Anthony and Kay, 1993; Strait, 1993a; Meldrum and Kay, 1997); however, SQ is highly phylogenetically interdependent and can only be used on closely-related groups with known frugivorous species (Kay and Ungar, 1997; Ungar, 2005).

3.1.1 Shearing ratios.

The use of SQs was later expanded by Strait (1993a, 1993b), who developed a new measurement called a shearing ratio (SRA). Unlike SQ, which is calculated based on the length of the tooth, SRA is calculated using the occlusal footprint area (area of the crown in occlusal view). The basic equation for calculating SRA is $\frac{CL}{\sqrt{A2D}}$, where CL is the total crest length and A2D is the occlusal footprint area of the tooth. The use of area is intended to account for variations in tooth shape, ostensibly allowing SRA values to be compared among groups with

differently shaped teeth. Furthermore, SRA does not require a set of known frugivores to be included. Strait (1993a) calculated SRA for microchiropterans, eulipotyphlans, and primates, and found that species that eat soft-bodied insects have higher SRA values compared to those that eat hard-bodied insects (e.g. beetles). However, the distinction was only easy to detect in closely related taxa, indicating that SRA has some phylogenetic dependence. Strait (1993b) also used SRA to distinguish between frugivorous and faunivorous primates, marsupials, and microchiropterans, finding that frugivores have lower SRA values than faunivores. She later used SRA to elucidate the diets of omomyid primates (Strait, 2001).

SRA has since been applied to other primate datasets, but it is typically incorporated into a suite of measurements rather than used independently (Bunn et al., 2011; Winchester et al., 2014). SRA has also been applied to a large, phylogenetically-corrected marsupial dataset (Hogue and ZiaShakeri, 2010). For both primates and marsupials, insectivorous and folivorous species have higher SRA values than closely-related frugivorous and hard-object eating species (Hogue and ZiaShakeri, 2010; Bunn et al., 2011; Winchester et al., 2014).

Recent work has demonstrated that SRA is influenced by body size (Hogue and ZiaShakeri, 2010; Christensen, 2012, 2014). For example, teeth with larger occlusal footprint areas tend to have higher SRA values than those with smaller areas. This means that, for mammals with similar body sizes, SRA can be used to differentiate among diets, but SRA may not be a good dietary proxy if the studied taxa are outside of the body size range of the comparative dataset.

Christensen (2012, 2014) applied SRA (called Shearing Crest Scores in her papers) to a broad sampling of mammalian clades, including multituberculates. Her therian mammal (marsupials and placentals) results reaffirmed the findings of earlier studies. Small-bodied

mammals have SRA differences between insectivores and high-fiber herbivores. For larger

mammals (>10 kg), carnivores have lower SRA values than herbivores. SRA cannot be used to

distinguish among different types of herbivory. It should be noted that Christensen (2012, 2014)

only included felids, hyaenids, and *Thylacinus* in her "carnivorous" group, so the low SRA

values do not reflect the entire carnivorous morphospace. Unlike previous studies (Strait, 1993a;

Hogue and ZiaShakeri, 2010), Christensen did not observe a phylogenetic signal in her data

(Christensen, 2012, 2014).

SRA is typically calculated from m2s, although m3s have been used for marsupials

(Hogue and ZiaShakeri, 2010). Using a specific tooth locus is feasible when large datasets are

available but can be problematic at smaller sample sizes. Christensen (2012) compensated for

this limitation by including molar data from four positions (M1/m1, M2/m2) in her analysis. She

studied whether SRA was affected by tooth position and noted that, within a species, SRA was

not significantly different between first and second molars or between upper and lower molars.

Unfortunately, Christensen (2012) had very low sample sizes for her comparisons: multiple

comparisons had n = 2 for each tooth. Low sample sizes mean that significant differences may

have gone undetected because of lower statistical power.

3.1.2 Shearing ratios applied to multituberculates.

Christensen (2012) calculated SRA values of several multituberculate species.

She determined that two species, *Meniscoessus robustus* and *Taeniolabis taoensis*, had SRA

values high enough to be suggestive of herbivory (SRA = 3.45 and 2.49, respectively). However,

it should be noted that she assumed small-bodied multituberculates could not have been

herbivorous and thus excluded some smaller multituberculates from the analysis despite them

having equally high SRA values (e.g. *Mesodma thompsoni* = 3.33). This conclusion relies on the

assumption that multituberculates and placentals have similar metabolic requirements, but even placentals and marsupials, both therians, differ in their metabolic requirements (for example, there are folivorous marsupials that fall below Kay's Threshold; Hogue and ZiaShakeri, 2010). As such, it is unlikely that a size threshold based on placental data holds for the non-therian multituberculates. Functional shearing capabilities can be compared across clades, but dietary inferences based on therian SRA values may not be accurate for multituberculates. Furthermore, multituberculate molars typically do not have shearing crests – rather, they have parallel or subparallel rows of cusps unconnected by crests. Christensen (2012) considered these cusp rows to be equivalent to shearing crests, but it is not clear that the two served the same function. The multituberculate SRA calculation proposed by Christensen (2012) may simply be quantifying differences in overall tooth morphology rather than calculating shearing crest lengths. Given this uncertainty, I refer to SRA values calculated for multituberculates as "Cusp Row Ratios" (CRR) in this study.

3.2 Methods

Previous work has demonstrated that there are clade-level offsets in SRA (e.g. prosimians versus platyrrhines) that make cross-clade comparisons unreliable (Strait, 1993b). Multituberculate phylogenetics are not well resolved, rendering phylogenetic corrections impractical for the group (Weil and Krause, 2008). As such, I have not used any corrections on the data.

SRA (and CRR) is a landmark-based metric that relies on unworn or slightly worn teeth. Some groups, such as primates, have established scoring guides used to classify wear stages of teeth (e.g. Scott, 1979; Elgart, 2010; Galbany et al., 2011; Pampush et al., 2016). This is not the

case for multituberculates. Creating a wear scale for multituberculates is challenging because multituberculate teeth wear differently based on the taxon, tooth type, and position of the tooth in the tooth row. I chose to use three broad categories to describe cheek tooth wear: low wear, medium wear, and high wear (Appendix D). Only teeth in the low wear category were used for CRR.

As previously discussed, calculating CRR for multituberculates can be difficult because most multituberculate molars do not have distinct shearing crests, but rather have subparallel rows of cusps. For the sake of comparison, I followed the assumptions of Christensen (2012) and treated each cusp row as the equivalent of a single shearing crest. I measured the length of each cusp row and then summed the lengths to get the total cusp row length. Accessory cuspules and distobuccal cingula were included when present. Specimens with minor damage (e.g. a chipped cusp) were accepted if the length of the cusp row and occlusal footprint area could still be measured.

Calibrated images of m1s and m2s were taken with a Dino-Lite Edge imaging system (AM4815ZTL Dino-Lite Premier, AnMo Electronics Corporation, Taiwan). Images were then imported to Fiji (available https://imagej.net/Fiji) for processing. The scale bar on each Dino-Lite image was used to set the correct scale in Fiji. I then used a modified version of Christensen's (2012) methods to collect measurements as follows: whereas Christensen (2012) used the Segmented Line tool in Fiji to measure crest lengths, I measured these with the Freehand Line tool, as this protocol was better able to capture the natural curvature of the cusp rows (Figure 3.1). To calculate tooth area, I used the Freehand Selections tool to outline the occlusal footprint of the crown (following (Strait, 1993b, 1993c)), unlike Christensen (2012), who used the length

x width of a tooth to approximate area (Figure 3.1). The CRR values for individual specimens can be found in Appendix E.
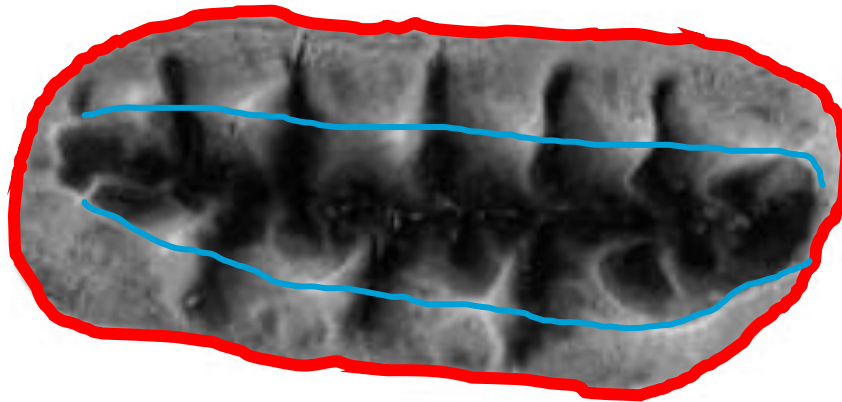
Figure 3.1. Multituberculate right m1. The lines used to measure the crest row length (CRL) are in blue and the outline of the occlusal footprint area (A2D) is in red.

All statistical analyses were performed in RStudio (v. 1.1.383, RStudio Team, 2016). I first compared the CRR of m1s and m2s to determine whether there were differences between the teeth. A Shapiro-Wilk test determined that the values for m1 and m2 were not normally distributed, so a nonparametric Mann-Whitney-Wilcoxon test was run to compare the CRRs. Only taxa with both m1 and m2 measurements were included.

Average m1 and m2 CRR values were calculated for each taxon. These values were calculated by taking the average cusp row length (CRL) and dividing it by the square root of the occlusal footprint area (A2D), defined as the area of the tooth crown when held in occlusal view. The equation for CRR is: $\frac{\overline{CRL}}{\sqrt{\overline{A2D}}}$. Error propagation was employed to determine the standard

deviations and standard errors of these averages. A detailed calculation of the error propagation equations can be found in Appendix F.

I compared the CRR values of the m1s to the CRR values of the m2s for three taxa. The taxa used were *Valenopsalis joyneri, Cimolomys* sp., and Cimolomyid 1. These three taxa had the greatest number of m1s and m2s in the sample, with n ≥ 3 in each case. The data were not normally distributed for any of the taxa, so nonparametric Mann-Whitney-Wilcoxon tests were used.

I also compared m1 and m2 CRR values among taxa. Four taxa had a large enough (n ≥ 3) m1 sample: *Cimolomys* sp., Cimolomyid 1, *Mesodma* sp., and *V. joyneri*. Only three taxa had enough (n ≥ 3) m2s for a comparison: *Cimolomys* sp., Cimolomyid 1, and *V. joyneri*. Kruskal-Wallis H tests were performed to test for the effect of taxon on m1 and m2 CRR values. A Dunn's post-hoc test with Bonferroni correction was used when significant differences were found.

A combined molar row (m1 + m2) CRR was calculated for each taxon with available specimens. To do this, I calculated the average cusp row length (CRL) and area (A2D) for each tooth (m1 and m2), based on individual values, and summed the averages. I then used the combined averages in the CRR equation:

$$\frac{\overline{(m1\ CRL)} + \overline{(m2\ CRL)}}{\sqrt{(\overline{(m1\ A2D)} + \overline{(m2\ A2D)})}}$$

Error propagation calculations for the resultant standard errors can be found in Appendix F. The m1 + m2 CRR value is here referred to as "molar row CRR". It is possible that the multituberculate p4 is also a molar (Clemens and Lillegraven, 1986; Greenwald, 1988; Luckett,

1993; Wible and Rougier, 2000), but this tooth was not included in the CRR calculations because the p4s are involved primarily in a different phase of the multituberculate masticatory cycle (Krause, 1982).

Bivariate plots of CRR and SRA compared to body size were created to compare Christensen's (2012) multituberculate data and Christensen's (2014) extant mammal data to the multituberculate data in this study. As Christensen's (2012, 2014) CRR and SRA values were reported as species averages, I calculated these for the data in this study by taking the average of individual m1 and m2 CRR values. Average tooth area was used as a proxy for body size.

3.3 Results

Cusp row ratios were calculated for species with little-worn m1s and m2s. For the m1s, *T. taoensis* had the highest CRR (3.90), while *Catopsalis alexanderi* had the lowest (M = 2.65, SD = 0.14) (**Figure 3.2**; Table 3.1). *Taeniolabis taoensis* also had the highest species m2 CRR (M = 2.16, SD = 0.17) (Figure 3.3; Table 3.1). However, the overall highest m2 CRR (2.34) belonged to a specimen of Cimolomyid 1. *Catopsalis calgariensis* had the lowest m2 CRR (1.61). Values for individual specimens can be found in Appendix E. A Mann-Whitney-Wilcoxon test revealed that the CRR values of m1s and m2s are significantly different (Z = -6.51, p < 0.001), with the group median of m1 (Mdn = 2.98) larger than the group median of m2 (Mdn = 2.05).

Table 3.1. Mean cusp row ratios of multituberculate taxa.

Table abbreviations: **N** – number of specimens; **SD** – standard deviation; **CV** – coefficient of variation; **SE** – standard error.

Taxon	Tooth	N	Mean CRR	SD	CV	SE
cf. *Acheronodon vossae*	m1	1	2.66	--	--	--
Catopsalis alexanderi	m1	2	2.62	0.14	0.053	0.070
Catopsalis calgariensis	m2	1	1.61	--	--	--
Catopsalis cf. *calgariensis*	m1	2	3.44	0.10	0.029	0.048
Catopsalis cf. *calgariensis*	m2	1	1.70	--	--	--
Catopsalis fissidens	m1	2	3.16	0.52	0.16	0.26
Catopsalis fissidens	m2	1	2.00	--	--	--
Catopsalis johnstoni	m1	1	2.74	--	--	--
Catopsalis kakwa	m1	1	2.69	--	--	--
Catopsalis kakwa	m2	1	1.96	--	--	--
Catopsalis waddleae	m1	1	2.43	--	--	--
Cimolomyid 1	m1	8	3.01	0.53	0.17	0.066
Cimolomyid 1	m2	9	1.75	1.03	0.50	0.11
Cimolomys sp.	m1	4	2.81	0.77	0.27	0.19
Cimolomys sp.	m2	6	1.92	0.34	0.18	0.057
Meniscoessus major	m1	2	2.91	0.28	0.10	0.14
Meniscoessus major	m2	1	2.12	--	--	--
Mesodma sp.	m1	6	2.89	0.81	0.28	0.14
Mesodma sp.	m2	1	1.97	--	--	--
Ptilodus sp.	m1	2	2.98	1.07	0.36	0.54
Stygimys kuszmauli	m1	1	3.08	--	--	--
Taeniolabis taoensis	m1	1	3.90	--	--	--
Taeniolabis taoensis	m2	2	2.16	0.17	0.08	0.083
Valenopsalis joyneri	m1	6	2.81	0.59	0.21	0.098
Valenopsalis joyneri	m2	3	2.13	0.22	0.10	0.074

Cimolomys sp., Cimolomyid 1, *Mesodma* sp., and *V. joyneri* were included in a Kruskal-Wallis H test to determine whether m1 CRR values differed among taxa. Significant differences were found (x^2 (3) = 10.19, p = 0.017). A post-hoc comparison using Dunn's post-hoc test with Bonferroni correction revealed that *V. joyneri* (Med = 2.93) and Cimolomyid 1 (Med = 2.88)

were significantly different (p = 0.025). The results of all other pairings were non-significant (Table 3.2). A visual inspection of the data indicates that many other species have larger and smaller CRR values than the four species included in the Kruskal-Wallis H test (Figure 3.2), with *T. taoensis* being notably larger (3.90), and several species being smaller. Whether or not these differences are significant cannot be determined with the limited sample sizes.

Table 3.2. Post-hoc results of m1 CRR comparisons between species. Significant *p*-values are in bold. α/2 = 0.025.

	Cimolomyid 1	*Cimolomys* sp.	*Mesodma* sp.
Cimolomys sp.	0.033	-	-
Mesodma sp.	1.00	0.31	-
V. joyneri	**0.0248**	1.00	0.33

There were sufficient numbers of m2s of *Cimolomys* sp., *V. joyneri*, and Cimolomyid 1 for statistical analysis. There were no significant differences among the taxa (x^2 (2) = 3.51, p = 0.17). The m2 CRR values are not as disparate as the m1 CRR values (Figure 3.3), with most m2 values clustering around 2.0 (Figure 3.3). *Catopsalis calgariensis* has the lowest m2 CRR (1.61), notably lower than those of the others (Figure 3.3). *Taeniolabis taoensis* (M = 2.16, SD = 0.17) has an m2 CRR similar to that of *V. joyneri* (M = 2.13, SD = 0.22).
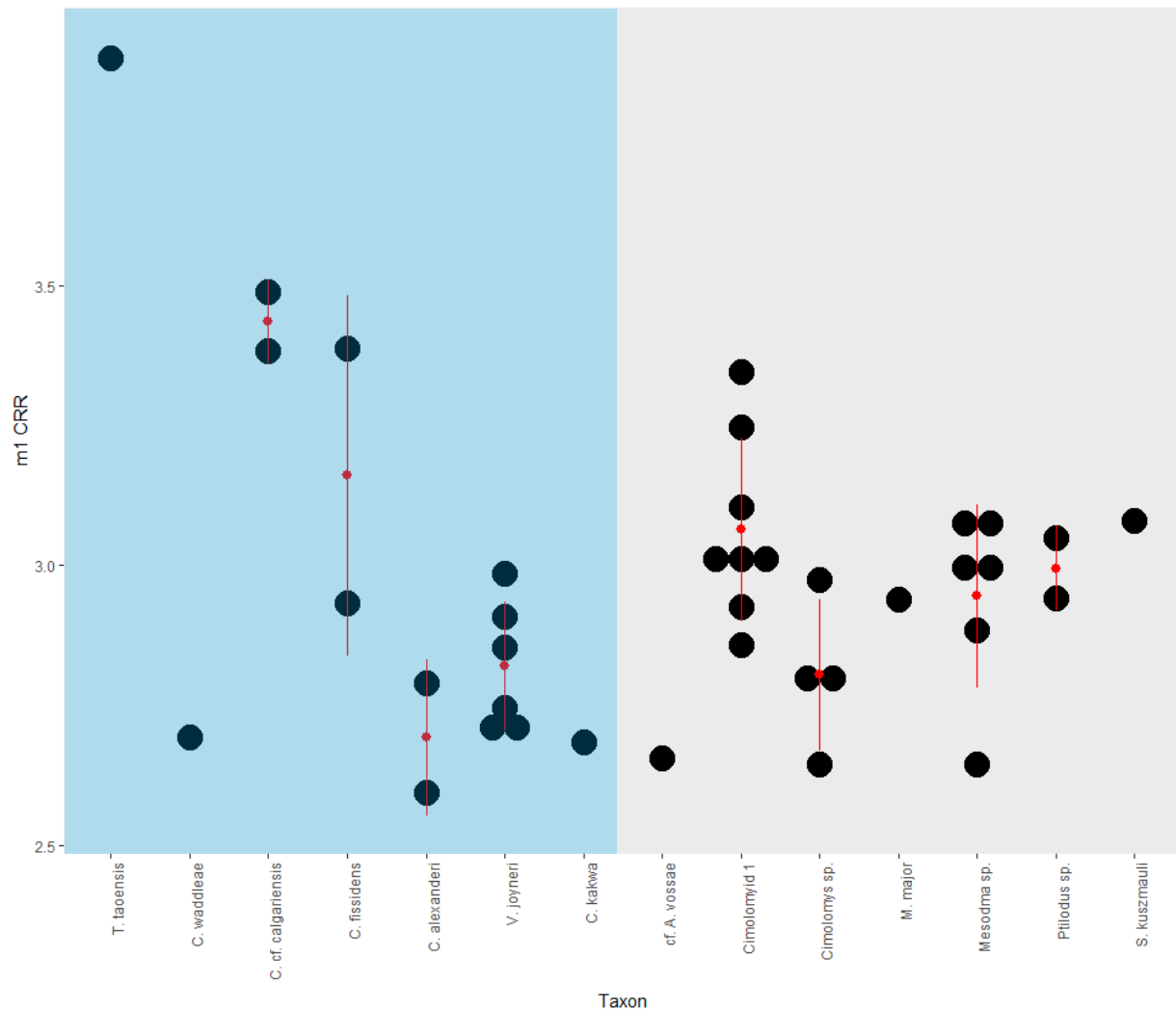
Figure 3.2. Dot plots of m1 CRRs by taxon. Each taxon mean is represented by a solid red circle with the red line representing one standard deviation from the mean. Taeniolabidoids are in the shaded blue area and are organized by inferred body size, with the largest-bodied taxon (*T. taoensis*) on the left and the smallest-bodied taxon (*C. kakwa*) on the right. Non-taeniolabidoids are in the shaded grey area and are not organized by inferred body size.
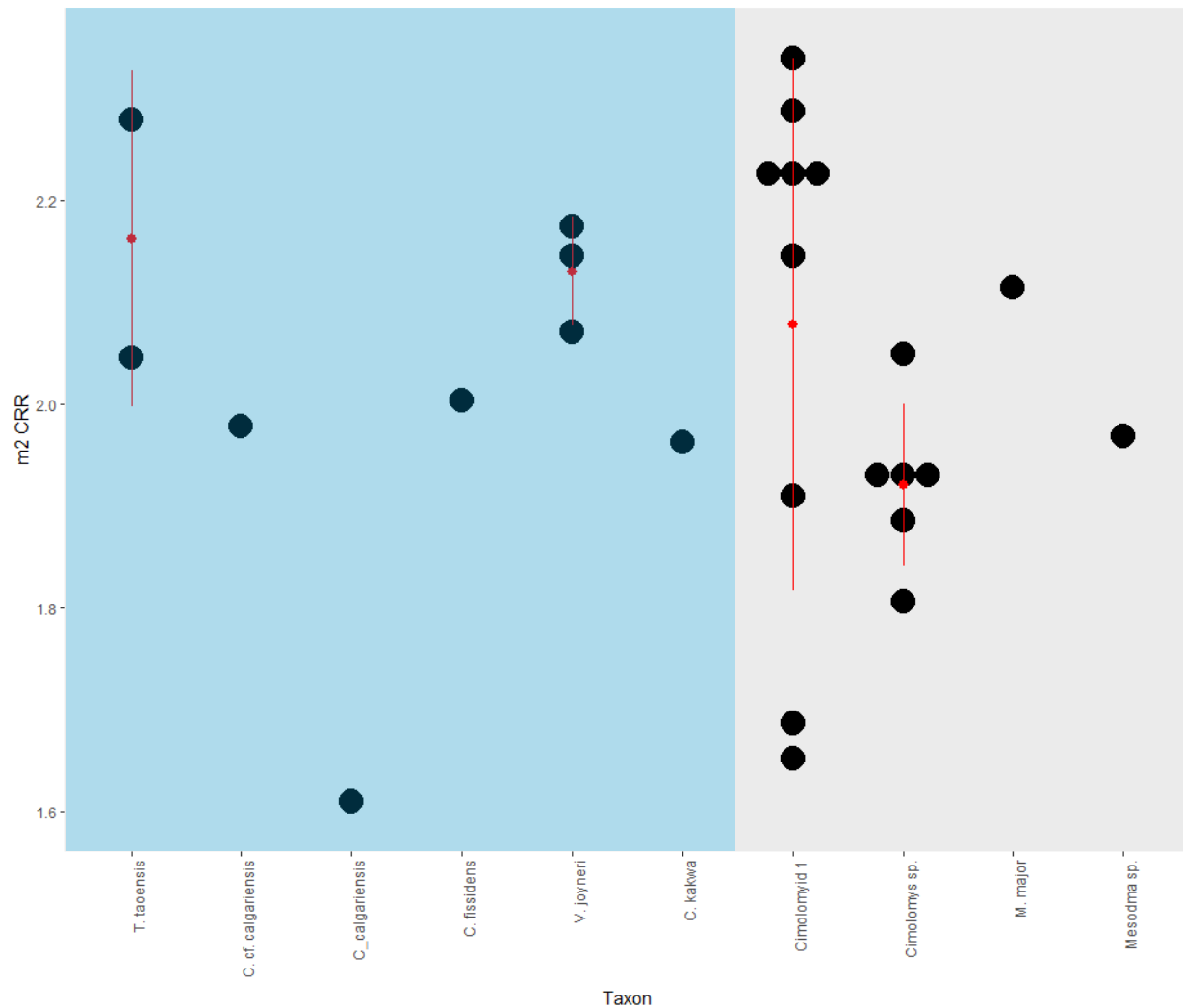
Figure 3.3. Dot plots of m2 CRRs by taxon. Each taxon mean is represented by a solid red circle with the red line representing one standard deviation from the mean. Taeniolabidoids are in the shaded blue area and are organized by inferred body size, with the largest-bodied taxon (*T. taoensis*) on the left and the smallest-bodied taxon (*C. kakwa*) on the right. Non-taeniolabidoids are in the shaded grey area and are not organized by inferred body size.

The combined molar row CRR values cannot be analyzed statistically, but there are some obvious differences in the values (Figure 3.4; Table 3.3). *Taeniolabis taoensis* has the highest molar row CRR (4.42, SE = 0.05), well above all other taxa. *Catopsalis* cf. *calgariensis* (3.92, SE = 0.04) also has a high molar row CRR value, but it is much more similar to those of other taxa (Figure 3.4). The molar row CRR of *C. kakwa* was calculated from a single m1 and m2, so there is no standard error in the measurement. *Catopsalis kakwa* has the lowest molar row CRR (3.31), but it is within the range of *Cimolomys* sp. (3.36, SE = 0.14).

Table 3.3. Molar row CRRs of multituberculate taxa. Values are calculated from a combination of m1s and m2s.

Table abbreviation: **SE** – standard error.

Taxon	CRR	SE
Cimolomyid 1	3.67	0.09
Catopsalis cf. *calgariensis*	3.92	0.04
Catopsalis fissidens	3.73	0.21
Catopsalis kakwa	3.31	--
Cimolomys sp.	3.36	0.14
Meniscoessus major	3.58	0.10
Mesodma sp.	3.53	0.10
Taeniolabis taoensis	4.42	0.05
Valenopsalis joyneri	3.51	0.08
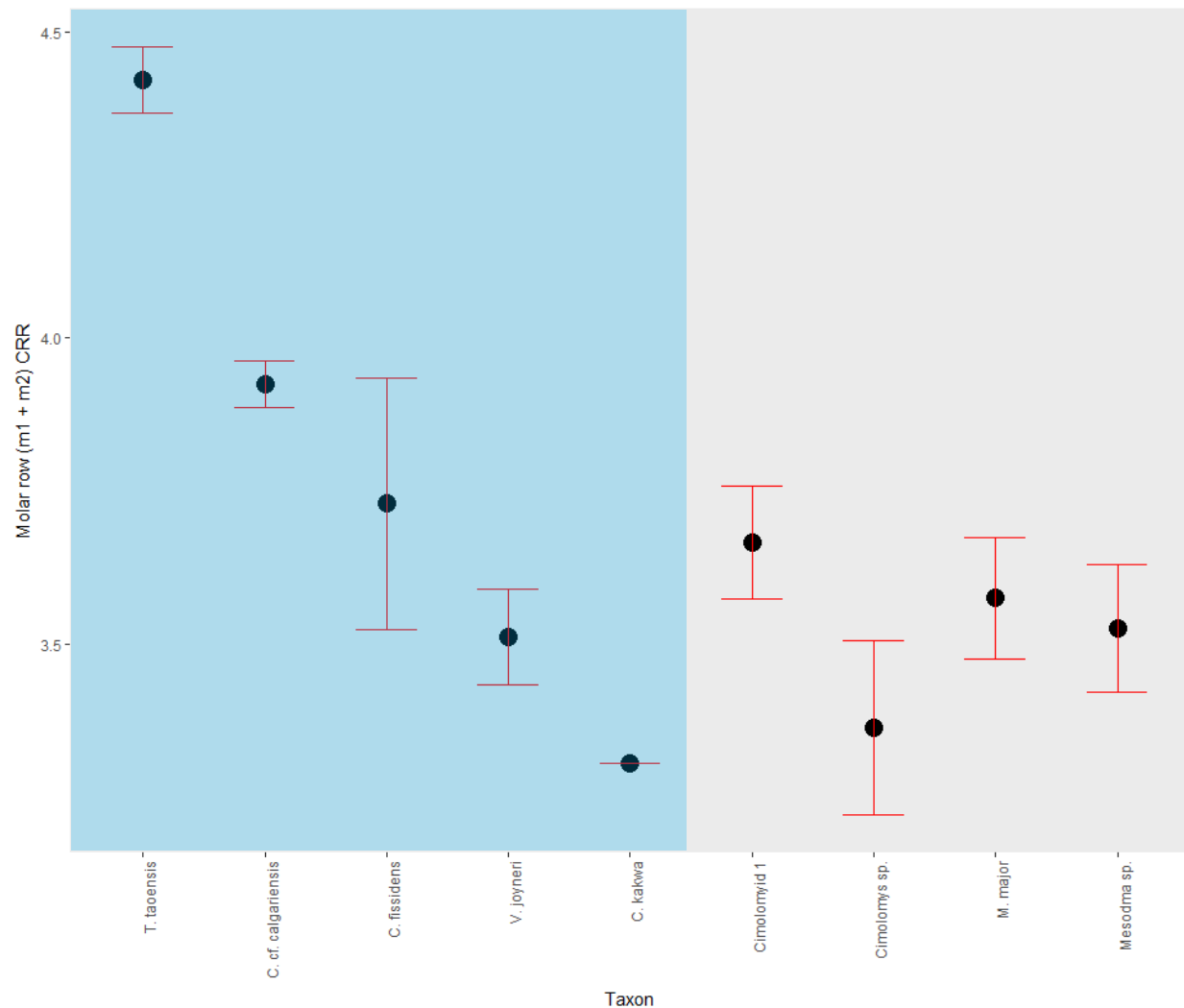
Figure 3.4. Molar row CRRs by taxon. Each molar row CRR is represented by a solid black circle with the red error bar representing one standard error. Taeniolabidoids are in the shaded blue area and are organized by inferred body size, with the largest-bodied taxon (*T. taoensis*) on the left and the smallest-bodied taxon (*C. kakwa*) on the right. Non-taeniolabidoids are in the shaded grey area and are not organized by inferred body size.

Bivariate plots demonstrate how multituberculate CRR values compare with the SRA values of therian mammals, and with multituberculate CRR values from a previous study. Most of the multituberculate CRR values from this study fall within the range of multituberculate CRR values calculated by Christensen (2012); the one exception is *C. calgariensis*, which is represented by a single m2 that has an unusually low CRR for its occlusal footprint area (Figure 3.5). When compared to therians, multituberculates CRR values appear to be overall higher than carnivore SRA values (Figure 3.5). Those multituberculates with smaller occlusal footprint areas have CRR values equivalent to insectivore and hard-object feeder SRA values, whereas those with larger occlusal footprint areas have CRR values comparable to hard-object feeder, grazer, and browser SRA values (Table 3.4). Bivariate plots also demonstrate that multituberculates may be assigned to different dietary categories depending on whether their m1 CRR values or their m2 CRR values are used (Figure 3.6, Table 3.4).
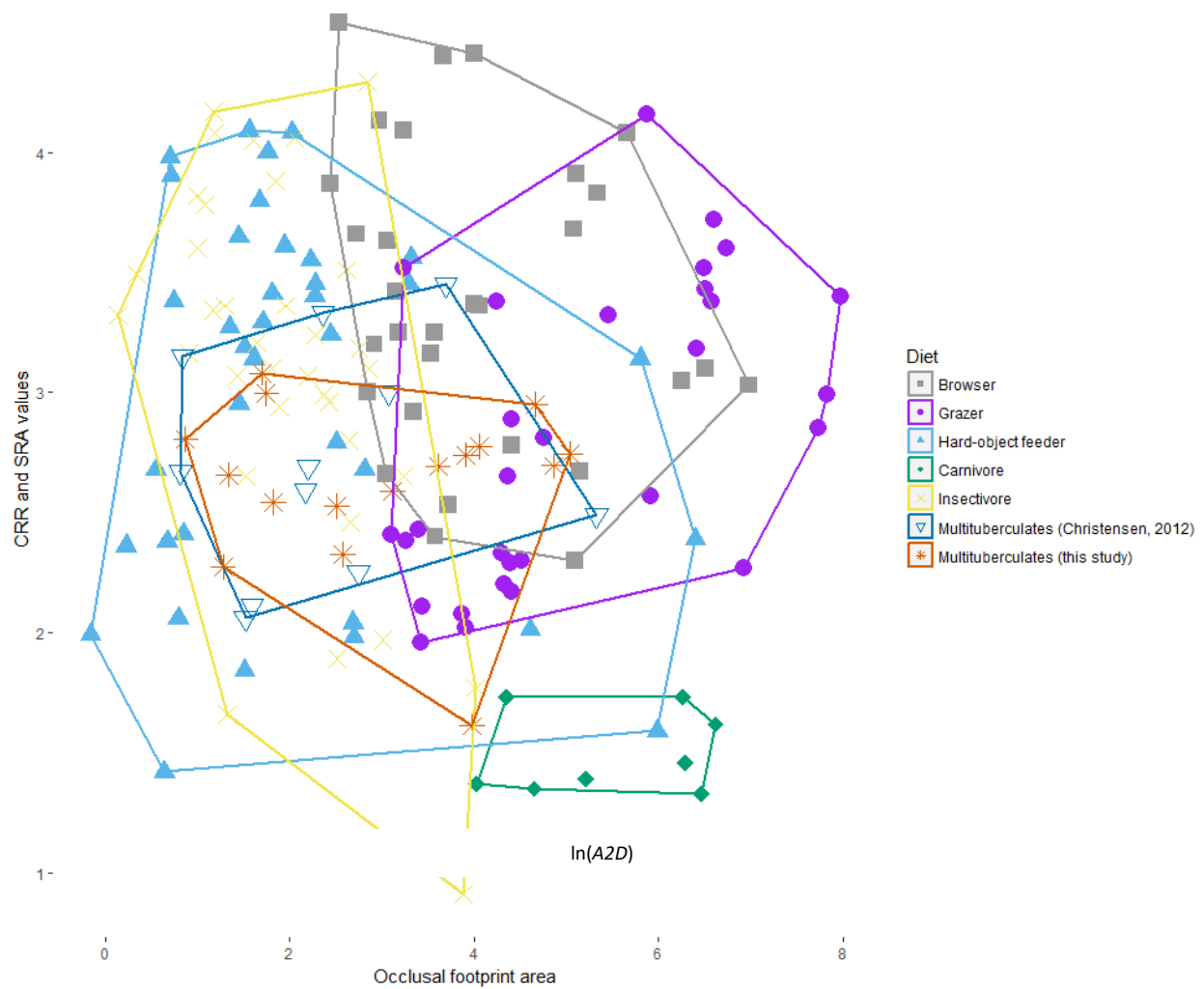
Figure 3.5. Minimum convex hull polygons of CRR (for multituberculates) and SRA (for therians) values by the natural log of occlusal footprint area. Therian mammal data are grouped by dietary category, based on Christensen (2014). Multituberculate data are taken from Christensen (2012) and this study.
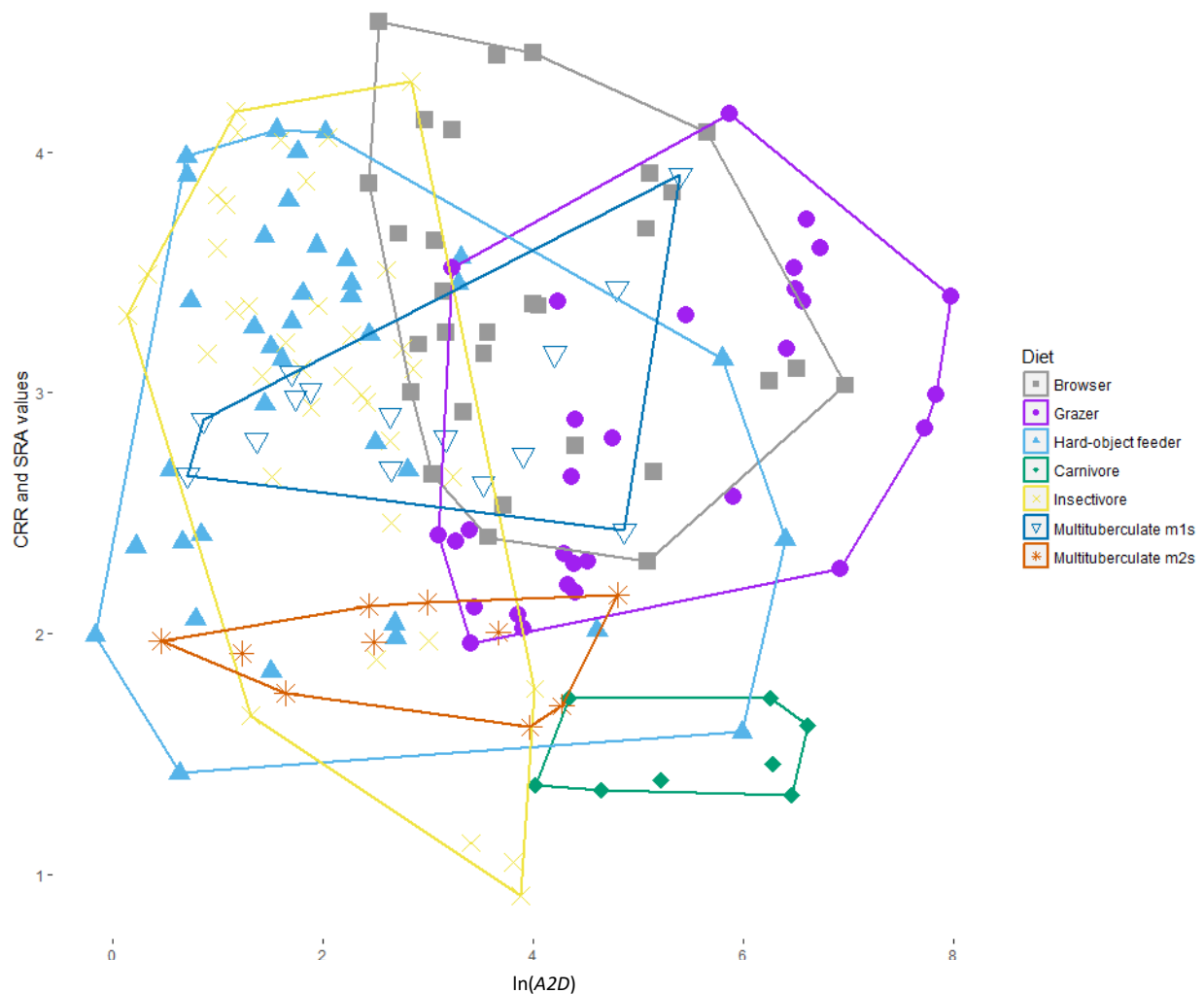
Figure 3.6. Minimum convex hull polygons of CRR (for multituberculates) and SRA (for therians) values by the natural log of occlusal footprint area. Therian mammal data are grouped by dietary category, based on Christensen (2014). Multituberculate data are separated by tooth (m1 and m2) and are from this study only.

Table 3.4. Inferred dietary categories of multituberculate taxa based on a comparison to therian SRA values from Christensen (2014).

Table abbreviations: **B** – browser; **C** – carnivore; **G** – grazer; **HO** – hard-object feeder; **I** – insectivore

Taxon	Tooth	Mean CRR	Dietary Category
cf. *Acheronodon vossae*	m1	2.66	HO/I
Catopsalis alexanderi	m1	2.62	B/G/HO/I
Catopsalis calgariensis	m2	1.61	HO/I
Catopsalis cf. *calgariensis*	m1	3.44	B/G
Catopsalis cf. *calgariensis*	m2	1.70	HO
Catopsalis fissidens	m1	3.16	B/G/HO
Catopsalis fissidens	m2	2.00	G/HO/I
Catopsalis johnstoni	m1	2.74	B/G/HO
Catopsalis kakwa	m1	2.69	HO/I
Catopsalis kakwa	m2	1.96	HO/I
Catopsalis waddleae	m1	2.43	B/G/HO
Cimolomyid 1	m1	3.01	HO/I
Cimolomyid 1	m2	1.75	HO/I
Cimolomys sp.	m1	2.81	HO/I
Cimolomys sp.	m2	1.92	HO/I
Meniscoessus major	m1	2.91	HO/I
Meniscoessus major	m2	2.12	HO/I
Mesodma sp.	m1	2.89	HO/I
Mesodma sp.	m2	1.97	HO
Ptilodus sp.	m1	2.98	HO/I
Stygimys kuszmauli	m1	3.08	HO/I
Taeniolabis taoensis	m1	3.90	B/G
Taeniolabis taoensis	m2	2.16	G/HO
Valenopsalis joyneri	m1	2.81	B/G/HO/I
Valenopsalis joyneri	m2	2.13	HO/I

3.4 Discussion

3.4.1 CRR of lower molars.

Multituberculates differ in the CRRs of their m1s and m2s. The higher CRR values of the m1s indicate longer cusp rows in relation to tooth area. This is unsurprising given the shape of

the teeth. The m1s and m2s tend to have similar widths, but m1s are much longer. Given that the equation of CRR is $\frac{CRL}{\sqrt{A2D}}$, an equivalent increase in both cusp row length (CRL) and tooth length, with width held constant, would result in the numerator increasing at a greater rate than the denominator. These data contradict Christensen (2012), who found that CRR values did not significantly differ between m1s and m2s within a taxon. This discrepancy may arise from Christensen's (2012) small sample sizes (in some cases, n = 2) for her comparisons.

Despite m1s having higher CRR values than m2s for all taxa, those with a larger m1 CRR do not consistently have a larger m2 CRR. Even within the taeniolabidoids, there are morphological differences that affect the CRR of a tooth, such as distobuccal cingula, which were counted as part of the crest row length. A prime example of this is in the molars of *C.* cf. *calgariensis* and *Catopsalis waddleae*. The two taxa have m1s of similar size, but *C. waddleae* lacks the distobuccal cingulum found on the m1 of *C.* cf. *calgariensis* (the absence of the m1 cingulum is considered the distinguishing feature between the two taxa; Buckley, 1995). Whereas *C.* cf. *calgariensis* has a high m1 CRR, *C. waddleae* has one of the lowest.

3.4.2 CRR of lower molar rows.

When taken separately, multituberculate m1s and m2s have different CRRs. However, this comparison is somewhat artificial because the m1s and m2s are two parts of a single tooth row. A more informative value may be the combined CRR of m1 and m2. There are two ways to approach calculating a CRR value for more than one tooth: combining individual tooth CRR values or averaging individual tooth CRR values. The combined CRR values give the total cusp row ratio of the molar row, whereas the averaged CRR values provide the average cusp row ratio of the molar row.

There are differences in molar row CRR between taxa. *Taeniolabis taoensis*, *C.* cf. *calgariensis*, and *C. fissidens* all have a high molar CRRs, meaning that the larger-bodied taeniolabidoids had longer cusp rows relative to occlusal footprint area. The high values of these three taeniolabidoid taxa appear to be driven by their m1s. For example, whereas *T. taoensis* does have high CRR values for both m1 and m2, the m2 CRR is equivalent to that of *V. joyneri* and Cimolomyid 1, both of which have a lower molar row CRR. Furthermore, *C.*cf. *calgariensis* has a mid-range m2 CRR, but nonetheless has a high molar row CRR. *Catopsalis kakwa* has the lowest molar row CRR, which appears to be driven by a low m1 CRR. *Cimolomys* sp. also has a rather low molar row CRR, but the standard errors overlap those of other taxa. The same may be true for *C. kakwa* if more specimens were available for measurement. However, it should be noted that there are larger-bodied taeniolabidoids, particularly *C. waddleae*, that have relatively low CRR values, so the observed patterns may not hold for all taxa.

3.4.3 Comparisons to therian taxa.

SRA is a measure of shearing capability, with higher SRA values corresponding to greater shearing ability for therians. Multituberculate molars do not have shearing crests, so multituberculate SRA values (called CRR values in this study) may not actually be a measurement of shearing capability. Furthermore, most SRA studies have used individual, homologous teeth, although a few have averaged multiple teeth within a tooth row. Because the homologies of multituberculate to therian molars are unclear (Janis and Weil, 2008), there is no justification to focus preferentially on a particular tooth.

Previous studies have indicated that SRA can be used to help distinguishing different dietary preferences. However, as SRA is heavily influenced by body size, direct comparisons can only be made between similar-sized individuals (Christensen, 2014). SRA also likely has a

phylogenetic component (Strait, 1993b; Hogue and ZiaShakeri, 2010; Winchester et al., 2014), but phylogeny does not always seem to influence SRA (Christensen, 2014). The lack of phylogenetic signal in Christensen's (2014) data may be partially explained by her calculations: she included teeth from different positions in the tooth row (M1/m1, M2/m2) when calculating average SRA (and multituberculate CRR). The averaging resulted in an SRA that reflected the functional shearing capabilities of the entire molar row rather than the individual teeth. This could have eliminated some of the morphology-based clade-level offsets that come from individual tooth comparisons (e.g. only m2s). However, the generalizability of tooth SRA versus tooth row SRA has not been tested.

The multituberculate CRR values calculated in this study are comparable to those calculated by Christensen (2012), although the *T. taoensis* CRR values calculated in this study are higher than the value reported by Christensen (2012). This is likely because Christensen (2012) calculated her *T. taoensis* CRR value from an M2, while the values in the present study come from m1s and m2s. The present study found that multituberculate CRR values significantly differ between molar positions.

Bivariate plots indicate that most multituberculates have CRR values equivalent to those of similar-sized therian insectivore and hard-object feeder SRA values, based on Christensen's (2014) data. For many multituberculates, the insectivores and hard-object feeders were the only comparative groups of similar body size. A few multituberculates have large enough teeth that they fall into the carnivore/browser/grazer area of the plot. All multituberculates have mid-range CRR values, regardless of body size – all dietary groups (except carnivores) have members with both higher and lower ratios.

Given that both body size and phylogeny can affect SRA values, and that multituberculate molars do not have shearing crests, comparisons of multituberculate CRR values to those of therian mammal SRA values should be approached cautiously. Body mass is difficult to estimate for multituberculates because different body mass equations produce vastly different numbers (Scott et al., 2018). Multituberculates are non-therian mammals (Janis and Weil, 2008; Weil and Krause, 2008) and, because multituberculate molars are not necessarily homologous with those of therians (Janis and Weil, 2008), there is no justification for comparing a particular multituberculate tooth to the therian tooth in the same position (e.g. comparing multituberculate m2s to therian m2s) Furthermore, it is unlikely that multituberculates had the same metabolic demands as therians. Therefore, while CRR values can be calculated with a modification of the SRA equation, they may not be a good proxy for multituberculate diets. More work is needed to determine whether multituberculate CRR values are truly comparable to therian SRA values and, if not, whether CRR values have use as a dietary proxy.

3.5 Literature Cited

Anthony, M. R. L., and R. F. Kay. 1993. Tooth form and diet in ateline and alouattine primates: reflections on the comparative method. American Journal of Science 293A:356–382.

Buckley, G. A. 1995. The multituberculate *Catopsalis* from the early Paleocene of the Crazy Mountains Basin in Montana. Acta Palaeontologica Polonica 40:389–398.

Bunn, J. M., D. M. Boyer, Y. Lipman, E. M. St. Clair, J. Jernvall, and I. Daubechies. 2011. Comparing Dirichlet normal surface energy of tooth crowns, a new technique of molar shape quantification for dietary inference, with previous methods in isolation and in combination. American Journal of Physical Anthropology 145:247–261.

Christensen, H. B. 2012. Mammalian adaptation to herbivory in the aftermath of the KT extinction. The University of Chicago, 112 pp.

Christensen, H. B. 2014. Similar associations of tooth microwear and morphology indicate similar diet across marsupial and placental mammals. PLoS ONE 9:1–11.

Cope, E. D. 1883. On the trituberculate type of molar tooth in the Mammalia. Proceedings of the American Philosophical Society 21:324–326.

Cuvier, G. 1833. The Animal Kingdom: Arranged in Conformity with Its Organization. G. & C. H. Carvill, 532 pp.

Elgart, A. A. 2010. Dental wear, wear rate, and dental disease in the African apes. American Journal of Primatology 72:481–491.

Galbany, J., J. Altmann, A. Pérez-Pérez, and S. C. Alberts. 2011. Age and individual foraging behavior predict tooth wear in *Amboseli baboons*. American Journal of Physical Anthropology 144:51–59.

Hogue, A. S., and S. ZiaShakeri. 2010. Molar crests and body mass as dietary indicators in marsupials. Australian Journal of Zoology 58:56–68.

Hunter, J. 1778. The Natural History of Human Teeth: Explaining Their Structure, Use, Formation, Growth and Diseases (J. Johnson (ed.)). 246 pp.

Janis, C. M., and A. Weil. 2008. Non-eutherian Mammal Summary; pp. 7–18 in C. M. Janis, G. F. Gunnell, and M. D. Uhen (eds.), Evolution of Tertiary Mammals of North America. Volume 2: Small Mammals, Xenarthrans, and Marine Mammals. Cambridge University Press, New York.

Kay, R. F. 1975. The functional adaptation of primate molar teeth. American Journal of Physical Anthropology 43:195–216.

Kay, R. F. 1978. Molar structure and diet in extant Cercopithecidae; pp. 309–339 in P. M. Butler

and K. A. Joysey (eds.), Development, Function and Evolution of Teeth. Academic Press,

New York.

Kay, R. F., and H. H. Covert. 1984. Anatomy and behavior of extinct primates; pp. 467–508 in

D. J. Chivers, B. A. Wood, and A. Bilsborough (eds.), Food Acquisition and Processing in

Primates. Plenum Press, New York.

Kay, R. F., and P. S. Ungar. 1997. Dental evidence for diet in some Miocene catarrhines with

comments on the effects of phylogeny on the interpretation of adaptation; pp. 131–151 in D.

R. Begun, C. Ward, and M. Rose (eds.), Function, Phylogeny and Fossils: Miocene

Hominoids and Great Ape and Human Origins. Plenum Press, New York.

Krause, D. W. 1982. Jaw movement, dental function, and diet in the Paleocene multituberculate

Ptilodus. Paleobiology 8:265–281.

Meldrum, D. J., and R. F. Kay. 1997. *Nuciruptor rubricae*, a new pitheciine seed predator from

the Miocene of Colombia. American Journal of Physical Anthropology 102:407–427.

Osborn, H. F. 1907. Evolution of Mammalian Molar Teeth (Macmillan (ed.)). 264 pp.

Owen, R. 1840. Odontography or, a Treaties on the Comparative Anatomy of the Teeth.

Hippolyte Bailliere, 168 pp.

Pampush, J. D., J. P. Spradley, P. E. Morse, A. R. Harrington, K. L. Allen, D. M. Boyer, and R.

F. Kay. 2016. Wear and its effects on dental topography measures in howling monkeys

(*Alouatta palliata*). American Journal of Physical Anthropology 161:705–721.

R Core Team (2016). R: A language and environment for statistical computing. R Foundation for

Statistical Computing, Vienna, Austria. https://www.R-project.org/.

Scott, C. S., A. Weil, and J. M. Theodor. 2018. A new, diminutive species of *Catopsalis* (Mammalia, Multituberculata, Taeniolabidoidea) from the early Paleocene of southwestern Alberta, Canada. Journal of Paleontology 1–15.

Scott, E. C. 1979. Dental wear scoring technique. American Journal of Physical Anthropology 51:213–218.

Strait, S. G. 1993a. Molar morphology and food texture among small-bodied insectivorous mammals. American Society of Mammalogists 74:391–402.

Strait, S. G. 1993b. Differences in occlusal morphology and molar size in frugivores and faunivores. Journal of Human Evolution 25:471–484.

Strait, S. G. 2001. Dietary reconstruction of small-bodied omomyoid primates. Journal of Vertebrate Paleontology 21:322–334.

Ungar, P. S. 2005. Dental evidence for the diets of fossil primates from Rudabanya, northeastern Hungary with comments on extant primate analogs and "noncompetitive" sympatry. Palaeontographica Italica 90:97–111.

Weil, A., and D. W. Krause. 2008. Multituberculata; pp. 19–38 in C. M. Janis, G. F. Gunnell, and M. D. Uhen (eds.), Evolution of Tertiary Mammals of North America. Volume 2: Small Mammals, Xenarthrans, and Marine Mammals. Cambridge University Press, New York.

Winchester, J. M., D. M. Boyer, E. M. St. Clair, A. D. Gosselin-Ildari, S. B. Cooke, and J. A. Ledogar. 2014. Dental topography of platyrrhines and prosimians: Convergence and contrasts. American Journal of Physical Anthropology 153:29–44.

Chapter Four: Dental Topographic Measures Applied to Multituberculate Lower Cheek Teeth

4.1 Introduction

Three-dimensional imaging techniques have revolutionized our ability to quantify tooth shape. The first steps towards digitizing teeth were made at the end of the 20th century with reflex microscopes (Reed, 1997), electromagnetic digitizers (Zuccotti et al., 1998), and laser confocal microscopes (Jernvall and Selänne, 1999). While these techniques were able to produce three-dimensional images, they were limited in their ability to process large samples of variably sized teeth (M'Kirera and Ungar, 2003). The popularization of laser scanners and computed tomography (CT) scanners alleviated this problem. The ability to produce large quantities of high-quality scans has allowed researchers to explore a new set of quantitative parameters that can be used for dental topographic analysis (DTA).

4.1.1 Relief index.

The relief index (RFI) of a tooth is a measure of the crown surface area compared to the occlusal footprint area (Ungar and Williamson, 2000; M'Kirera and Ungar, 2003; Boyer, 2008). In this case, the occlusal footprint refers to the outline of the crown in occlusal view. Species that consume high amounts of structural carbohydrates in their diet (i.e. folivores and insectivores) tend to have higher RFI values than omnivores and frugivores (Boyer, 2008; Bunn and Ungar, 2009; Bunn et al., 2011; Winchester et al., 2014), while hard-object feeders have lower RFI values than frugivores (Ledogar et al., 2013; Winchester et al., 2014; Allen et al., 2015; Thiery et al., 2017).

The first version of RFI was introduced by Ungar and Williamson (2000) and elaborated on by M'Kirera and Ungar (2003). This version calculated the raw ratio of crown surface area to occlusal footprint area:

$$\text{RFI} = \frac{A3D}{A2D}$$

with *A3D* equivalent to the surface area of the tooth crown and *A2D* equivalent to the occlusal footprint area of the tooth (Pampush et al., 2016a).

M'Kirera and Ungar (2003) considered RFI to be a type of three-dimensional shearing quotient (SQ) – given that shearing crests contribute to the surface area of a tooth, the ratio of the crown area to the occlusal footprint area is similar to the ratio of shearing crest length to tooth length. To measure RFI, M'Kirera and Ungar (2003) used a laser scanner to generate 2.5D (a full three-dimensional representation could not be generated with a laser scanner) representations of chimpanzee and gorilla m2s. They then used geographic information systems (GIS) software to crop the scans and calculate RFI values. M'Kirera and Ungar (2003) chose to crop the teeth at the lowest point of the occlusal basin so that only the functional part of the tooth remained. The authors found that RFI values could be used to distinguish between chimpanzee and gorilla molars; gorillas, which are folivores, have higher RFI values than the largely frugivorous chimpanzees, and this distinction remained even when RFI was calculated from moderately worn teeth. The results of M'Kirera and Ungar (2003) have been supported by other primate studies (Ungar and M'Kirera, 2003; Dennis et al., 2004; Ulhass et al., 2004; King et al., 2005; Ungar and Bunn, 2008; Bunn and Ungar, 2009; Venkataraman et al., 2014; Ungar et al., 2018).

Boyer (2008) further explored the applications of RFI by testing it on a set of euarchontan m2s, including those of tree shrews and dermopterans. He modified the RFI formula

to make it more applicable to large, multi-clade datasets that may not have normal distributions (Boyer, 2008):

$$\text{RFI} = \ln\left(\frac{\sqrt{A3D}}{\sqrt{A2D}}\right)$$

Unlike earlier studies, Boyer (2008) cropped his scans at the crown-root junction so that the entire crown was accounted for in the calculation. He argued that the functional part of the crown often extends below the level of the occlusal basin, and therefore data are lost when the tooth is cropped above the crown-root junction (Boyer, 2008). Boyer (2008) pioneered the use of a µCT scanner rather than a laser scanner in RFI studies, ensuring that his data were fully 3D.

Like M'Kirera and Ungar (2003), Boyer's (2008) study showed that RFI is relatively insensitive to tooth wear; whereas the RFI value of a tooth does decrease with increased wear, teeth at the same stage of wear in different taxa nonetheless retain significantly different RFI values (Boyer, 2008). The differences across taxa only disappear for very highly worn teeth (Boyer, 2008). This general principle continues to be supported in the literature (Pampush et al., 2016b; Berthaume et al., 2018).

Boyer's version of RFI has been preferred over the earlier version, with respect to both formula and cropping location (e.g. Boyer et al., 2010; Bunn et al., 2011; Ledogar et al., 2013; Winchester et al., 2014; Pampush et al., 2016). RFI has only been applied to Euarchontoglires, so it is unclear how transferable the metric is to other clades (Boyer et al., 2010; Bunn et al., 2011; Ledogar et al., 2013; Keller, 2014; Venkataraman et al., 2014; Winchester et al., 2014; Allen et al., 2015; Pampush et al., 2016b; Thiery et al., 2017; Ungar et al., 2018). It should also be noted that RFI varies significantly based on tooth position (Bunn and Ungar, 2009; Allen et al., 2015; Pampush et al., 2016b; Yamashita et al., 2016).

4.1.2 Orientation patch count and orientation patch count rotated.

Orientation patch count (OPC) was introduced by Evans et al. (2007) as a putatively homology-free method for quantifying functional surfaces on a tooth row. The explanation for OPC is that teeth are tools for processing food, and that resistant foods are more difficult to process than soft foods. OPC rests on the principle that the processing ability of a tooth increases as the number of facets in contact with the food increases, which in turn increases the surface complexity of the tooth. Thus, animals that consume more resistant foods have greater tooth complexity.

Orientation Patch Count Rotated (OPCR) is a modification of OPC (Evans and Jernvall, 2009). For OPC, patches (i.e. facets), are calculated while the tooth is held in a fixed position, which can lead to counting errors if the tooth is not properly oriented. This problem was addressed by modifying the methods: for OPCR, multiple patch counts are performed while the tooth is rotated around a fixed axis, and the counts are then averaged to produce a composite OPCR value. OPC and OPCR values are highly correlated, and the two counts are comparable (Evans and Jernvall, 2009; Wilson et al., 2012). In this thesis, the two measurements are collectively referred to as OPC/R. OPC versus OPCR will be specified when discussing individual studies.

Evans et al. (2007) compared the OPC values of the molar rows of carnivorans and rodents. They found that values are higher in the dentitions of herbivorous mammals than in those of carnivorous (including faunivorous and insectivorous) mammals. Likewise, but to a lesser degree, OPC is higher in plant-dominated omnivores than in animal-dominated omnivores. However, examination of other clades has shown that these trends do not always hold, and OPC/R cannot be used to distinguish among all dietary categories (e.g. insectivores vs. folivores;

91

omnivores vs. frugivores) (Bunn et al., 2011; Santana et al., 2011; Winchester et al., 2014; Thiery et al., 2017).

OPC/R analyses have been conducted on many extant taxa including rodents (Evans et al., 2007; Evans and Jernvall, 2009; Keller, 2014), carnivorans (Evans et al., 2007; Evans and Jernvall, 2009; Smits and Evans, 2012), phyllostomid bats (Santana et al., 2011), dasyurids (Smits and Evans, 2012), and euarchontans including dermopterans (Bunn et al., 2011), scandentians (Bunn et al., 2011), prosimians (Bunn et al., 2011; Godfrey et al., 2012), platyrrhines (Ledogar et al., 2013; Winchester et al., 2014; Ungar et al., 2018), and catarrhines (Thiery et al., 2017). In fact, OPC/R is the only DTA metric that has been used in analyses of taxa outside of Euarchontoglires. Furthermore, the overall OPC/R of a tooth does not vary greatly between low and moderate tooth wear (individual patches may change, but total number does not), so variably worn teeth can be included in analyses (Pampush et al., 2016b; Ungar et al., 2018).

The extensive use of OPC/R has led to a variety of modifications to the original methodology. Some studies use individual teeth (e.g. Bunn et al., 2011; Godfrey et al., 2012; Ledogar et al., 2013; Winchester et al., 2014; Thiery et al., 2017) while others use partial or full tooth rows (e.g. Evans et al., 2007; Evans and Jernvall, 2009; Santana et al., 2011; Smits and Evans, 2012). The choice is important, for it can greatly affect the results of OPC/R analyses given the functional diversity of teeth in a row. For example, if OPC/R values for *Crocuta crocuta* (spotted hyaena) are calculated from only lower molars (m1), then the tooth predominantly used for bone cracking (p4) is excluded from the analysis. Furthermore, the length of the tooth row can impact OPC/R results (Smits and Evans, 2012). For example, dasyurids (marsupials) have higher OPC/R values than carnivorans (placentals) with similar

diets, in part because dasyurids have are greater number of molars (4) than carnivorans (1 to 3) (Smits and Evans, 2012). Some of these differences can be mitigated with downsampling and averaging procedures, but they do make cross-study comparisons more difficult (Smits and Evans, 2012).

Another potential problem with OPC/R is the amount of downsampling performed on each scan before the scan is analyzed. There is a linear relationship between scan resolution and OPC/R, with higher resolutions producing higher values (Evans and Janis, 2014). Some changes in OPC/R can be detected at low resolutions, but it requires higher resolutions to detect certain patterns of dietary change (e.g. evolution of grazing in horses) (Evans and Janis, 2014). Low resolutions may be sufficient for gross categorizations (e.g. carnivore vs. herbivore), but they may not be enough to distinguish among finer categories or to recognize minor shape differences (Evans and Janis, 2014).

4.1.3 Dirichlet normal energy.

Dirichlet normal energy (DNE) quantifies the curvature of a tooth by measuring how greatly the tooth shape differs from that of a planar surface (Bunn et al., 2011). Higher values of DNE correspond to teeth that are less planar and that have more undulations. Essentially, DNE measures the "curviness" of a tooth. DNE is calculated as follows (Bunn et al., 2011; Pampush et al., 2016a, 2016b):

$$\text{DNE} = \sum e(p) \times area(p)$$

In the above equation, $e(p)$ is the Dirichlet Energy Density at point p, and $area(p)$ is the area of point p. The term $e(p)$ is a measurement of how the normal map expands at point p:

$$e(p) = \|n_u\|^2 + \|n_v\|^2$$

93

where n is the normal at point p and u and v are orthonormal directions on the surface (Bunn et al., 2011). The terms n_u and n_v denote the derivatives of the normal n in the directions u and v (Bunn et al., 2011). For a more detailed explanation of Dirichlet Energy Density and how DNE is calculated, please refer to Bunn et al. (2011), Pampush et al. (2016a-b), and Winchester (2016).

Unlike OPC/R and RFI, DNE is independent of the initial position, orientation, and scale of the scan (Bunn et al., 2011). Furthermore, DNE is less sensitive to cropping techniques than RFI (Bunn et al., 2011; Prufrock et al., 2016a). However, DNE is greatly affected by smoothing protocols, which makes cross-study comparisons difficult (Spradley et al., 2017). Both too little and too much smoothing can lead to aberrant DNE values (Spradley et al., 2017). DNE is also affected by tooth wear (Pampush et al., 2016b; Berthaume et al., 2018).

DNE has so far been calculated from isolated euarchontan teeth (Bunn et al., 2011; Godfrey et al., 2012; Ledogar et al., 2013; Winchester et al., 2014; Pampush et al., 2016b; Berthaume and Schroer, 2017; Thiery et al., 2017). In general, DNE values can be used to distinguish insectivores from frugivores, with insectivorous species having the highest DNE values and frugivorous species (including seed-eaters) having the lowest (Bunn et al., 2011; Ledogar et al., 2013; Winchester et al., 2014). Folivores and omnivores have intermediate values (Bunn et al., 2011; Winchester et al., 2014). It is not known whether these patterns hold for non-euarchontan mammals.

4.1.4 Combined dental topographic analysis.

Different DTA metrics quantify different, but highly correlated, aspects of tooth shape. OPC/R is a measurement of surface complexity, RFI is a measurement of topographic relief, and DNE is a measurement of curvature. OPC/R is not strongly correlated with either RFI or DNE,

and OPC/R can produce very different relative values than the other metrics (Boyer et al., 2010; Bunn et al., 2011; Winchester et al., 2014). For example, pitheciine seed eaters have brachydont, flat teeth with crenulated enamel. Unworn pitheciine teeth have OPC/R scores that are higher than those of other frugivorous primates, but their RFI scores are lower (Ledogar et al., 2013). RFI and DNE are correlated, although the strength of the correlation varies with group (Bunn et al., 2011; Winchester et al., 2014). Given this, it stands to reason that a suite of metrics would perform better than a single metric at classifying diet, and multiple topographic metrics are often employed with fossils to check whether classifications are consistent among metrics (Boyer et al., 2010; Boyer and Lipman, 2012; Prufrock et al., 2016a).

4.1.5 Is dental topographic analysis homology free?

Dental topographic analysis, specifically OPC/R, was introduced as a homology-free technique for classifying diets (Evans et al., 2007). Evans et al. (2007) argued that the similarities in OPC values between carnivorans and rodents indicated that OPC was reliable between clades regardless of tooth shape, type, quantity, replacement, and chewing motion. The only significant difference in OPC between rodents and carnivorans was in the "carnivore" category – Evans et al. (2007) explained that this was likely because carnivorous rodents tend to be insectivorous while carnivorous carnivorans tend to consume vertebrates. However, the authors did not perform any phylogenetic corrections on their data to check their assertions.

Results from further OPC/R studies have challenged the assumption of phylogenetic independence. Perhaps the most notable example is that of carnivorans and dasyurids: dasyurids have significantly higher tooth row OPC values than carnivorans with similar diets (Smits and Evans, 2012). A study on phyllostomid bats also found that bat OPC values are much higher than those of rodents and carnivorans with similar diets (Santana et al., 2011), however, the bat scans

may have been processed differently from the rodent and carnivoran scans (Evans, pers. comm., 2018).

Boyer (2008) encountered a similar problem when he published a modified version of RFI. He tested his version of RFI on a sample of euarchontans, including dermopterans and tree shrews. The results raised some concerns – RFI could be used to distinguish among frugivores, folivores, insectivores, and omnivores when only primates were included in the analysis. When the non-primate euarchontans were included, insectivores and folivores were no longer distinguishable. This suggested that there was a phylogenetic component to RFI.

The implications of these OPC/R and RFI studies were not immediately addressed. DTA was used without phylogenetic corrections, both on living and extinct taxa. Subsequently, Winchester et al. (2014) demonstrated that a phylogenetic signal is present in DTA. They found that, when phylogenetic interdependence is accounted for, OPCR can no longer be used to distinguish among dietary categories for prosimians and platyrrhines. Furthermore, although DNE could still be used to differentiate between some diets, the differences were not as strong, and some diets became indistinguishable. Conversely, for RFI, differences among dietary categories became more pronounced, suggesting that RFI may be a better metric for partitioning diets when phylogenetic corrections are performed. These results demonstrate that much of the dietary differentiation observed using DTA may actually be a phylogenetic signal. Even closely-related groups can have phylogenetic interdependence: DNE can be used to partition great apes into dietary categories when phylogeny is ignored, but when phylogeny is included, dietary signals disappear (Berthaume and Schroer, 2017). Essentially, DTA should not be used without phylogenetic corrections, especially when comparisons are being made across clades. Many, but

not all, DTA studies are now including phylogenetic corrections (Allen et al., 2015; Berthaume and Schroer, 2017; Thiery et al., 2017)

4.1.6 Dental topographic analysis applied to the fossil record.

DTA has been used many times on extinct taxa to examine changes in morphology through time, to compare morphologies among clades, and to infer diets. Most studies that have made explicit dietary predictions have been primate studies (Ungar, 2004; Merceron et al., 2006; Godfrey et al., 2012; Berthaume et al., 2018). Primates are an ideal group for DTA because the extant taxa have been extensively studied, they are highly variable in tooth morphology, and they have well-resolved and widely accepted phylogenies (Winchester et al., 2014; Berthaume and Schroer, 2017). Relationships are close enough that DFAs can be used (e.g. subfossil lemurs) (Godfrey et al., 2012) and phylogenetic interdependence can be taken into account (Thiery et al., 2017; Berthaume et al., 2018). Closely-related extant groups and well-resolved phylogenies are not available for all extinct clades. Even with these caveats, much can be learned from the analysis of fossils.

DTA is a good method for studying evolutionary trends in ecomorphology. For example, both OPC and RFI values increased for plesiadapids during the Paleocene-Eocene Thermal Maximum (Boyer et al., 2010). Boyer et al. (2010) suggested that this increase meant that plesiadapids were becoming more herbivorous over time. López-Torres et al. (2018) found the same trend in paromomyids. Another study found that OPCR of horses increased from the Eocene to the Pleistocene (Evans and Janis, 2014). Evans and Janis (2014) did not compare the horse OPCR values to those of modern perissodactyls, and they did not make dietary predictions. Instead, they noted the likely diet of each species based on previous research and related the OPCR values back to those predicted diets. Comparison of DTA values over time is a good

approach for fossil taxa, especially if there are other lines of evidence supporting particular dietary categories.

Niche partitioning can also be tested using DTA. Significant differences between sympatric species are generally taken to indicate niche partitioning. Based on this, niche-partitioning has been inferred among plesiadapiforms and between plesiadapiforms and early rodents (Boyer and Lipman, 2012; Prufrock et al., 2016b, 2016a). However, paleontological studies of DTA are unavoidably affected by phylogenetic relationships. This is especially true when comparisons are being made between clades, or between extinct and extant groups. More extensive studies with phylogenetically-corrected extant data may clarify the extent of clade offset, but until then, comparisons between clades need to be viewed with caution. In spite of these issues, DTA has merit and may still be used in informative ways on fossil datasets as long as phylogenetic interdependence is recognized.

4.1.7 Dental topographic analysis of multituberculates.

One DTA study has previously been conducted on multituberculates. Wilson et al. (2012) used OPC to infer the diets of multituberculates from the middle Jurassic to the late Eocene. Multituberculates pose an interesting problem for DTA because they do not have any extant close relatives. The relationship of multituberculates to other mammals is controversial and the homologies of multituberculate teeth to those of other mammals remain unclear (Janis and Weil, 2008).

Wilson et al. (2012) found that multituberculate teeth from latest Cretaceous and early Paleocene had the highest OPC values and the greatest spread of OPC values. The authors chose to compare their OPC results to those of carnivorans and rodents. Compared to the extant clades, most multituberculates fall into carnivorous and omnivorous categories (Evans et al., 2007;

Wilson et al., 2012). Only five species have OPC values characteristic of herbivory: *Catopsalis alexanderi*, *Catopsobaatar catopsaloides*, *Cimolomys gracilis*, *Lambdopsalis bulla*, and *Taeniolabis taoensis* (Wilson et al., 2012). *Taeniolabis taoensis* has the highest OPC, with a value exceeding those of extant rodents and carnivorans (Wilson et al., 2012).

Wilson et al. (2012) chose to use the full cheek tooth row of multituberculates. Multituberculates can have up to six lower cheek teeth (Kielan-Jaworowska et al., 2004, p. 301), while the comparative set of carnivorans and rodents included up to three teeth (Evans et al., 2007). This may have inadvertently introduced some error into the comparison – the number of teeth in the tooth row can greatly affect OPC/R values (Smits and Evans, 2012). This means that, even ignoring the phylogenetic interdependence of the method, the multituberculate OPC values may not be directly comparable to the carnivoran and rodent values.

4.2 Methods

All statistical analyses were run in RStudio (v. 1.1.383, RStudio Team, 2016).

Previous work has demonstrated that DTA is not homology free. There are clade-level offsets in metrics, which make comparisons across clades unreliable (Winchester et al., 2014; Allen et al., 2015). Phylogenetic corrections have been helpful in reducing the phylogenetic signal present in the measurements, but accurate results require well-resolved phylogenies for the groups in questions (Winchester et al., 2014; Allen et al., 2015; Berthaume and Schroer, 2017; Thiery et al., 2017). Multituberculate phylogenetics are not well-resolved (Weil and Krause, 2008). As such, I have chosen not to perform any phylogenetic corrections on my data.

DTA, which is not landmark-based, has proven to be useful for both low and moderate wear stages. Therefore, both low and moderately worn teeth were included. An analysis of wear stage effects on DTA for the present study can be found in Appendix I.

RFI and DNE are typically calculated from lower m2s. OPC/R has been calculated using both isolated teeth and tooth rows, depending on the study. Therefore, all available lower cheek teeth (p4, m1, m2) were included in this analysis. Premolars function in a different part of the multituberculate masticatory cycle (Krause, 1982), but previous studies have included premolars as part of the tooth row for OPC/R (Wilson et al., 2012). Most specimens in the present study were isolated teeth, but tooth rows were included when available for comparisons to published tooth row OPC/R data. Specimens were scanned with a Scanco Medical µCT 35 at 70 kV and 114 µA. Most teeth were scanned at standard resolution, which produced scans with an isotropic voxel size of 30 µm. This resolution was judged to be adequate because it typically produced scans with more than 10,000 faces (the eventual downsampled resolution). For some of the smaller teeth, scans at standard resolution were too coarse. These small teeth were scanned at high resolution and had an isotropic voxel size of 15 µm (Appendix G). A few scans had less than 10,000 faces at the high resolution. These scans were included in the analysis, but their reduced faces are noted in Appendix G.

Actual specimens were scanned when possible, but some teeth were embedded in bone and were thus too large for the scanner. When this occurred, casts of the teeth were made using an epoxy resin (see Chapter Two Methods for details) and those casts were scanned. There may be some effect of material on DTA (López-Torres et al., 2018). This is especially true of OPCR, which seems to be inflated by casts (López-Torres et al., 2018). The use of casts was unavoidable in this study, but most of the scans were made from fossils (Appendix G).

Scans were reconstructed using the Scanco µCT Evaluation Program (v.6.5-3). After reconstruction, scans were imported into Amira (v. 5.6.0, FEI Visualization Sciences, Hillsborough, OR, USA) and a surface was extracted. This surface was then trimmed at the crown/root junction so that only the tooth crown remained. The scans were then exported to MeshLab (v.2016.12; Cignoni et al., 2008) where the Cleaning and Repairing function Remove Isolated Pieces was used to further trim them. Once trimming was complete, the scans were uniformly oriented using the Transform > Rotate function. The scans were oriented so that the anterior side of the tooth faced left and the occlusal surface was in the z-plane as per Pampush et al. (2016).

4.2.1 Processing scans with SurferManipulator for OPC/R.

SurferManipulator (available at http://evomorph.org/surfermanipulator/; Evans et al., 2007) is a Surfer® (Golden Software, LLC, Golden, Colorado) plugin created by A. Evans to calculate OPC/R. SurferManipulator is designed to handle scans produced by a laser scanner, not a CT scanner – this means that the program is equipped to handle 2.5D data, and fully 3D scans need to be trimmed (i.e. "undercuts" removed) before OPC/R can be calculated (Evans et al., 2007). Instructions for processing scans in Surfer® using SurferManipulator can be found at http://evomorph.org/surfermanipulator/. After preparing the scans in Surfer®, I imported the scans into SurferManipulator and processed them following the methods of Evans et al. (2007). Each tooth was downsampled to 50 rows. For partial or full tooth rows, the appropriate multiple of 50 was used (e.g. two teeth = 100 rows). The OPCR of these downsampled scans was then calculated in SurferManipulator (Figure 4.1).

OPCR values calculated with SurferManipulator are not comparable to OPCR values produced with other programs such as molaR and MorphoTester (Pampush et al., 2016a;

101

Winchester, 2016). I chose to calculate OPCR values with SurferManipulator because Wilson et al. (2012) used the program when they calculated the OPC of multituberculates.
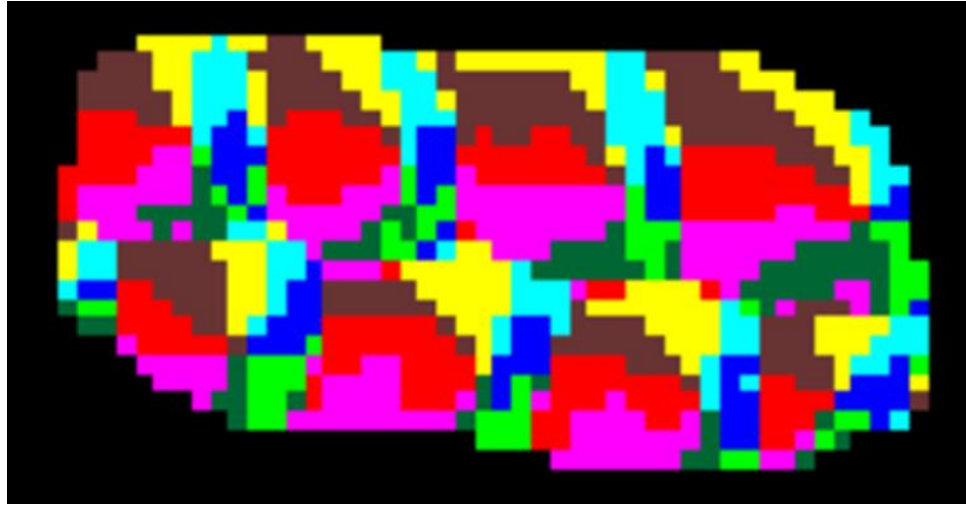
Figure 4.1. Coloured representation of the OPCR of a *V. joyneri* m1 (UALVP 28167) calculated in SurferManipulator. Patches with similar orientations share the same colour. The tooth was downsampled to 50 rows prior to the calculation.

4.2.2 Preparing scans for molaR.

molaR is an R package (R Core Team, 2016) designed to calculate DTA (Pampush et al., 2016a). It can calculate OPC/R, RFI, and DNE with various parameters, and it can batch process scans. A similar python program, MorphoTester, is also available (Winchester, 2016), but MorphoTester was not used in this study because all analysis in the present study were run in RStudio.

Scans for molaR require extra processing in Amira and MeshLab. Once a scan was fully trimmed, the crown was then simplified to 10,000 faces in Amira using the Simplification editor and smoothed (iterations = 100, lambda = 0.6) using the SmoothSurface module, following standard procedures for preparing scans (Pampush et al., 2016a). Each tooth was independently

simplified to 10,000 faces. For tooth rows containing multiple teeth, the scan was simplified to the appropriate multiple of 10,000. For example, a tooth row containing two teeth would be simplified to 20,000 faces.

Calculating DNE requires further preparation. This is because the original software (Teether) used to calculate DNE included an additional smoothing step after smoothing in Amira (Pampush et al., 2016a). A somewhat equivalent, but not identical, smoothing process can be performed in MeshLab using the Laplacian Smooth operation, set at three steps, 1D boundary smoothing, and with cotangent weighting enabled (Pampush et al., 2016a). For a few scans, this smoothing produced a spike-like protrusion in the mesh (Appendix G). These spikes were selected and deleted, and any non-manifold edges were removed and then the Close Holes operation was used.

Over-smoothing scans for DNE can distort the results (Spradley et al., 2017). While most protocols recommend 100 iterations of smoothing in Amira, this smoothing may eliminate meaningful curvature or may result in artificial curvatures being produced, sometimes increasing the DNE beyond its original value (Spradley et al., 2017). The effects are even worse when addition smoothing steps, such as Laplacian Smooth, are included (Spradley et al., 2017). Spradley et al. (2017) recommended running 20-30 smoothing iterations in Amira to retain natural DNE values. I smoothed a set of scans using 30 iterations to determine how much smoothing affects DNE for multituberculates. I compared the 30-iteration scans to the 100-iteration scans and to the 100-iterations + Laplacian Smooth scans (Appendix H).

4.2.3 Processing scans with molaR.

Scans were processed using the molar_batch function, which is capable of running OPC/R, RFI, and DNE at the same time (Figure 4.2).

103
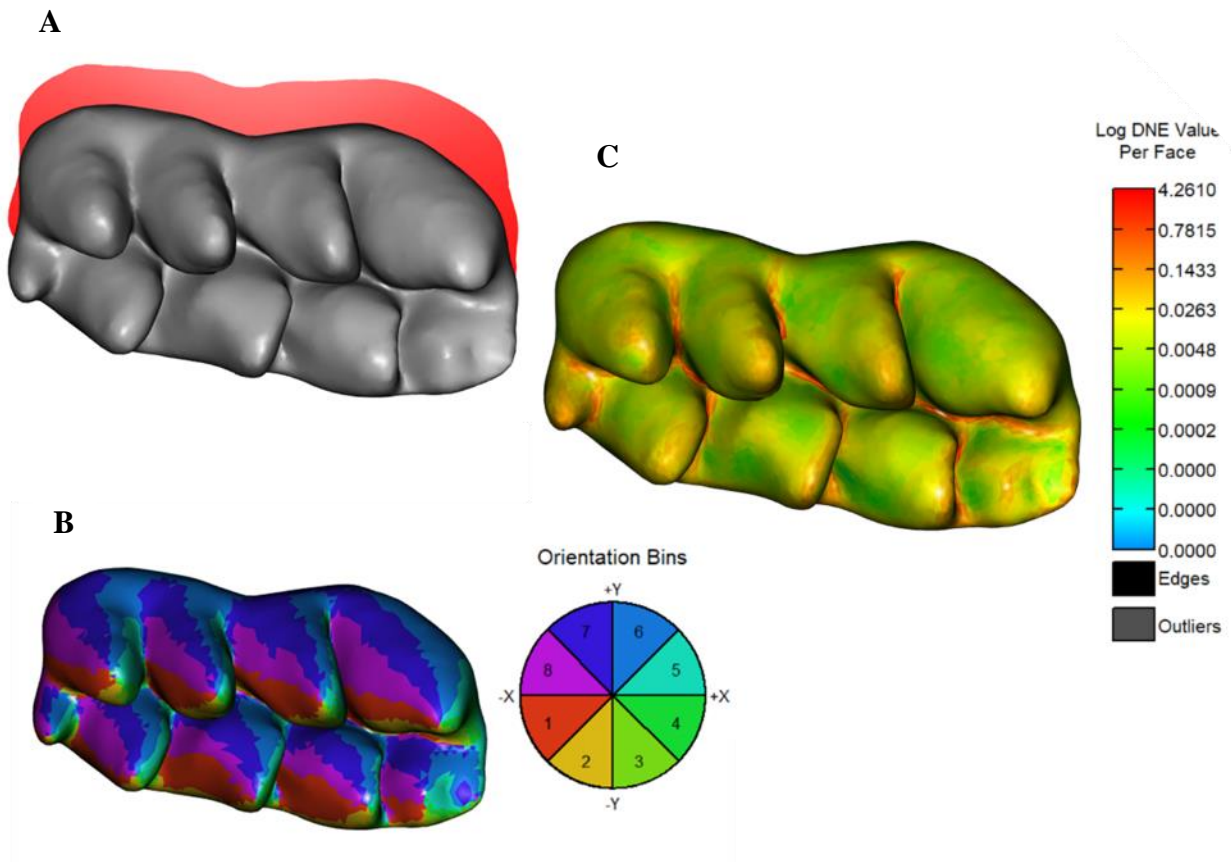
Figure 4.2. Coloured representation of the DTA of a *V. joyneri* m1 (UALVP 28167) calculated in molaR. The tooth was downsampled to 10,000 faces prior to the calculation. A) RFI – the grey 3D tooth represents the crown surface area (A3D) and the red shadow represented the occlusal footprint area (A2D). B) OPCR – the colouring indicates patch orientation, grouped into eight orientation bins. C) DNE – the tooth is coloured with a heat map that represents the distribution of log-scaled DNE values, with warmer colours representing higher values.

RFI was calculated as per Boyer (2008). The RFI_alpha, which controls the sensitivity of the occlusal footprint trace, was automatically set to 0.01. I change the setting to 0.06, as

suggested by Pampush (pers. comm., 2018). The higher alpha level results in fewer molaR errors. When an error still occurred, I manually adjusted the alpha level (Appendix G).

Both OPC and OPCR can be calculated with molaR. I only calculated OPCR because it is less prone to errors. Occasionally, because of computational overload, molaR was able to calculate the OPC but not the OPCR of a scan. When this occurred, I used the OPC value in my analysis (Appendix G).

The OPCr function automatically performs eight rotations, each of $5.625°$, and counts any faces that have a minimum patch size of three. These settings reflect the parameters introduced by Evans and Jernvall (2009). I kept the automatic settings for one iteration, but I also ran an OPCR calculation with a minimum patch size of five. The larger patch size reflects the parameters often used in MorphoTester (Winchester, 2016; Berthaume et al., 2018). The larger size is meant to compensate for the relatively low downsampling of Amira scans compared to SurferManipulator scans (Winchester, 2016). To help distinguish between SurferManipulator and molaR OPCR results, I will refer to data from molaR as 3D-OPCR. This is a term first coined by Winchester (2016) to describe OPCR calculated from fully 3D scans. Only SurferManipulator OPCR and 3-patch minimum 3D-OPCR values were included in the main analysis. Comparisons among the OPCR programs and parameters can be found in Appendix H.

The DNE function in molaR automatically excludes boundary faces and faces containing the highest 0.1% of the Dirichlet Energy Densities (Pampush et al., 2016a). There are times that the exclusion of the highest 0.1% is not enough, especially with fossils that may have cracks (Berthaume et al., 2018). I ran three iterations of DNE: one with the automatic settings, one adjusted to exclude the top 1.0% of densities, and one adjusted to exclude the top 5.0% of densities. All outlier exclusions were performed on the 100-iteration scans. I also calculated

DNE of all three smoothing parameters with both 0.1% outlier exclusion and 5.0% outlier exclusion. All DNE protocols (outlier exclusions and smoothing techniques) were run with the BoundaryDiscard = "Vertex" argument. This prompted R to exclude any faces that had at least one vertex on the boundary, which results in DNE values more reflective of an object's actual shape (Spradley et al., 2017). Comparisons among all DNE parameters can be found in Appendix H. After making the comparisons, I chose to include the Laplacian Smooth scans with 0.1% outlier exclusion and the 30-iteration smoothed scans with 5.0% outlier exclusion in my main analysis.

4.2.4 Constructing composite tooth rows.

Most of the multituberculate specimens included in this study were isolated teeth. This is useful for evaluating the topography of individual teeth, but not for evaluating full tooth rows. Wilson et al. (2012) encountered a similar problem when constructing their dataset. Their solution was to build composite tooth rows from multiple specimens, preferably of the same species but sometimes only of the same genus (Wilson et al., 2012). Whether this construction occurred in the scanning stage or the calculation stage is not clear. I have chosen to take a similar approach with my data. In my case, I constructed the composites after DTA calculations.

I only constructed composite tooth rows for OPCR because both RFI and DNE rely on individual teeth. OPCR is a summation of values from points on a surface. Therefore, composite OPCR values can be calculated by adding each tooth OPCR value (e.g. $OPCR_{p4} + OPCR_{m1} + OPCR_{m2} = OPCR_{tooth\ row}$). When multiple specimens of the same tooth were available (e.g. m1), the OPCR values were average together before being added to the composite total. Propagation of uncertainty was accounted for when calculating composite standard deviations.

4.2.5 Statistical analyses.

The p4 DTA results could not be evaluated statistically because of low sample size. Statistical comparisons were performed on the m1 and m2 DTA results for the taxa with three or more specimens. Non-normality was assumed for the data. Levene's Test was used to check for heteroscedasticity – all data were homoscedastic, so Kruskal-Wallis H-tests were used. A Dunn's post-hoc test with a Bonferroni correction was performed when significant differences were detected. For the m1s, the following taxa were included in the statistical analysis: *Catopsalis alexanderi*, *Catopsalis* cf. *calgariensis*, *Cimolomys* sp., *Meniscoessus major*, *Mesodma* sp., *Taeniolabis taoensis*, and *Valenopsalis joyneri*. For the m2s, the following taxa were included in the statistical analysis: *C.* cf. *calgariensis*, *M. major*, *T. taoensis*, and *V. joyneri*.

One specimen included in the RFI and OPCR analyses was excluded from the DNE analysis. This specimen was UALVP 16058 (*Catopsalis johnstoni*). I chose to exclude UALVP 16058 because its DNE value was clearly an outlier that was unlikely to be biologically meaningful; even with 30 iterations of smoothing and an outlier exclusion of 5.0%, the specimen had a DNE value of over 1,400 while all other isolated teeth had DNE values of less than 1,000 (Appendix H, J).

4.3 Results

4.3.1 RFI.

4.3.1.1 RFI of p4s.

RFI values could only be calculated for the p4s of five taxa (Table 4.1). Of these taxa, *C. alexanderi* had the lowest RFI (0.48) and *M. major* had the highest RFI (0.69). *Catopsalis kakwa* (0.66, SD = 0.022) and *V. joyneri* (0.65, SD = 0.039) had equivalent values, both of which were

just slightly lower than that of *M. major*. *Taeniolabis taoensis* (0.54, SD = 0.028) had a value closest to that of *C. alexanderi*.

Table 4.1. Mean p4 RFI values by taxon.

Table abbreviations: **N** – number of specimens; **SD** – standard deviation; **CV** – coefficient of variation.

Taxon	N	RFI (SD)	CV
Catopsalis alexanderi	1	0.48 (--)	--
Catopsalis kakwa	2	0.66 (0.022)	0.033
Meniscoessus major	1	0.69 (--)	--
Taeniolabis taoensis	2	0.54 (0.028)	0.051
Valenopsalis joyneri	3	0.65 (0.039)	0.059

4.3.1.2 RFI of m1s.

Most taxa have m1 RFI values that range from 0.47 to 0.59 (Table 4.2). The only exceptions are some of the taeniolabidoids: *C. alexanderi*, *Catopsalis fissidens*, and *T. taoensis*. *Taeniolabis taoensis* has the lowest m1 RFI score (0.37, SD = 0.010), followed by *C. alexanderi* and *C. fissidens* (0.43, SD = 0.11; 0.43, SD = 0.019, respectively). Taeniolabidoids (*C. kakwa* and *V. joyneri*) also have the some of the highest RFI scores (0.58, SD 0.014; 0.57, SD = 0.069, respectively). In fact, the only taxon with a higher score is Cimolomyid 1 (0.59, SD = 0.015). The other taxa all fall between *C. alexanderi*/*C. fissidens* and *C. kakwa*/*V. joyneri*.

Table 4.2. Mean m1 RFI values by taxon.

Table abbreviations: **N** – number of specimens; **SD** – standard deviation; **CV** – coefficient of variation.

Taxon	N	RFI (SD)	CV
cf. *Acheronodon*	1	0.53 (--)	--
Catopsalis alexanderi	3	0.43 (0.11)	0.25
Catopsalis cf. *calgariensis*	3	0.51 (0.082)	0.16
Catopsalis fissidens	2	0.43 (0.019)	0.045
Catopsalis johnstoni	1	0.54 (--)	--
Catopsalis kakwa	2	0.58 (0.014)	0.024
Catopsalis waddleae	1	0.54 (--)	--
Cimolomyid 1	2	0.59 (0.015)	0.025
Cimolomys sp.	3	0.54 (0.029)	0.055
Meniscoessus major	4	0.49 (0.054)	0.11
Mesodma sp.	4	0.47 (0.059)	0.13
Neoplagiaulacid	1	0.51 (--)	--
Ptilodus sp.	1	0.49 (--)	--
Stygimys kuszmauli	1	0.53 (--)	--
Taeniolabis taoensis	3	0.37 (0.010)	0.027
Valenopsalis joyneri	6	0.57 (0.069)	0.12

A Kruskal-Wallis test detected significant differences among the taxa (x^2 (6) = 14.0, p = 0.03). Upon further inspection, only *T. taoensis* (median = 0.37) and *V. joyneri* (median = 0.60) have a statistically significant difference (p = 0.008) (Table 4.3). This is understandable given that *T. taoensis* has the overall lowest RFI, and *V. joyneri* has the highest RFI of the taxa included in the statistical analysis.

Table 4.3. Results of Dunn's post-hoc test with Bonferroni correction for m1 RFI comparisons among taxa. The significant *p*-value is in bold. α/2 = 0.025.

	C. alexanderi	*C.* cf. *calgariensis*	*Cimolomys* sp.	*M. major*	*Mesodma* sp.	*T. taoensis*
C. cf. *calgariensis*	1.00	--	--	--	--	--
Cimolomys sp.	1.00	1.00	--	--	--	--
M. major	1.00	1.00	1.00	--	--	--
Mesodma sp.	1.00	1.00	1.00	1.00	--	--
T. taoensis	1.00	0.92	0.23	1.00	1.00	--
V. joyneri	0.22	1.00	1.00	0.83	0.53	**0.008**

4.3.1.3 RFI of m2s.

The m2 RFI values follow similar patterns to the m1 RFI values (Table 4.4; Figure 4.3). *Taeniolabis taoensis* (0.38, SD = 0.033), *C. alexanderi* (0.39), and *C. fissidens* (0.39, SD = 0.017) have the lowest values, while *C. kakwa* (0.66, SD = 0.045) and *V. joyneri* (0.57, SD = 0.045) have some of the highest values. As with the m1s, Cimolomyid 1 (0.62) also has a high

RFI. The rest of the taxa have RFIs between 0.42 and 0.55. *Meniscoessus robustus* (0.43) is notable for having a relatively low RFI value, similar than that of *C. calgariensis* (0.42, SD = 0.062). A Kruskal-Wallis test did not detect any significant differences among taxa (x^2 (3) = 7.73, p = 0.052).

Table 4.4. Mean m2 RFI values by taxon.

Table abbreviations: **N** – number of specimens; **SD** – standard deviation; **CV** – coefficient of variation.

Taxon	N	RFI (SD)	CV
Catopsalis alexanderi	1	0.39 (--)	--
Catopsalis calgariensis	2	0.42 (0.063)	0.15
Catopsalis cf. *calgariensis*	3	0.48 (0.060)	0.13
Catopsalis fissidens	2	0.39 (0.017)	0.044
Catopsalis kakwa	2	0.66 (0.045)	0.068
Cimolomyid 1	1	0.62 (--)	--
Cimolomys sp.	1	0.50 (--)	--
Meniscoessus major	3	0.55 (0.079)	0.14
Meniscoessus robustus	1	0.43 (--)	--
Mesodma sp.	1	0.54 (--)	--
Taeniolabis taoensis	3	0.38 (0.033)	0.086
Valenopsalis joyneri	4	0.57 (0.045)	0.079

Within a taxon, the p4 tends to have the highest RFI value (Figure 4.3). The only exceptions to this are *C. kakwa*, which has similar p4 and m2 values, and *C. alexanderi*, which has similar p4 and m1 values. The m1 and m2 values tend to be similar within a taxon, although there is often a lot of intra-taxon spread in the data.
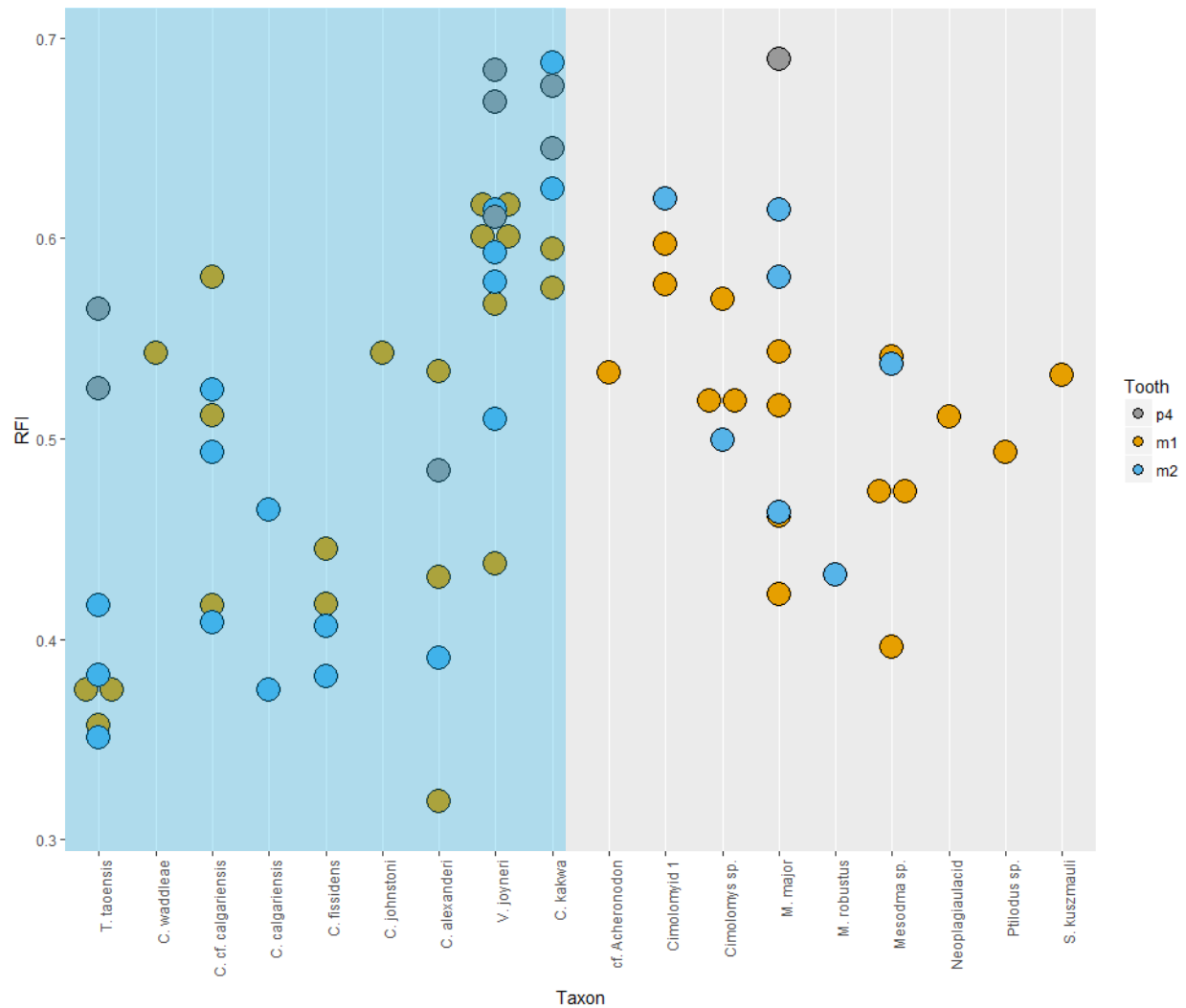
Figure 4.3. Dot plots of RFI values by tooth and taxon. Coloured circles represent individual specimens. Grey circles are p4s, orange circles are m1s, and blue circles are m2s. Taeniolabidoids are in the shaded blue area and are organized by inferred body size, with the largest-bodied taxon (*T. taoensis*) on the left and the smallest-bodied taxon (*C. kakwa*) on the right. Non-taeniolabidoids are in the shaded grey area and are not organized by inferred body size.

4.3.2 OPCR.

4.3.2.1 OPCR of p4.

Of the taxa evaluated, *T. taoensis* has the highest p4 3D-OPCR (58.9, SD = 9.72) and *C. alexanderi* has the lowest p4 3D-OPCR (22.4) (Table 4.5). *Catopsalis kakwa* has a 3D-OPCR similar to that of *C. alexanderi*. *Meniscoessus major* and *V. joyneri*, which have similar values to each other, fall in-between *T. taoensis* and *C. alexanderi*.

Table 4.5. Mean p4 OPCR values by taxon.

Table abbreviations: **N** – number of specimens; **SD** – standard deviation; **CV** – coefficient of variance; **3D-OPCR** – OPCR calculated with molaR; **SM OPCR** – OPCR calculated with SurferManipulator.

Taxon	N	3D-OPCR (SD)	3D-OPCR CV	SM OPCR (SD)	SM OPCR CV
Catopsalis alexanderi	1	22.4 (--)	--	19.4 (--)	--
Catopsalis kakwa	2	24.2 (1.15)	0.047	16.9 (1.50)	0.089
Meniscoessus major	1	44.00 (--)	--	12.5 (--)	--
Taeniolabis taoensis	2	58.9 (9.72)	0.17	34.6 (10.9)	0.31
Valenopsalis joyneri	3	40.0 (7.01)	0.18	26.0 (1.88)	0.072

All of the SurferManipulator values are lower than the equivalent 3D-OPCR values (Table 4.5). This is expected. The distribution of SurferManipulator values differs somewhat from that of the 3D-OPCR values: *Taeniolabis taoensis* still has the highest value (34.6, SD = 10.9), but *C. alexanderi* no longer has the lowest value. Instead, *M. major* is the lowest (12.5).

This contrasts with the 3D-OPCR values where *M. major* had the second-highest value.

Furthermore, for SurferManipulator, *C. kakwa* has a lower value than *C. alexanderi.*

4.3.2.2 OPCR of m1.

The OPCR values of the m1s are much higher than those of the p4s (Figure 4.4; Table

4.6). *Taeniolabis taoensis* has the highest 3D-OPCR value (207, SD = 9.02), closely followed by

Stygimys kuszmauli (205), *C. kakwa* (203, SD = 11.2), and *Catopsalis johnstoni* (201).

Catopsalis waddleae (113) and cf. *Acheronodon* (115) have the lowest 3D-OPCR values.

Table 4.6. Mean m1 OPCR values by taxon.

Table abbreviations: N – number of specimens; **SD** – standard deviation; **CV** – coefficient of
variance; **3D-OPCR** – OPCR calculated with molaR; **SM OPCR** – OPCR calculated with
SurferManipulator.

Taxon	N	3D-OPCR (SD)	3D-OPCR CV	SM OPCR (SD)	SM OPCR CV
cf. *Acheronodon vossae*	1	115 (--)	--	77.4 (--)	--
Catopsalis alexanderi	3	140 (11.0)	0.079	80.8 (4.89)	0.060
Catopsalis cf. *calgariensis*	3	169 (18.1)	0.11	89.1 (3.31)	0.037
Catopsalis fissidens	2	157 (3.27)	0.021	92.5 (3.54)	0.038
Catopsalis johnstoni	1	201 (--)	--	76.0 (--)	--
Catopsalis kakwa	2	203 (11.2)	0.055	103 (2.65)	0.026
Catopsalis waddleae	1	113 (--)	--	78.4 (--)	--

Cimolomyid 1	2	183 (12.6)	0.069	84.6 (2.12)	0.025
Cimolomys sp.	3	152 (12.5)	0.082	77.3 (3.93)	0.051
Meniscoessus major	4	152 (16.0)	0.11	70.4 (13.7)	0.19
Mesodma sp.	4	125 (18.5)	0.15	75.2 (2.14)	0.029
Neoplagiaulacid	1	145 (--)	--	75.8 (--)	--
Ptilodus sp.	1	141 (--)	--	84.7 (--)	--
Stygimys kuszmauli	1	205 (--)	--	76.3 (--)	--
Taeniolabis taoensis	3	207 (9.02)	0.044	97.2 (7.31)	0.075
Valenopsalis joyneri	6	147 (39.2)	0.27	78.0 (15.1)	0.19

A Kruskal-Wallis H-test detected significant differences among taxa (x^2 (6) = 13.7, p = 0.033). The only significant difference is between *T. taoensis* and *Mesodma* sp. (p = 0.016) (Table 4.7), the former of which has a median 3D-OPCR of 205 and the latter of which has a median 3D-OPCR of 119 (Appendix J).

Table 4.7. Results of Dunn's post-hoc test with Bonferroni correction for m1 3D-OPCR comparisons among taxa. Significant *p*-values are in bold. α/2 = 0.025.

	C. alexanderi	*C.* cf. *calgariensis*	*Cimolomys* sp.	*M. major*	*Mesodma* sp.	*T. taoensis*
C. cf. *calgariensis*	1.00	--	--	--	--	--
Cimolomys sp.	1.00	1.00	--	--	--	--

M. major	1.00	1.00	1.00	--	--	--
Mesodma sp.	1.00	0.22	0.97	0.68	--	--
T. taoensis	0.20	1.00	1.00	1.00	**0.016**	--
V. joyneri	1.00	1.00	1.00	1.00	1.00	0.14

As with the p4s, the m1s have a lower OPCR when the values are calculated with SurferManipulator (Figure 4.5; Table 4.6). There is also less spread in the SurferManipulator data (**Error! Reference source not found.**). *Catopsalis kakwa* has the highest value (103, SD = 2.65), followed by *T. taoensis* (97.2, SD = 7.31) and *C. fissidens* (92.5, SD = 3.54). This is somewhat different from the 3D-OPCR values – *C. kakwa* and *T. taoensis* have high values regardless of method, but *C. johnstoni* and *S. kuszmauli* have low SurferManipulator values while having high 3D-OPCR values. *Catopsalis waddleae* and cf. *A. vossae* still have relatively low values, but they are no longer the lowest. In fact, *C. johnstoni* (76.0) and *S. kuszmauli* (76.3) have lower values that *C. waddleae* and cf. *A. vossae* when OPCR is calculated with SurferManipulator. Unlike the 3D-OPCR values, there are no significant differences among taxa for the SurferManipulator OPCR values. A Kruskal-Wallis test reported marginally significant differences (x^2 (6) = 12.8, p = 0.0455), but these differences were not enough to be detected by a Dunn's post-hoc test with Bonferroni correction.

4.3.2.3 OPCR of m2.

Meniscoessus robustus has the highest m2 3D-OPCR value (208) (Table 4.8). *Taeniolabis taoensis* has the second-highest value (150, SD = 39.8), which is approximately 25% less than that of *M. robustus.* Most of the other taxa have values higher than 90 and lower than 140. *Mesodma* sp. is notable for having the lowest value (72.1) of the included taxa. No

significant differences were detected when a Kruskal-Wallis test was performed (x^2 (3) = 1.98, p = 0.56).

As with the other teeth, the m2 OPCR values calculated with SurferManipulator are lower than the 3D-OPCR values (Table 4.8). *Meniscoessus robustus* and *T. taoensis* still have the highest values, but with SurferManipulator, *T. taoensis* has a higher value (111, SD = 26.5) than *M. robustus* (83.9). *Mesodma* sp. also still has the lowest value (55.0), but *V. joyneri* now also had a relatively low value (58.9, SD = 9.68). There are no significant differences among the groups included in the statistical analysis (x^2 (3) = 7.20, p = 0.066).

Table 4.8. Mean m2 OPCR values by taxon.

Table abbreviations: **N** – number of specimens; **SD** – standard deviation; **CV** – coefficient of variance; **3D-OPCR** – OPCR calculated with molaR; **SM OPCR** – OPCR calculated with SurferManipulator.

Taxon	N	3D-OPCR (SD)	3D-OPCR CV	SM OPCR (SD)	SM OPCR CV
Catopsalis alexanderi	1	127 (--)	--	64.8 (--)	--
Catopsalis calgariensis	2	99.6 (28.8)	0.29	68.2 (13.3)	0.20
Catopsalis cf. *calgariensis*	3	116 (40.2)	0.35	71.8 (19.0)	0.26
Catopsalis fissidens	2	96.5 (22.8)	0.24	71.5 (20.2)	0.28
Catopsalis kakwa	2	105 (6.72)	0.064	77.8 (0.71)	0.009
Cimolomyid 1	1	137 (--)	--	74.0 (--)	--

Cimolomys sp.	1	135 (--)	--	66.5 (--)	--
Meniscoessus major	3	130 (25.1)	0.19	74.5 (6.36)	0.085
Meniscoessus robustus	1	208 (--)	--	83.9 (--)	--
Mesodma sp.	1	72.1 (--)	--	55.0 (--)	--
Taeniolabis taoensis	3	150 (39.8)	0.27	111 (26.5)	0.24
Valenopsalis joyneri	4	119 (22.5)	0.19	58.9 (9.68)	0.16

The p4s consistently have lower OPCR values than the molars, regardless of the OPCR program used. The distribution of m1 and m2 values is not as consistent (Figure 4.4Figure 4.5). For 3D-OPCR, all taxa have lower m2 values than m1 values. Even when there are overlapping values from individual specimens, the majority of the m2s have lower values than the majority of the m1s (e.g. *C. alexanderi*, *C.* cf. *calgariensis*, *M. major*, *V. joyneri*). The SurferManipulator values generally follow the same trend, but *M. major* and *T. taoensis* have relatively high m2 values. For *T. taoensis*, the m2 values are higher than the m1 values.
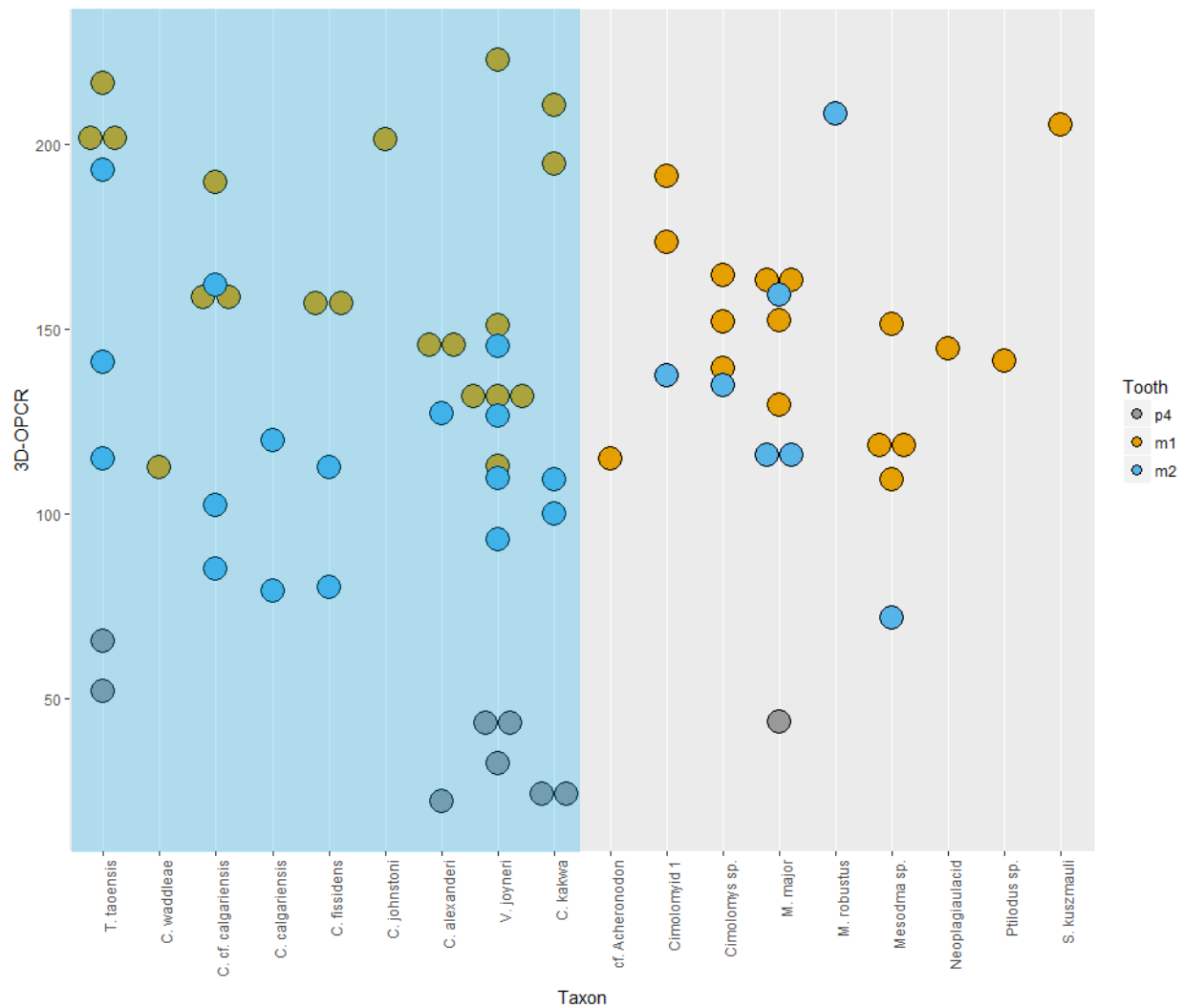
Figure 4.4. Dot plots of 3D-OPCR values by tooth and taxon. Coloured circles represent individual specimens. Grey circles are p4s, orange circles are m1s, and blue circles are m2s. Taeniolabidoids are in the shaded blue area and are organized by inferred body size, with the largest-bodied taxon (*T. taoensis*) on the left and the smallest-bodied taxon (*C. kakwa*) on the right. Non-taeniolabidoids are in the shaded grey area and are not organized by inferred body size.
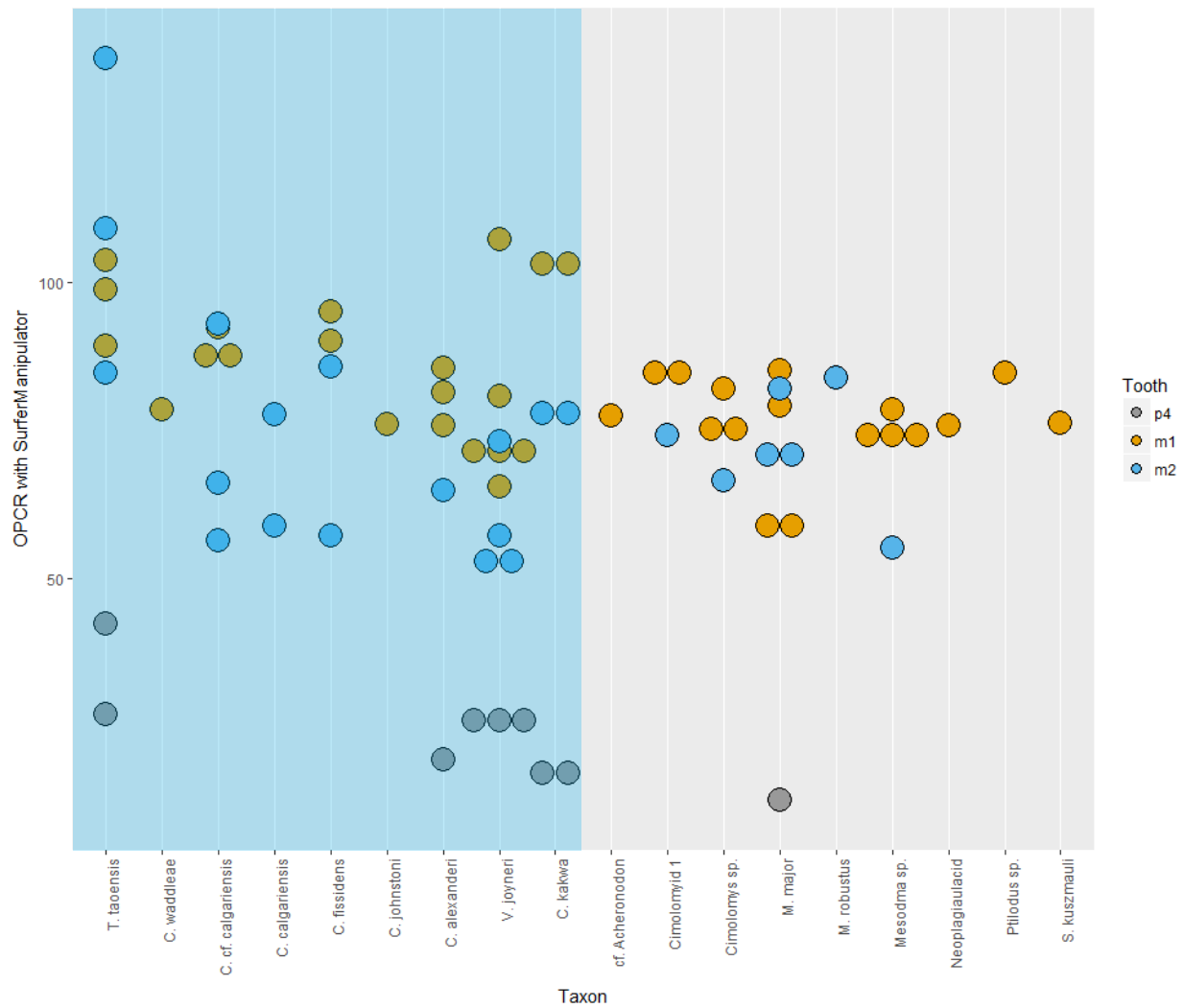
Figure 4.5. Dot plots of OPCR values (calculated in SurferManipulator) by tooth and taxon. Coloured circles represent individual specimens. Grey circles are p4s, orange circles are m1s, and blue circles are m2s. Taeniolabidoids are in the shaded blue area and are organized by inferred body size, with the largest-bodied taxon (*T. taoensis*) on the left and the smallest-bodied taxon (*C. kakwa*) on the right. Non-taeniolabidoids are in the shaded grey area and are not organized by inferred body size.

121

4.3.2.4 OPCR of tooth rows.

Taeniolabis taoensis has the highest 3D-OPCR for the whole tooth row (468, SD = 39.2) (Table 4.9). This is approximately 25% more than the second-highest 3D-OPCR value, which belongs to *C. alexanderi* (361). Of the taxa with full tooth rows, *V. joyneri* has the lowest 3D-OPCR (305, SD = 60.6). *Meniscoessus major*, the only non-taeniolabidoid included, has a 3D-OPCR value in the middle of the range (341).

Table 4.9. Mean tooth row OPCR values by taxon. Composite tooth rows are indicated with an asterisk (*).

Table abbreviations: **SD** – standard deviation; **CV** – coefficient of variance; **3D-OPCR** – OPCR calculated with molaR; **SM OPCR** – OPCR calculated with SurferManipulator

Taxon	3D-OPCR (SD)	3D-OPCR CV	SM OPCR (SD)	SM OPCR CV
Catopsalis alexanderi	361 (--)	--	198 (--)	--
Catopsalis kakwa*	332 (22.7)	0.068	198 (5.41)	0.027
Meniscoessus major	341 (--)	--	130 (--)	--
Taeniolabis taoensis	468 (39.2)	0.084	313 (28.9)	0.092
Valenopsalis joyneri*	305 (60.6)	0.20	163 (23.9)	0.15

Taeniolabis taoensis also has the highest tooth row OPCR (313, SD = 28.9) with SurferManipulator (Table 4.9). For the SurferManipulator values, the OPCR of *T. taoensis* is

approximately 50% higher than that of the next-highest taxa, *C. alexanderi* (198) and *C. kakwa* (198, SD = 5.41). *Meniscoessus major* has the lowest OPCR value (130).

4.3.3 DNE.

4.3.3.1 DNE of p4.

DNE was calculated from two sets of scans: Laplacian Smoothed scans with 0.1% outlier exclusion (LS scans) and 30-iteration smoothed scans with 5.0% outlier exclusion (30i scans). *Catopsalis alexanderi* has the lowest p4 DNE value for both sets of scans (54.6 for LS; 54.7 for 30i) and *T. taoensis* has the highest p4 DNE values for both sets of scans (368, SD = 25.9 for LS; 130, SD = 6.42 for 30i) (Table 4.10). *Valenopsalis joyneri* consistently has the second-highest p4 DNE value. *Meniscoessus major* has a higher value than *C. kakwa* for LS, but *C. kakwa* has a slightly higher value than *M. major* for 30i.

Table 4.10. Mean p4 DNE values by taxon.

SD – standard deviation; **CV** – coefficient of variance; **LS** – Laplacian Smoothing with 0.1% outlier exclusion; **30i** – 30 iterations of smoothing with 5.0% outlier exclusion.

Taxon	N	LS DNE (SD)	LS CV	30i DNE (SD)	30i CV
Catopsalis alexanderi	1	54.6 (--)	--	54.7 (--)	--
Catopsalis kakwa	2	86.2 (3.41)	0.040	67.2 (4.00)	0.059
Meniscoessus major	1	134 (--)	--	65.1 (--)	--
Taeniolabis taoensis	2	268 (25.9)	0.10	130 (6.42)	0.049
Valenopsalis joyneri	3	145 (32.7)	0.23	112 (28.5)	0.25

4.3.3.2 DNE of m1s.

The LS DNE values tend to be much higher than the 30i DNE values (Table 4.11). The LS values also have more spread, both within and among taxa (Table 4.11). The highest LS DNE value belongs to *Catopsalis kakwa* (4248, SD = 3042) and the lowest value belongs to *Mesodma* sp. (309, SD = 55.8). A Kruskal-Wallis test reported significant differences among the taxa (x^2 (6) = 17.6, p =0.007) – *Mesodma* sp. (Mdn = 298) has a significantly lower DNE value than *V. joyneri* (Mdn = 2006) (Table 4.12).

Table 4.11. Mean m1 DNE values by taxon.

Table abbreviations: **N** – number of specimens; **SD** – standard deviation; **CV** – coefficient of variance; **LS** – Laplacian Smoothing with 0.1% outlier exclusion; **30i** – 30 iterations of smoothing with 5.0% outlier exclusion.

Taxon	N	LS DNE (SD)	LS CV	30i DNE (SD)	30i CV
cf. *Acheronodon*	1	429 (--)	--	301 (--)	--
Catopsalis alexanderi	3	1161 (842)	0.73	362 (72.9)	0.20
Catopsalis cf. *calgariensis*	3	4062 (3076)	0.76	480 (96.3)	0.20
Catopsalis fissidens	2	493 (6.38)	0.013	436 (6.29)	0.014
Catopsalis kakwa	2	4248 (3042)	0.72	689 (102)	0.15
Catopsalis waddleae	1	1293 (--)	--	314 (--)	--
Cimolomyid 1	2	3850 (1176)	0.46	727 (46.5)	0.064
Cimolomys sp.	3	1253 (295)	0.24	452 (30.4)	0.067
Meniscoessus major	4	918 (464)	0.51	422 (151)	0.36

Mesodma sp.	4	309 (55.8)	0.18	295 (60.7)	0.21
Neoplagiaulacid	1	424 (--)	--	403 (--)	--
Ptilodus sp.	1	332 (--)	--	318 (--)	--
Stygimys kuszmauli	1	1263 (--)	--	498 (--)	--
Taeniolabis taoensis	3	954 (1046)	1.10	466 (127)	0.27
Valenopsalis joyneri	6	2953 (1155)	0.39	516 (71.1)	0.14

Table 4.12. Results of Dunn's post-hoc test with Bonferroni correction for m1 DNE comparisons among taxa, calculated with 0.1% outlier exclusion and Laplacian Smoothing. The significant *p*-value is in bold. α/2 = 0.025.

	C. alexanderi	*C.* cf. *calgariensis*	*Cimolomys* sp.	*M. major*	*Mesodma* sp.	*T. taoensis*
C. cf. *calgariensis*	1.00	--	--	--	--	--
Cimolomys sp.	1.00	1.00	--	--	--	--
M. major	1.00	0.78	1.00	--	--	--
Mesodma sp.	1.00	0.030	0.69	1.00	--	--
T. taoensis	1.00	0.92	1.00	1.00	1.00	--
V. joyneri	0.78	1.00	1.00	0.26	**0.003**	0.38

When 30i was used to calculate DNE, Cimolomyid 1 attained the highest value (727, SD = 46.5), although *C. kakwa* was the second highest (689, SD = 102). *Mesodma* sp. still had the

lowest value (295, SD = 60.7). There were significant differences among the 30i DNE values (x^2 (6) = 12.8, p = 0.046). Once again, the DNE of *Mesodma* sp. (Mdn = 273) was significantly lower than the DNE of *V. joyneri* (Mdn = 505) (Table 4.13).

Table 4.13. Results of Dunn's post-hoc test with Bonferroni correction for m1 DNE comparisons among taxa, calculated with 5.0% outlier exclusion and 30 iterations of smoothing. The significant *p*-value is in bold. α/2 = 0.025.

	C. alexanderi	*C.* cf. *calgariensis*	*Cimolomys* sp.	*M. major*	*Mesodma* sp.	*T. taoensis*
C. cf. calgariensis	1.00	--	--	--	--	--
Cimolomys sp.	1.00	1.00	--	--	--	--
M. major	1.00	1.00	1.00	--	--	--
Mesodma sp.	1.00	0.29	0.51	0.54	--	--
T. taoensis	1.00	1.00	1.00	1.00	0.45	--
V. joyneri	0.35	1.00	1.00	1.00	**0.013**	1.00

4.3.3.3 DNE of m2s.

The m2 LS DNE values are much higher than the m2 30i DNE values, and the LS values have a lot more spread (Figure 4.6Figure 4.7; Table 4.14). Cimolomyid 1 (6709) has the highest m2 LS DNE value, and *C. fissidens* (193, SD = 69.8) has the lowest. For the m2 30i DNE values, *M. robustus* (529) has the highest and Cimolomyid 1(524) has the second highest. *Mesodma* sp.

126

(111) has the lowest value. There were no significant differences among taxa for the m2 LS DNE values (x^2 (3) = 6.90, p = 0.075) or for m2 30i DNE values (x^2 (3) = 3.27, p = 0.35).

Table 4.14. Mean m2 DNE values by taxon.

Table abbreviations: **SD** – standard deviation; **CV** – coefficient of variance; **LS** – Laplacian Smoothing with 0.1% outlier exclusion; **30i** – 30 iterations of smoothing with 5.0% outlier exclusion.

Taxon	N	LS DNE (SD)	LS CV	30i DNE (SD)	30i CV
Catopsalis alexanderi	1	501 (--)	--	174 (--)	--
Catopsalis calgariensis	2	862 (944)	1.01	178 (38.7)	0.22
Catopsalis cf. *calgariensis*	3	3454 (2453)	0.71	315 (124)	0.39
Catopsalis fissidens	2	193 (69.8)	0.36	183 (52.5)	0.29
Catopsalis kakwa	2	3077 (3049)	0.99	365 (124)	0.34
Cimolomyid 1	1	6709 (--)	--	524 (--)	--
Cimolomys sp.	1	3056 (--)	--	444 (--)	--
Meniscoessus major	3	790 (437)	0.55	415 (172)	0.41
Meniscoessus robustus	1	1074 (--)	--	529 (--)	--
Mesodma sp.	1	210 (--)	--	111 (--)	--
Taeniolabis taoensis	3	430 (259)	0.60	293 (45.5)	0.16
Valenopsalis joyneri	4	4613 (2635)	0.57	437 (154)	0.35
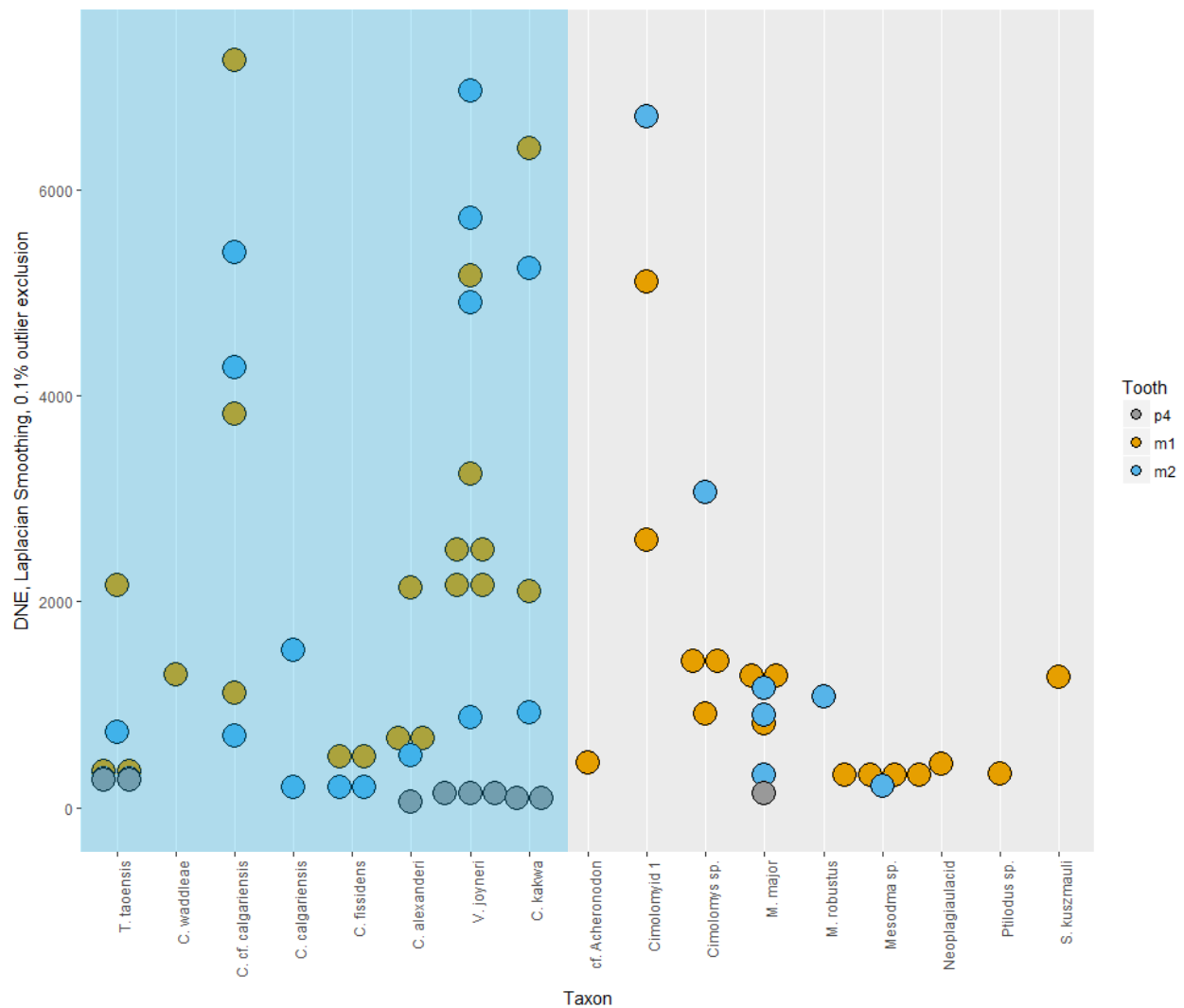
Figure 4.6. Dot plot of DNE values (Laplacian Smoothing, 0.1% outlier exclusion) by tooth and taxon. Coloured circles represent individual specimens. Grey circles are p4s, orange circles are m1s, and blue circles are m2s. Taeniolabidoids are in the shaded blue area and are organized by inferred body size, with the largest-bodied taxon (*T. taoensis*) on the left and the smallest-bodied taxon (*C. kakwa*) on the right. Non-taeniolabidoids are in the shaded grey area and are not organized by inferred body size.
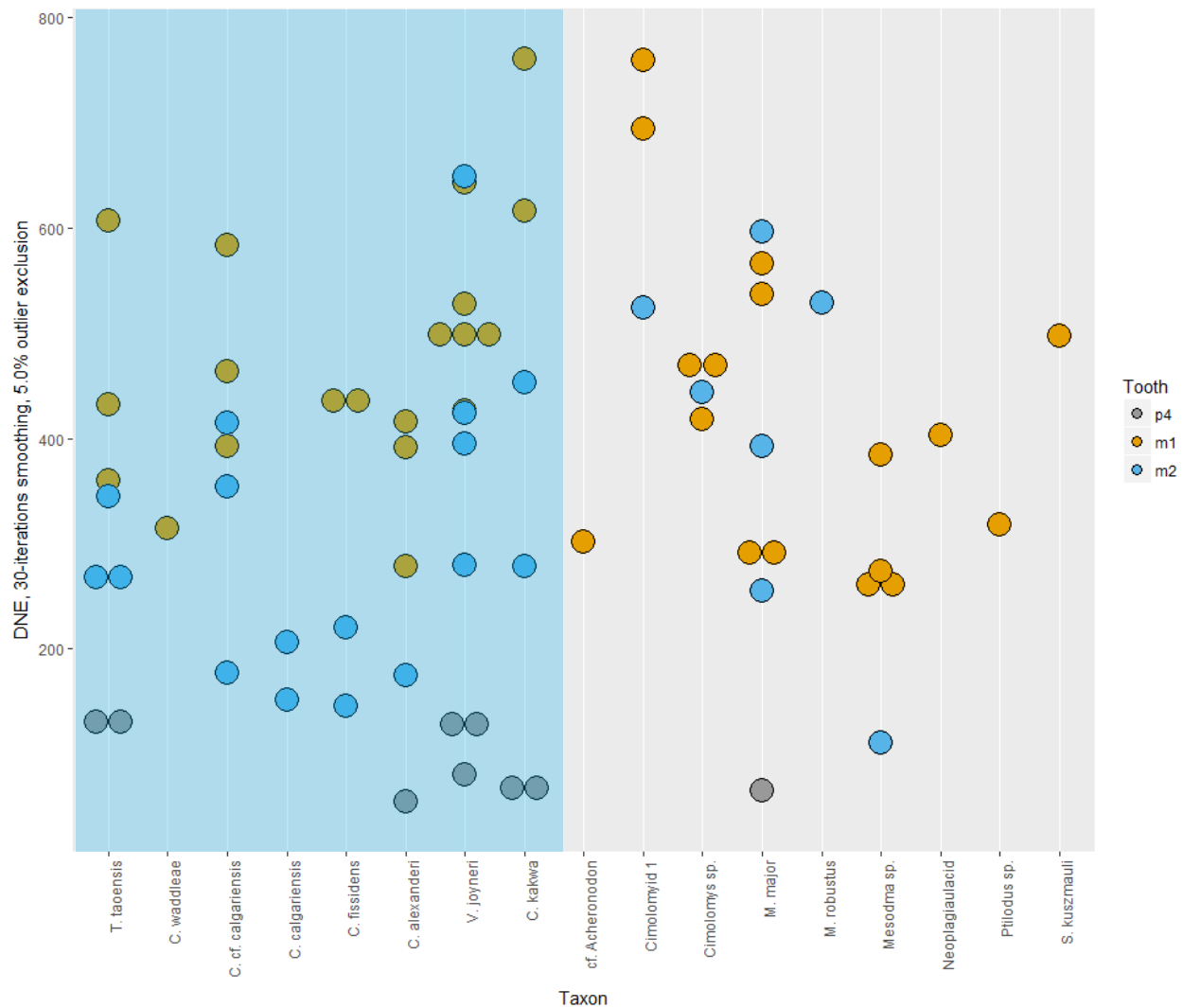
Figure 4.7. Dot plots of DNE values (30 iterations of smoothing, 5.0% outlier exclusion) by tooth and taxon. Coloured circles represent individual specimens. Grey circles are p4s, orange circles are m1s, and blue circles are m2s. Taeniolabidoids are in the shaded blue area and are organized by inferred body size, with the largest-bodied taxon (*T. taoensis*) on the left and the smallest-bodied taxon (*C. kakwa*) on the right. Non-taeniolabidoids are in the shaded grey area and are not organized by inferred body size.

When DNE is calculated using the LS scans, the p4s have relatively low values, but there is some overlap between p4 and molar values for individual specimens (Figure 4.6). The m1s and m2s tend to have similar values. The is more separation of DNE values by tooth for the 30i scans. The p4s have distinctly lower values for all taxa, and the m2s often have lower values than the m1s (Figure 4.7).

4.3.4 Comparisons among dental topographic measures.

The distribution of p4 DTA values varies among taxa (Figure 4.8). For example, *C. alexanderi* is the only taxon with consistently low DTA values. *Catopsalis kakwa* has a high RFI value, but low OPCR and DNE values. Conversely, *T. taoensis* has a low RFI value and high OPCR and DNE values. *Meniscoessus major* has a high RFI, mid-range OPCR value, and low DNE value. *Valenopsalis joyneri* also has a high RFI value a mid-range OPCR value, but it has a high DNE value.

The m1 OPCR and DNE values are similar in their distributions (Figure 4.9): taxa with relatively low OPCR values also have relatively low DNE values. The one exception is *T. taoensis*, which has some of the highest OPCR values but has mid-range DNE values. RFI values do not have the same distribution as the OPCR and DNE values. Some taxa, such as cf. *A. vossae, Mesodma* sp., and *C. waddleae*, have relatively high RFI values while having very low OPCR and DNE values. Conversely, *T. taoensis* has the lowest RFI value, but has relatively high OPCR and DNE values. Still other taxa have consistently high RFI, OPCR, and DNE values (*C. kakwa*, *Cimolomys* sp.). There are no taxa with consistently low values.

The m2 DTA values follow a pattern similar to those of the m1s: taxa with lower OPCR values tend to have lower DNE values too (Figure 4.10). *Taeniolabis taoensis* once again has a relatively high OPCR value compared to its DNE value. *Catopsalis alexanderi* also has a

130

relatively high m2 OPCR value, which is not something that was observed in the m1s. The RFI

values seem to be more closely correlated with the OPCR and DNE values for the m2s.

However, there are a few exceptions: *C. kakwa* and *Mesodma* sp. have high RFI values but mid-

to low-range OPCR and DNE values. Conversely, *M. robustus* has a low RFI value but very high

OPCR and DNE values.

The RFI and OPCR values calculated in this study can be used to infer multituberculate

diets through comparisons to published datasets (Table 4.15). Isolated p4s are included in these

comparisons, but it should be noted that the p4s are involved in the slicing-crushing part of the

multituberculate masticatory cycle while the m1s and m2s are involved in the grinding part of

the cycle (Krause, 1982). OPCR comparisons can only be made with the OPCR values calculated

by SurferManipulator: there are currently no published datasets of lower molar 3D-OPCR values

for multiple dietary categories. DNE comparisons cannot be made because, in this study, the

DNE values calculated with the standard parameters are unrealistically high (Appendix I).

Table 4.15. Inferred dietary categories of multituberculate taxa based on a comparison to

therian RFI and OPCR values. RFI and individual tooth OPCR values are compared to

values from Boyer (2008) and Winchester et al. (2014). OPCR tooth row values are

compared to values from Evans et al. (2007).

Table abbreviations: Am – ambiguous; **AD-Om** – animal-dominated omnivore; **F** – folivore;

Fr – frugivore; **H** – herbivore; **HO** – hard-object feeder; **In** – insectivore; **PD-OM** – plant-

dominated omnivore. Asterisk (*) indicates a value outside the range reported for extant taxa.

Taxon	Tooth	RFI	RFI Diet	OPCR	OPCR Tooth Diet	OPCR Row	OPCR Tooth Row Diet
cf. *Acheronodon*	m1	0.53	Am/F/Fr/ Om	77.4	Fr/HO	--	--
Catopsalis alexanderi	p4	0.48	Am/Om	19.4	F/Fr*		
Catopsalis alexanderi	m1	0.43	Am/Fr	80.8	Fr/HO	198	PD-Om/H
Catopsalis alexanderi	m2	0.39	Fr/HO	64.8	Fr/HO/ In		
Catopsalis calgariensis	m2	0.42	Fr	68.2	Fr/HO/ In		
Catopsalis cf. *calgariensis*	m1	0.51	Am/F/Fr/ Om	89.1	Fr/HO		
Catopsalis cf. *calgariensis*	m2	0.48	Am/Om	71.8	Fr/HO		
Catopsalis fissidens	m1	0.43	Am/Fr	92.5	HO		
Catopsalis fissidens	m2	0.39	Fr/HO	71.5	Fr/HO		

Catopsalis johnstoni	m1	0.54	Am/F/Fr/ Om	76.0	Fr/HO		
Catopsalis kakwa	p4	0.66	F/In	16.9	F/Fr*		
Catopsalis kakwa	m1	0.58	F/In	103	HO*	198	PD-Om/H
Catopsalis kakwa	m2	0.66	F/In	77.8	Fr/HO		
Catopsalis waddleae	m1	0.54	Am/F/Fr/ Om	78.4	Fr/HO		
Cimolomyid 1	m1	0.59	F/In	84.6	Fr/HO		
Cimolomyid 1	m2	0.62	F/In	74.0	Fr/HO		
Cimolomys sp.	m1	0.54	Am/F/Fr/ Om	77.3	Fr/HO		
Cimolomys sp.	m2	0.50	Am/F/Fr/ Om	66.5	Fr/HO/ In		
Meniscoessus major	p4	0.69	F/In	12.5	F/Fr*		
Meniscoessus major	m1	0.49	Am/F/Fr/ Om	70.4	Fr/HO	130	C/AD-Om
Meniscoessus major	m2	0.55	F/In/Om	74.5	Fr/HO		
Meniscoessus robustus	m2	0.43	Am/Fr	83.9	Fr/HO		

Mesodma sp.	m1	0.47	Am/F/Fr/ Om	75.2	Fr/HO		
Mesodma sp.	m2	0.54	Am/F/Fr/ Om	55.0	F/Fr/ HO/In/ Om		
Neoplagiaulacid	m1	0.51	Am/F/Fr/ Om	75.8	Fr/HO		
Ptilodus sp.	m1	0.49	Am/F/Fr/ Om	84.7	Fr/HO		
Stygimys kuszmauli	m1	0.53	Am/F/Fr/ Om	76.3	Fr/HO		
Taeniolabis taoensis	p4	0.54	Am/F/Fr/ Om	34.6	F/Fr/ HO		
Taeniolabis taoensis	m1	0.37	Fr/HO	97.2	HO*	313	H*
Taeniolabis taoensis	m2	0.38	Fr/HO	111	HO*		
Valenopsalis joyneri	p4	0.65	F/In	26.0	F/Fr*	163	AD- Om/PD-Om
Valenopsalis joyneri	m1	0.57	F/In	78.0	Fr/HO		

Valenopsalis	m2	0.57	F/In	58.9	F/Fr/
joyneri					HO/In/
					Om
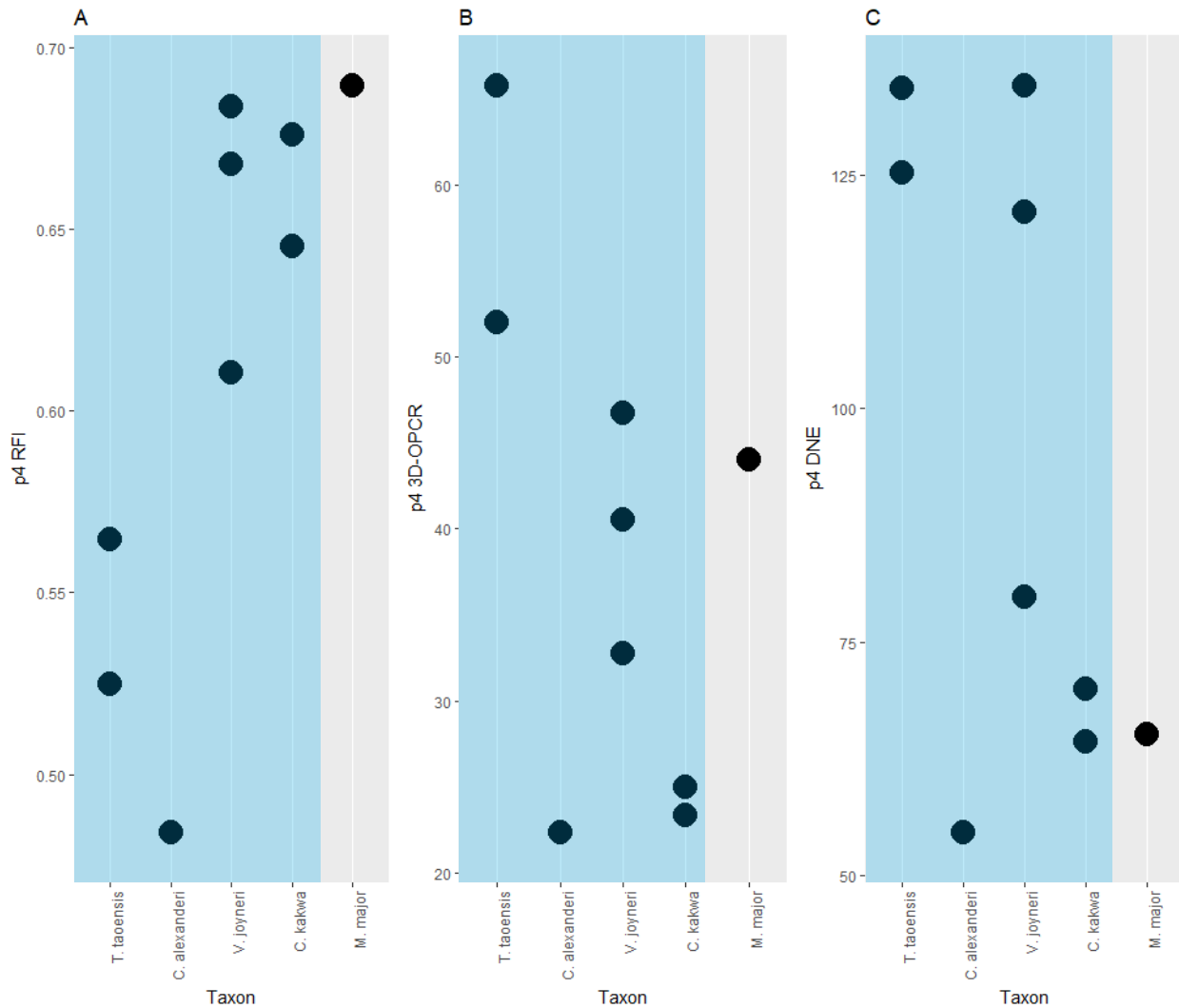
Figure 4.8. Dot plots of p4 A) RFI values B) 3D-OPCR values C) DNE values (30 iterations of smoothing, 5.0% outlier exclusion) by taxon. Taeniolabidoids are in the shaded blue area and are organized by inferred body size, with the largest-bodied taxon (*T. taoensis*) on the left and the smallest-bodied taxon (*C. kakwa*) on the right. The non-taeniolabidoid *M. major* is in the shaded grey area.
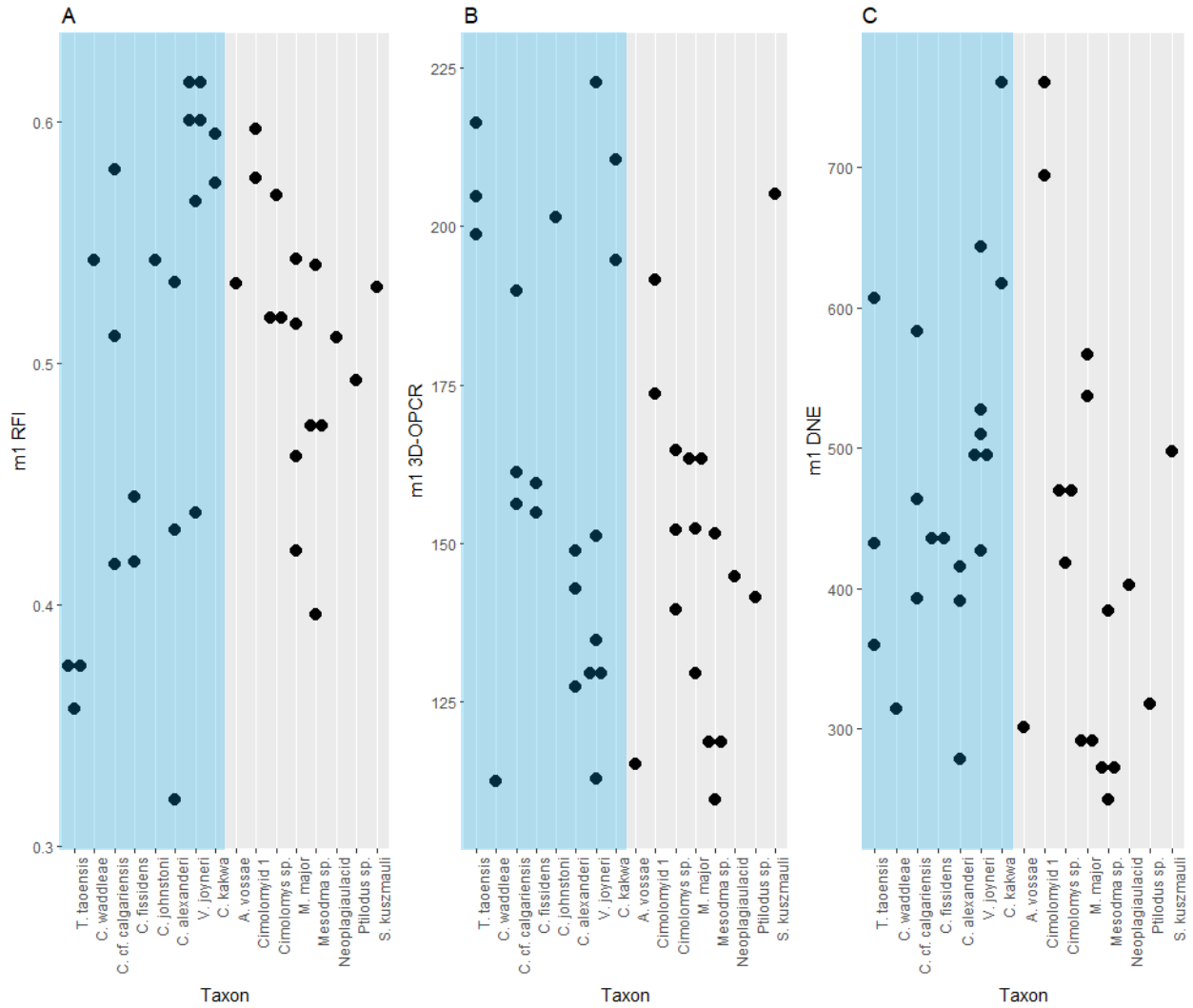
Figure 4.9. Dot plots of m1 A) RFI values B) 3D-OPCR values C) DNE values (30 iterations of smoothing, 5.0% outlier exclusion) by taxon. Taeniolabidoids are in the shaded blue area and are organized by inferred body size, with the largest-bodied taxon (*T. taoensis*) on the left and the smallest-bodied taxon (*C. kakwa*) on the right. The non-taeniolabidoids are in the shaded grey area and are not ordered by inferred body size.
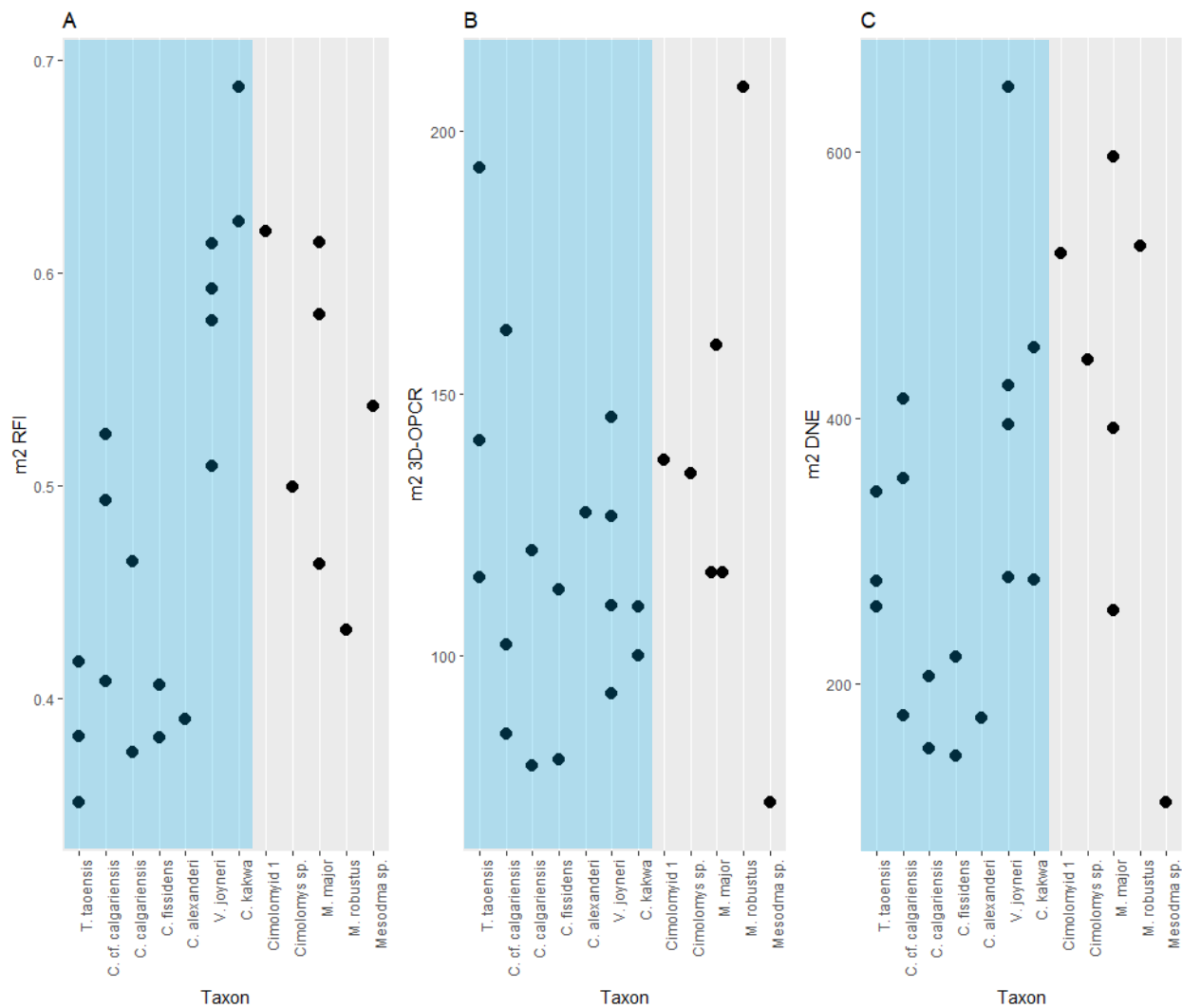
Figure 4.10. Dot plots of m2 A) RFI values B) 3D-OPCR values C) DNE values (30 iterations of smoothing, 5.0% outlier exclusion) by taxon. Taeniolabidoids are in the shaded blue area and are organized by inferred body size, with the largest-bodied taxon (*T. taoensis*) on the left and the smallest-bodied taxon (*C. kakwa*) on the right. The non-taeniolabidoids are in the shaded grey area and are not ordered by inferred body size.

4.4 Discussion.

DTA can be used to make predictions about multituberculate diets, but these predictions may not always be accurate. RFI, OPCR, and DNE are all somewhat phylogenetically

138

interdependent (Winchester et al., 2014). Therefore, there are inherent problems in comparing multituberculate DTA values to those of therian mammals; there is a chance that the values are not equivalent between the groups. Furthermore, RFI and DNE values have only been calculated for isolated teeth, typically m2s, and the m2s of multituberculates are not necessarily homologous to the m2s of therians. Table 4.15 shows that multituberculate m1s and m2s typically have values indicative of the same dietary category when the same metric is used, but there are some exceptions (e.g. *C. fissidens* RFI values). When multiple metrics are used, dietary classifications often differ among the metrics (Table 4.15). Some very broad statements can be made (e.g. more complex teeth tend to be better at processing tough foods), but dietary categories are assigned tentatively. Furthermore, because ranges often vary among groups (Winchester et al., 2014), it is difficult to say what amount of disparity indicates a true difference in diet. Thus, a discussion of multituberculate DTA values must be approached with caution.

4.4.1 RFI.

RFI values follow a consistent pattern in multituberculates: taxa with relatively low RFI values for one tooth usually have relatively low RFI values for all the teeth in the tooth row. Within a taxon, the p4s tend to have higher RFI values than the molars (Figure 4.3). This is understandable given that multituberculate p4s have a small occlusal footprint relative to their crown surface area.

The m1s and m2s do differ in their RFI values, but the differences are fairly minor (Figure 4.3). Often, there is just as much intra-molar variation as there is inter-molar variation for a taxon. This suggests that the m1s and m2s performed similar functions in the tooth row, unlike the p4s.

Euarchontan RFI values have a range of less than 0.20 for any one dietary category, regardless of clade (Boyer, 2008; Bunn et al., 2011; Winchester et al., 2014). This indicates that RFI values have a consistent spread, although non-euarchontan RFI data are needed to determine if this pattern truly holds. Based on the euarchontan ranges, the amount of variation observed in the multituberculate data is high for a single dietary category, at least when the molars are considered (Figure 4.3). This suggests that multiple dietary categories may be represented in this study. The significant difference between the *T. taoensis* and *V. joyneri* m1 values further supports this conclusion. There would likely be significant differences among more taxa (e.g. *T. taoensis* compared to *C. kakwa* and Cimolomyid 1) if larger sample sizes were available.

Based on trends in euarchontan data, higher RFI values indicate diets rich in fibers and structural carbohydrates (Boyer, 2008). This would mean that some taxa, namely *V. joyneri*, *C. kakwa*, and Cimolomyid 1, were eating more fibers and/or structural carbohydrates than other taxa, namely *T. taoensis*, *C. fissidens*, and *C. alexanderi*. The rest of the taxa have RFI values that fall in-between these end-members. Whether the diets of these intermediate taxa were more similar to those of the *V. joyneri* cohort or the *T. taoensis* cohort cannot be folivores and insectivores based on therian data, while *T. taoensis*, *C. fissidens*, and *C. alexanderi* would be classified as frugivores and hard-object eaters (Table 4.15). The intermediate taxa would be classified as omnivores, folivores, or frugivores (Table 4.15).

4.4.2 OPCR.

OPCR was calculated in two different ways: SurferManipulator was used to calculate OPCR from 2.5D scans, while molaR was used to calculate 3D-OPCR from fully 3D scans. Differences in scan-dimensionality and downsampling mean that OPCR results from SurferManipulator and molaR are not directly comparable (Pampush et al., 2016a).

SurferManipulator consistently produces lower results than molaR in the present study (Appendix H), which concurs with the published literature (Pampush et al., 2016a). The distribution of values among the taxa also differs between the two programs. As an example, when calculated with molaR, the 3D-OPCR of the *C. alexanderi* p4 is lower than the 3D-OPCR of the *M. major* p4 (Table 4.5). When calculated with SurferManipulator, the *M. major* p4 has a lower value than the *C. alexanderi* p4. Similar differences are seen with the molars. These discrepancies likely result from scan trimming; undercuts must be removed before scans can be processed in SurferManipulator. Trimming the scans removes some of the surface, which in turn removes some of the patches. Some teeth must be trimmed more than others, so patch removal is not consistent across specimens. Furthermore, difficulties with program compatibility resulted in the scans being manually trimmed, which introduced an extra element of human error. The molaR results are probably a more accurate measure OPCR given that the molaR scans did not require extra trimming. However, most published studies have used SurferManipulator to calculate OPCR, so these values are necessary when making comparisons to the published literature.

Comparisons to published literature are particularly problematic for OPCR because high OPCR values are not always indicative of the same diets, even in eutherians. Relatively high OPCR values have been consistently recovered for folivores, but they have also been recovered for some frugivores (Santana et al., 2011; Winchester et al., 2014), insectivores (Bunn et al., 2011; Winchester et al., 2014), and hard-object eaters (Winchester et al., 2014). This is a problem because in other groups, relatively low OPCR values have been found for frugivores (Godfrey et al., 2012; Winchester et al., 2014), insectivores (Evans et al., 2007), and seed-eaters (Thiery et al., 2017). Hypercarnivores and carnivores seem to have the lowest values, but even

these values may not be consistent across groups (Evans et al., 2007; Smits and Evans, 2012). Ranges of OPCR values also vary among diets and clades (Bunn et al., 2011; Winchester et al., 2014; Ungar et al., 2018). Based on these discrepancies, perhaps the most that can be said about OPCR is that higher OPCR values are correlated with an increased ability to process tough foods.

4.4.2.1 Individual teeth.

The p4s have much lower OPCR values than the molars. This is understandable given that p4s have fewer (if any) cusps and, in most cases, a preponderance of large planar surfaces. Molars have many more cusps and fewer large planar surfaces. Because higher patch counts are associated with an increased ability to process tough foods (Evans et al., 2007), it stands to reason that multituberculate molars were more equipped for breaking down tough foods than multituberculate premolars were. It also stands to reason that multituberculates with higher molar OPCR values had molars that were better-able to process tough foods. For example, *Mesodma* sp. has a relatively low m2 OPCR (55.0 from SurferManipulator) while *T. taoensis* has a relatively high m2 OPCR (111, SD = 26.5 from SurferManipulator). This indicates that *T. taoensis* had a greater ability to process tough foods.

The spread of data for both m1s and m2s is higher with 3D-OPCR, and there are more differences between the m1 and m2 values. There is also a significant difference between the *Mesodma* sp. and *T. taoensis* m1 3D-OPCR values but not between their m1 OPCR SurferManipulator values. This indicates that 3D-OPCR is more sensitive to small differences in patch counts, which may also mean that 3D-OPCR is more informative about processing capabilities. If statistically significant differences are biologically meaningful, then other taxa with low 3D-OPCR values, such as cf. *A. vossae* and *C. waddleae,* may have had teeth that were

142

less equipped to handle tough items than taxa with high m1 3D-OPCR values, such as *S. kuszmauli*, *C. kakwa*, and *C. johnstoni*.

Many studies have used isolated cheek teeth to examine the OPCR of eutherians. When considering these results, it appears that the multituberculate p4s have lower OPCR values than most eutherian cheek teeth (Boyer et al., 2010; Bunn et al., 2011; Godfrey et al., 2012; Evans and Janis, 2014; Winchester et al., 2014; Prufrock et al., 2016b; Thiery et al., 2017; Berthaume et al., 2018; López-Torres et al., 2018; Ungar et al., 2018). The only species that falls into the eutherian OPCR range is *T. taoensis*, and this is on the low-end of the range. The multituberculate molars have OPCR values comparable to the eutherian teeth. All of the included multituberculate molars have values equivalent to, if not greater than, those of euarchontan folivores (Winchester et al., 2014). The multituberculates would be classified as folivores, frugivores, and hard-object feeders based on their molar OPCR values (Table 4.15).

4.4.2.2 Tooth rows.

Of the five taxa with full tooth rows included in this study, *T. taoensis* has the highest OPCR value from both SurferManipulator and molaR. However, the rest of the taxa do not follow the same patterns. *Catopsalis kakwa* and *V. joyneri* have lower 3D-OPCR values than *M. major*, but higher SurferManipulator OPCR values than *M. major*. *Catopsalis alexanderi* has a higher 3D-OPCR than *C. kakwa*, but the two species have identical OPCR values from SurferManipulator. These differences are probably a result of scan trimming, as with the individual teeth. OPCR values for single dietary categories can have ranges of more than 100 when full tooth rows are considered (Evans et al., 2007), and the overall range of OPCR values for the included multituberculate taxa (excepting *T. taoensis*) is far less than 100, so the discrepancies are probably not a point of concern.

The OPCR of multituberculate tooth rows has been calculated once before (Wilson et al., 2012). The SurferManipulator value for *T. taoensis* (313, SD = 28.9) is similar to that recovered by Wilson et al. (2012) (OPCR = 347.625). The OPCR value for *C. alexanderi* found in this study (198) is also similar to the one recovered by Wilson et al. (2012) (OPCR = 215.125). The values in this study are slightly lower, probably because of the manual removal of undercuts.

Wilson et al. (2012) suggested that the high OPCR values of *T. taoensis* and *C. alexanderi* indicated herbivory, while the low OPCR values of many other taxa indicated carnivory and omnivory. It is true that the values of *T. taoensis* and *C. alexanderi* fall into (or above) the herbivore range for extant carnivorans and rodents while other taxa fall into the carnivore/omnivore range (Evans et al., 2007). At the time of Wilson et al. (2012), the phylogenetic-dependence of OPCR was not yet realized; a comparison between multituberculates and extant therians was reasonable given the available data. Admittedly, the relatively high OPCR values of *T. taoensis* and *C. alexanderi* (along with others, such as *M. robustus*) do suggest that these taxa were processing different foods than taxa with very low OPCR values. The trouble lies in making predictions about multituberculate diets based on the OPCR ranges of eutherians – for example, *Ctenacodon serratus* (OPCR = 84.375) has an OPCR of a eutherian hypercarnivore (Evans et al., 2007; Wilson et al., 2012), but this does not mean that *C. serratus* was actually a hypercarnivore: it means is that *C. serratus* did not have as much cusp complexity as *T. taoensis* and was therefore probably not consuming substances with the same structural properties as *T. taoensis*.

4.4.3 DNE.

Traditionally, DNE is calculated using scans that have been iteratively smoothed and then processed with either Implicit Fairing or Laplacian Smoothing (Pampush et al., 2016a;

Winchester, 2016). The top 0.1% of Dirichlet Normal Energies are then excluded from the final

DNE value in an effort to eliminate outliers (Pampush et al., 2016a; Winchester, 2016). Concerns

have been raised about using these smoothing techniques (Spradley et al., 2017) and exclusion

criteria (Berthaume et al., 2018), especially when fossils are being studied (Berthaume et al.,

2018). My own analysis has demonstrated that the "standard" smoothing and exclusion

parameters produce unrealistic results. A detailed explanation of this can be found in Appendix

H . More realistic DNE values are obtained when scans are smoothed for 30 iterations (without

Implicit Fairing or Laplacian Smoothing) and a 5.0% outlier exclusion is used. Unfortunately,

these modified parameters make comparisons difficult because most DNE studies have used the

"standard" parameters. However, the scans processed with the "standard" parameters are also

unhelpful – the highest euarchontan DNE values currently known are slightly above 350 (Bunn

et al., 2011; Winchester et al., 2014; Thiery et al., 2017), while many multituberculates have

values over 1000 (Table 4.11, Table 4.14). These high energy values are clearly a result of

outlier inclusion, not biologically meaningful curvature (Appendix H). Therefore, direct

comparisons to published data will not be attempted for DNE. All further discussion of DNE in

this study refers to the values obtained through 30 iterations of smoothing and 5.0% outlier

exclusion.

The multituberculate p4s consistently have lower DNE values than the molars (Figure 4.7).

This is not surprising given that DNE measures tooth curvature – visual inspection shows that

multituberculate p4s do not have as much curvature as multituberculate molars. The taxon with

the highest p4 DNE – *T. taoensis* – also has the most rounded p4 (Granger and Simpson, 1929).

Similarly, the m2s tend to have lower DNE values than the m1s: within a taxon, the m2s have

fewer cusps than the m1s (e.g. Granger and Simpson, 1929; Clemens and Kielan-Jaworowska,

1979; Kielan-Jaworowska et al., 2004; Weil and Krause, 2008). This means that the m2s have fewer inflection points with high curvature.

A more interesting result is the distribution of molar DNE values across taxa. Some taxa, such as *Mesodma* sp., have consistently lower values than other taxa, such as Cimolomyid 1 and *V. joyneri*. These differences are probably indicative of true differences in tooth curvature. High DNE values are typically found in taxa that process structural carbohydrates, such as insectivores and folivores (Bunn et al., 2011; Winchester et al., 2014). Therefore, the multituberculates with higher DNE values may have been consuming more structural carbohydrates, or other substances with similar properties. However, not much more can be said about the multituberculate DNE values given the parameters used in this study.

4.4.4 Comparisons among dental topographic measures.

4.4.4.1 *p4*.

Multituberculate p4s have an inconsistent distribution of DTA values. *Catopsalis alexanderi* has low values for all DTA metrics, suggesting that its p4 has low relief, little curvature, and few facets. This is different from the other small-bodied taeniolabidoids. *Catopsalis kakwa* has a high RFI value, but low OPCR and DNE values, while *V. joyneri* has high RFI and DNE values, along with a mid-range OPCR value. The DTA results of *C. kakwa* are easily explained – the *C. kakwa* p4 is relatively tall and narrow (high RFI), and it lacks some of the cuspules found on other taeniolabidoid p4s (low OPCR, DNE) (Scott et al., 2018). The differences between *C. alexanderi* and *V. joyneri* are more surprising because the two species have similar p4 morphologies (Middleton, 1982). The *C. alexanderi* p4 was in the middle stage of wear, so some of the tooth topography may have been lost, leading to lower values. A larger sample of *C. alexanderi* p4s would help clarify the discrepancies.

Taeniolabis taoensis is the only large taeniolabidoid with a p4 included in the analysis.

Taeniolabis taoensis has a low p4 RFI and a high p4 OPCR and DNE. This is again

understandable given the morphology of *T. taoensis* p4s. The teeth are fairly short (low RFI), but

they are rounded with many cuspules (high OPCR, DNE) (Granger and Simpson, 1929).

The only non-taeniolabidoid p4 included was the p4 of *M. major*. The p4 of *M. major* is

tall and laterally compressed (Fox, 1980), which explains its high RFI value. The tooth has a

serrated apical edge, but the sides are essentially flat planes (Fox, 1980), which means that it has

some facets but very little curvature. This is probably why *M. major* has a mid-range OPCR

value and a low DNE value.

4.4.4.2 Lower molars.

The molars usually have both high OPCR and DNE values, or both low OPCR and DNE

values. This can be explained by the molar morphology. Multituberculate molars are dominated

by rows of cusps, so an increase in cusp complexity or number will increase both the number of

facets and the amount of curvature of the tooth. This also explains why the m1s, which have

more cusps than the m2s, have higher OPCR and DNE values. *Taeniolabis taoensis* is an

interesting exception to the OPCR/DNE correlation – *T. taoensis* has relatively high OPCR

values compared to DNE values for both m1s and m2s. This suggests that the molars of *T.*

taoensis have facets that do not greatly contribute to tooth curvature.

The RFI values of m1 and m2 (particularly m1) do not align with the OPCR and DNE

values. This is unusual given that RFI and DNE are usually more closely correlated to each other

than either is to OPCR (Bunn et al., 2011; Winchester et al., 2014). In multituberculates, many

taxa have molars with high RFI values compared to their OPCR and DNE values. This would

suggest that the teeth have a lot of occlusal relief but relatively simple cusps. *Taeniolabis*

taoensis and *M. robustus* are the reverse, with a low RFI but high OPCR/DNE. *Taeniolabis taoensis* molars have broad bases with blunt cusps (Granger and Simpson, 1929), so the low RFI is understandable. The higher OPCR/DNE values can be explained by the bulbous nature of the cusps, as well as the frequent addition of auxiliary cuspules (Granger and Simpson, 1929). *Meniscoessus robustus* has extremely crescentic molar cusps that form posteriorly-oriented crescentic wear facets (Clemens, 1964; Fox, 1980; Archibald, 1982). This unusual cusp shape and wear pattern is likely the cause of the high *M. robustus* OPCR and DNE values. The taxa with high RFI, OPCR, and DNE values (e.g. *C. kakwa*, *Cimolomys* sp.) appear to have molars with high relief, relatively complex cusps, and lots of tooth curvature.

RFI, OPCR, and DNE values are not consistent within the taeniolabidoids, even when body size is considered (Figure 4.9Figure 4.10). For example, within the large-bodied taeniolabidoids (*C. calgariensis*, *C.* cf. *calgariensis*, *C. waddleae*, *T. taoensis*), *T. taoensis* and *C. waddleae* have opposite results: *T. taoensis* has a low RFI but a high OPCR and DNE while *C. waddleae* has a high RFI but a low OPCR and DNE. The small-bodied taeniolabidoids (*C. alexanderi*, *C. kakwa*, *V. joyneri*) are equally dissimilar, as are the intermediate taeniolabidoids (*C. johnstoni*, *C. fissidens*). The distribution of values is not even consistent between the m1s and m2s of a single species, and there is often a large range of values for a single tooth (e.g. DNE of *V. joyneri* m2s).

Disparate DTA measures are found within the non-taeniolabidoid cimolodontans too. This disparity may be explained by the morphology of multituberculate molars. Multituberculate teeth are not as consistent in their morphologies as therian teeth: specimens of a single multituberculate species can have different cusp counts and crown shapes (e.g. Granger and Simpson, 1929; Clemens and Kielan-Jaworowska, 1979; Kielan-Jaworowska et al., 2004). This

148

is a problem because DTA quantifies aspects of morphology. Changes to cusp count and crown shape can influence topographic metrics, as evidenced by differences in DTA values across wear stages (Pampush et al., 2016b). Therefore, some of the intra-taxon disparity observed in the present study is quite likely a result of inconsistent tooth morphologies. The problem may be accentuated by the measurement of isolated teeth; tooth row complexity may be more consistent than individual tooth complexity within a species. However, such a comparison was not in the scope of this study.

4.4.5 Dental topographic analysis as a dietary proxy.

DTA values are often used to make dietary inferences about extinct clades. Given the disparity of DTA values in this study, it is clear that the inferences would differ depending on which metric was used (Table 4.15). For example, based on therian RFI values, *C. kakwa* was an insectivore/folivore, but based on OPCR values from the same dataset, *C. kakwa* was a frugivore/hard-object eater (Winchester et al., 2014). Furthermore, *C. kakwa* and *T. taoensis* would be placed in different dietary categories based on their RFI values, but the two taxa would be placed in the same category based on their OPCR values (Winchester et al., 2014). In some cases, the same taxon would even be placed in different categories depending on which molar is used: the m1 OPCR value of *V. joyneri* is equivalent to that of a primate frugivore/hard-object feeder, but the m2 OPCR value of *V. joyneri* is low enough that it falls into an ambiguous range of values that correspond to insectivores, folivores, and omnivores, as well as frugivores and hard-object feeders (Winchester et al., 2014).

The current study brings some conclusions from a previous multituberculate study (Wilson et al., 2012) into question. Wilson et al. (2012) applied OPCR to multituberculate specimens and used the resultant values to make dietary inferences about the studied taxa. Using OPCR alone, it

would appear that species such as *T. taoensis* and *C. alexanderi* were herbivorous while others, such as *Mesodma* sp., were carnivorous (including insectivory) or were animal-dominated omnivores (Wilson et al., 2012). However, based on the present study, OPCR alone may not be the best predictor of diet. In fact, based on the RFI results from the present study, *Mesodma* sp. was either insectivorous or folivorous, while *T. taoensis* and *C. alexanderi* were likely frugivorous (Boyer, 2008; Winchester et al., 2014). Furthermore, when calculated with the "standard" parameters, both *Mesodma* sp. and *T. taoensis* have DNE values characteristic of insectivores and folivores (both strongly leaning toward insectivory) and *C. alexanderi* has values exceeding those of extant insectivores.

4.5 Summary and Conclusions

DTA metrics do not produce consistent results when applied to multituberculate teeth: RFI, OPCR, and DNE each have a unique pattern of variation along the tooth row and among taxa. Compared to the molars, the p4s have lower OPCR and DNE values and higher RFI values. Within the molars, the m1s have higher DTA values than the m2s. The RFI values of the p4s increase with increasing body size, but otherwise, there is no clear relationship between DTA values and body size. Furthermore, the taeniolabidoids and non-taeniolabidoids do not have noticeably different DTA values. This is contrary to what was expected given differences in taeniolabidoid and non-taeniolabidoid molar morphology. However, the categorizations are not always implausible. For example, both RFI and OPCR (DNE was not use for comparisons) were used to recovered *T. taoensis* as a frugivore or hard-object eater – this categorization is conceivable given the reduced p4, bulbous and blunt molar cusps, and (inferred) strong temporalis muscles of *T. taoensis* (Broom, 1914; Granger and Simpson, 1929; Miao, 1988; Gambaryan and Kielan-Jaworowska, 1995).

In extant mammals, DTA metrics are not equally useful for categorizing diets (Bunn et al., 2011; Winchester et al., 2014), and there are a few instances of contradictory results among the metrics (Ledogar et al., 2013; Winchester et al., 2014; Pampush et al., 2016b; Ungar et al., 2018). Furthermore, OPCR may only work well on full tooth rows (Boyer et al., 2010; Winchester et al., 2014; Pampush et al., 2016b). Given these problems, it is unsurprising that multituberculates do not have consistent trends in their DTA values. The disparity of values is almost certainly an indication of different dietary niches, but little can be said about which niches are represented. This demonstrates a fundamental problem with DTA in its current state –DTA has not been used to fully explore the niches and morphospace of extant therians, so the relationships among metrics are poorly understood. Even when phylogenetic dependence is ignored, DTA is still difficult to apply to non-therians because the reference dataset is incomplete. This is not to say that DTA has no place in paleontology. DTA can be very informative, as evidenced by its use in many fossil studies (Boyer et al., 2010; Boyer and Lipman, 2012; Wilson et al., 2012; Ledogar et al., 2013; Prufrock et al., 2016b, 2016a; Thiery et al., 2017; Berthaume et al., 2018; López-Torres et al., 2018). However, all but one of these studies involved euarchontans, which have a well-established dataset of DTA values of extant taxa. The limits of DTA need to be better understood and a more robust dataset of extant mammals needs to be developed before conclusions about distantly-related extinct clades are made.

4.6 Literature Cited

Allen, K. L., S. B. Cooke, L. A. Gonzales, and R. F. Kay. 2015. Dietary inference from upper and lower molar morphology in platyrrhine primates. PLoS ONE 10:1–22.

Archibald, J. D. 1982. A study of Mammalia and geology across the Cretaceous-Tertiary

boundary in Garfield County, Montana. University of California Publications in Geological

Sciences 122:1–286.

Berthaume, M. A., and K. Schroer. 2017. Extant ape dental topography and its implications for

reconstructing the emergence of early *Homo*. Journal of Human Evolution 112:15–29.

Berthaume, M. A., L. K. Delezene, and K. Kupczik. 2018. Dental topography and the diet of

Homo naledi. Journal of Human Evolution 118:14–26.

Boyer, D. M. 2008. Relief index of second mandibular molars is a correlate of diet among

prosimian primates and other euarchontan mammals. Journal of Human Evolution 55:1118–

1137.

Boyer, D. M., and Y. Lipman. 2012. Earliest record of *Platychoerops* (Primates, Plesiadapidae),

a new species from Mouras Quarry, Mont de Berru, France. American Journal of Physical

Anthropology 149:329–346.

Boyer, D. M., A. R. Evans, and J. Jernvall. 2010. Evidence of dietary differentiation among late

paleocene-early eocene plesiadapids (Mammalia, Primates). American Journal of Physical

Anthropology 142:194–210.

Broom, R. 1914. On the sturcture and affinities of the Multituberculata. Bulletin of The

American Museum of Natural History.

Bunn, J. M., and P. S. Ungar. 2009. Dental topography and diets of four old world monkey

species. American Journal of Primatology 71:466–477.

Bunn, J. M., D. M. Boyer, Y. Lipman, E. M. St. Clair, J. Jernvall, and I. Daubechies. 2011.

Comparing Dirichlet normal surface energy of tooth crowns, a new technique of molar

shape quantification for dietary inference, with previous methods in isolation and in

combination. American Journal of Physical Anthropology 145:247–261.

Cignoni, P., M. Callieri, M. Corsini, M. Dellepiane, F. Ganovelli, and G. Ranzuglia. 2008.
MeshLab: an open-source mesh processing tool. Proceedings of the 2008 Eurographics
Italian Chapter Conference 978-3–9056:129–136.

Clemens, W. A. 1964. Fossil mammals of the type Lance Formation, Wyoming: Part I.
Introduction and Multituberculata. University of California Publications in Geological
Sciences 48:1–105.

Clemens, W. A., and Z. Kielan-Jaworowska. 1979. Multituberculata; pp. 99–149 in J. A.
Lillegraven, Z. Kielan-Jaworowska, and W. A. Clemens (eds.), Mesozoic mammals: the
first two-thirds of mammalian history. University of California Press, Berkeley.

Dennis, J. C., P. S. Ungar, M. F. Teaford, and K. E. Glander. 2004. Dental topography and molar
wear in *Alouatta palliata* From Costa Rica. American Journal of Physical Anthropology
161:152–161.

Evans, A. R., and J. Jernvall. 2009. Patterns and constraints in carnivoran and rodent dental
complexity and tooth size. Journal of Vertebrate Paleontology 29:24A.

Evans, A. R., and C. M. Janis. 2014. The evolution of high dental complexity in the horse
lineage. Annales Zoologici Fennici 51:73–79.

Evans, A. R., G. P. Wilson, M. Fortelius, and J. Jernvall. 2007. High-level similarity of
dentitions in carnivorans and rodents. Nature 445:78–81.

Fox, R. C. 1980. Mammals from the Upper Cretaceous Oldman formation, Alberta. II. *Pediomys*
Marsh (Marsupialia). Canadian Journal of Earth Sciences 16:103–113.

Gambaryan, P. P., and Z. Kielan-Jaworowska. 1995. Masticatory musculature of Asian
taeniolabidoid multituberculate mammals. Acta Palaeontol. Pol. 40:45–108.

Godfrey, L. R., J. M. Winchester, S. J. King, D. M. Boyer, and J. Jernvall. 2012. Dental topography indicates ecological contraction of lemur communities. American Journal of Physical Anthropology 148:215–227.

Granger, W., and G. G. Simpson. 1929. A revision of the Tertiary Multituberculata. Bulletin of the American Museum of Natural History 56:601–676.

Janis, C. M., and A. Weil. 2008. Non-eutherian Mammal Summary; pp. 7–18 in C. M. Janis, G. F. Gunnell, and M. D. Uhen (eds.), Evolution of Tertiary Mammals of North America. Volume 2: Small Mammals, Xenarthrans, and Marine Mammals. Cambridge University Press, New York.

Jernvall, J., and L. Selänne. 1999. Laser confocal microscopy and geographic information systems in the study of dental morphology. Palaeontologia Electronica 2:1–17.

Keller, J. S. 2014. Dental ecometrics predict trophic categories of North American rodents. GSA Annual Meeting in Vancouver, British Columbia 289–11A

Kielan-Jaworowska, Z., R. L. Cifelli, and Z.-X. Luo. 2004. Mammals from the Age of Dinosaurs: Origins, Evolution, and Structure. Columbia University Press, New York, 630 pp.

King, S. J., S. J. Arrigo-Nelson, S. T. Pochron, G. M. Semprebon, L. R. Godfrey, P. C. Wright, and J. Jernvall. 2005. Dental senescence in a long-lived primate links infant survival to rainfall. Proceedings of the National Academy of Sciences 102:16579–16583.

Krause, D. W. 1982. Jaw movement, dental function, and diet in the Paleocene multituberculate Ptilodus. Paleobiology 8:265–281.

Ledogar, J. A., J. M. Winchester, E. M. St. Clair, and D. M. Boyer. 2013. Diet and dental topography in pitheciine seed predators. American Journal of Physical Anthropology

150:107–121.

López-Torres, S., K. R. Selig, K. A. Prufrock, D. Lin, and M. T. Silcox. 2018. Dental

topographic analysis of paromomyid (Plesiadapiformes, Primates) cheek teeth: more than

15 million years of changing surfaces and shifting ecologies. Historical Biology 30:76–88.

Lucas, S. G., T. E. Williamson, and M. D. Middleton. 1997. *Catopsalis* (Mammalia:

Multituberculata) from the Paleocene of New Mexico and Utah: taxonomy and

biochronological significance. Journal of Paleontology 71:484–493.

M'Kirera, F., and P. S. Ungar. 2003. Occlusal relief changes with molar wear in *Pan troglodytes

troglodytes* and *Gorilla gorilla gorilla*. American Journal of Primatology 60:31–41.

Merceron, G., S. Taylor, R. Scott, Y. Chaimanee, and J.-J. Jaeger. 2006. Dietary characterization

of the hominoid *Khoratpithecus* (Miocene of Thailand): evidence from dental topographic

and microwear texture analyses. Naturwissenschaften 93:329–333.

Miao, D. 1988. Skull morphology of *Lambdopsalis bulla* (Mammalia, Multituberculata) and its

implications to mammalian evolution. Contributions to Geology, University of Wyoming,

Special Paper 4:1–104.

Middleton, M. D. 1982. A new species and additional material of *Catopsalis* (Mammalia,

Multituberculata) from the Western Interior of North America. Journal of Paleontology

56:1197–1206.

Pampush, J. D., J. M. Winchester, P. E. Morse, A. Q. Vining, D. M. Boyer, and R. F. Kay.

2016a. Introducing molaR: a new R package for quantitative topographic analysis of teeth

(and other topographic surfaces). Journal of Mammalian Evolution 23:397–412.

Pampush, J. D., J. P. Spradley, P. E. Morse, A. R. Harrington, K. L. Allen, D. M. Boyer, and R.

F. Kay. 2016b. Wear and its effects on dental topography measures in howling monkeys

(*Alouatta palliata*). American Journal of Physical Anthropology 161:705–721.

Prufrock, K. A., D. M. Boyer, and M. T. Silcox. 2016a. The first major primate extinction: An evaluation of paleoecological dynamics of North American stem primates using a homology free measure of tooth shape. American Journal of Physical Anthropology 159:683–697.

Prufrock, K. A., S. López-Torres, M. T. Silcox, and D. M. Boyer. 2016b. Surfaces and spaces: troubleshooting the study of dietary niche space overlap between North American stem primates and rodents. Surface Topography: Metrology and Properties 4:024005.

Reed, D. N. 1997. Contour mapping as a new method for interpreting diet from tooth morphology. American Journal of Physical Anthropology Supplemental 24:194.

Santana, S. E., S. Strait, and E. R. Dumont. 2011. The better to eat you with: Functional correlates of tooth structure in bats. Functional Ecology 25:839–847.

Scott, C. S., A. Weil, and J. M. Theodor. 2018. A new, diminutive species of *Catopsalis* (Mammalia, Multituberculata, Taeniolabidoidea) from the early Paleocene of southwestern Alberta, Canada. Journal of Paleontology 1–15.

Smits, P. D., and A. R. Evans. 2012. Functional constraints on tooth morphology in carnivorous mammals. BMC Ecolutionary Biology 12:1–11.

Spradley, J. P., J. D. Pampush, P. E. Morse, and R. F. Kay. 2017. Smooth operator: The effects of different 3D mesh retriangulation protocols on the computation of Dirichlet normal energy. American Journal of Physical Anthropology 163:94–109.

Strait, S. G. 1993. Molar morphology and food texture among small-bodied insectivorous mammals. American Society of Mammalogists 74:391–402.

R Core Team (2016). R: A language and environment for statistical computing. R Foundation for Statistical Computing, Vienna, Austria. https://www.R-project.org/.

Thiery, G., G. Gillet, V. Lazzari, G. Merceron, and F. Guy. 2017. Was *Mesopithecus* a seed eating colobine? Assessment of cracking , grinding and shearing ability using dental topography. Journal of Human Evolution 112:79–92.

Ulhass, L., O. Kuhmer, F. Schrenk, and W. Henke. 2004. A new 3-d approach to determine functional morphology of cercopithecoid molars. Annals of Anatomy 186:487–493.

Ungar, P. 2004. Dental topography and diets of *Australopithecus afarensis* and early *Homo*. Journal of Human Evolution 46:605–622.

Ungar, P., and M. Williamson. 2000. Exploring the effects of tooth wear on functional morphology: a preliminary study using dental topographic analysis. Palaeontologia Electronica 3:1–18.

Ungar, P. S., C. Healy, A. Karme, M. Teaford, M. Fortelius, P. S. Ungar, C. Healy, A. Karme, M. Teaford, and M. Fortelius. 2018. Dental topography and diets of platyrrhine primates. Historical Biology 30:1–12.

Ungar, P. S., and F. M'Kirera. 2003. A solution to the worn tooth conundrum in primate functional anatomy. Proceedings of the National Academy of Sciences 100:3874–3877.

Ungar, P. S., and J. M. Bunn. 2008. Primate dental topographic analysis and functional morphology; pp. 253–265 in J. D. Irish and G. C. Nelson (eds.), Techniques and Application in Dental Anthropology. Cambridge University Press, New York.

Venkataraman, V. V, H. Glowacka, J. Fritz, M. Clauss, C. Seyoum, N. Nguyen, and P. J. Fashing. 2014. Effects of dietary fracture toughness and dental wear on chewing efficiency in Geladas (*Theropithecus gelada*). American Journal of Physical Anthropology 32:17–32.

Weil, A., and D. W. Krause. 2008. Multituberculata; pp. 19–38 in C. M. Janis, G. F. Gunnell,

and M. D. Uhen (eds.), Evolution of Tertiary Mammals of North America. Volume 2: Small
Mammals, Xenarthrans, and Marine Mammals. Cambridge University Press, New York.

Wilson, G. P., A. R. Evans, I. J. Corfe, P. D. Smits, M. Fortelius, and J. Jernvall. 2012. Adaptive
radiation of multituberculate mammals before the extinction of dinosaurs. Nature 483:457–
460.

Winchester, J. M. 2016. MorphoTester: An open source application for morphological
topographic analysis. PLoS ONE 1–18.

Winchester, J. M., D. M. Boyer, E. M. St. Clair, A. D. Gosselin-Ildari, S. B. Cooke, and J. A.
Ledogar. 2014. Dental topography of platyrrhines and prosimians: Convergence and
contrasts. American Journal of Physical Anthropology 153:29–44.

Yamashita, N., F. P. Cuozzo, M. L. Sauther, E. Fitzgerald, A. Riemenschneider, and P. S. Ungar.
2016. Mechanical food properties and dental topography differentiate three populations of
Lemur catta in southwest Madagascar. Journal of Human Evolution 98:66–75.

Zuccotti, L. F., M. D. Williamson, W. F. Limp, and P. S. Ungar. 1998. Technical note:
Modelling primate occlusal topography using Geographic Information Systems technology.
American Journal of Physical Anthropology 107:137–142.

Chapter Five: Conclusions

In this thesis, a variety of dietary proxies were applied to a sample of North American cimolodontan multituberculates. The goal was to determine if there were detectable dietary differences among North American taeniolabidoids, specifically between the small-bodied and large-bodied taxa, and between taeniolabidoids and non-taeniolabidoid cimolodontans.

Previous studies have used shearing ratios (SRA), Orientation patch count (OPC), and dental microwear as proxies for multituberculate diet. Christensen (2012) classified two large-bodied cimolodontans, *Taeniolabis taoensis* and *Meniscoessus robustus*, as herbivores based on their microwear signals and SRA values. Wilson et al. (2012) also classified *T. taoensis* as an herbivore, this time based on OPC values. One small-bodied taeniolabidoid, *Catopsalis alexanderi*, was also classified as an herbivore based on its OPC value (Wilson et al., 2012). *Meniscoessus robustus* was classified as a plant-dominated omnivore rather than an herbivore (Wilson et al., 2012).

Given these previous studies, I elected to use dental microwear analysis, SRA, and dental topographic analysis (DTA – includes Relief Index (RFI), Orientation Patch Count Rotated (OPCR), Dirichlet Normal Energy (DNE)) to infer diet. Dental microwear was counted from scanning electron microscope (SEM) images of the specimens. SRA was calculated using photographs of the specimens taken with a Dino-Lite digital microscope. DTA was calculated from computed tomography (CT) scans of the specimens. The values produced by each dietary proxy were compared among the studied taxa and, when possible, to published datasets.

5.1 Correlations with Taeniolabidoid Body Size

There are very few body-size-specific differences in the dietary proxies. All taeniolabidoids have similar microwear scratch-to-pit ratios, regardless of body size. The large-bodied taeniolabidoids (*T. taoensis*, *Catopsalis calgariensis*, *Catopsalis* cf. *calgariensis*) do have slightly lower fine-to-coarse microwear ratios than the smaller taeniolabidoids, which could indicate that the larger taeniolabidoids were consuming relatively resistant substances, but the differences are minor and may be a result of low sample size.

Premolar OPCR and DNE values do not appear to have any correlation with taeniolabidoid body size. The p4 SRA and RFI values do have a correlation with body size – the small-bodied taeniolabidoids (*Catopsalis kakwa*, *Valenopsalis joyneri*) have higher p4 SRA and RFI values than the large-bodied taeniolabidoids (*Catopsalis* cf. *calgariensis*, *T. taoensis*). RFI has been described as a three-dimensional shearing quotient (M'Kirera and Ungar, 2003; Dennis et al., 2004), and SRA and RFI are often highly correlated (Bunn et al., 2011; Winchester et al., 2014), so the similarity in distributions is unsurprising. The relatively high SRA and RFI values mean that the p4s of the small-bodied taeniolabidoids had more shearing ability and topographic relief than the p4s of the large-bodied taeniolabidoids.

The m1 SRA values are also correlated with body size: the large-bodied taeniolabidoids have higher m1 SRA values than the smaller taeniolabidoids. However, this pattern is not present in the m2 SRA values, or in any of the DTA values. This lack of correlation suggests that differences in taeniolabidoid molar morphologies are not closely tied to body size. The differences may be influenced by phylogeny, but correcting for phylogenetic-dependence was not possible in the present study.

5.2 Differences between Taeniolabidoids and Non-taeniolabidoids

Taeniolabidoids and non-taeniolabidoids have a similar spread of SRA and DTA values. Most of the differences between the studied taeniolabidoids and non-taeniolabidoids come from dental microwear analysis. Taeniolabidoids have lower scratch-to-pit ratios and fine-to-coarse feature ratios than the non-taeniolabidoids. These differences suggest that taeniolabidoids were consuming more resistant substances and less exogenous grit than the non-taeniolabidoids. However, the differences are small, and a larger sample size is needed to determine if they are significant.

One unexpected result of the microwear analysis was the microwear signal detected on *Mesodma* sp. Two included specimens of *Mesodma* sp. have much higher scratch-to-pit ratios than all other specimens in the analysis. Similarly, one specimen of *Mesodma* sp. has a much higher fine-to-coarse feature ratio than all other specimens. This disparity suggests that some of the included *Mesodma* sp. specimens come from the Cretaceous while others come from the Paleocene: a significant change in microwear signal across the K-Pg boundary has been observed for *Mesodma thompsoni* (Weil and Pignataro, 2007a-b). Weil and Pignataro (2007a-b) suggested that this change in microwear indicates that *Mesodma thompsoni* was a generalist. It is interesting to note that *Mesodma* sp. also has the lowest molar OPCR and DNE values of the studied taxa. This means that, compared to the other included multituberculates, *Mesodma* sp. has "simpler" molars with fewer facets and less curvature.

5.3 Differences Along the Tooth Row

Premolar microwear was not documented in this study, and molar microwear was not differentiated by tooth position, so microwear cannot be compared along the tooth row.

161

However, CRR and DTA values were calculated for individual cheek teeth. The molars of the studied multituberculates have higher OPCR, and DNE values, but lower RFI values, than the p4s. This means that multituberculate molars have less topographic relief than the p4s, despite having more facets and more curvature. The discrepancy between RFI and DNE indicates that the two metrics are not always highly correlated and illustrates how the DTA values of multituberculate molars differ from those of euarchontans.

The included m1s tend to have higher CRR and DTA values than m2s, but the relative size of the m1 and m2 values is fairly consistent: for example, taxa with relatively high m1 values usually also have relatively high m2 values. OPCR and DNE seem to be more highly correlated with each other than either is to RFI, meaning that teeth with more facets also tend to have more curvature, but not necessarily more topographic relief. CRR also appears to be more highly correlated with OPCR and DNE than RFI. This means that molars with longer crest rows also tend to have more facets and more curvature.

The variation in values between the m1s and m2s and across metrics illustrates a problem with applying CRR and DTA to multituberculates: the values are usually calculated from isolated teeth. This approach works well when the teeth are homologous and are from closely-related clades, but the homologies of multituberculate and therian teeth are not well established (Janis and Weil, 2008). Given the unclear homologies and the differences in CRR/DTA values along the molar row, it is best not to compare individual multituberculate and therian teeth to each other. Full tooth row comparisons may be more informative. Unfortunately, OPCR is the only metric that has been calculated using full tooth rows at present and, for some metrics, the inclusion of p4 in the tooth row may lead to a different signal given that multituberculate p4s are involved in a different part of the multituberculate masticatory cycle (Krause, 1982).

162

5.4 Dietary Proxies and Gross Morphology

Dental, cranial, and post-cranial evidence suggest that taeniolabidoids were occupying different ecological niches than non-taeniolabidoids. Taeniolabidoids have reduced premolars and bulbous molar cusps with predominately apical wear (Granger and Simpson, 1929; Miao, 1986; Kielan-Jaworowska et al., 2004). Conversely, non-taeniolabidoid cimolodontans tend to have arcuate blade-like p4s, and the molar cusps of non-taeniolabidoid cimolodontans tend to wear laterally and medially (Kielan-Jaworowska et al., 2004). These morphological differences indicate that taeniolabidoid cheek teeth were engaged in more grinding than non-taeniolabidoid cheek teeth. Furthermore, taeniolabidoids may have had a relatively strong medial temporalis, which is one of the masticatory muscles used for crushing and grinding (Broom, 1914; Granger and Simpson, 1929; Miao, 1988; Gambaryan and Kielan-Jaworowska, 1995). Based on crania and post-crania, taeniolabidoids are inferred to have been terrestrial (and possibly fossorial) (Miao, 1988; Kielan-Jaworowska and Qi, 1990; Kielan-Jaworowska and Gambaryan, 1994), while some non-taeniolabidoids are inferred to have been scansorial (Simpson and Elftman, 1928; Jenkins and Krause, 1983; Krause and Jenkins, 1983). These features suggest that taeniolabidoids were terrestrial herbivores, while some non-taeniolabidoid cimolodontans may have been scansorial omnivores or insectivores (Kielan-Jaworowska et al., 2004; Weil and Krause, 2008).

The microwear signals recovered in this study were unexpected given the inferred locomotor modes of taeniolabidoids (terrestrial/fossorial) and non-taeniolabidoids (scansorial). Typically, organisms feeding closer to the ground (e.g. terrestrial organisms) have higher scratch-to-pit ratios than those feeding in trees (e.g. scansorial organisms) (Teaford and Walker, 1984; Solounias and Semprebon, 2002). However, some extant ground squirrels do have

163

relatively high pit and coarse feature frequencies compared to scansorial squirrels (Nelson et al., 2005), meaning that the taeniolabidoid microwear signal is not unheard of for small-bodied terrestrial mammals. The signal is also plausible given that taeniolabidoid cheek teeth are relatively well-adapted for grinding resistant materials.

The DTA results were also unexpected given the morphological differences between the taeniolabidoids and non-taeniolabidoids. Based on the DTA values, the taeniolabidoids and non-taeniolabidoids have the same dietary categories, and the taxa often have "intermediate" DTA values that are indicative of multiple diets (Table 4.15). Even so, there are some consistencies in classification. For example, *T. taoensis* is classified as a frugivore/hard-object eater based on both RFI and individual tooth OPCR values. It is conceivable that *T. taoensis* engaged in frugivory and hard-object eating given the dental morphology of the taxon. This dietary classification also aligns with the *T. taoensis* microwear signal. However, the metrics are not always so consistent – *M. major* is classified in an ambiguous category of folivores, frugivores, omnivores, and insectivores based on its RFI values, but it is classified as a frugivore or hard-object eater based on its individual OPCR values, and the microwear signal of *M. major* suggest relatively little consumption of resistant items. The cheek teeth of *M. major* are not as well-adapted for grinding as the cheek teeth of the taeniolabidoids, so it stands to reason that *M. major* would have a different microwear signal and different DTA values than the taeniolabidoids. The ambiguity of the *M. major* classifications (and similar ambiguity for many of the other taxa) may be the result of phylogenetic-dependence and unclear homologies. However, it may also be an indication that multituberculate dentitions are not as specialized as those of therians, and that many multituberculates were generalists. This interpretation concurs with Weil and Pignataro's

164

(2007a-b) suggestion that *Mesodma* and *Cimexomys* microwear signals changed across the K-Pg boundary because the taxa were generalists.

5.5 Conclusions and Future Directions

None of the dietary proxies used in this thesis were able to detect clear and consistent differences in the included taxa. This could mean that the included taxa all had similar diets, or it could mean that the selected dietary proxies are not good a discriminating among multituberculate diets. These findings also suggest that some previous conclusions made about multituberculate diets (Christensen, 2012; Wilson et al., 2012) may need to be re-examined.

The dental microwear analysis did detect some small differences among taxa, but strong conclusions could not be drawn because of insufficient sample size. More specimens need to be included in the analysis to determine whether the observed differences are significant. Microwear should also be compared between first and second molars, and between anterior and posterior cusps. These comparisons will help determine if microwear varies along the multituberculate tooth row.

Shearing ratios (CRR in this study) may not be a good proxy for multituberculate diets because multituberculate molars do not have shearing crests. More work needs to be done to determine whether multituberculate CRR values are actually a measure of shearing ability before CRR can be applied as a dietary proxy.

DTA was not good at discriminating among the multituberculates in this study. This suggests that, in its present state, dental topographic analysis may not be a good dietary proxy for multituberculates. Multituberculates may have had more generalist diets than therians, but this cannot be determined until a much more robust dataset of extant taxa needs to be developed, and

relationships among the metrics need to be better understood. Furthermore, there may be some problems in applying DTA to isolated teeth, especially given that multituberculate molars are not homologous to therian molars. A better approach may be to compare tooth row values. OPCR is currently the only metric that has been calculated from full tooth rows, and OPCR values are more strongly correlated with dietary categories when full tooth rows are used (Evans et al., 2007; Bunn et al., 2011; Winchester et al., 2014). Now, RFI, and DNE values need to be calculated from full tooth rows so that similar comparisons can be made. Multituberculate DTA values can be revisited once tooth rows values are calculated, the relationships among metrics are better understood, and a larger comparative dataset is established.

5.6 Literature Cited

Broom, R. 1914. On the sturcture and affinities of the Multituberculata. Bulletin of The American Museum of Natural History 33:115–134.

Bunn, J. M., D. M. Boyer, Y. Lipman, E. M. St. Clair, J. Jernvall, and I. Daubechies. 2011. Comparing Dirichlet normal surface energy of tooth crowns, a new technique of molar shape quantification for dietary inference, with previous methods in isolation and in combination. American Journal of Physical Anthropology 145:247–261.

Christensen, H. B. 2012. Mammalian adaptation to herbivory in the aftermath of the KT extinction. The University of Chicago, 112 pp.

Dennis, J. C., P. S. Ungar, M. F. Teaford, and K. E. Glander. 2004. Dental topography and molar wear in *Alouatta palliata* from Costa Rica. American Journal of Physical Anthropology 161:152–161.

Evans, A. R., G. P. Wilson, M. Fortelius, and J. Jernvall. 2007. High-level similarity of

dentitions in carnivorans and rodents. Nature 445:78–81.

Gambaryan, P. P., and Z. Kielan-Jaworowska. 1995. Masticatory musculature of Asian taeniolabidoid multituberculate mammals. Acta Palaeontol. Pol. 40:45–108.

Granger, W., and G. G. Simpson. 1929. A revision of the Tertiary Multituberculata. Bulletin of the American Museum of Natural History 56:601–676.

Janis, C. M., and A. Weil. 2008. Non-eutherian Mammal Summary; pp. 7–18 in C. M. Janis, G. F. Gunnell, and M. D. Uhen (eds.), Evolution of Tertiary Mammals of North America. Volume 2: Small Mammals, Xenarthrans, and Marine Mammals. Cambridge University Press, New York.

Jenkins, F. A. J., and D. W. Krause. 1983. Adaptations for climbing in North American multituberculates (Mammalia). Science, New Series 220:712–715.

Kielan-Jaworowska, Z., and T. Qi. 1990. Fossorial adaptations of a taeniolabidoid multituberculate mammal from the Eocene of China. Vertebrata PalAsiatica 28:81–94.

Kielan-Jaworowska, Z., and P. P. Gambaryan. 1994. Postcranial anatomy and habits of Asian multituberculate mammals. Fossils & Strata 36:1–92.

Kielan-Jaworowska, Z., R. L. Cifelli, and Z.-X. Luo. 2004. Mammals from the Age of Dinosaurs: Origins, Evolution, and Structure. Columbia University Press, New York, 630 pp.

Krause, D. W. 1982. Jaw movement, dental function, and diet in the Paleocene multituberculate *Ptilodus*. Paleobiology 8:265–281.

Krause, D. W., and F. A. J. Jenkins. 1983. The postcranial skeleton of North American multituberculates. Bulletin of the Museum of Comparative Zoology 150:199–246.

Miao, D. 1986. Dental anatomy and ontogeny of *Lambdopsalis bulla* (Mammalia,

Multituberculata). Contributions to Geology, University of Wyoming 24:65–76.

Miao, D. 1988. Skull morphology of *Lambdopsalis bulla* (Mammalia, Multituberculata) and its

implications to mammalian evolution. Contributions to Geology, University of Wyoming,

Special Paper 4:1–104.

M'Kirera, F., and P. S. Ungar. 2003. Occlusal relief changes with molar wear in Pan troglodytes

troglodytes and Gorilla gorilla gorilla. American Journal of Primatology 60:31–41.

Nelson, S., C. Badgley, and E. Zakem. 2005. Microwear in modern squirrels in relation to diet.

Palaeontologia Electronica 8:1–15.

Simpson, G. G., and H. O. Elftman. 1928. Hind limb musculature and habits of a Paleocene

multituberculate. American Museum Novitates 333:1–19.

Solounias, N., and G. Semprebon. 2002. Advances in the reconstruction of ungulate

ecomorphology with application to early fossil equids. American Museum Novitates

3366:1–49.

Teaford, M. F., and A. Walker. 1984. Quantitative differences in dental microwear between

primate species with different diets and a comment on the presumed diet of *Sivapithecus*.

American Journal of Physical Anthropology 64:191–200.

Weil, A., and F. Pignataro. 2007a. Dietary inferences from dental microwear in multituberculate

mammals from the Hell Creek and Tullock formations of Eastern Montana. Journal of

Vertebrate Paleontology 27:163A–164A.

Weil, A., and F. Pignataro. 2007b. Dental microwear in multituberculate mammals and dietary

change across the K/T boundary in Eastern Montana. Journal of Morphology 268:1148A.

Wilson, G. P., A. R. Evans, I. J. Corfe, P. D. Smits, M. Fortelius, and J. Jernvall. 2012. Adaptive

radiation of multituberculate mammals before the extinction of dinosaurs. Nature 483:457–

460.

Winchester, J. M., D. M. Boyer, E. M. St. Clair, A. D. Gosselin-Ildari, S. B. Cooke, and J. A. Ledogar. 2014. Dental topography of platyrrhines and prosimians: Convergence and contrasts. American Journal of Physical Anthropology 153:29–44.

Appendix A: Specimen Spatiotemporal Information

Institutional abbreviations: **AMNH** – American Museum of Natural and Cultural History (New York, NY, USA); **NMMNH** – New Mexico Museum of Natural History and Science (Albuquerque, NM, USA); **ROM** – Royal Ontario Museum (Toronto, ON, Canada); **TMP** – Royal Tyrrell Museum of Palaeontology (Drumheller, AB, Canada); **UALVP** – University of Alberta Laboratory for Vertebrate Paleontology (Edmonton, AB, Canada); **UCM** – University of Colorado Museum of Natural History (Boulder, CO, USA); **UM** – University of Michigan Museum of Paleontology (Ann Arbor, MI, USA); **UW** – University of Wyoming Geological Museum (Laramie, WY, USA).

Table abbreviations: **Ma** – mega-annum; **NALMA** – North American Land Mammal Age

Species	Specimen Number	Locality	NALMA	Series/Epoch	Reference
cf. *Acheronodon*	TMP 2015.069.0174	Trainspotting locality, Paskapoo formation, AB	earliest Tiffanian (Ti1)	Late Paleocene	TMP Database
Catopsalis alexanderi	TMP 1987.151.0027	Alexander locality (UCM locality 77267), Denver Formation, Arapahoe County, CO	early Puercan (Pu1)	Early Paleocene	(Middleton, 1982; Eberle, 2003; Lofgren et al., 2004)
Catopsalis alexanderi	UCM 34136	Alexander locality (UCM locality 77267), Denver Formation, Arapahoe County, CO	early Puercan (Pu1)	Early Paleocene	(Middleton, 1982; Eberle, 2003; Lofgren et al., 2004)
Catopsalis alexanderi	UCM 34139	Alexander locality (UCM locality 77267), Denver Formation, Arapahoe County, CO	early Puercan (Pu1)	Early Paleocene	(Middleton, 1982; Eberle, 2003; Lofgren et al., 2004)
Catopsalis alexanderi	UCM 34141	Alexander locality (UCM locality 77267), Denver Formation, Arapahoe County, CO	early Puercan (Pu1)	Early Paleocene	(Middleton, 1982; Eberle, 2003; Lofgren et al., 2004)
Catopsalis alexanderi	UCM 34332	Alexander locality (UCM locality 77267), Denver Formation, Arapahoe County, CO	early Puercan (Pu1)	Early Paleocene	(Middleton, 1982; Eberle, 2003; Lofgren et al., 2004)

Catopsalis alexanderi	UCM 34596	Alexander locality (UCM locality 77267), Denver Formation, Arapahoe County, CO	early Puercan (Pu1)	Early Paleocene	(Middleton, 1982; Eberle, 2003; Lofgren et al., 2004)
Catopsalis alexanderi	UCM 34608	Alexander locality (UCM locality 77267), Denver Formation, Arapahoe County, CO	early Puercan (Pu1)	Early Paleocene	(Middleton, 1982; Eberle, 2003; Lofgren et al., 2004)
Catopsalis alexanderi	UCM 34939	Alexander locality (UCM locality 77267), Denver Formation, Arapahoe County, CO	early Puercan (Pu1)	Early Paleocene	(Middleton, 1982; Eberle, 2003; Lofgren et al., 2004)
Catopsalis alexanderi	UCM 38857	Alexander locality (UCM locality 77267), Denver Formation, Arapahoe County, CO	early Puercan (Pu1)	Early Paleocene	(Middleton, 1982; Eberle, 2003; Lofgren et al., 2004)
Catopsalis calgariensis	TMP 127	Calgary2E locality, Porcupine Hills Formation, AB	?early Torrejonian (To1)	Early Paleocene	(Russell, 1926)
Catopsalis calgariensis	TMP 2015.023.0001	Calgary2E locality, Porcupine Hills Formation, AB	?early Torrejonian (To1)	Early Paleocene	TMP Database
Catopsalis cf. *calgariensis*	UW 6387	Shotgun (Twin Buttes) localities (UW V-60014 and V-60016), Shotgun Member of the Fort Union Formation, Fremont Co., WY	earliest Tiffanian (Ti1)	Late Paleocene	(Middleton, 1982; Lofgren et al., 2004)
Catopsalis cf. *calgariensis*	UW 6387	Shotgun (Twin Buttes) localities (UW V-60014 and V-60016), Shotgun Member of the Fort Union Formation, Fremont Co., WY	earliest Tiffanian (Ti1)	Late Paleocene	(Middleton, 1982; Lofgren et al., 2004)
Catopsalis cf. *calgariensis*	UW 6388	Shotgun (Twin Buttes) localities (UW V-60014 and V-60016), Shotgun Member of the Fort Union Formation, Fremont Co., WY	earliest Tiffanian (Ti1)	Late Paleocene	(Middleton, 1982; Lofgren et al., 2004)
Catopsalis cf. *calgariensis*	UW 6388	Shotgun (Twin Buttes) localities (UW V-60014 and V-60016), Shotgun Member of the Fort Union Formation, Fremont Co., WY	earliest Tiffanian (Ti1)	Late Paleocene	(Middleton, 1982; Lofgren et al., 2004)
Catopsalis cf. *calgariensis*	UW 6407	Shotgun (Twin Buttes) localities (UW V-60014 and V-60016), Shotgun Member of the Fort Union Formation, Fremont Co., WY	earliest Tiffanian (Ti1)	Late Paleocene	(Middleton, 1982; Lofgren et al., 2004)

Catopsalis cf. *calgariensis*	UW 14051	Shotgun (Twin Buttes) localities (UW V-60014 and V-60016), Shotgun Member of the Fort Union Formation, Fremont Co., WY	earliest Tiffanian (Ti1)	Late Paleocene	(Middleton, 1982; Lofgren et al., 2004)
Catopsalis cf. *calgariensis*	UW 14055	Shotgun (Twin Buttes) localities (UW V-60014 and V-60016), Shotgun Member of the Fort Union Formation, Fremont Co., WY	earliest Tiffanian (Ti1)	Late Paleocene	(Middleton, 1982; Lofgren et al., 2004)
Catopsalis cf. *calgariensis*	UW 14058	Shotgun (Twin Buttes) localities (UW V-60014 and V-60016), Shotgun Member of the Fort Union Formation, Fremont Co., WY	earliest Tiffanian (Ti1)	Late Paleocene	(Middleton, 1982; Lofgren et al., 2004)
Catopsalis cf. *calgariensis*	UW 15100	Shotgun (Twin Buttes) localities (UW V-60014 and V-60016), Shotgun Member of the Fort Union Formation, Fremont Co., WY	earliest Tiffanian (Ti1)	Late Paleocene	(Middleton, 1982; Lofgren et al., 2004)
Catopsalis cf. *calgariensis*	UW 15102	Shotgun (Twin Buttes) localities (UW V-60014 and V-60016), Shotgun Member of the Fort Union Formation, Fremont Co., WY	earliest Tiffanian (Ti1)	Late Paleocene	(Middleton, 1982; Lofgren et al., 2004)
Catopsalis fissidens	NMMNH 8608	Chico Springs locality, Nacimiento Formation, San Juan Basin, NM	Torrejonian (?To1/To2)	Early Paleocene	(Lucas et al., 1997)
Catopsalis fissidens	NMMNH 8608	Chico Springs locality, Nacimiento Formation, San Juan Basin, NM	Torrejonian (?To1/To2)	Early Paleocene	(Lucas et al., 1997)
Catopsalis fissidens	NMMNH 8609	Chico Springs locality, Nacimiento Formation, San Juan Basin, NM	Torrejonian (?To1/To2)	Early Paleocene	(Lucas et al., 1997)
Catopsalis fissidens	NMMNH 8613	Chico Springs locality, Nacimiento Formation, San Juan Basin, NM	Torrejonian (?To1/To2)	Early Paleocene	(Lucas et al., 1997)
Catopsalis fissidens	NMMNH 62373	Chico Springs locality, Nacimiento Formation, San Juan Basin, NM	Torrejonian (?To1/To2)	Early Paleocene	(Williamson et al., 2015)
Catopsalis fissidens	NMMNH 62398	Chico Springs locality, Nacimiento Formation, San Juan Basin, NM	Torrejonian (?To1/To2)	Early Paleocene	(Williamson et al., 2015)
Catopsalis fissidens	NMMNH 19500	Chico Springs locality, Nacimiento Formation, San Juan Basin, NM	Torrejonian (?To1/To2)	Early Paleocene	(Lucas et al., 1997)

Catopsalis johnstoni	UALVP 16058	Medicine Hat Brick and Tile Quarry, 3 km NW Ravenscrag, Saskatchewan, Ravenscrag Formation, Long Fall horizon	Lancian	Latest Cretaceous	(Fox, 1989)
Catopsalis kakwa	TMP 2009.133.0041	Zagas Quarry (TMP locality L2391), Porcupine Hills Formation, AB, Canada	Torrejonian (To2/3)	Early Paleocene	(Scott et al., 2018)
Catopsalis kakwa	TMP 2009.133.0114	Zagas Quarry (TMP locality L2391), Porcupine Hills Formation, AB, Canada	Torrejonian (To2/3)	Early Paleocene	(Scott et al., 2018)
Catopsalis kakwa	TMP 2010.097.0015	Narcissus locality, Porcupine Hills formation, AB	middle Torrejonian (To2)	Early Paleocene	(Scott et al., 2018)
Catopsalis kakwa	TMP 2010.097.0020	Narcissus locality, Porcupine Hills formation, AB	middle Torrejonian (To2)	Early Paleocene	(Scott et al., 2018)
Catopsalis kakwa	TMP 2012.024.0063	Zagas Quarry (TMP locality L2391), Porcupine Hills Formation, AB, Canada	Torrejonian (To2/3)	Early Paleocene	(Scott et al., 2018)
Catopsalis kakwa	TMP 2012.024.0225	Zagas Quarry (TMP locality L2391), Porcupine Hills Formation, AB, Canada	Torrejonian (To2/3)	Early Paleocene	(Scott et al., 2018)
Catopsalis kakwa	TMP 2015.071.0141	Jumpingpound Creek Site 1, Porcupine Hills formation, AB	middle Torrejonian (To2)	Early Paleocene	(Scott et al., 2018)
Catopsalis kakwa	UALVP 57538	Nordic Ski Quarry, Porcupine Hills Formation, AB	late Torrejonian (To3)	Early Paleocene	(Scott et al., 2018)
Catopsalis kakwa	UALVP 57541	Nordic Ski Quarry, Porcupine Hills Formation, AB	late Torrejonian (To3)	Early Paleocene	(Scott et al., 2018)
Catopsalis kakwa	UALVP 57542	Nordic Ski Quarry, Porcupine Hills Formation, AB	late Torrejonian (To3)	Early Paleocene	(Scott et al., 2018)
Catopsalis kakwa	UALVP 57543	Nordic Ski Quarry, Porcupine Hills Formation, AB	late Torrejonian (To3)	Early Paleocene	(Scott et al., 2018)
Catopsalis waddleae	UM 90042	Bear Formation, Crazy Mountains Basin, Simpson Quarry, Wheatland county, MT	Puercan (Pu2/3)	Early Paleocene	(Buckley, 1995; Lofgren et al., 2004)
Cimolomyid 1	TMP 87.73.2	DPP, Dinosaur Park formation, AB	Judithian	Late Cretaceous	TMP Database
Cimolomyid 1	TMP 95.6.6	Dinosaur Provincial Park - Sabo's Site 1 (2), Dinosaur Park formation, AB	Judithian	Late Cretaceous	TMP Database
Cimolomyid 1	UALVP 1766	Irvine locality, Dinosaur Park Formation, AB, Canada (near Irvine, east of Medicine Hat)	Judithian	Late Cretaceous	UALVP Database

Cimolomyid 1	UALVP 2010	Irvine locality, Dinosaur Park Formation, AB, Canada (near Irvine, east of Medicine Hat)	Judithian	Late Cretaceous	UALVP Database
Cimolomyid 1	UALVP 2158	Irvine locality, Dinosaur Park Formation, AB, Canada (near Irvine, east of Medicine Hat)	Judithian	Late Cretaceous	UALVP Database
Cimolomyid 1	UALVP 4233	Irvine locality, Dinosaur Park Formation, AB, Canada (near Irvine, east of Medicine Hat)	Judithian	Late Cretaceous	UALVP Database
Cimolomyid 1	UALVP 30004	Irvine locality, Dinosaur Park Formation, AB, Canada (near Irvine, east of Medicine Hat)	Judithian	Late Cretaceous	UALVP Database
Cimolomyid 1	UALVP 30008	Irvine locality, Dinosaur Park Formation, AB, Canada (near Irvine, east of Medicine Hat)	Judithian	Late Cretaceous	UALVP Database
Cimolomyid 1	UALVP 30038	Irvine locality, Dinosaur Park Formation, AB, Canada (near Irvine, east of Medicine Hat)	Judithian	Late Cretaceous	UALVP Database
Cimolomyid 1	UALVP 30040	Irvine locality, Dinosaur Park Formation, AB, Canada (near Irvine, east of Medicine Hat)	Judithian	Late Cretaceous	UALVP Database
Cimolomyid 1	UALVP 30053	Irvine locality, Dinosaur Park Formation, AB, Canada (near Irvine, east of Medicine Hat)	Judithian	Late Cretaceous	UALVP Database
Cimolomyid 1	UALVP 30092	Medicine Hat #12, Dinosaur Park Formation, Medicine Hat, AB	Judithian	Late Cretaceous	UALVP Database
Cimolomyid 1	UALVP 30093	Irvine locality, Dinosaur Park Formation, AB, Canada (near Irvine, east of Medicine Hat)	Judithian	Late Cretaceous	UALVP Database
Cimolomyid 1	UALVP 30096	Irvine locality, Dinosaur Park Formation, AB, Canada (near Irvine, east of Medicine Hat)	Judithian	Late Cretaceous	UALVP Database

Cimolomyid 1	UALVP 30112	Irvine locality, Dinosaur Park Formation, AB, Canada (near Irvine, east of Medicine Hat)	Judithian	Late Cretaceous	UALVP Database
Cimolomyid 1	UALVP 30549	Irvine locality, Dinosaur Park Formation, AB, Canada (near Irvine, east of Medicine Hat)	Judithian	Late Cretaceous	UALVP Database
Cimolomyid 1	UALVP 30558	Irvine locality, Dinosaur Park Formation, AB, Canada (near Irvine, east of Medicine Hat)	Judithian	Late Cretaceous	UALVP Database
Cimolomyid 1	UALVP 30568	Irvine locality, Dinosaur Park Formation, AB, Canada (near Irvine, east of Medicine Hat)	Judithian	Late Cretaceous	UALVP Database
Cimolomyid 1	UALVP 30575	Irvine locality, Dinosaur Park Formation, AB, Canada (near Irvine, east of Medicine Hat)	Judithian	Late Cretaceous	UALVP Database
Cimolomyid 1	UALVP 30593	Irvine locality, Dinosaur Park Formation, AB, Canada (near Irvine, east of Medicine Hat)	Judithian	Late Cretaceous	UALVP Database
Cimolomyid 1	UALVP 30605	Irvine locality, Dinosaur Park Formation, AB, Canada (near Irvine, east of Medicine Hat)	Judithian	Late Cretaceous	UALVP Database
Cimolomyid 1	UALVP 30640	Irvine locality, Dinosaur Park Formation, AB, Canada (near Irvine, east of Medicine Hat)	Judithian	Late Cretaceous	UALVP Database
Cimolomyid 1	UALVP 30641	Irvine locality, Dinosaur Park Formation, AB, Canada (near Irvine, east of Medicine Hat)	Judithian	Late Cretaceous	UALVP Database
Cimolomyid 1	UALVP 30616	Irvine locality, Dinosaur Park Formation, AB, Canada (near Irvine, east of Medicine Hat)	Judithian	Late Cretaceous	UALVP Database
Cimolomyid 1	TMP 90.33.100	Onefour - DPP Unit Site 1, Dinosaur Park Formation, AB	--	Late Cretaceous	TMP Database
Cimolomyid 1	TMP 99.19.7	HOS (Hoodoo Site), Foremost formation, AB	Judithian	Late Cretaceous	TMP Database

Cimolomys sp.	TMP 87.99.62	DPP, Dinosaur Park Formation, AB	Judithian	Late Cretaceous	TMP Database
Cimolomys sp.	TMP 88.212.72	Dinosaur Provincial Park - Sabo's Site 1 (2), Dinosaur Park formation, AB	Judithian	Late Cretaceous	TMP Database
Cimolomys sp.	TMP 93.138.2	Dinosaur Provincial Park - D-2, Oldman Formation, AB	Judithian	Late Cretaceous	TMP Database
Cimolomys sp.	TMP 95.169.19	DPP, Dinosaur Park formation, AB	Judithian	Late Cretaceous	TMP Database
Cimolomys sp.	TMP 99.1.5	HAS (Hanna's Ankylosaur Site), Oldman Formation, AB	Judithian	Late Cretaceous	TMP Database
Cimolomys sp.	TMP 99.13.5	CS (Confluence Site), Oldman formation, AB	Judithian	Late Cretaceous	TMP Database
Cimolomys sp.	UALVP 709	Steveville #12, Dinosaur Park Formation, AB, Canada	Judithian	Late Cretaceous	UALVP Database
Cimolomys sp.	UALVP 2141	Irvine locality, Dinosaur Park Formation, AB, Canada (near Irvine, east of Medicine Hat)	Judithian	Late Cretaceous	UALVP Database
Cimolomys sp.	UALVP 30052	Dinosaur Provincial Park #4, Oldman Formation, AB	Judithian	Late Cretaceous	UALVP Database
Cimolomys sp.	UALVP 30108	Dinosaur Provincial Park #4, Oldman Formation, AB	Judithian	Late Cretaceous	UALVP Database
Cimolomys sp.	UALVP 30112	Irvine locality, Dinosaur Park Formation, AB, Canada (near Irvine, east of Medicine Hat)	Judithian	Late Cretaceous	UALVP Database
Cimolomys sp.	UALVP 30605	Irvine locality, Dinosaur Park Formation, AB, Canada (near Irvine, east of Medicine Hat)	Judithian	Late Cretaceous	UALVP Database
Cimolomys sp.	UALVP 30729	Irvine locality, Dinosaur Park Formation, AB, Canada (near Irvine, east of Medicine Hat)	Judithian	Late Cretaceous	UALVP Database
Meniscoessus major	UALVP 15164	Irvine locality, Dinosaur Park Formation, AB, Canada (near Irvine, east of Medicine Hat)	Judithian	Late Cretaceous	UALVP Database
Meniscoessus major	UALVP 15165	Irvine locality, Dinosaur Park Formation, AB, Canada (near Irvine, east of Medicine Hat)	Judithian	Late Cretaceous	UALVP Database

Meniscoessus major	UALVP 15167	Irvine locality, Dinosaur Park Formation, AB, Canada (near Irvine, east of Medicine Hat)	Judithian	Late Cretaceous	UALVP Database
Meniscoessus major	UALVP 15172	Irvine locality, Dinosaur Park Formation, AB, Canada (near Irvine, east of Medicine Hat)	Judithian	Late Cretaceous	UALVP Database
Meniscoessus major	UALVP 15173	Irvine locality, Dinosaur Park Formation, AB, Canada (near Irvine, east of Medicine Hat)	Judithian	Late Cretaceous	UALVP Database
Meniscoessus major	UALVP 15174	Irvine locality, Dinosaur Park Formation, AB, Canada (near Irvine, east of Medicine Hat)	Judithian	Late Cretaceous	UALVP Database
Meniscoessus major	UALVP 15180	Irvine locality, Dinosaur Park Formation, AB, Canada (near Irvine, east of Medicine Hat)	Judithian	Late Cretaceous	UALVP Database
Meniscoessus major	UALVP 15181	Irvine locality, Dinosaur Park Formation, AB, Canada (near Irvine, east of Medicine Hat)	Judithian	Late Cretaceous	UALVP Database
Meniscoessus major	UALVP 15182	Irvine locality, Dinosaur Park Formation, AB, Canada (near Irvine, east of Medicine Hat)	Judithian	Late Cretaceous	UALVP Database
Meniscoessus major	UALVP 15187	Irvine locality, Dinosaur Park Formation, AB, Canada (near Irvine, east of Medicine Hat)	Judithian	Late Cretaceous	UALVP Database
Meniscoessus major	UALVP B	--	--	--	--
Meniscoessus robustus	ROM M	Bug Creek Anthills, Hell Creek Formation, MT (Lancian or early Puercan)	Lancian/Puercan (Pu1)	Latest Cretaceous/Early Paleocene	ROM Database
Meniscoessus robustus	ROM N	Bug Creek Anthills, Hell Creek Formation, MT (Lancian or early Puercan)	Lancian/Puercan (Pu1)	Latest Cretaceous/Early Paleocene	ROM Database
Meniscoessus robustus	TMP 83.215.15	Bushy Tailed Blowout, Lance Formation, WY	Lancian	Late Cretaceous	UALVP Database
Meniscoessus robustus	UALVP 1581	Bushy Tailed Blowout #1, Lance Formation, WY	Lancian	Late Cretaceous	UALVP Database

Meniscoessus robustus	UALVP 27189	Bug Creek Anthills, Hell Creek Formation, MT (Lancian or early Puercan)	Lancian/Puercan (Pu1)	Latest Cretaceous/Early Paleocene	UALVP Database
Meniscoessus robustus	UALVP 27243	Bushy Tailed Blowout #1, Lance Formation, WY	Lancian	Late Cretaceous	UALVP Database
Meniscoessus robustus	UALVP 27244	Bushy Tailed Blowout #1, Lance Formation, WY	Lancian	Late Cretaceous	UALVP Database
Mesodma formosa	ROM B1	Bug Creek Anthills, Hell Creek Formation, MT	Lancian/Puercan (Pu1)	Latest Cretaceous/Early Paleocene	--
Mesodma formosa	ROM V	Bug Creek Anthills, Hell Creek Formation, MT	Lancian/Puercan (Pu1)	Latest Cretaceous/Early Paleocene	--
Mesodma thompsoni	ROM A1	Bug Creek Anthills, Hell Creek Formation, MT	Lancian/Puercan (Pu1)	Latest Cretaceous/Early Paleocene	--
Mesodma sp.	ROM P	Bug Creek Anthills, Hell Creek Formation, MT	Lancian/Puercan (Pu1)	Latest Cretaceous/Early Paleocene	--
Mesodma sp.	ROM R	Bug Creek Anthills, Hell Creek Formation, MT	Lancian/Puercan (Pu1)	Latest Cretaceous/Early Paleocene	--
Mesodma sp.	ROM X	Bug Creek Anthills, Hell Creek Formation, MT	Lancian/Puercan (Pu1)	Latest Cretaceous/Early Paleocene	--
Mesodma sp.	ROM T	Bug Creek Anthills, Hell Creek Formation, MT	Lancian/Puercan (Pu1)	Latest Cretaceous/Early Paleocene	--
Mesodma sp.	ROM U	Bug Creek Anthills, Hell Creek Formation, MT	Lancian/Puercan (Pu1)	Latest Cretaceous/Early Paleocene	--
Mesodma sp.	ROM Y	Bug Creek Anthills, Hell Creek Formation, MT	Lancian/Puercan (Pu1)	Latest Cretaceous/Early Paleocene	--
Mesodma thompsoni	ROM Z	Bug Creek Anthills, Hell Creek Formation, MT	Lancian/Puercan (Pu1)	Latest Cretaceous/Early Paleocene	--
Mesodma sp.	UALVP 7278	Bug Creek Anthills, Hell Creek Formation, MT	Lancian/Puercan (Pu1)	Latest Cretaceous/Early Paleocene	UALVP Database; (Lofgren, 1995)
Mesodma sp.	UALVP 7288	Bug Creek Anthills, Hell Creek Formation, MT	Lancian/Puercan (Pu1)	Latest Cretaceous/Early Paleocene	UALVP Database; (Lofgren, 1995)
Mesodma sp.	UALVP 7429	Bug Creek Anthills, Hell Creek Formation, MT	Lancian/Puercan (Pu1)	Latest Cretaceous/Early Paleocene	UALVP Database; (Lofgren, 1995)
Mesodma sp.	UALVP 7433	Bug Creek Anthills, Hell Creek Formation, MT	Lancian/Puercan (Pu1)	Latest Cretaceous/Early Paleocene	UALVP Database; (Lofgren, 1995)
Neoplagiaulacid	TMP 2009.132.0239	Sheeps Ahoy locality, Willow Creek formation, AB	Puercan (?Pu2/3)	Early Paleocene	TMP Database
Ptilodus sp. C	TMP 2015.069.0174	Trainspotting locality, Paskapoo formation, AB	earliest Tiffanian (Ti1)	Late Paleocene	TMP Database
Ptilodus sp. C	TMP 2015.069.0663	Trainspotting locality, Paskapoo formation, AB	earliest Tiffanian (Ti1)	Late Paleocene	TMP Database
Ptilodus sp.	TMP 2015.069.0902	Trainspotting locality, Paskapoo formation, AB	earliest Tiffanian (Ti1)	Late Paleocene	TMP Database

Ptilodus sp. C	TMP 2014.047.0181	Trainspotting locality, Paskapoo formation, AB	earliest Tiffanian (Ti1)	Late Paleocene	TMP Database
Ptilodus sp. C	TMP 2016.039.0004	Trainspotting locality, Paskapoo formation, AB	earliest Tiffanian (Ti1)	Late Paleocene	TMP Database
Ptilodus sp. C	TMP 2017.025.0289	Trainspotting locality, Paskapoo formation, AB	earliest Tiffanian (Ti1)	Late Paleocene	TMP Database
Ptilodus sp. C	UALVP 46291	Blindman River DW-2, Paskapoo Formation, AB	middle Tiffanian (Ti3)	Late Paleocene	UALVP Database
Ptilodus wyomingensis	TMP 2010.097.0126	Narcissus locality, Porcupine Hills formation, AB	middle Torrejonian (To2)	Early Paleocene	TMP Database
Stygimys kuszmauli	UALVP 6533	Bug Creek Anthills, Hell Creek Formation, MT	Lancian/Puercan (Pu1)	Latest Cretaceous/Early Paleocene	UALVP Database; (Lofgren, 1995)
Taeniolabis taoensis	AMNH 727	Nacimiento formation (T-P zone), San Juan Basin, NM	Late Puercan (Pu 3)	Early Paleocene	(Williamson, 1996; Lofgren et al., 2004; Williamson et al., 2015)
Taeniolabis taoensis	AMNH 27728	Nacimiento formation (T-P zone), San Juan Basin, NM	Late Puercan (Pu 3)	Early Paleocene	(Williamson, 1996; Lofgren et al., 2004; Williamson et al., 2015)
Taeniolabis taoensis	AMNH 163007.001	Nacimiento formation (T-P zone), San Juan Basin, NM	Late Puercan (Pu 3)	Early Paleocene	(Williamson, 1996; Lofgren et al., 2004; Williamson et al., 2015)
Taeniolabis taoensis	AMNH 163007.002	Nacimiento formation (T-P zone), San Juan Basin, NM	Late Puercan (Pu 3)	Early Paleocene	(Williamson, 1996; Lofgren et al., 2004; Williamson et al., 2015)
Taeniolabis taoensis	NMMNH 2763	Nacimiento formation (T-P zone), San Juan Basin, NM	Late Puercan (Pu 3)	Early Paleocene	(Williamson, 1996; Lofgren et al., 2004; Williamson et al., 2015)
Taeniolabis taoensis	NMMNH 2765	Nacimiento formation (T-P zone), San Juan Basin, NM	Late Puercan (Pu 3)	Early Paleocene	(Williamson, 1996; Lofgren et al., 2004; Williamson et al., 2015)
Taeniolabis taoensis	NMMNH 2935	Nacimiento formation (T-P zone), San Juan Basin, NM	Late Puercan (Pu 3)	Early Paleocene	(Williamson, 1996; Lofgren et al., 2004; Williamson et al., 2015)
Taeniolabis taoensis	NMMNH 2941	Nacimiento formation (T-P zone), San Juan Basin, NM	Late Puercan (Pu 3)	Early Paleocene	(Williamson, 1996; Lofgren et al., 2004; Williamson et al., 2015)
Taeniolabis taoensis	NMMNH 8615	Nacimiento formation (T-P zone), San Juan Basin, NM	Late Puercan (Pu 3)	Early Paleocene	(Williamson, 1996; Lofgren et al., 2004; Williamson et al., 2015)
Taeniolabis taoensis	NMMNH 8631	Nacimiento formation (T-P zone), San Juan Basin, NM	Late Puercan (Pu 3)	Early Paleocene	(Williamson, 1996; Lofgren et al., 2004; Williamson et al., 2015)
Taeniolabis taoensis	NMMNH 8632	Nacimiento formation (T-P zone), San Juan Basin, NM	Late Puercan (Pu 3)	Early Paleocene	(Williamson, 1996; Lofgren et al., 2004; Williamson et al., 2015)
Taeniolabis taoensis	NMMNH 12387	Nacimiento formation (T-P zone), San Juan Basin, NM	Late Puercan (Pu 3)	Early Paleocene	(Williamson, 1996; Lofgren et al., 2004; Williamson et al., 2015)

Taeniolabis taoensis	NMMNH 42938	Nacimiento formation (T-P zone), San Juan Basin, NM	Late Puercan (Pu 3)	Early Paleocene	(Williamson, 1996; Lofgren et al., 2004; Williamson et al., 2015)
Taeniolabis taoensis	NMMNH 42939	Nacimiento formation (T-P zone), San Juan Basin, NM	Late Puercan (Pu 3)	Early Paleocene	(Williamson, 1996; Lofgren et al., 2004; Williamson et al., 2015)
Taeniolabis taoensis	NMMNH 44417	Nacimiento formation (T-P zone), San Juan Basin, NM	Late Puercan (Pu 3)	Early Paleocene	(Williamson, 1996; Lofgren et al., 2004; Williamson et al., 2015)
Taeniolabis taoensis	NMMNH 47445	Nacimiento formation (T-P zone), San Juan Basin, NM	Late Puercan (Pu 3)	Early Paleocene	(Williamson, 1996; Lofgren et al., 2004; Williamson et al., 2015)
Taeniolabis taoensis	NMMNH 47447	Nacimiento formation (T-P zone), San Juan Basin, NM	Late Puercan (Pu 3)	Early Paleocene	(Williamson, 1996; Lofgren et al., 2004; Williamson et al., 2015)
Valenopsalis joyneri	ROM I	Bug Creek Anthills, Hell Creek Formation, MT	early Puercan (Pu1)	Early Paleocene	(Lofgren, 1995; Lofgren et al., 2004; Wilson, 2013)
Valenopsalis joyneri	ROM H	Bug Creek Anthills, Hell Creek Formation, MT	early Puercan (Pu1)	Early Paleocene	(Lofgren, 1995; Lofgren et al., 2004; Wilson, 2013)
Valenopsalis joyneri	UALVP 6596	Bug Creek Anthills, Hell Creek Formation, MT	early Puercan (Pu1)	Early Paleocene	(Lofgren, 1995; Lofgren et al., 2004; Wilson, 2013)
Valenopsalis joyneri	UALVP 6608	Bug Creek Anthills, Hell Creek Formation, MT	early Puercan (Pu1)	Early Paleocene	(Lofgren, 1995; Lofgren et al., 2004; Wilson, 2013)
Valenopsalis joyneri	UALVP 6609	Bug Creek Anthills, Hell Creek Formation, MT	early Puercan (Pu1)	Early Paleocene	(Lofgren, 1995; Lofgren et al., 2004; Wilson, 2013)
Valenopsalis joyneri	UALVP 6610	Bug Creek Anthills, Hell Creek Formation, MT	early Puercan (Pu1)	Early Paleocene	(Lofgren, 1995; Lofgren et al., 2004; Wilson, 2013)
Valenopsalis joyneri	UALVP 7278	Bug Creek Anthills, Hell Creek Formation, MT	early Puercan (Pu1)	Early Paleocene	(Lofgren, 1995; Lofgren et al., 2004; Wilson, 2013)
Valenopsalis joyneri	UALVP 7288	Bug Creek Anthills, Hell Creek Formation, MT	early Puercan (Pu1)	Early Paleocene	(Lofgren, 1995; Lofgren et al., 2004; Wilson, 2013)
Valenopsalis joyneri	UALVP 7393	Bug Creek Anthills, Hell Creek Formation, MT	early Puercan (Pu1)	Early Paleocene	(Lofgren, 1995; Lofgren et al., 2004; Wilson, 2013)
Valenopsalis joyneri	UALVP 7394	Bug Creek Anthills, Hell Creek Formation, MT	early Puercan (Pu1)	Early Paleocene	(Lofgren, 1995; Lofgren et al., 2004; Wilson, 2013)
Valenopsalis joyneri	UALVP 7395	Bug Creek Anthills, Hell Creek Formation, MT	early Puercan (Pu1)	Early Paleocene	(Lofgren, 1995; Lofgren et al., 2004; Wilson, 2013)
Valenopsalis joyneri	UALVP 7412	Bug Creek Anthills, Hell Creek Formation, MT	early Puercan (Pu1)	Early Paleocene	(Lofgren, 1995; Lofgren et al., 2004; Wilson, 2013)
Valenopsalis joyneri	UALVP 28167	Bug Creek Anthills, Hell Creek Formation, MT	early Puercan (Pu1)	Early Paleocene	(Lofgren, 1995; Lofgren et al., 2004; Wilson, 2013)
Valenopsalis joyneri	UALVP 28170	Bug Creek Anthills, Hell Creek Formation, MT	early Puercan (Pu1)	Early Paleocene	(Lofgren, 1995; Lofgren et al., 2004; Wilson, 2013)
Valenopsalis joyneri	UALVP 28172	Bug Creek Anthills, Hell Creek Formation, MT	early Puercan (Pu1)	Early Paleocene	(Lofgren, 1995; Lofgren et al., 2004; Wilson, 2013)
Valenopsalis joyneri	UALVP 28175	Bug Creek Anthills, Hell Creek Formation, MT	early Puercan (Pu1)	Early Paleocene	(Lofgren, 1995; Lofgren et al., 2004; Wilson, 2013)

Valenopsalis joyneri	UALVP 28178	Bug Creek Anthills, Hell Creek Formation, MT	early Puercan (Pu1)	Early Paleocene	(Lofgren, 1995; Lofgren et al., 2004; Wilson, 2013)
Valenopsalis joyneri	UALVP 28186	Bug Creek Anthills, Hell Creek Formation, MT	early Puercan (Pu1)	Early Paleocene	(Lofgren, 1995; Lofgren et al., 2004; Wilson, 2013)
Valenopsalis joyneri	UALVP 28202	Bug Creek Anthills, Hell Creek Formation, MT	early Puercan (Pu1)	Early Paleocene	(Lofgren, 1995; Lofgren et al., 2004; Wilson, 2013)
Valenopsalis joyneri	UALVP 28203	Bug Creek Anthills, Hell Creek Formation, MT	early Puercan (Pu1)	Early Paleocene	(Lofgren, 1995; Lofgren et al., 2004; Wilson, 2013)
Valenopsalis joyneri	UALVP 28204	Bug Creek Anthills, Hell Creek Formation, MT	early Puercan (Pu1)	Early Paleocene	(Lofgren, 1995; Lofgren et al., 2004; Wilson, 2013)
Valenopsalis joyneri	UALVP 28205	Bug Creek Anthills, Hell Creek Formation, MT	early Puercan (Pu1)	Early Paleocene	(Lofgren, 1995; Lofgren et al., 2004; Wilson, 2013)
Valenopsalis joyneri	UALVP 28206	Bug Creek Anthills, Hell Creek Formation, MT	early Puercan (Pu1)	Early Paleocene	(Lofgren, 1995; Lofgren et al., 2004; Wilson, 2013)
Valenopsalis joyneri	UALVP 28207	Bug Creek Anthills, Hell Creek Formation, MT	early Puercan (Pu1)	Early Paleocene	(Lofgren, 1995; Lofgren et al., 2004; Wilson, 2013)
Valenopsalis joyneri	UALVP 28211	Bug Creek Anthills, Hell Creek Formation, MT	early Puercan (Pu1)	Early Paleocene	(Lofgren, 1995; Lofgren et al., 2004; Wilson, 2013)
Valenopsalis joyneri	UALVP 28187	Bug Creek Anthills, Hell Creek Formation, MT	early Puercan (Pu1)	Early Paleocene	(Lofgren, 1995; Lofgren et al., 2004; Wilson, 2013)

Literature Cited

Buckley, G. A. 1995. The multituberculate *Catopsalis* from the early Paleocene of the Crazy

Mountains Basin in Montana. Acta Palaeontologica Polonica 40:389–398.

Eberle, J. J. 2003. Puercan mammalian systematics and biostratigraphy in the Denver Formation,

Denver Basin, Colorado. Rocky Mountain Geology 38:143–169.

Fox, R. C. 1989. The Wounded Knee local fauna and mammalian evolution near the Cretaceous-

Tertiary boundary, Saskatchewan, Canada. Paleontographica Abteilung A 208:11–59.

Lofgren, D. L. 1995. The Bug Creek problem and the Cretaceous-Tertiary transition at McGuire

Creek, Montana. University of California Publications in Geological Sciences 140:1–185.

Lofgren, D. L., J. A. Lillegraven, W. A. Clemens, P. D. Gingerich, and T. E. Williamson. 2004.

Paleocene biochronology: The Puercan through Clarkforkian Land Mammal Ages; pp. 43–

105 in M. O. Woodburne (ed.), Cenozoic Mammals of North America: Geochronology and

Biostratigraphy. Columbia University Press, New York.

Lucas, S. G., T. E. Williamson, and M. D. Middleton. 1997. *Catopsalis* (Mammalia: Multituberculata) from the Paleocene of New Mexico and Utah: taxonomy and biochronological significance. Journal of Paleontology 71:484–493.

Middleton, M. D. 1982. A new species and additional material of *Catopsalis* (Mammalia, Multituberculata) from the Western Interior of North America. Journal of Paleontology 56:1197–1206.

Russell, L. S. 1926. A new species of the genus *Catopslais* Cope from the Paskapoo Formation of Alberta. American Journal of Science 12:230–234.

Scott, C. S., A. Weil, and J. M. Theodor. 2018. A new, diminutive species of *Catopsalis* (Mammalia, Multituberculata, Taeniolabidoidea) from the early Paleocene of southwestern Alberta, Canada. Journal of Paleontology 1–15.

Williamson, T. E. 1996. The beginning of the age of mammals in the San Juan Basin, New Mexico: biostratigraphy and evolution of Paleocene mammals of the Nacimiento Formation. Bulletin of the New Mexico Museum of Natural History and Science 8:1–141.

Williamson, T. E., S. L. Brusatte, R. Secord, and S. Shelley. 2015. A new taeniolabidoid multituberculate (Mammalia) from the middle Puercan of the Nacimiento Formation, New Mexico, and a revision of taeniolabidoid systematics and phylogeny. Zoological Journal of the Linnean Society 177:183–208.

Wilson, G. P. 2013. Mammals across the K/Pg boundary in northeastern Montana , U.S.A.: dental morphology and body-size patterns reveal extinction selectivity and immigrant-fueled ecospace filling. Paleobiology 39:429–469.

Institutional abbreviations: **AMNH** – American Museum of Natural and Cultural History (New York, NY, USA); **NMMNH** – New Mexico Museum of Natural History and Science (Albuquerque, NM, USA); **ROM** – Royal Ontario Museum (Toronto, ON, Canada); **TMP** – Royal Tyrrell Museum of Palaeontology (Drumheller, AB, Canada); **UALVP** – University of Alberta Laboratory for Vertebrate Paleontology (Edmonton, AB, Canada); **UCM** – University of Colorado Museum of Natural History (Boulder, CO, USA); **UW** – University of Wyoming Geological Museum (Laramie, WY, USA).

Table abbreviations: **MC** – molding compound; **S** – Sinclair molding compound; **P** – President molding compound; **SP** – small pit; **MP** – medium pit; **LP** – large pit; **FS** – fine scratch; **MS** – medium scratch; **LS** – large scratch.

Counts for each region of interest (ROI) are presented separately. Average counts for each specimen are in the grey rows.

Taxon	MC	SEM Mag.	Specimen Number	Tooth	Row	Cusp	SP	MP	LP	FS	MS	LS	Gouges	Flakes
Cimolomyid 1	S	200	TMP 1990.033.0100	RM2	Lingual	2	17	4	1	18	0	0	0	1
							18	2	2	28	1	0	1	0
							17.5	3	1.5	23	0.5	0	0.5	0.5
Cimolomyid 1	S	200	UALVP 1766	Rm1	Lingual	5	19	5	3	22	2	1	0	0
							15	1	2	28	2	1	0	0
							17	3	2.5	25	2	1	0	0
Cimolomyid 1	S	200	UALVP 2158	RM1	Middle	7	43	9	1	42	0	0	0	0
							29	6	2	34	0	1	0	0
							36	7.5	1.5	38	0	0.5	0	0
Cimolomyid 1	S	200	UALVP 30004	RM1	Middle	7	35	3	5	14	4	0	0	0
							19	3	3	15	1	0	0	0
							27	3	4	14.5	2.5	0	0	0
Cimolomyid 1	S	200	UALVP 30008	LM1	Middle	5	21	3	6	15	4	1	0	0
							18	1	3	36	2	0	1	0
							19.5	2	4.5	25.5	3	0.5	0.5	0
Cimolomyid 1	S	200	UALVP 30549	Lm1	Lingual	4	37	4	3	35	2	1	1	0
							24	8	3	42	2	0	5	0
							30.5	6	3	38.5	2	0.5	3	0
Cimolomyid 1	S	200	UALVP 30575	Rm1	Lingual	2	17	5	1	25	1	0	0	0
							14	7	2	22	0	0	0	0
							15.5	6	1.5	23.5	0.5	0	0	0
Cimolomys sp.	S	200	TMP 1995.169.0019	LM2	Lingual	3	14	3	0	25	3	0	0	0
							13	5	0	26	2	2	1	0
							13.5	4	0	25.5	2.5	1	0.5	0
Cimolomys sp.	S	200	UALVP 2141	Rm1	Lingual	4	14	4	1	15	1	0	1	0
							33	3	4	23	0	0	0	1
							23.5	3.5	2.5	19	0.5	0	0.5	0.5
Cimolomys sp.	S	200	UALVP 30052	LM1	Middle	6	33	8	5	27	3	0	0	0
							16	9	2	31	3	1	1	0
							24.5	8.5	3.5	29	3	0.5	0.5	0
Cimolomys sp.	S	200	UALVP 30053	LM2	Middle	2	22	4	3	25	1	0	0	1

							10	5	4	30	3	0	0	0
							16	4.5	3.5	27.5	2	0	0	0.5
Cimolomys sp.	S	200	UALVP 30729	LM1	Middle	1	43	6	5	44	0	0	0	0
							30	8	3	30	1	1	0	1
							36.5	7	4	37	0.5	0.5	0	0.5
Catopsalis alexanderi	S	100	UALVP 34136	Lm2	Lingual	2	14	6	0	14	2	0	0	1
							15	3	0	19	4	0	0	0
							14.5	4.5	0	16.5	3	0	0	0.5
Catopsalis alexanderi	S	100	UALVP 34141	Lm1	Lingual	4	28	6	3	23	1	0	1	1
							34	5	2	17	4	0	0	0
							31	5.5	2.5	20	2.5	0	0.5	0.5
Catopsalis alexanderi	S	100	UALVP 34596	RM2	Lingual	2	30	9	1	24	2	0	0	0
							42	6	2	21	1	1	1	0
							36	7.5	1.5	22.5	1.5	0.5	0.5	0
Catopsalis alexanderi	S	100	UALVP 34949	RM1	Middle	7	11	3	0	10	0	3	1	3
							13	4	2	19	1	0	2	0
							12	3.5	1	14.5	0.5	1.5	1.5	1.5
Catopsalis alexanderi	S	100	UALVP 38857	Lm2	Lingual	1	47	10	1	29	1	0	0	1
							33	7	2	21	0	2	2	0
							40	8.5	1.5	25	0.5	1	1	0.5
Catopsalis calgariensis	S	100	TMP 2015.025.0001	Lm2	Lingual	1	16	6	4	6	3	1	2	0
							8	2	1	13	0	0	0	0
							12	4	2.5	9.5	1.5	0.5	1	0
Catopsalis cf. *calgariensis*	S	100	UW 6387	Rm1	Lingual	4	14	6	5	17	0	0	3	0
							25	4	4	12	0	1	4	1
							19.5	5	4.5	14.5	0	0.5	3.5	0.5
Catopsalis cf. *calgariensis*	S	100	UW 6387	Lm2	Lingual	2	13	7	0	10	1	3	0	1

Taxon														
							14	3	3	10	3	1	0	1
							13.5	5	1.5	10	2	2	0	1
Catopsalis cf. *calgariensis*	S	100	UW 6407	RM1	Middle	5	4	3	1	11	3	0	0	0
							14	3	1	6	4	0	0	0
							9	3	1	8.5	3.5	0	0	0
Catopsalis cf. *calgariensis*	S	100	UW 14055	RM1	Middle	4	12	5	1	18	4	0	0	0
							12	3	0	15	3	1	0	0
							12	4	0.5	16.5	3.5	0.5	0	0
Catopsalis cf. *calgariensis*	S	100	UW 14058	LM2	Lingual	2	5	3	4	15	2	0	0	2
							13	6	2	18	4	0	2	0
							9	4.5	3	16.5	3	0	1	1
Catopsalis fissidens	S	100	NMMNH 8608	RM1	Middle	9	27	6	3	28	0	1	0	0
							25	9	0	24	2	0	1	0
							26	7.5	1.5	26	1	0.5	0.5	0
Catopsalis fissidens	S	100	NMMNH 8608	Lm1	Lingual	4	21	7	3	20	2	0	0	1
							33	9	4	15	1	1	0	2
							27	8	3.5	17.5	1.5	0.5	0	1.5
Catopsalis fissidens	S	100	NMMNH 8608	Lm2	Lingual	1	43	5	0	15	1	0	0	1
							42	4	1	13	1	0	1	0
							42.5	4.5	0.5	14	1	0	0.5	0.5
Catopsalis fissidens	P	100	NMMNH 62373	Lm1	Lingual	2	17	6	3	25	1	1	1	1
							20	3	2	22	0	2	0	0
							18.5	4.5	2.5	23.5	0.5	1.5	0.5	0.5
Catopsalis fissidens	P	100	NMMNH 62373	Lm2	Lingual	2	17	10	2	20	1	0	0	0
							31	3	3	31	0	0	0	0
							24	6.5	2.5	25.5	0.5	0	0	0

Catopsalis kakwa	S	100	TMP 2009.133.0014	Rm1	Labial	3	10	4	0	14	0	0	0	0
							12	2	1	11	0	0	0	0
							11	3	0.5	12.5	0	0	0	0
Catopsalis kakwa	S	100	TMP 2010.097.0020	Rm1	Labial	2	8	4	3	13	1	0	1	2
							10	0	4	7	2	0	0	0
							9	2	3.5	10	1.5	0	0.5	1
Catopsalis kakwa	S	100	TMP 2012.024.0063	Lm1	Lingual	3	16	6	1	9	0	1	1	2
							25	9	2	29	3	0	1	1
							20.5	7.5	1.5	19	1.5	0.5	1	1.5
Catopsalis kakwa	S	100	TMP 2012.024.0225	RM1	Labial	2	7	6	0	9	1	0	0	0
							7	3	0	9	0	0	0	0
							7	4.5	0	9	0.5	0	0	0
Catopsalis kakwa	S	100	UALVP 57542	Rm1	Lingual	2	13	4	2	16	1	0	1	3
							6	5	0	22	0	0	0	1
							9.5	4.5	1	19	0.5	0	0.5	2
Meniscoessus major	S	100	UALVP 15164	Rm1	Lingual	3	12	5	5	15	3	1	0	0
							17	4	3	27	1	0	0	0
							14.5	4.5	4	21	2	0.5	0	0
Meniscoessus major	S	100	UALVP 15165	Rm1	Lingual	4	18	1	3	23	1	0	0	0
							7	1	2	14	1	0	0	0
							12.5	1	2.5	18.5	1	0	0	0
Meniscoessus major	S	100	UALVP 15172	LM1	Middle	8	26	5	1	29	1	0	1	0
							20	6	2	25	2	0	0	0
							23	5.5	1.5	27	1.5	0	0.5	0
Meniscoessus major	S	100	UALVP 15174	RM1	Middle	2	26	5	4	26	0	0	0	0
							16	2	2	21	0	0	2	0
							21	3.5	3	23.5	0	0	1	0
Meniscoessus major	S	100	UALVP 15180	LM2	Lingual	3	22	5	6	25	4	0	0	0

Taxon			Specimen	Tooth	Position	No.								
							22	2	1	30	1	0	0	0
							22	3.5	3.5	27.5	2.5	0	0	0
Meniscoessus robustus	S	100	ROM M	Lm2	Lingual	2	13	3	2	12	2	2	0	0
							17	4	0	14	2	0	0	0
							15	3.5	1	13	2	1	0	0
Meniscoessus robustus	S	200	TMP 1987.215.0015	m1	?	4	24	6	0	21	0	0	0	0
							20	3	0	26	0	0	0	1
							22	4.5	0	23.5	0	0	0	0.5
Meniscoessus robustus	S	100	UALVP 27189	RM1	Middle	4	18	3	1	12	1	1	0	0
							19	4	0	11	1	1	0	2
							18.5	3.5	0.5	11.5	1	1	0	1
Meniscoessus robustus	S	100	UALVP 27243	Rm2	Lingual	2	21	6	3	13	0	0	3	1
							11	3	0	30	0	0	0	0
							16	4.5	1.5	21.5	0	0	1.5	0.5
Meniscoessus robustus	S	100	UALVP 27244	LM2	Lingual	1	9	3	1	6	4	2	0	0
							18	5	0	18	1	0	0	1
							13.5	4	0.5	12	2.5	1	0	0.5
Mesodma sp.	S	200	ROM A1	LM1	Middle	10	17	1	1	22	4	0	0	1
							23	3	0	29	3	0	0	0
							20	2	0.5	25.5	3.5	0	0	0.5
Mesodma sp.	S	200	ROM P	LM2	Lingual	4	12	6	1	15	2	0	4	0
							16	2	3	22	1	0	1	0
							14	4	2	18.5	1.5	0	2.5	0
Mesodma sp.	S	200	ROM U	Rm1	Lingual	2 and 3	17	1	4	26	0	0	0	0
							18	3	4	25	0	0	0	0
							17.5	2	4	25.5	0	0	0	0
Mesodma sp.	S	200	UALVP 7429	RM1	Middle	8	31	3	0	18	3	0	0	0
							29	5	0	26	2	0	0	0
							30	4	0	22	2.5	0	0	0

Taxon														
Mesodma sp.	S	200	UALVP 7433	RM1	Middle	2	33	0	3	40	0	0	1	1
							-	-	-	-	-	-	-	-
							33	0	3	40	0	0	1	1
Ptilodus sp.	S	200	TMP 1999.019.0007	RM2	Lingual	2	10	8	1	13	1	0	0	0
							13	6	1	19	2	0	0	1
							11.5	7	1	16	1.5	0	0	0.5
Ptilodus sp.	S	100	TMP 2017.025.0289	LM1	Middle	5	21	4	1	17	1	1	1	0
							14	3	0	16	1	1	0	2
							17.5	3.5	0.5	16.5	1	1	0.5	1
Ptilodus sp.	S	200	UALVP 46291	RM1	Middle	6	16	5	1	29	1	0	1	0
							21	3	3	27	0	1	1	0
							18.5	4	2	28	0.5	0.5	1	0
Ptilodus sp.	S	200	UALVP 46291	RM2	Lingual	2	22	2	0	19	1	1	0	0
							7	6	4	8	4	1	0	0
							14.5	4	2	13.5	2.5	1	0	0
Ptilodus sp.	S	100	UALPV 46291	Lm2	Lingual	2	12	3	2	20	2	0	0	0
							22	9	0	27	0	0	0	0
							17	6	1	23.5	1	0	0	0
Taeniolabis taoensis	P	100	AMNH 163.007.001	Rm1	Lingual	5	25	4	0	15	5	0	0	0
							21	7	0	16	7	0	0	0
							23	5.5	0	15.5	6	0	0	0
Taeniolabis taoensis	P	100	AMNH 727	Rm1	Lingual	6	34	11	3	19	1	0	1	1
							29	5	2	22	1	0	0	0
							31.5	8	2.5	20.5	1	0	0.5	0.5
Taeniolabis taoensis	P	100	AMNH 27728	Lm2	Lingual	3	24	2	8	20	1	0	0	1
							12	8	4	13	5	1	3	0
							18	5	6	16.5	3	0.5	1.5	0.5
Taeniolabis taoensis	S	100	NMMNH 12387	RM1	Middle	2	10	6	3	10	0	2	0	0
							11	2	5	16	2	0	0	1

Species														
							10.5	4	4	13	1	1	0	0.5
Taeniolabis taoensis	S	100	NMMNH 44417	Rm1	Lingual	6	22	8	1	13	2	0	0	1
							30	9	1	14	1	0	0	0
							26	8.5	1	13.5	1.5	0	0	0.5
Valenopsalis joyneri	S	100	UALVP 6596	Rm1	Lingual	3	21	9	5	12	3	3	0	0
							17	10	5	27	3	1	1	1
							19	9.5	5	19.5	3	2	0.5	0.5
Valenopsalis joyneri	S	100	UALVP 28167	Rm1	Lingual	3	13	4	3	17	0	0	0	0
							28	2	1	16	0	0	0	0
							20.5	3	2	16.5	0	0	0	0
Valenopsalis joyneri	S	100	UALVP 28175	Rm1	Lingual	2	19	8	1	13	3	1	0	1
							26	8	3	24	2	1	0	0
							22.5	8	2	18.5	2.5	1	0	0.5
Valenopsalis joyneri	S	100	UALVP 28186	RM1	Middle	7	32	9	2	16	2	1	0	0
							28	9	2	27	1	0	0	2
							30	9	2	21.5	1.5	0.5	0	1
Valenopsalis joyneri	S	100	UALVP 28202	Lm2	Lingual	1	12	2	2	15	3	0	0	0
							7	5	5	19	1	0	0	0
							9.5	3.5	3.5	17	2	0	0	0

Appendix C: Microwear Counting Colour Scheme

Colour		Microwear Feature
Yellow	▬▬▬	Small pits
Green	▬▬▬	Medium pits
Magenta	▬▬▬	Large pits
Teal	▬▬▬	Fine scratches
Dark blue	▬▬▬	Medium scratches
White		Large scratches
Red	▬▬▬	Shallow gouges
Orange	▬▬▬	Deep gouges

Appendix D: Operational Definitions of Multituberculate Cheek Teeth Wear Stages

Definitions modified from Krause (1982).

Wear Stage	Operational Definition
Low wear	Dentine is not exposed or, if dentine is exposed, there are no noticeable changes to tooth morphology.
Moderate wear	Dentine is exposed, but the occlusal surfaces of the cusps still retain enamel. The cusps are in positive relief above the midline basin of tooth. The cusps are distinct, and a majority of the dentine pools are not connected. In the case of taeniolabidoid molars, the teeth may have posterior cusps with high wear, but the anterior cusps are still mostly unworn.
High wear	Dentine is exposed, cusps are close to being flush with the occlusal basin. The cusps do not retain their original shape.

Literature Cited

Krause, D. W. 1982. Jaw movement, dental function, and diet in the Paleocene multituberculate *Ptilodus*. Paleobiology 8:265–281.

Appendix E: Cusp Row Ratios of Individual Specimens

Institutional abbreviations: **NMMNH** – New Mexico Museum of Natural History and Science (Albuquerque, NM, USA); **ROM** – Royal Ontario Museum (Toronto, ON, Canada); **TMP** – Royal Tyrrell Museum of Palaeontology (Drumheller, AB, Canada); **UALVP** – University of Alberta Laboratory for Vertebrate Paleontology (Edmonton, AB, Canada); **UCM** – University of Colorado Museum of Natural History (Boulder, CO, USA); **UM** – University of Michigan Museum of Paleontology (Ann Arbor, MI, USA); **UW** – University of Wyoming Geological Museum (Laramie, WY, USA)

Table abbreviations: **CRL** – cusp row length; **CRR** – cusp row ratio

Genus	Species	Repository	Specimen Number	Tooth	Total CRL (mm)	Tooth Area (mm^2)	CRR
cf. *Acheronodon*	*vossae*	TMP	2015.069.0174	Lm1	3.798	2.043	2.657179
Cimolomyid 1		UALVP	1766	Rm1	7.804	6.755	3.002649
Cimolomyid 1		UALVP	30575	Rm1	8.025	6.68	3.104966
Cimolomyid 1		UALVP	30593	Rm1	7.364	6.332	2.926465
Cimolomyid 1		UALVP	4233	Lm1	7.811	7.47	2.857895
Cimolomyid 1		TMP	95.6.6	Rm1	8.556	6.537	3.346428
Cimolomyid 1		UALVP	30568	Rm1	7.864	6.897	2.994425
Cimolomyid 1		UALVP	30558	Lm1	8.63	7.07	3.245646
Cimolomyid 1		UALVP	2010	Rm1	7.661	6.388	3.031119
Cimolomyid 1		UALVP	30633	Rm2	3.542	4.405	1.687624
Cimolomyid 1		UALVP	30096	Rm2	3.826	5.365	1.65181
Cimolomyid 1		UALVP	30098	Lm2	4.629	5.873	1.910105
Cimolomyid 1		TMP	87.73.2	Lm2	5.261	5.542	2.234781
Cimolomyid 1		UALVP	30640	Rm2	5.669	5.872	2.339448
Cimolomyid 1		UALVP	30616	Rm2	5.513	6.177	2.218192
Cimolomyid 1		UALVP	30092	Rm2	5.152	5.761	2.14648

Cimolomyid 1		UALVP	30093	Rm2	5.579	6.274	2.227328
Cimolomyid 1		UALVP	30641	Rm2	5.176	5.118	2.287937
Catopsalis	*alexanderi*	UCM	34141	Lm1	16.048	38.262	2.594401
Catopsalis	*alexanderi*	UCM	34332	Rm1	16.611	35.408	2.791548
Catopsalis	cf. *calgariensis*	UW	15100	Rm1	37.305	121.651	3.382277
Catopsalis	cf. *calgariensis*	UW	6388	Rm1	38.345	120.845	3.488144
Catopsalis	cf. *calgariensis*	UW	14051	Rm2	17.032	74.114	1.978406
Catopsalis	calgariensis	TMP	2015.023.0001	Lm2	11.731	53.071	1.610299
Catopsalis	*fissidens*	NMMNH	8607	Lp4	6.625	11.027	1.995066
Catopsalis	*fissidens*	NMMNH	8608	Lm1	28.015	68.377	3.387939
Catopsalis	*fissidens*	NMMNH	8613	Rm1	23.802	65.852	2.933114
Catopsalis	*fissidens*	NMMNH	8613	Rm2	12.538	39.157	2.003658
Catopsalis	*johnstoni*	UALVP	16058	Lm1	19.32	49.708	2.740274
Catopsalis	*kakwa*	TMP	2015.071.0141	Lp4	4.239	2.134	2.901792
Catopsalis	*kakwa*	UALVP	57541	Rp4	4.463	2.888	2.626203
Catopsalis	*kakwa*	TMP	2012.024.0063	Lm1	10.103	14.148	2.68598
Catopsalis	*kakwa*	TMP	2009.133.0041	Rm2	6.803	12.012	1.962876
Catopsalis	*waddleae*	UM	90042	Lm1	30.627	129.178	2.694698
Cimolomys	sp.	UALVP	2141	Rm1	6.149	4.272	2.975013
Cimolomys	sp.	UALVP	30108	Rm1	5.543	3.967	2.783004
Cimolomys	sp.	UALVP	709	Rm1	5.903	4.391	2.817027
Cimolomys	sp.	UALVP	30112	Lm1	4.668	3.112	2.646129
Cimolomys	sp.	TMP	93.138.2	Lm2	3.335	3.008	1.922901
Cimolomys	sp.	UALVP	30605	Lm2	3.756	3.827	1.919978
Cimolomys	sp.	TMP	87.99.62	Rm2	3.5	3.251	1.941152
Cimolomys	sp.	TMP	99.13.5	Lm2	3.458	3.362	1.885932
Cimolomys	sp.	TMP	88.212.72	Lm2	3.772	3.386	2.049879
Cimolomys	sp.	TMP	99.1.5	Rm2	3.256	3.25	1.806104
Meniscoessus	*major*	IALVP	15182[T]	Lp4	6.686	9.948	2.119818
Meniscoessus	*major*	UALVP	15164	Rm1	11.218	15.136	2.883433

Meniscoessus	*major*	UALVP	15165	Rm1	10.582	12.964	2.938991
Meniscoessus	*major*	UALVP	B	Rm2	7.164	11.472	2.115125
Mesodma	*formosa*	ROM	B1	Rm1	4.721	2.362	3.071808
Mesodma	sp.	ROM	T	Rm1	4.519	2.295	2.982984
Mesodma	sp.	ROM	U	Rm1	4.93	2.685	3.008672
Mesodma	sp.	ROM	Y	Rm1	5.285	2.942	3.081227
Mesodma	sp.	UALVP	7278	Lm1	4.425	2.796	2.646334
Mesodma	sp.	UALVP	7288	Lm1	4.093	2.014	2.884111
Mesodma	*formosa*	ROM	V	Lm2	2.479	1.585	1.969073
Ptilodus	sp.	TMP	2015.069.0902*	Lm1	6.154	4.374	2.942511
Ptilodus	sp. C	TMP	2014.047.0181	Lm1	8.1	7.061	3.048259
Stygimys	*kuszmauli*	UALVP	6533	Rm1	7.214	5.482	3.081106
Taeniolabis	*taoensis*	NMMNH	9631	Rp4	10.649	28.578	1.992016
Taeniolabis	*taoensis*	NMMNH	8631	Rm1	58.107	221.539	3.903942
Taeniolabis	*taoensis*	NMMNH	2763	Lm2	23.22	128.783	2.046129
Taeniolabis	*taoensis*	NMMNH	8631	Rm2	24.412	114.672	2.279684
Valenopsalis	*joyneri*	ROM	I	Lp4	6.244	7.149	2.335287
Valenopsalis	*joyneri*	UALVP	7395	Lp4	4.308	3.486	2.307342
Valenopsalis	*joyneri*	UALVP	7412	Lp4	4.958	4.325	2.38404
Valenopsalis	*joyneri*	UALVP	28167	Lm1	13.552	24.635	2.730405
Valenopsalis	*joyneri*	UALVP	28170	Rm1	12.751	22.402	2.69402
Valenopsalis	*joyneri*	UALVP	28172	Lm1	14.621	28.333	2.746824
Valenopsalis	*joyneri*	UALVP	28175	Lm1	13.933	22.928	2.909789
Valenopsalis	*joyneri*	UALVP	28193	Lm1	14.407	25.485	2.853851
Valenopsalis	*joyneri*	UALVP	6596	Lm1	13.054	19.102	2.986787
Valenopsalis	*joyneri*	UALVP	28202	Lm2	9.2	19.728	2.071316
Valenopsalis	*joyneri*	UALVP	28204	Lm2	9.981	21.635	2.145831
Valenopsalis	*joyneri*	UALPV	28207	Rm2	9.329	18.399	2.174893

[T] Molar row has medium wear, but p4 has low wear

* Tooth still embedded in rock. Measurements may be slightly underestimated

Appendix F: Crest Row Ratio Error Propagation Calculations

Error Propagation for Crest Row Ratios by Tooth

The SRA formula is $\frac{CL}{\sqrt{A2D}}$, where CL is the total crest length of a tooth and A2D is the occlusal

footprint area of the tooth. To calculate the average SRA for a taxon (e.g. Valenopsalis joyneri

m1), an average crest length and average area must be calculated. The resultant SRA equation is

$\frac{\overline{CL}}{\sqrt{\overline{A2D}}}$. Both the average CL and average A2D have an associated standard deviation. Thus, error

propagation must be considered when finding the standard deviation of the average tooth SRA.

The basic formula for Gaussian error propagation is:

$$s_{\bar{z}} \approx \sqrt{\left(\frac{\partial z}{\partial x}\, s_{\bar{x}}\right)^2 + \left(\frac{\partial z}{\partial y}\, s_{\bar{y}}\right)^2 + \left(\frac{\partial z}{\partial q}\, s_{\bar{q}}\right)^2 + \cdots}$$

For the SRA formula,

$$\frac{\partial z}{\partial CL} = \left(\frac{1}{\sqrt{\overline{A2D}}}\right)\left(\frac{\partial}{\partial CL} \cdot \overline{CL}\right) = \frac{1}{\sqrt{\overline{A2D}}}$$

$$\frac{\partial z}{\partial A2D} = (\overline{CL})\left(\frac{\partial}{\partial A2D} \cdot \overline{A2D}^{-\frac{1}{2}}\right) = (\overline{CL})\left(-\frac{1}{2} \cdot \overline{A2D}^{-\frac{3}{2}}\right) = -\frac{\overline{CL}}{2\left(\sqrt{\overline{A2D}}\right)^3}$$

The end formula is:

$$s_{\bar{z}} \approx \sqrt{\left(\frac{1}{\sqrt{\overline{A2D}}} \cdot s_{\overline{CL}}\right)^2 + \left(-\frac{1}{2}\frac{\overline{CL}}{\left(\sqrt{\overline{A2D}}\right)^3} \cdot s_{\overline{A2D}}\right)^2}$$

These partial derivatives are intended to be used with the standard error ($s_{\bar{z}}$) of the mean.

Because my measurements report standard deviations, I converted these to standard errors using

the formula $s_{\bar{z}} = \frac{s_z}{\sqrt{n}}$. The following table has both the standard deviations and standard errors of

the SRAs by tooth and taxon. Only taxa with more than one specimen are included.

Genus	Species	Tooth	N	Average CL (SD)	Average Area (SD)	CL SE	Area SE
Catopsalis	*alexanderi*	m1	2	16.3295 (0.398101)	36.835 (2.018083)	0.2815	1.427
Catopsalis	cf. *calgariensis*	m1	2	37.825 (0.735391)	121.248 (0.569928)	0.52	0.403
Catopsalis	*fissidens*	m1	2	25.9085 (2.979041)	67.1145 (1.785445)	2.1065	1.2625
Catopsalis	*kakwa*	p4	2	4.351 (0.1583919)	2.511 (0.5331585)	0.112	0.377
Cimolomyid 1	sp.	m1	8	7.964375 (0.432362)	6.766125 (0.377282)	0.152863	0.133389
Cimolomyid 1	sp.	m2	9	4.927444 (0.771563)	5.598556 (0.578852)	0.257188	0.192951
Cimolomys	sp.	m1	4	5.56575 (0.648175)	3.9355 (0.577309)	0.324087	0.288654
Cimolomys	sp.	m2	6	3.512833 (0.213099)	3.347333 (0.270441)	0.086997	0.110407
Meniscoessus	*major*	m1	2	10.9 (0.44972)	14.05 (1.535836)	0.318	1.086
Mesodma	sp.	m1	6	4.093 (0.415647)	2.014 (0.350142)	0.169687	0.142945
Ptilodus	sp.	m1	2	7.127 (1.37603)	5.7175 (1.899996)	0.973	1.3435
Taeniolabis	*taoensis*	m2	2	23.816 (0.842871)	121.7275 (9.977984)	0.596	7.0555
Valenopsalis	*joyneri*	p4	3	5.17 (0.9852573)	4.986667 (1.9190478)	0.568839	1.107963
Valenopsalis	*joyneri*	m1	6	13.71967 (0.740254)	23.81417 (3.126318)	0.302207	1.276314
Valenopsalis	*joyneri*	m2	3	9.503333 (0.41867)	19.92067 (1.626581)	0.241719	0.939107

Error propagation was also required for molar row SRA. The formula for the molar row

SRA is similar to that of the individual teeth averages, but it involves combining the average m1

and average m2 SRA values:

$$\text{Molar row SRA} = \frac{\overline{(m1\ CL)} + \overline{(m2\ CL)}}{\sqrt{((m1\ A2D) + \overline{(m2\ A2D)})}}$$

The partial derivatives for this formula are as follows:

$$\frac{\partial z}{\partial\ m1CL} = \left(\frac{\partial}{\partial m1CL}\left(\frac{\overline{m1CL}}{\sqrt{\overline{m1A2D} + \overline{m2A2D}}} + \frac{\overline{m2CL}}{\sqrt{\overline{m1A2D} + \overline{m2A2D}}}\right)\right)$$

$$= \left(\frac{\partial}{\partial m1CL} \cdot \frac{\overline{m1CL}}{\sqrt{\overline{m1A2D} + \overline{m2A2D}}}\right) + 0 = \frac{1}{\sqrt{\overline{m1A2D} + \overline{m2A2D}}}$$

$$\frac{\partial z}{\partial\ m2CL} = \left(\frac{\partial}{\partial m2CL}\left(\frac{\overline{m1CL}}{\sqrt{\overline{m1A2D} + \overline{m2A2D}}} + \frac{\overline{m2CL}}{\sqrt{\overline{m1A2D} + \overline{m2A2D}}}\right)\right)$$

$$= 0 + \left(\frac{\partial}{\partial m2CL} \cdot \frac{\overline{m2CL}}{\sqrt{\overline{m1A2D} + \overline{m2A2D}}}\right) = \frac{1}{\sqrt{\overline{m1A2D} + \overline{m2A2D}}}$$

$$\frac{\partial z}{\partial\ m1A2D} = (\overline{m1CL} + \overline{m2CL})\frac{\partial z}{\partial\ m1A2D}\left(\frac{1}{\sqrt{\overline{m1A2D} + \overline{m2A2D}}}\right) =$$

Using the chain rule, $f = u^{-\frac{1}{2}}, u = (\overline{m1A2D} + \overline{m2A2D})$

$$(\overline{m1CL} + \overline{m2CL})\frac{\partial}{\partial u}\left(u^{-\frac{1}{2}}\right)\frac{\partial}{\partial\ m1A2D}(\overline{m1A2D} + \overline{m2A2D}) = (\overline{m1CL} + \overline{m2CL})\left(\frac{u^{-\frac{3}{2}}}{-2}\right)$$

$$= -\frac{1}{2}\frac{(\overline{m1CL} + \overline{m2CL})}{\left(\sqrt{(\overline{m1A2D} + \overline{m2A2D})}\right)^3}$$

Similarly,

$$\frac{\partial z}{\partial\ m2A2D} = (\overline{m1CL} + \overline{m2CL})\frac{\partial z}{\partial\ m2A2D}\left(\frac{1}{\sqrt{\overline{m1A2D} + \overline{m2A2D}}}\right)$$

$$= (\overline{m1CL} + \overline{m2CL})\frac{\partial}{\partial u}\left(u^{-\frac{1}{2}}\right)\frac{\partial}{\partial\ m2A2D}(\overline{m1A2D} + \overline{m2A2D})$$

$$= (\overline{m1CL} + \overline{m2CL})\left(\frac{u^{-\frac{3}{2}}}{-2}\right) = -\frac{1}{2}\frac{(\overline{m1CL} + \overline{m2CL})}{\left(\sqrt{(\overline{m1A2D} + \overline{m2A2D})}\right)^3}$$

The partial derivatives are then added to the Gaussian error propagation equation:

$$\sqrt{\begin{array}{c}\left(\frac{1}{\sqrt{\overline{m1A2D} + \overline{m2A2D}}}\cdot s_{\overline{m1CL}}\right)^2 + \left(\frac{1}{\sqrt{\overline{m1A2D} + \overline{m2A2D}}}\cdot s_{\overline{m2CL}}\right)^2 + \\[2em] \left(-\frac{1}{2}\frac{(\overline{m1CL} + \overline{m2CL})}{\left(\sqrt{(\overline{m1A2D} + \overline{m2A2D})}\right)^3}\cdot s_{\overline{m1A2D}}\right)^2 + \left(-\frac{1}{2}\frac{(\overline{m1CL} + \overline{m2CL})}{\left(\sqrt{(\overline{m1A2D} + \overline{m2A2D})}\right)^3}\cdot s_{\overline{m2A2D}}\right)^2\end{array}}$$

The error propagation for tooth row SRAs is very similar to that of molar row SRAs. The only difference is that the CL and A2D of the p4 is included in the calculation:

$$Tooth\ row\ SRA = \frac{(\overline{p4\ CL}) + (\overline{m1\ CL}) + (\overline{m2\ CL})}{\sqrt{((\overline{p4\ A2D}) + (\overline{m1\ A2D}) + (\overline{m2\ A2D}))}}$$

The partial derivatives for this formula are as follows:

$$\frac{\partial z}{\partial\, p4CL} = \left(\frac{\partial}{\partial p4CL}\left(\frac{\overline{p4CL}}{\sqrt{(p4\ A2D) + (m1\ A2D) + \ (m2\ A2D)}}\right.\right.$$

$$+ \frac{\overline{m1CL}}{\sqrt{(p4\ A2D) + (m1\ A2D) + \ (m2\ A2D)}}$$

$$\left.\left.+ \frac{\overline{m2CL}}{\sqrt{(p4\ A2D) + (m1\ A2D) + \ (m2\ A2D)}}\right)\right)$$

$$= \left(\frac{\partial}{\partial p4CL} \cdot \frac{\overline{p4CL}}{\sqrt{(p4\ A2D) + (m1\ A2D) + \ (m2\ A2D)}}\right) + 0$$

$$= \frac{1}{\sqrt{(p4\ A2D) + (m1\ A2D) + \ (m2\ A2D)}}$$

$$\frac{\partial z}{\partial\, m1CL} = \left(\frac{\partial}{\partial m1CL}\left(\frac{\overline{p4CL}}{\sqrt{(p4\ A2D) + (m1\ A2D) + \ (m2\ A2D)}}\right.\right.$$

$$+ \frac{\overline{m1CL}}{\sqrt{(p4\ A2D) + (m1\ A2D) + \ (m2\ A2D)}}$$

$$\left.\left.+ \frac{\overline{m2CL}}{\sqrt{(p4\ A2D) + (m1\ A2D) + \ (m2\ A2D)}}\right)\right)$$

$$= \left(\frac{\partial}{\partial m1CL} \cdot \frac{\overline{m1CL}}{\sqrt{(p4\ A2D) + (m1\ A2D) + \ (m2\ A2D)}}\right) + 0$$

$$= \frac{1}{\sqrt{(p4\ A2D) + (m1\ A2D) + \ (m2\ A2D)}}$$

$$\frac{\partial z}{\partial\ m2CL} = \left(\frac{\partial}{\partial m2CL}\left(\frac{\overline{p4CL}}{\sqrt{(\overline{p4\ A2D}) + (\overline{m1\ A2D}) + (\overline{m2\ A2D})}}\right.\right.$$

$$+ \frac{\overline{m1CL}}{\sqrt{(\overline{p4\ A2D}) + (\overline{m1\ A2D}) + (\overline{m2\ A2D})}}$$

$$\left.\left.+ \frac{\overline{m2CL}}{\sqrt{(\overline{p4\ A2D}) + (\overline{m1\ A2D}) + (\overline{m2\ A2D})}}\right)\right)$$

$$= \left(\frac{\partial}{\partial m2CL} \cdot \frac{\overline{m2CL}}{\sqrt{(\overline{p4\ A2D}) + (\overline{m1\ A2D}) + (\overline{m2\ A2D})}}\right) + 0$$

$$= \frac{1}{\sqrt{(\overline{p4\ A2D}) + (\overline{m1\ A2D}) + (\overline{m2\ A2D})}}$$

$$\frac{\partial z}{\partial\ p4A2D} = (\overline{p4CL} + \overline{m1CL} + \overline{m2CL})\frac{\partial z}{\partial\ p4A2D}\left(\frac{1}{\sqrt{\overline{p4A2D} + \overline{m1A2D} + \overline{m2A2D}}}\right) =$$

Using the chain rule, $f = u^{-\frac{1}{2}}, u = (\overline{p4CL} + \overline{m1CL} + \overline{m2CL})$

$$(\overline{p4CL} + \overline{m1CL} + \overline{m2CL})\frac{\partial}{\partial u}\left(u^{-\frac{1}{2}}\right)\frac{\partial}{\partial\ p4A2D}(\overline{p4A2D} + \overline{m1A2D} + \overline{m2A2D})$$

$$= (\overline{p4CL} + \overline{m1CL} + \overline{m2CL})\left(\frac{u^{-\frac{3}{2}}}{-2}\right) = -\frac{1}{2}\frac{(\overline{p4CL} + \overline{m1CL} + \overline{m2CL})}{\left(\sqrt{\overline{p4A2D} + \overline{m1A2D} + \overline{m2A2D}}\right)^3}$$

$$\frac{\partial z}{\partial\ m1A2D} = (\overline{p4CL} + \overline{m1CL} + \overline{m2CL})\frac{\partial z}{\partial\ m1A2D}\left(\frac{1}{\sqrt{\overline{p4A2D} + \overline{m1A2D} + \overline{m2A2D}}}\right) =$$

$$(\overline{p4CL} + \overline{m1CL} + \overline{m2CL})\frac{\partial}{\partial u}\left(u^{-\frac{1}{2}}\right)\frac{\partial}{\partial\ m1A2D}(\overline{p4A2D} + \overline{m1A2D} + \overline{m2A2D})$$

$$= (\overline{p4CL} + \overline{m1CL} + \overline{m2CL})\left(\frac{u^{-\frac{3}{2}}}{-2}\right) = -\frac{1}{2}\frac{(\overline{p4CL} + \overline{m1CL} + \overline{m2CL})}{\left(\sqrt{\overline{p4A2D} + \overline{m1A2D} + \overline{m2A2D}}\right)^3}$$

$$\frac{\partial z}{\partial\, m2A2D} = (\overline{p4CL} + \overline{m1CL} + \overline{m2CL})\frac{\partial z}{\partial\, m2A2D}\left(\frac{1}{\sqrt{\overline{p4A2D} + \overline{m1A2D} + \overline{m2A2D}}}\right) =$$

$$(\overline{p4CL} + \overline{m1CL} + \overline{m2CL})\frac{\partial}{\partial u}\left(u^{-\frac{1}{2}}\right)\frac{\partial}{\partial\, m2A2D}(\overline{p4A2D} + \overline{m1A2D} + \overline{m2A2D})$$

$$= (\overline{p4CL} + \overline{m1CL} + \overline{m2CL})\left(\frac{u^{-\frac{3}{2}}}{-2}\right) = -\frac{1}{2}\frac{(\overline{p4CL} + \overline{m1CL} + \overline{m2CL})}{\left(\sqrt{\overline{p4A2D} + \overline{m1A2D} + \overline{m2A2D}}\right)^3}$$

The resultant equation is:

$$\sqrt{\begin{aligned}&\left(\frac{1}{\sqrt{(\overline{p4\,A2D}) + (\overline{m1\,A2D}) + (\overline{m2\,A2D})}}\cdot s_{\overline{p4CL}}\right)^2 + \left(\frac{1}{\sqrt{(\overline{p4\,A2D}) + (\overline{m1\,A2D}) + (\overline{m2\,A2D})}}\cdot s_{\overline{m1CL}}\right)^2 +\\[2mm]&\left(\frac{1}{\sqrt{(\overline{p4\,A2D}) + (\overline{m1\,A2D}) + (\overline{m2\,A2D})}}\cdot s_{\overline{m2CL}}\right)^2 + \left(-\frac{1}{2}\frac{(\overline{p4CL} + \overline{m1CL} + \overline{m2CL})}{\left(\sqrt{\overline{p4A2D} + \overline{m1A2D} + \overline{m2A2D}}\right)^3}\cdot s_{\overline{p4A2D}}\right)^2 +\\[2mm]&\left(-\frac{1}{2}\frac{(\overline{p4CL} + \overline{m1CL} + \overline{m2CL})}{\left(\sqrt{\overline{p4A2D} + \overline{m1A2D} + \overline{m2A2D}}\right)^3}\cdot s_{\overline{m1A2D}}\right)^2 + \left(-\frac{1}{2}\frac{(\overline{p4CL} + \overline{m1CL} + \overline{m2CL})}{\left(\sqrt{\overline{p4A2D} + \overline{m1A2D} + \overline{m2A2D}}\right)^3}\cdot s_{\overline{m2A2D}}\right)^2\end{aligned}}$$

Appendix G: CT Scanning and Processing Parameters

Institutional abbreviations: **NMMNH** – New Mexico Museum of Natural History and Science (Albuquerque, NM, USA); **ROM** –

Royal Ontario Museum (Toronto, ON, Canada); **TMP** – Royal Tyrrell Museum of Palaeontology (Drumheller, AB, Canada); **UALVP**

– University of Alberta Laboratory for Vertebrate Paleontology (Edmonton, AB, Canada); **UCM** – University of Colorado Museum of

Natural History (Boulder, CO, USA); **UM** – University of Michigan Museum of Paleontology (Ann Arbor, MI, USA); **UW** –

University of Wyoming Geological Museum (Laramie, WY, USA).

Table terms: **Scan Faces** – the number of faces on the initial CT scan; **RFI alpha adjustment** – the alpha level set when calculating

RFI, if different from the standard (0.60); **Healed LS scan** – was the scan healed after Laplacian Smoothing was performed

Specimen	Taxon	Tooth	Scan Resolution	Specimen Material	Scan Faces	Simplification Factor	RFI alpha adjustment	Healed LS scan?
TMP 2015.069.0174	Cf. *Acheronodon vossae*	Lm1	High	Tooth	10986	10,000	--	--
UCM 34136	*Catopsalis alexanderi*	Lp4-m2	Standard	Tooth	74,101	30,000	--	--
UCM 34136	*Catopsalis alexanderi*	Lm1	Standard	Tooth	37,255	10,000	--	--
UCM 34136	*Catopsalis alexanderi*	Lm2	Standard	Tooth	26,520	10,000	--	--
UCM 34136	*Catopsalis alexanderi*	Lp4	Standard	Tooth	9279	--	--	--
UCM 34141	*Catopsalis alexanderi*	Lm1	Standard	Tooth	42,676	10,000	--	--
UCM 34332	*Catopsalis alexanderi*	Rm1	Standard	Tooth	47,757	10,000	--	--
TMP 2015.023.0001	*Catopsalis calgariensis*	Lm2	Standard	Tooth	74,762	10,000	--	--

TMP 127	*Catopsalis calgariensis*	Rm2	Standard	Cast	68,613	10,000	--	--
UW 14051	*Catopsalis* cf. *calgariensis*	Rm2	Standard	Tooth	107,158	10,000	--	--
UW 15100	*Catopsalis* cf. *calgariensis*	Rm1	Standard	Tooth	203,588	10,000	--	--
UW 15102	*Catopsalis* cf. *calgariensis*	Rm2	Standard	Tooth	80,455	10,000	--	Yes
UW 6387	*Catopsalis* cf. *calgariensis*	Lm2	Standard	Tooth	127,935	10,000	--	Yes
UW 6387	*Catopsalis* cf. *calgariensis*	Rm1	Standard	Tooth	114,021	10,000	--	--
UW 6388	*Catopsalis* cf. *calgariensis*	Lm2	Standard	Tooth	68,407	10,000	--	Yes
UW 6388	*Catopsalis* cf. *calgariensis*	Rm1	Standard	Tooth	80,455	10,000	--	--
NMMNH 8608	*Catopsalis fissidens*	Lp4-m2	Standard	Cast	167,354	30,000	0.70	--
NMMNH 8608	*Catopsalis fissidens*	Lm1	Standard	Cast	16,599	10,000	--	--
NMMNH 8608	*Catopsalis fissidens*	Lm2	Standard	Cast	93,999	10,000	--	Yes
NMMNH 8609	*Catopsalis fissidens*	Lm1-2	Standard	Cast	53,306	10,000	--	--
NMMNH 8609	*Catopsalis fissidens*	Lm1	Standard	Cast	135,987	20,000	--	--
NMMNH 8609	*Catopsalis fissidens*	Lm2	Standard	Cast	82,705	10,000	--	--
NMMNH 8613	*Catopsalis fissidens*	Rm1-2	Standard	Cast	52,027	10,000	--	--
NMMNH 8613	*Catopsalis fissidens*	Rm1	Standard	Cast	150,494	20,000	--	--
NMMNH 8613	*Catopsalis fissidens*	Rm2	Standard	Cast	95,671	10,000	--	Yes
UALVP 16058	*Catopsalis johnstoni*	Lm1	Standard	Tooth	56,727	10,000	--	--
TMP 2009.133.0041	*Catopsalis kakwa*	Rm2	Standard	Tooth	56,727	10,000	--	--
TMP 2009.133.0114	*Catopsalis kakwa*	Rm1	Standard	Tooth	19,307	10,000	--	Yes
TMP 2010.097.0015	*Catopsalis kakwa*	Rm2	Standard	Tooth	18,838	10,000	--	--

TMP 2010.097.0020	*Catopsalis kakwa*	Rm1	Standard	Tooth	20,920	10,000	--	--
TMP 2015.071.0141	*Catopsalis kakwa*	Lp4	High	Tooth	27,030	10,000	--	--
UALVP 57541	*Catopsalis kakwa*	Rp4	High	Tooth	14,674	10,000	--	--
UM 90042	*Catopsalis waddleae*	Lm1	Standard	Cast	193,497	10,000	--	--
UALVP 1766	Cimolomyid 1	Rm1	High	Tooth	39,977	10,000	--	--
UALVP 30096	Cimolomyid 1	Rm2	High	Tooth	30,992	10,000	--	--
UALVP 30593	Cimolomyid 1	Rm1	High	Tooth	38,598	10,000	--	--
UALVP 2141	*Cimolomys* sp.	Rm1	High	Tooth	21,636	10,000	--	--
UALVP 30112	*Cimolomys* sp.	Lm1	High	Tooth	19,793	10,000	0.70	--
UALVP 30605	*Cimolomys* sp.	Lm2	High	Tooth	18,258		--	--
UALVP 709	*Cimolomys* sp.	Rm1	High	Tooth	21,794	10,000	--	--
UALVP 15164	*Meniscoessus major*	Rm1	Standard	Tooth	21,227	10,000	--	--
UALVP 15165	*Meniscoessus major*	Rm1	Standard	Tooth	18,279	10,000	--	--
UALVP 15167	*Meniscoessus major*	Rm1	Standard	Tooth	16,802	10,000	--	--
UALVP 15182	*Meniscoessus major*	Lp4-m2	Standard	Tooth	50,057	30,000	--	--
UALVP 15182	*Meniscoessus major*	Lm1	Standard	Tooth	17,500	10,000	0.80	--
UALVP 15182	*Meniscoessus major*	Lm2	Standard	Tooth	15,416	10,000	--	--
UALVP 15182	*Meniscoessus major*	Lp4	Standard	Tooth	15,211	10,000	--	--
UALVP 15187	*Meniscoessus major*	Rm2	Standard	Tooth	16,391	10,000	--	--
UALVP B	*Meniscoessus major*	Rm2	Standard	Tooth	17,945	10,000	--	--
ROM M	*Meniscoessus robustus*	Lm2	Standard	Tooth	28,169	10,000	--	--
ROM B1	*Mesodma* sp.	Rm1	High	Tooth	14,854	10,000	--	--
ROM T	*Mesodma* sp.	Rm1	High	Tooth	8271	--	--	--
ROM V	*Mesodma* sp.	Lm2	High	Tooth	<10,000	--	--	--
UALVP 7278	*Mesodma* sp.	Lm1	High	Tooth	10,467	10,000	--	--
UALVP 7288	*Mesodma* sp.	Lm1	High	Tooth	7446	--	--	--
TMP 2009.132.0239	Neoplagiaulacid	Lm1	Standard	Tooth	20,445	10,000	--	--

TMP 2010.097.0126	*Ptilodus wyomingensis*	Lm1	High	Tooth	25,890	10,000	--	--
UALVP 6533	*Stygimys kuszmauli*	Rm1	High	Tooth	31,876	10,000	--	--
NMMNH 2763	*Taeniolabis taoensis*	Lm2	Standard	Tooth	191,835	10,000	--	--
NMMNH 42938	*Taeniolabis taoensis*	Rm2	Standard	Tooth	24,512	10,000	--	--
NMMNH 42939	*Taeniolabis taoensis*	Lm2	Standard	Cast	166,827	10,000	--	--
NMMNH 44417	*Taeniolabis taoensis*	Rm1	Standard	Cast	157,984	10,000	--	--
NMMNH 47445	*Taeniolabis taoensis*	Rm1-2	Standard	Tooth	231,096	10,000	--	Yes
NMMNH 47445	*Taeniolabis taoensis*	Rm1	Standard	Cast	358,511	20,000	--	--
NMMNH 47445	*Taeniolabis taoensis*	Rm2	Standard	Cast	210,558	10,000	--	--
NMMNH 47447	*Taeniolabis taoensis*	Rm2	Standard	Cast	166,072	10,000	--	--
NMMNH 8631	*Taeniolabis taoensis*	Rp4-m2	Standard	Cast	468,878	30,000	--	--
NMMNH 8631	*Taeniolabis taoensis*	Rm1	Standard	Cast	50,053	10,000	--	--
NMMNH 8631	*Taeniolabis taoensis*	Rm2	Standard	Cast	242,273	10,000	--	--
NMMNH 8631	*Taeniolabis taoensis*	Rp4	Standard	Cast	174,295	10,000	--	--
NMMNH 8632	*Taeniolabis taoensis*	Rp4-m2	Standard	Cast	413,189	30,000	0.70	Yes
NMMNH 8632	*Taeniolabis taoensis*	Rm1	Standard	Cast	39,185	10,000	--	--
NMMNH 8632	*Taeniolabis taoensis*	Rm2	Standard	Cast	220,125	10,000	--	--
NMMNH 8632	*Taeniolabis taoensis*	Rp4	Standard	Cast	149,753	10,000	0.70	--
ROM H	*Valenopsalis joyneri*	Lm2	Standard	Tooth	20,640	10,000	--	--
ROM I	*Valenopsalis joyneri*	Lp4	Standard	Tooth	9479	--	--	--
UALVP 28167	*Valenopsalis joyneri*	Rm1	Standard	Tooth	32,960	10,000	0.70	--
UALVP 28170	*Valenopsalis joyneri*	Lm1	Standard	Tooth	28,526	10,000	--	--

UALVP 28172	*Valenopsalis joyneri*	Rm1	Standard	Tooth	35,180	10,000	--	--
UALVP 28175	*Valenopsalis joyneri*	Rm1	Standard	Tooth	30,056	10,000	--	--
UALVP 28178	*Valenopsalis joyneri*	Lm1	Standard	Tooth	21,920	10,000	--	--
UALVP 28202	*Valenopsalis joyneri*	Lm2	Standard	Tooth	29,546	10,000	--	--
UALVP 28203	*Valenopsalis joyneri*	Rm2	Standard	Tooth	21,112	10,000	--	--
UALVP 28204	*Valenopsalis joyneri*	Lm2	Standard	Tooth	31,357	10,000	--	--
UALVP 28205	*Valenopsalis joyneri*	Lm2	Standard	Tooth	28,120	10,000	--	--
UALVP 28207	*Valenopsalis joyneri*	Rm2	Standard	Tooth	28,788	10,000	--	Yes
UALVP 28211	*Valenopsalis joyneri*	Rp4	High	Tooth	22,461	10,000	--	--
UALVP 6596	*Valenopsalis joyneri*	Rm1	Standard	Tooth	21,901	10,000	--	--
UALVP 6608	*Valenopsalis joyneri*	Rm2	Standard	Tooth	27,177	10,000	--	--
UALVP 6609	*Valenopsalis joyneri*	Rm2	Standard	Tooth	21,671	10,000	--	--
UALVP 6610	*Valenopsalis joyneri*	Rm2	Standard	Tooth	21,122	10,000	--	--
UALVP 7394	*Valenopsalis joyneri*	Lm1	Standard	Tooth	17,414	10,000	--	--
UALVP 7395	*Valenopsalis joyneri*	Lp4	High	Tooth	21,020	10,000	--	--
UALVP 7412	*Valenopsalis joyneri*	Lp4	High	Tooth	21,640	10,000	--	--

Appendix H: Program and Parameter Comparisons for Dental Topographic Analysis

RFI

RFI is calculated using the crown surface area (A3D) and occlusal footprint area (A2D; the footprint of the crown in occlusal view) of a tooth (M'Kirera and Ungar, 2003; Boyer, 2008). There are two forms of the RFI equation – the version introduced by M'Kirera and Ungar (2003) ($\left(\frac{A3D}{A2D}\right)$), and the modification introduced by Boyer (2008) ($\ln(\frac{\sqrt{A3D}}{\sqrt{A2D}})$). Scans used for RFI can be cropped at two locations: the bottom of the occlusal basin or the crown-root junction. Boyer's (2008) equation and crown-root junction cropping are more common, but both equations and cropping locations continue to be used. The choice is dictated primarily by researcher preference. For multituberculates, the crown surface ventral to the occlusal basin may not have been involved in food processing. However, Boyer's (2008) equation and cropping location have been applied to vastly more taxa, so I elected to use these methods for the sake of comparisons. Cropping location is something that should be examined in the future, but it was not in the scope of this study. Because I only calculated RFI using one version of the equation and one cropping location, there are no program or parameter comparisons to make for RFI.

OPC/R

There are many options for calculating OPC/R. The measurement was initially performed with SurferManipulator (available at http://evomorph.org/surfermanipulator/), a Surfer® (Golden Software, LLC, Golden, Colorado) plug-in developed by A. Evans (Evans et al., 2007). This program uses 2.5D digital elevation models (DEMs) of teeth to calculate OPC/R. Many parameters can be set in SurferManipulator, including the level of downsampling and the minimum acceptable patch size (i.e. number of patches that constitute a countable facet). SurferManipulator (using Surfer) also blanks scans and removes undercuts. This renders scans

fully 2.5D. SurferManipulator calculations usually use a 3-patch minimum (Evans et al., 2007; Wilson et al., 2012; Winchester et al., 2014; Pampush et al., 2016a).

Two other programs for OPC/R are now available: molaR and MorphoTester. These programs can use fully 3D scans. Scans for molaR and MorphoTester are first trimmed, simplified, and smoothed in a program such as Amira or Avizo. OPC/R calculated from 3D scans is called 3D-OPCR (Winchester, 2016). This form of OPC/R is not directly comparable to SurferManipulator OPC/R because of differences in dimensionality and downsampling (Pampush et al., 2016a; Winchester, 2016). For 3D-OPCR, molaR has an automatic 3-patch minimum, while Winchester (2016) suggests a minimum patch size of 5 for MorphoTester (Pampush et al., 2016a). MorphoTester and molaR produce identical results when 3D-OPCR is calculated with the same parameters, and both 3-patch and 5-patch values can be used to detect species-level differences (Pampush et al., 2016a; Winchester, 2016). In both cases, 3D-OPCR values are significantly above those of SurferManipulator (Pampush et al., 2016a; Winchester, 2016).

The cross-compatibility of OPC/R is an issue. The OPC/R of multituberculates has only been calculated with SurferManipulator previously (Wilson et al., 2012). More recent studies of other clades have calculated OPC/R with molaR and MorphoTester, but with different patch count parameters. I compared OPCR results from SurferManipulator to 3D-OPCR results with 3-patch and 5-patch minimums from molaR. All scanned specimens were included in the comparison, including specimens that had taphonomic deformation. These deformed specimens were included because the purpose of the comparison was to evaluate OPCR parameters, not to examine biologically meaningful differences. Graphs show that SurferManipulator produced the lowest OPCR values and the 3-patch minimum in molaR produced the highest OPCR values

(Figure H1-2). This concurs with the established literature (Pampush et al., 2016a; Winchester, 2016). A Kruskal-Wallis test confirmed that there were significant differences among the conditions (x^2 (3) = 83.3, p < 0.001). A post-hoc Dunn test with a Bonferroni correction found that all conditions were significantly different from each other (all p < 0.001).
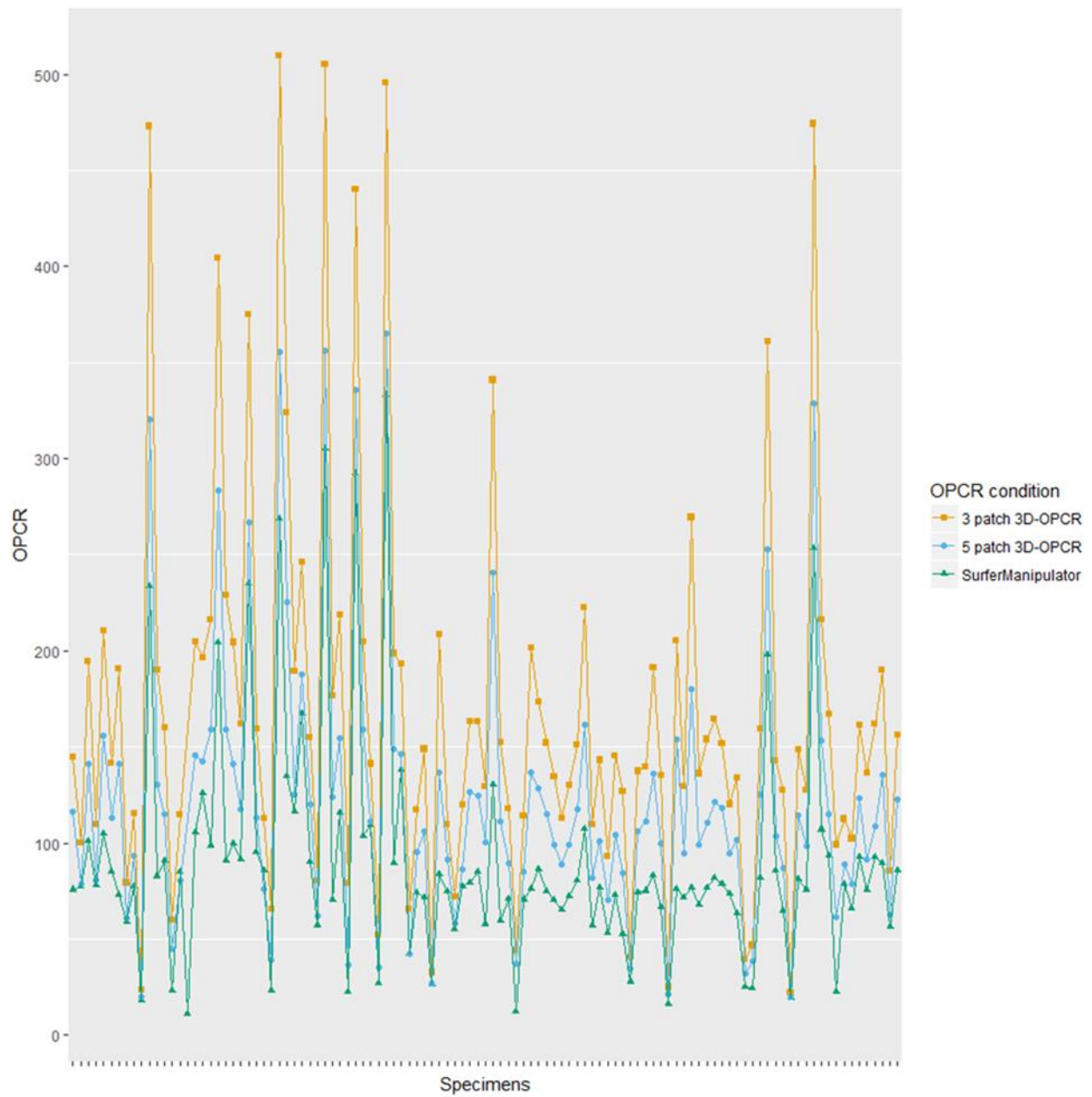
Figure H1. OPCR values of individual specimens calculated with various programs and patch-inclusion criteria. Each tick mark on the x-axis represents a specimen.
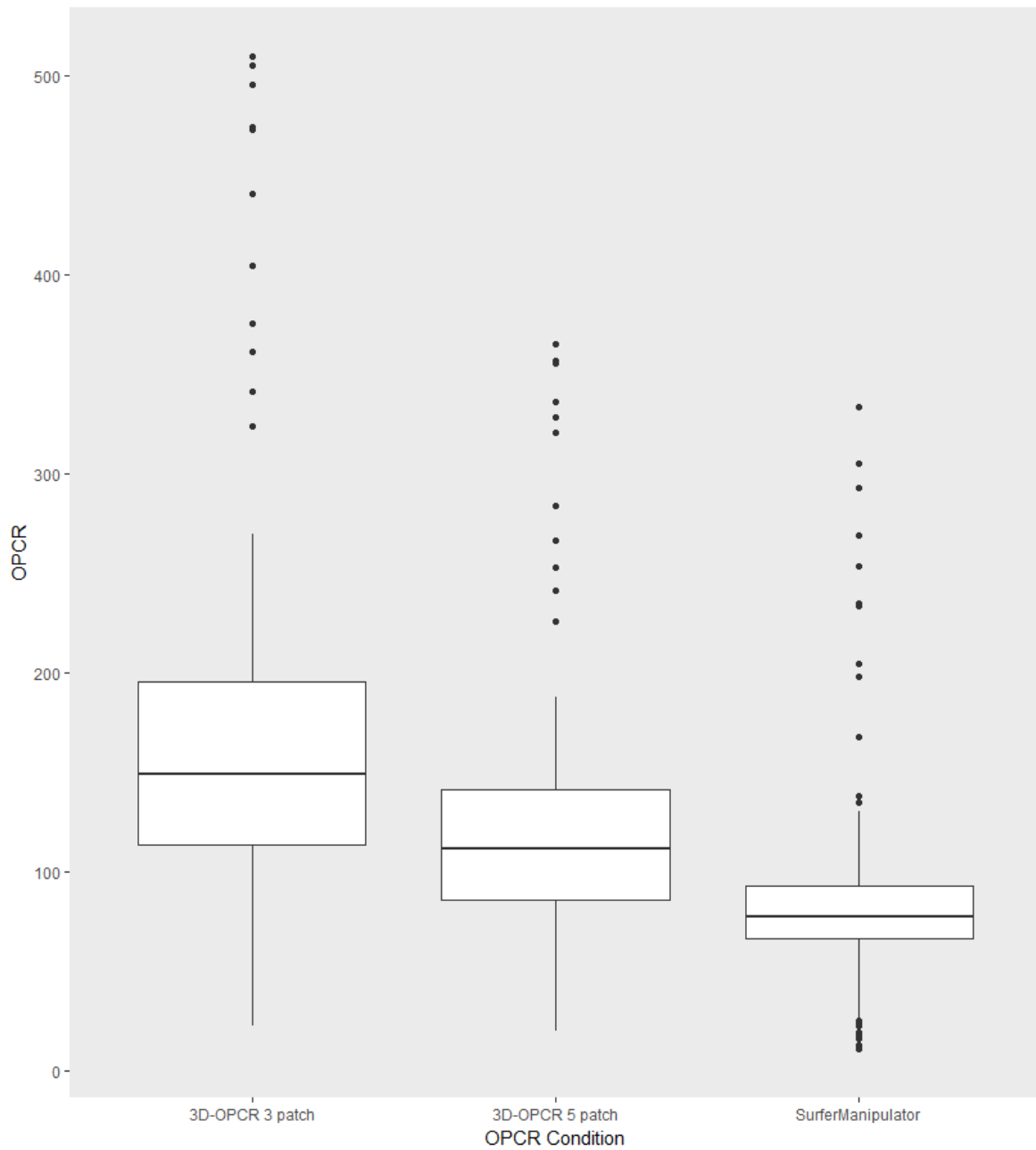
Figure H2. Box plot of OPCR values by condition. The centre line is the median, the boxes are the interquartile range, and the vertical lines (whiskers) are 1.5 times the interquartile range. Outliers are solid circles.

Sample variance was calculated for each of the three OPCR conditions. The 3D-OPCR 3-patch data had the largest variance (10,699) while the SurferManipulator data had the smallest (3,504). The 3D-OPCR 5-patch data had a variance (5,297) closer to the SurferManipulator values than the 3-patch values. This suggests that a higher patch-size threshold and more downsampling both result in a smaller spread of OPCR values.

OPCR variance by taxon.

The sample variance for each taxon was calculated for each OPCR condition. These variances were then compared with a set of paired-sample t-tests to determine if differences in programs and patch criteria affected the spread of OPCR values for each taxon. Natural log transformations were performed on all variance data to make them normally distributed. All t-tests detected significant differences (all $p < 0.001$). The SurferManipulator scans had the least variability and the 3-patch scans had the most (Table H1). The relatively small variability of the SurferManipulator scans is likely a result of high downsampling: increased downsampling is known to eliminate biologically meaningful differences in OPCR among taxa (Evans and Janis, 2014). It stands to reason that intra-taxon variability would also decrease. It also makes sense that the 5-patch inclusion criterion would have less variability than the 3-patch inclusion criterion given that the 5-patch criterion excludes more patches.

Table H1. OPCR and DNE variances for each taxon.

Taxon	OPCR SurferManipulator	3D-OPCR 3 patch	3D-OPCR 5 patch	DNE 100, 0.1%	DNE 100, 1.0%	DNE 100, 5.0%	DNE 30, 0.1%	DNE 30, 0.5%	DNE Laplacian Smooth, 0.1%	DNE Laplacian Smooth, 5.0%
Catopsalis kakwa	1316	6271	3242	563516	328912	118451	478751	124681	9727687	131146
Catopsalis alexanderi	5553	19741	9133	470981	156178	77640	589074	100132	2543372	47089
Taeniolabis taoensis	8053	17712	9712	104819	82094	45762	135786	65960	208642	27611
Catopsalis fissidens	5921	20347	10098	110652	96920	55910	162569	87179	109112	37243
Mesodma sp.	85	807	458	5464	5514	4294	15346	9534	4319	3141
Valenopsalis joyneri	477	3375	1520	272857	124049	30160	213569	32469	4441044	23064
Meniscoessus major	951	6347	3009	283057	88351	33283	283629	45895	4092388	23038
Cimolomyid 1	40	760	242	9890	7772	17141	3824	14883	4302422	16913
Cimolomys sp.	40	178	81	9917	5393	879	3919	637	872914	1289
Catopsalis cf. *calgariensis*	203	1346	709	315222	100552	20327	285939	25398	6884433	13888

OPCR parameter selection.

It is necessary to use SurferManipulator-processed scans to compare the current

multituberculate data with most published datasets. For comparisons within the current dataset, I

elected to use both SurferManipulator-processed scans and molaR-processed scans with a 3-

patch minimum. No studies have been conducted to determine an optimum patch size. Based on

previous work with downsampling, retention of finer features improves detection of biologically

meaningful differences in OPCR (Evans and Janis, 2014). Therefore, it stands to reason that a

minimum patch size of three is preferable to a minimum patch size of five for retaining

biologically relevant features. A few recent datasets have been processed with a 5-patch

minimum – the set of 5-patch scans can be used for comparisons to those datasets.

DNE

Dirichlet normal 3nergy (DNE) was initially calculated with Teether (Bunn et al., 2011).

Teether uses scans that are already simplified and smoothed, but the software also adds a

smoothing step (Implicit Fairing) beyond the standard Amira/Avizo procedure (Pampush et al.,

2016a). The same smoothing step is available in MorphoTester (Winchester, 2016). Implicit

fairing is not available in molaR. To mimic the additional smoothing step, scans need to be

smoothed in MeshLab with the Laplacian Smooth operation (Pampush et al., 2016a). The

smoothing procedures are not identical, but they produce quite similar results (Pampush et al.,

2016a).

The standard Amira scan smoothing (iterations = 100, $\lambda = 0.6$) plus the Implicit

Fairing/Laplacian Smoothing step have been accepted as the standard procedures for DNE.

However, they may not be the best ones for capturing the full range of Dirichlet energy values of

a tooth (Spradley et al., 2017). Over-smoothing scans can distort DNE values: many iterations of

Amira smoothing flatten a surface to point where its DNE value no longer reflects the DNE of the original surface (Spradley et al., 2017). The effects are even worse when additional smoothing steps, such as Laplacian Smoothing, are included (Spradley et al., 2017). In a few rare cases, smoothing may also result in artificial "horns" being produced, increasing the DNE beyond its original value (Spradley et al., 2017). Spradley et al. (2017) recommended running 20-30 smoothing iterations to retain natural DNE values while eliminating extraneous noise. This recommendation has not yet been employed in the published paleontological literature.

DNE is also sensitive to outliers. Previous work has indicated that surfaces often have a few areas with extremely high values that greatly increase the overall DNE. This is especially true for fossils. MorphoTester and molaR automatically exclude the top 0.1% outlier energies of a surface (Pampush et al., 2016a; Winchester, 2016). It is unclear from the literature whether Teether also excludes outliers. Berthaume et al. (2018) found that the automatic 0.1% exclusion was not enough for fossils: specimens tend to have broken edges and cracked faces that elevate DNE. Instead, a 1.0% or 5.0% exclusion should be used, with 5.0% being preferable (Berthaume et al., 2018). These broader exclusion criteria have not yet been employed in other published studies.

I calculated DNE in molaR using 100-iteration smoothed scans with the top 0.1%, 1.0%, and 5.0% of energy values excluded. I also calculated DNE for 30-iteration smoothed scans with 0.1% and 5.0% outlier exclusion. Finally, DNE calculations were performed at 0.1 % and 5.0% outlier exclusion on scans that had been smoothed with additional Laplacian Smoothing (3 steps, 1D boundary smoothing, cotangent weighting enabled) in MeshLab. The sole specimen of *Catopsalis johnstoni*, UALVP 16058, was excluded from the analysis because its DNE values were extremely high outliers (Appendix J) that were obscuring differences in the rest of the data.

216

The occasional occurrence of unusually high DNE values has been reported in extant taxa too (Renaud and Ledevin, 2017).

Laplacian smoothing with 0.1% outlier exclusion produced noticeably higher DNE values than other smoothing parameters (Figure H3-4). It is also apparent, although to a lesser extent, that all batches with 0.1% outlier exclusion have higher DNE values than the batches with 5.0% outlier exclusion (Figure H3-4).
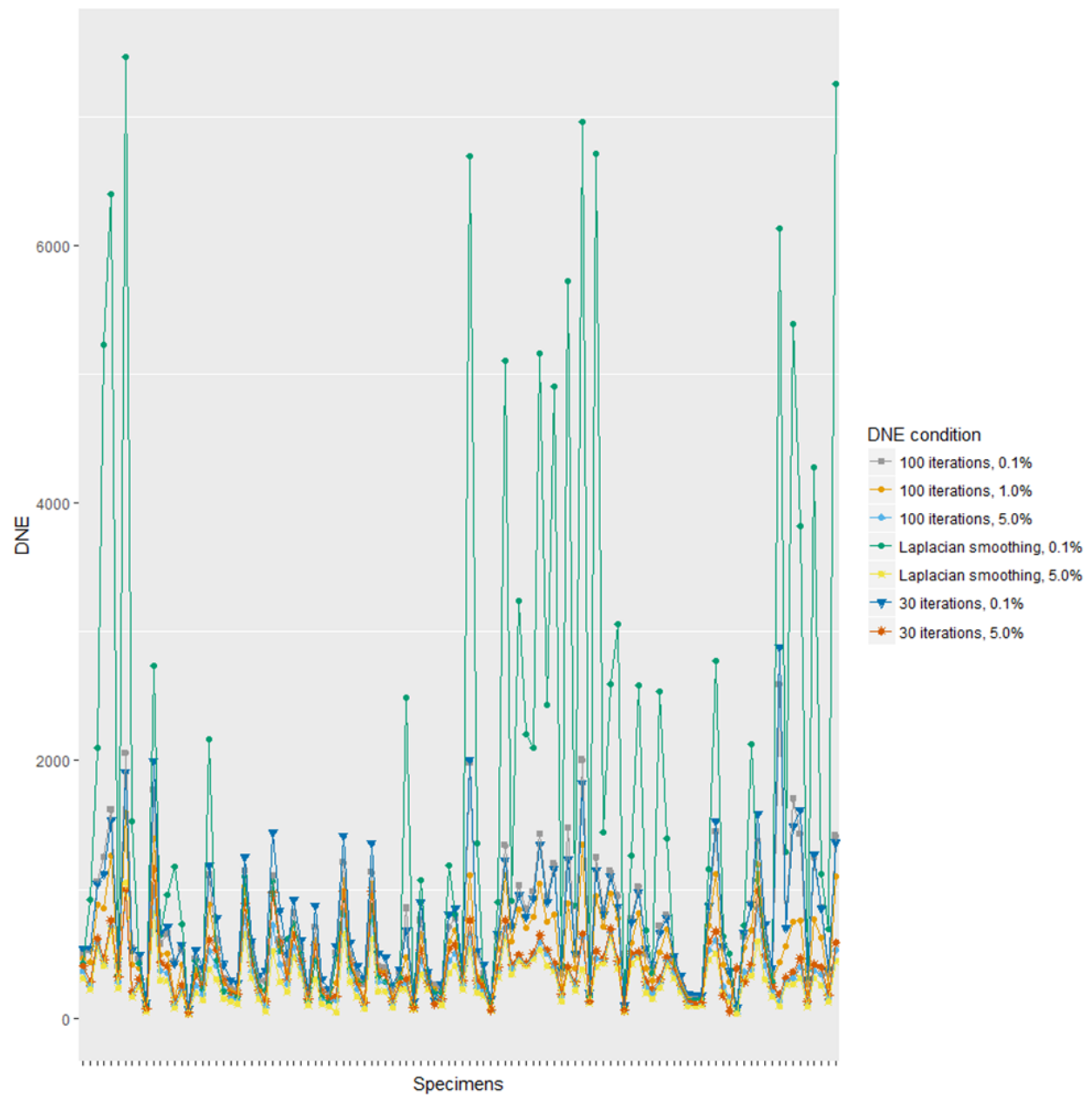
Figure H3. DNE values for individual specimens calculated with various smoothing and outlier exclusion parameters. Each tick mark on the x-axis represents a specimen.
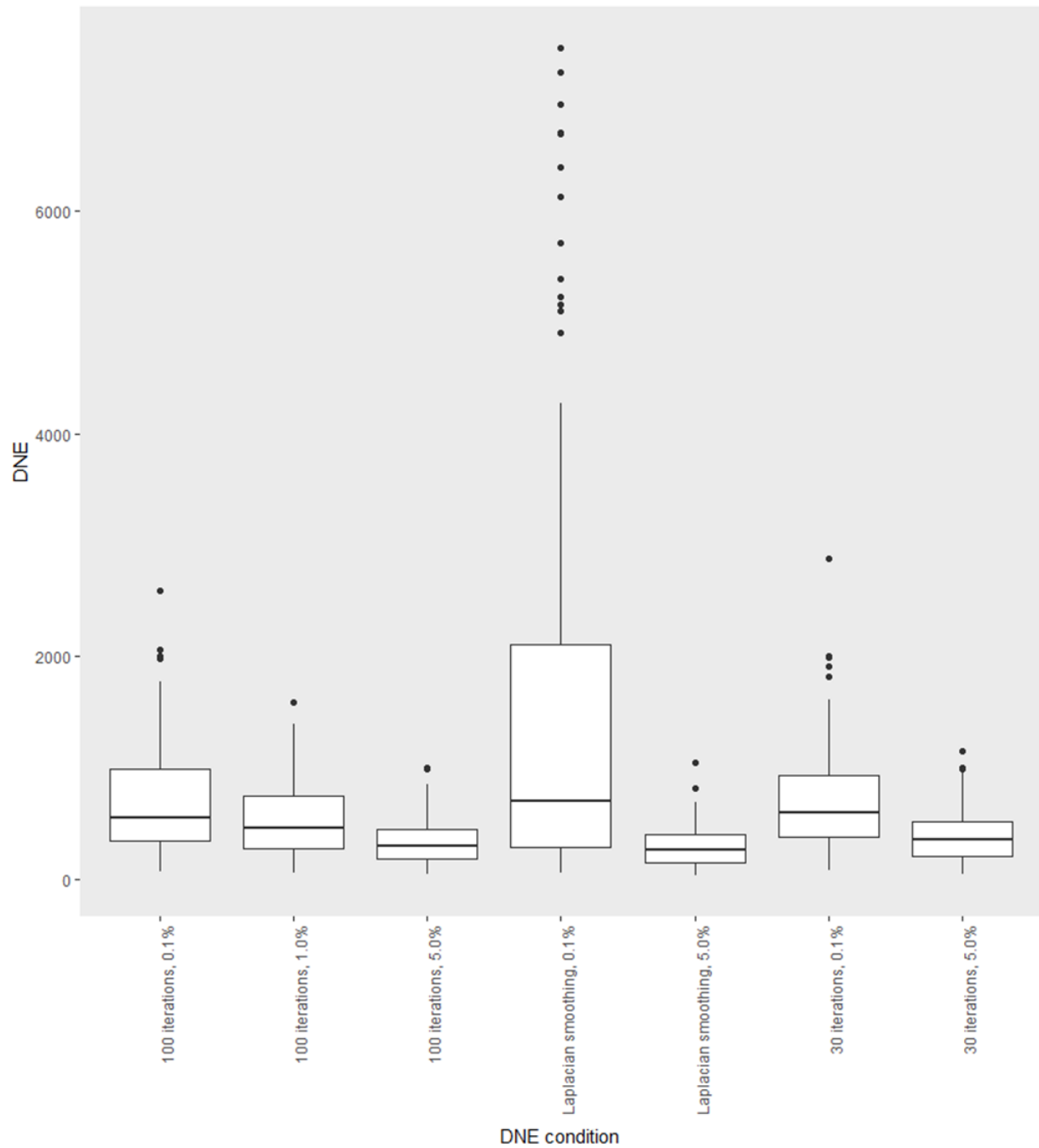
Figure H4. Box plot of DNE values by condition. The centre line is the median, the boxes are the interquartile range, and the vertical lines (whiskers) are 1.5 times the interquartile range. Outliers are solid circles.

Statistical comparisons were used to further explore differences among the groups. Shapiro-Wilks tests indicated that the DNE values were not normally distributed. A Kruskal-Wallis test indicated that there were significant differences among groups (x^2 (6) = 135, p < 0.001), and a Dunn's post-hoc test with a Bonferroni correction found that many of the conditions significantly differed from one another (Table H2). Unsurprisingly, given the graphs, the Laplacian smoothed scans with 0.1% outlier exclusion had the highest median DNE (732). This high value was unexpected given that extra smoothing usually results in lower DNE values (Spradley et al., 2017). It is likely that the combination of Amira and Laplacian smoothing created scans with artificial topography. This phenomenon has been documented before in over-smoothed scans (Spradley et al., 2017).

Table H2. Results of a Dunn post-hoc test with Bonferroni correction for DNE parameter comparisons. Significant p-values are in bold. Median DNE values are listed at the bottom of the table. α/2 = 0.025.

	100, 0.1%	100, 1.0%	100, 5.0%	30, 0.1%	30, 0.5%	Laplacian, 0.1%	Laplacian, 5.0%
100, 0.1%	-	1.00	**<0.001**	1.00	**<0.001**	1.00	**<0.001**
100, 1.0%	-	-	**0.002**	0.20	0.14	0.10	**<0.001**
100, 5.0%	-	-	-	**<0.001**	1.00	**<0.001**	1.00
30, 0.1%	-	-	-	-	**<0.001**	1.00	**<0.001**
30, 0.5%	-	-	-	-	-	**<0.001**	0.13
Laplacian, 0.1%	-	-	-	-	-	-	**<0.001**
Median DNE value	553	473	308	607	359	715	263

The 100-iteration smoothed scans with 0.1% outlier exclusion were not significantly different from those of the 30-iteraion and Laplacian Smoothed scans with 0.1% outlier exclusions (p = 1.00). This suggests that differences between smoothing parameters are negligible if the same outlier exclusion criterion is used. Spradley et al. (2017) suggested using 20-30 iterations of smoothing to reduce noise without adding artificial features. My data indicate that smoothing up to 100 iterations is probably acceptable, although a small amount of curvature is lost. Conversely, Laplacian Smoothing with a high outlier exclusion threshold clearly produces a lot more variance than either of the Amira smoothing protocols (Figure H4) and should not be used.

The 100-interion smoothed scans produced an expected decrease in DNE values with increased outlier exclusion criteria: the 0.1% exclusion batch had the highest median DNE (553), followed by the 1.0% exclusion batch (Mdn = 473) and the 5.0% exclusion batch (Mdn = 308). The DNE values of the 0.1% and 1.0% criteria were not significantly different from each other, but both were significantly higher than the 5.0% batch (Table H2). A 1.0% or 5.0% exclusion threshold was suggested by Berthaume et al. (2018) for fossils because specimens tend to have imperfections that inflate DNE. Berthaume et al. (2018) recommended using 5.0% over 1.0% – my data support this recommendation given that the 0.1% and 1.0% thresholds do not significantly differ.

All batches calculated with a 5.0% outlier exclusion had lower DNE values those calculated with a 0.1% outlier exclusion, regardless of smoothing protocol. The 30-iteration smoothed scans were slightly higher (Mdn = 359) than the 100-iterion smoothed scans (Mdn = 308), but this difference is negligible (Table H2). The more interesting result is that of the Laplacian Smoothed scans, which had the lowest median DNE of any protocol (Mdn = 263). The low value is interesting because it matches previous research that demonstrated that Laplacian Smoothing led to depressed DNE values (Spradley et al., 2017). This is in direct contrast to the Laplacian scans that were processed with 0.1% outlier exclusion. The large difference between the 0.1% and 5.0% batches demonstrates the strong effect of outlier exclusion criteria on DNE: a 0.1% outlier exclusion threshold was not enough to eliminate the supremely high DNE values produced by Laplacian Smoothing artifacts.

Most studies on extant and extinct taxa have used a 0.1% outlier exclusion threshold and have used either Laplacian Smoothing or Implicit Fairing in addition to 100 iterations of Amira smoothing. It is possible that the stringent outlier exclusion threshold counteracted the over-

smoothing and produced plausible DNE values. However, this does not mean the values were true to the teeth – they were likely high because of artificial topography rather than natural curvature. This problem may not have been noticed because most studies have used undamaged teeth from extant taxa. Fossilized teeth tend to have more imperfections and are therefore more susceptible to smoothing alterations. The effects of smoothing and outlier exclusion bear further exploration but are not in the scope of this study.

DNE variance by taxon.

The DNE variances were compared within each taxon to determine if DNE protocols affected the spread of values for individual taxa (Table H1). The variances were not normally distributed, even when log transformed, so a series of paired-sample Wilcoxon tests were used. Most differences were significant (Table H3). The overwhelming number of statistically significant differences demonstrates how much DNE protocols can affect results. Many parameters have taxon-specific differences in variance, even when they do not have significant differences between their median DNE values (Table H2). The two pairs of exceptions are the 30-iteration and 100-iteration scans with 0.1% outlier exclusion, and the 100-iterion and Laplacian Smoothed scans with 5.0% outlier exclusion. The lack of significant differences in taxon variability between the 30- and 100-iteration scans further suggests that the results between the two groups are comparable, despite a slight amount of curvature being lost from more smoothing. Interestingly, there are significant differences between the 30-iteration and 100-iteration sets when the 5.0% outlier exclusion criterion is used, but not between the 100-iteration and Laplacian Smoothed scans. This once again suggests that the retention of outliers can obscure underlying differences (or similarities) in curvature; when more outliers are retained (i.e. 0.1% exclusion), the Laplacian scans have artificially high DNE values despite extra smoothing.

The 100-iteration and Laplacian Smoothed scans with 5.0% outlier exclusion have similar median values and taxon-specific variances, so the two protocols can probably be compared to each other. However, neither set of parameters is common in the literature.

Table H3. Results of paired-sample Wilcoxon tests comparing taxon-level DNE variability between DNE parameters. Significant p-values are in bold.

	100, 0.1%	100, 1.0%	100, 5.0%	30, 0.1%	30, 0.5%	Laplacian, 0.1%	Laplacian, 5.0%
100, 0.1%	-	**0.004**	**0.006**	1.00	**0.010**	**0.010**	**0.006**
100, 1.0%	-	-	**0.010**	**0.010**	**0.014**	**0.004**	**0.010**
100, 5.0%	-	-	-	**0.010**	**0.010**	**0.002**	0.064
30, 0.1%	-	-	-	-	**0.010**	**0.010**	**0.010**
30, 0.5%	-	-	-	-	-	**0.004**	**0.037**
Laplacian, 0.1%	-	-	-	-	-	-	**0.002**

DNE Parameter Selection.

The Laplacian Smoothed scans with 0.1% outlier exclusion were for comparisons to established datasets. However, these comparisons may not be very accurate given the unrealistically high values produced by that set of scans. For comparisons within my dataset, I used the 30-iteration smoothed scans with 5.0% outlier exclusion. I chose to use the less-smoothed scans to avoid eliminating biologically meaningful curvature. I chose the more liberal exclusion threshold because, based on the comparisons I have conducted, more stringent

thresholds retain too many extreme values. A protocol with 30 iterations of smoothing and 5.0% outlier exclusion should produce DNE values that closely reflect the true curvature of the teeth.

Literature Cited

Berthaume, M. A., L. K. Delezene, and K. Kupczik. 2018. Dental topography and the diet of Homo naledi. Journal of Human Evolution 118:14–26.

Boyer, D. M. 2008. Relief index of second mandibular molars is a correlate of diet among prosimian primates and other euarchontan mammals. Journal of Human Evolution 55:1118–1137.

Bunn, J. M., D. M. Boyer, Y. Lipman, E. M. St. Clair, J. Jernvall, and I. Daubechies. 2011. Comparing Dirichlet normal surface energy of tooth crowns, a new technique of molar shape quantification for dietary inference, with previous methods in isolation and in combination. American Journal of Physical Anthropology 145:247–261.

Evans, A. R., and C. M. Janis. 2014. The evolution of high dental complexity in the horse lineage. Annales Zoologici Fennici 51:73–79.

Evans, A. R., G. P. Wilson, M. Fortelius, and J. Jernvall. 2007. High-level similarity of dentitions in carnivorans and rodents. Nature 445:78–81.

M'Kirera, F., and P. S. Ungar. 2003. Occlusal relief changes with molar wear in Pan troglodytes troglodytes and Gorilla gorilla gorilla. American Journal of Primatology 60:31–41.

Pampush, J. D., J. M. Winchester, P. E. Morse, A. Q. Vining, D. M. Boyer, and R. F. Kay. 2016. Introducing molaR: a New R Package for Quantitative Topographic Analysis of Teeth (and Other Topographic Surfaces). Journal of Mammalian Evolution 23:397–412.

Renaud, S., and R. Ledevin. 2017. Impact of wear and diet on molar row geometry and

topography in the house mouse. Archives of Oral Biology 81:31–40.

Spradley, J. P., J. D. Pampush, P. E. Morse, and R. F. Kay. 2017. Smooth operator: The effects of different 3D mesh retriangulation protocols on the computation of Dirichlet normal energy. American Journal of Physical Anthropology 163:94–109.

Wilson, G. P., A. R. Evans, I. J. Corfe, P. D. Smits, M. Fortelius, and J. Jernvall. 2012. Adaptive radiation of multituberculate mammals before the extinction of dinosaurs. Nature 483:457–460.

Winchester, J. M. 2016. MorphoTester: An Open Source Application for Morphological Topographic Analysis. PLoS ONE 1–18.

Winchester, J. M., D. M. Boyer, E. M. St. Clair, A. D. Gosselin-Ildari, S. B. Cooke, and J. A. Ledogar. 2014. Dental topography of platyrrhines and prosimians: Convergence and contrasts. American Journal of Physical Anthropology 153:29–44.

Appendix I: Effects of Tooth Wear on Dental Topographic Analysis

Comparing Wear Stages

Previous research has demonstrated that DTA can be used to detect dietary differences using worn teeth. Topographic measures change differently with wear. RFI shows an overall decrease with wear, but teeth at equivalent wear stages still have statistically significant differences among species (Ungar and Williamson, 2000; M'Kirera and Ungar, 2003; Ungar and M'Kirera, 2003; Boyer, 2008; Bunn and Ungar, 2009; Pampush et al., 2016b; Berthaume et al., 2018). DNE increases with wear in howler monkeys (Pampush et al., 2016b), but decreases in hominins (Berthaume et al., 2018). Like RFI, DNE can be used to distinguish between species when equivalent wear stages are compared. OPC/R is fairly insensitive to wear (Pampush et al., 2016b; Berthaume et al., 2018).

Large samples of unworn and slightly worn teeth are not always available. This is why many DTA studies have used variably worn teeth, including Wilson et al.'s (2012) multituberculate OPC/R study. OPC/R is not greatly influenced by wear in primates, but the effects of wear have not been tested in other groups. Both RFI and DNE are affected by wear. Therefore, I chose to test for wear effects on my data before conducting other analyses. For the comparisons, I calculated RFI using Boyer's (2008) formula and cropping parameters, I used 3D-OPCR calculated with a 3-patch minimum, and I calculated DNE with 5.0% outlier exclusion from scans that were smoothed for 30 iterations ($\lambda = 0.6$). All measures were calculated using the R package (R Core Team, 2016) molaR (Pampush et al., 2016a).

Pairwise comparisons were performed to determine if there were significant differences between wear stages. Teeth were grouped by taxon and wear stage, and averages of each grouping were taken (e.g. all low-wear m1s of *V. joyneri* were averaged together). Teeth were

only included in a comparison if there were representatives from multiple wear stages. For example, *C. kakwa* had low-wear m1s but no medium-wear m1s, so the low-wear m1s were not included in the low ~ medium wear comparison. However, the m1s of *C. kakwa* were used in the low ~ high wear comparison because both low-wear and high-wear m1s were available.

All statistical analyses were run in RStudio (v. 1.1.383, RStudio Team, 2016). Shapiro-Wilks tests and Levene's tests were used to check for normality and homoscedasticity. When both normality and homoscedasticity were met, independent sample t-tests were used to compare between wear stages for each topographic measurement. Mann-Whitney-Wilcoxon tests were used when the assumption of normality was violated.

RFI

The RFI data were homoscedastic, but the data for the low ~ high RFI comparison were not normally distributed. Results indicate that RFI values decrease with wear stage, but this decrease is fairly small (Figure I2). In fact, the medium ~ high RFI comparison is the only pairwise comparison with a significant difference between groups (Table I1). The decrease in RFI values with increased wear is consistent with documented RFI changes (Ungar and Williamson, 2000; M'Kirera and Ungar, 2003; Ungar and M'Kirera, 2003; Boyer, 2008; Bunn and Ungar, 2009; Pampush et al., 2016b; Berthaume et al., 2018) and is understandable given that multituberculate cusps tend to become blunter and shorter with wear (Figure I1).
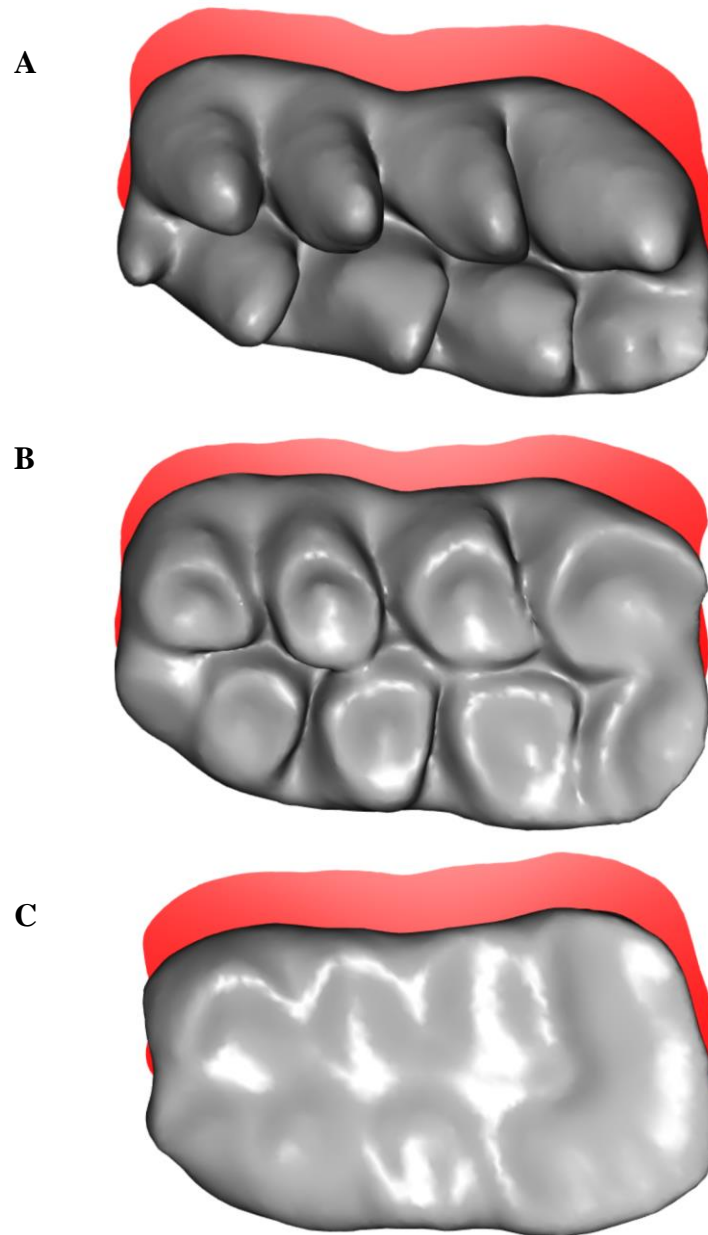
Figure I1. Examples of teeth used to calculate RFI. All teeth are *V. joyneri* left m1s. For each specimen, the grey 3D tooth represents the crown surface area and the red shadow represents the occlusal footprint area. A. Low wear (UALVP 28170) RFI = 0.61 B. Medium wear (UALVP 28178) RFI = 0.44 C. High wear (UALVP 7394) RFI = 0.40.
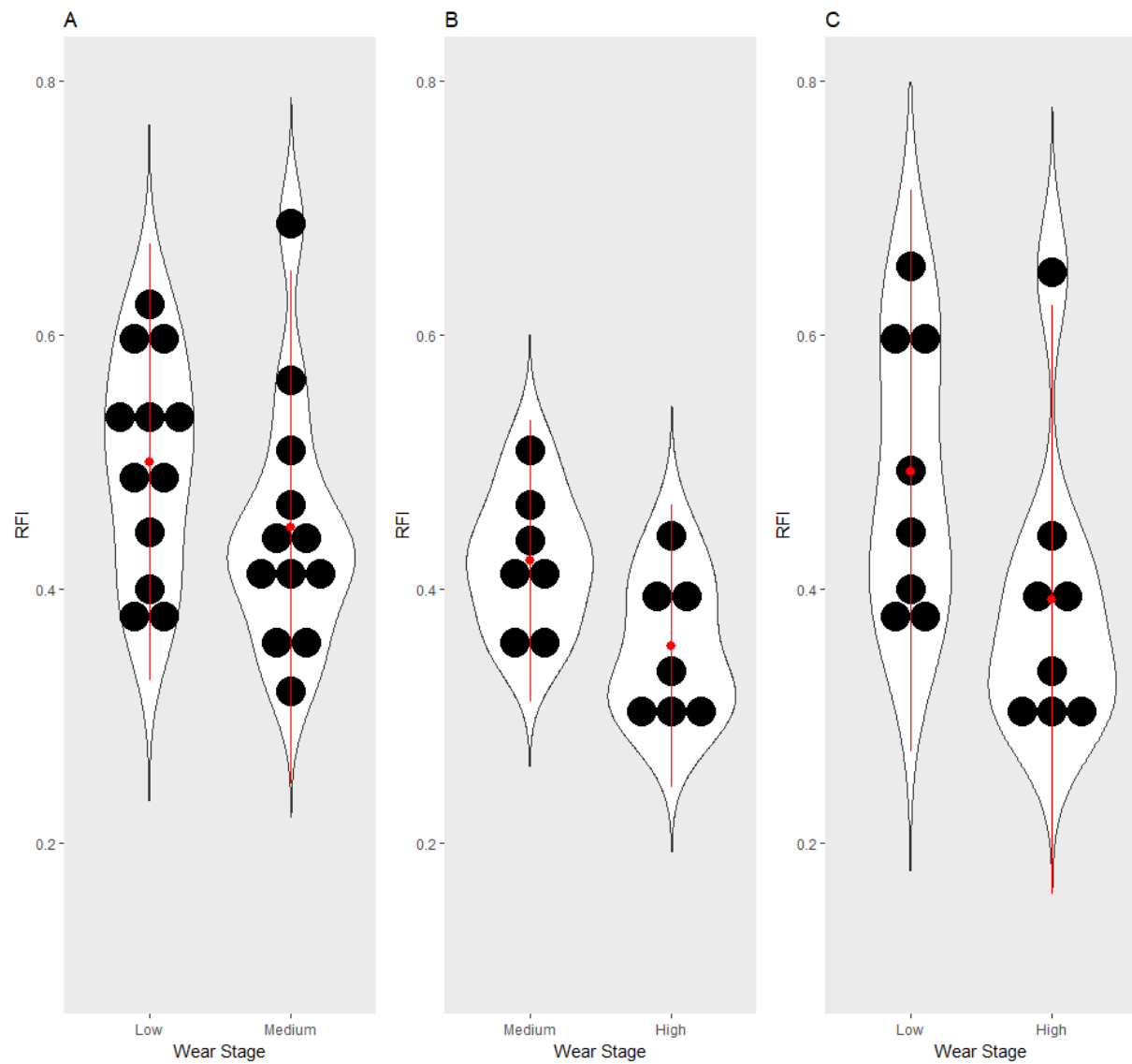
Figure I2. Dot plots of average RFI values by wear stage. Each solid black circle represents the mean RFI of a taxon. Each wear-stage mean is a solid red circle with the red line representing one standard deviation from the mean. A. Low and medium wear RFI values B. Medium and high wear RFI values C. Low and high wear RFI values.

OPCR

       All OPCR data were normally distributed and homoscedastic. None of the pairwise comparisons had significant differences (Table I1), which concurs with OPCR results reported in the primate literature (Pampush et al., 2016b; Berthaume et al., 2018). In the current dataset, OPCR values increase slightly with increased wear (Figure I3). There is also a larger spread of values with increased wear (Figure I3). This may be because dentine is exposed early in the wear process. Dentine is softer than enamel, and thus easier to deform. Over time, the dentine may become more faceted than the original enamel (Figure I4). More specimens are needed to determine if this apparent increase in average OPCR and OPCR spread is an artifact of small sample size.
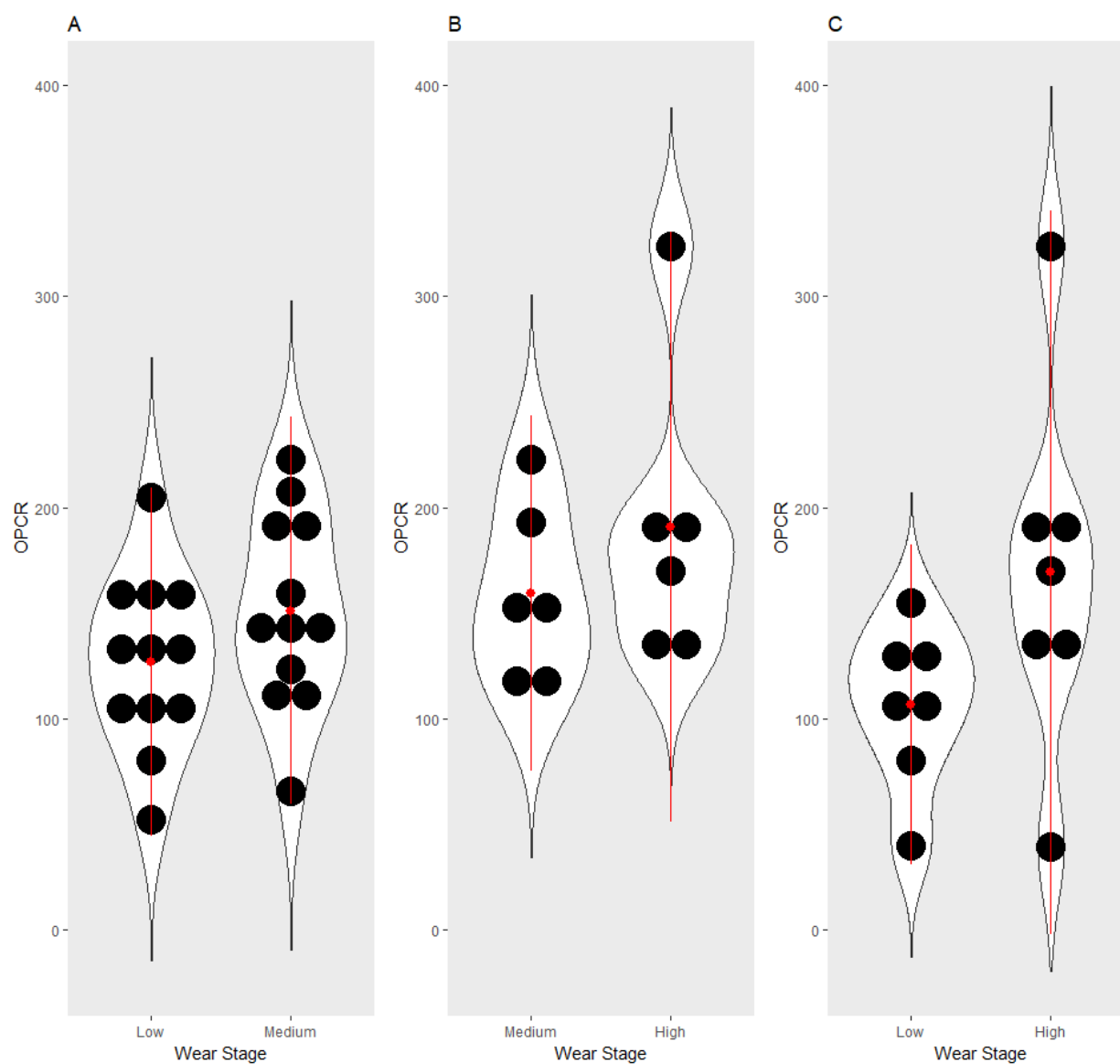
Figure I3. Dot plots of average OPCR values by wear stage. Each solid black circle represents the mean OPCR of a taxon. Each wear-stage mean is a solid red circle with the red line representing one standard deviation from the mean. A. Low and medium wear OPCR values B. Medium and high wear OPCR values C. Low and high wear OPCR values.
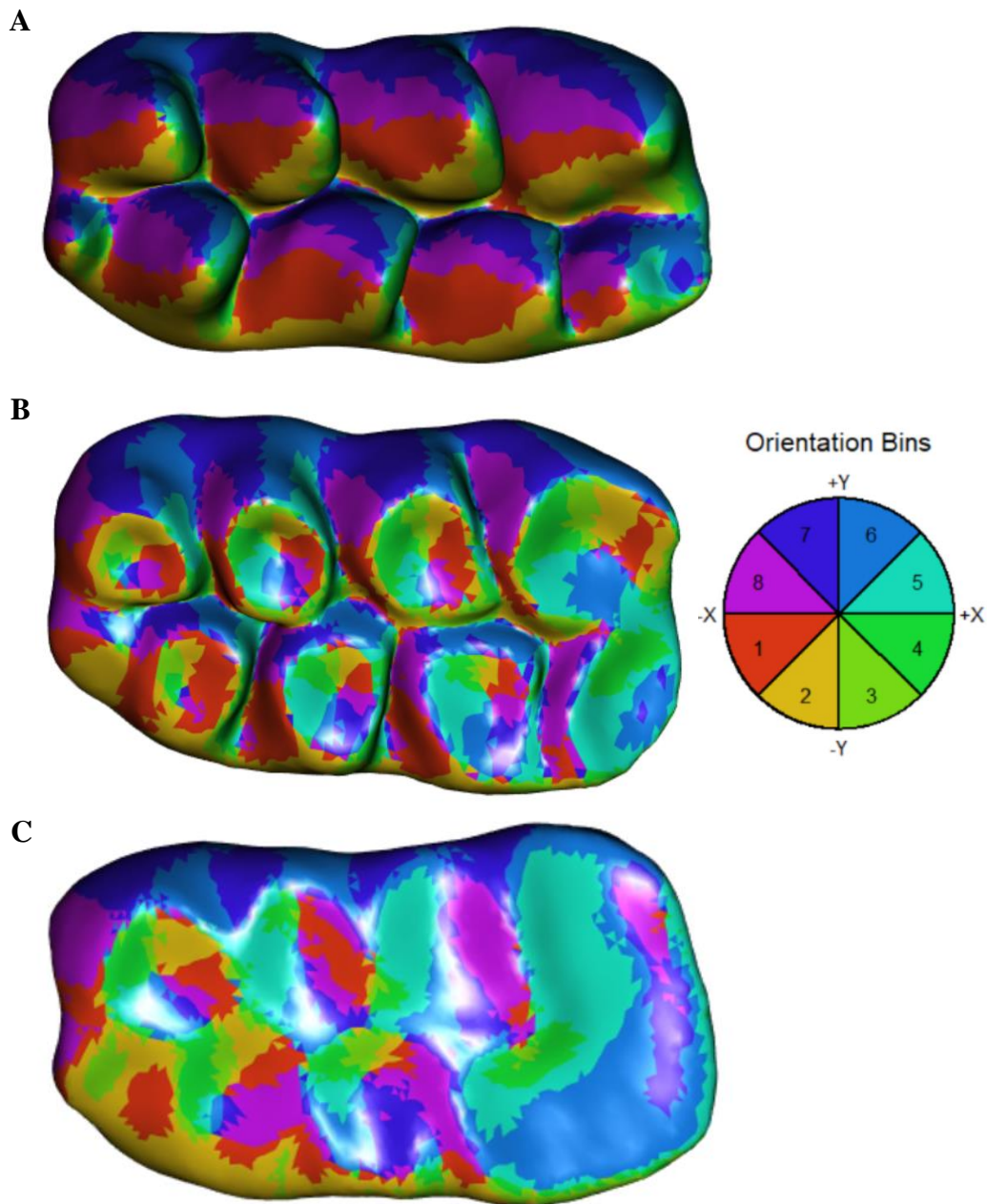
Figure I4. Examples of teeth used to calculate OPCR. All teeth are *V. joyneri* left m1s. The colouring indicates patch orientation, grouped into eight orientation bins. A. Low wear (UALVP 28170) OPCR = 113 B. Medium wear (UALVP 28178) OPCR = 223 C. High wear (UALVP 7394) OPCR = 134.

DNE

The DNE data were all homoscedastic and normally distributed. DNE values are quite similar across wear stages (Figure I5), and there are no statistically significant differences among the groups (Table I1). This suggests that the overall curvature of multituberculate teeth is not greatly affected by cusp wear. This may be because most unworn cusps have fairly planar sides: the curvature is predominantly at the tips of the cusps and the valleys between the cusps (Figure I6). The orientation and height of the cusp planes change with wear, but the valley curvature remains relatively constant and cusp-tip curvature only decreases slightly. There may be a more notable decrease in DNE at very high stages of wear (Figure I5), but more specimens are needed to determine if this is the case. Interestingly, DNE values have been observed to both increase and decrease with additional wear, depending on the clade in question additional wear, depending on the clade in question (Pampush et al., 2016b; Berthaume et al., 2018).
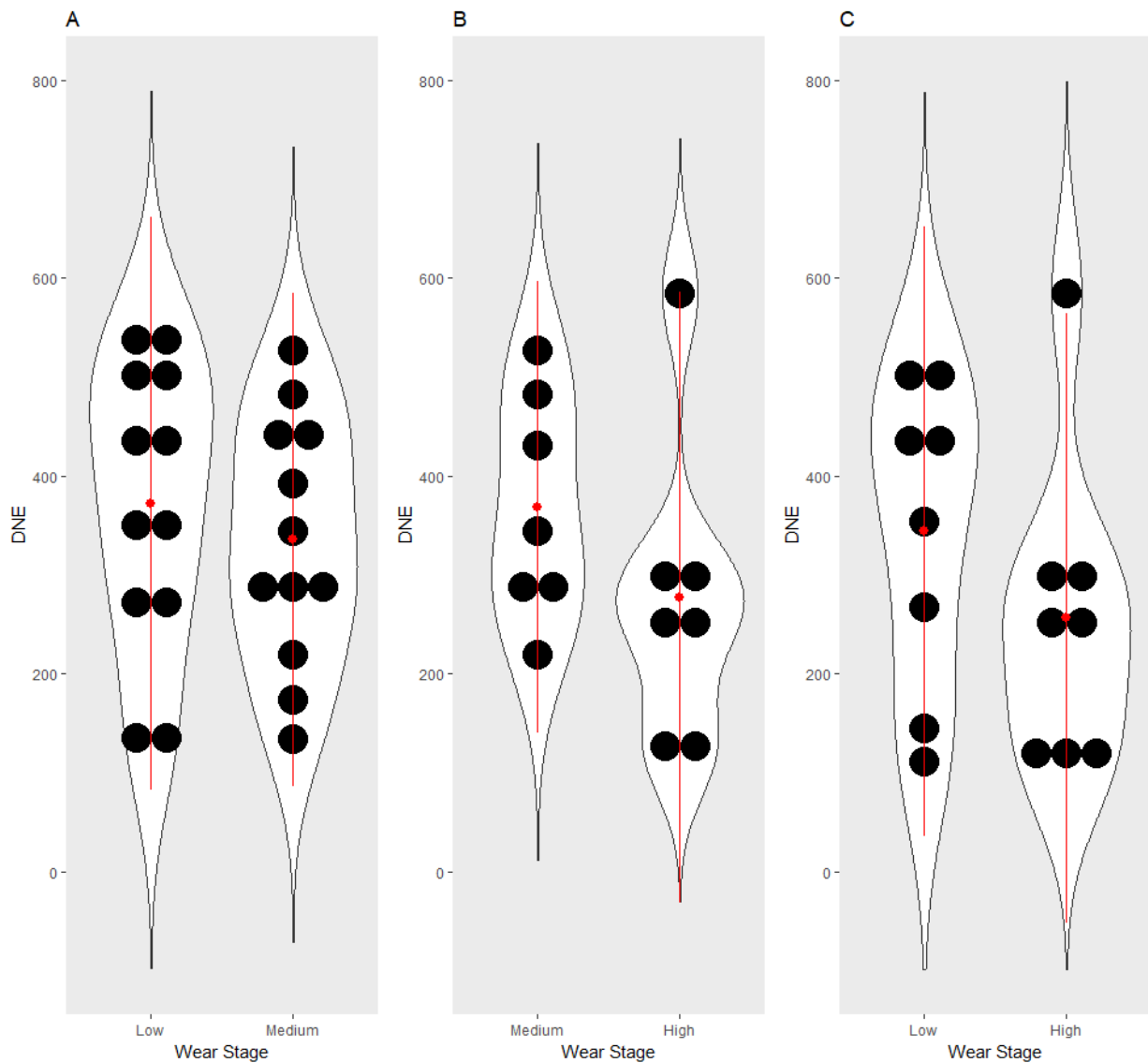
Figure I5. Dot plots of average DNE values by wear stage. Each solid black circle represents the mean DNE of a taxon. Each wear-stage mean is a solid red circle with the red line representing one standard deviation from the mean. A. Low and medium wear DNE values B. Medium and high wear DNE values C. Low and high wear DNE values.
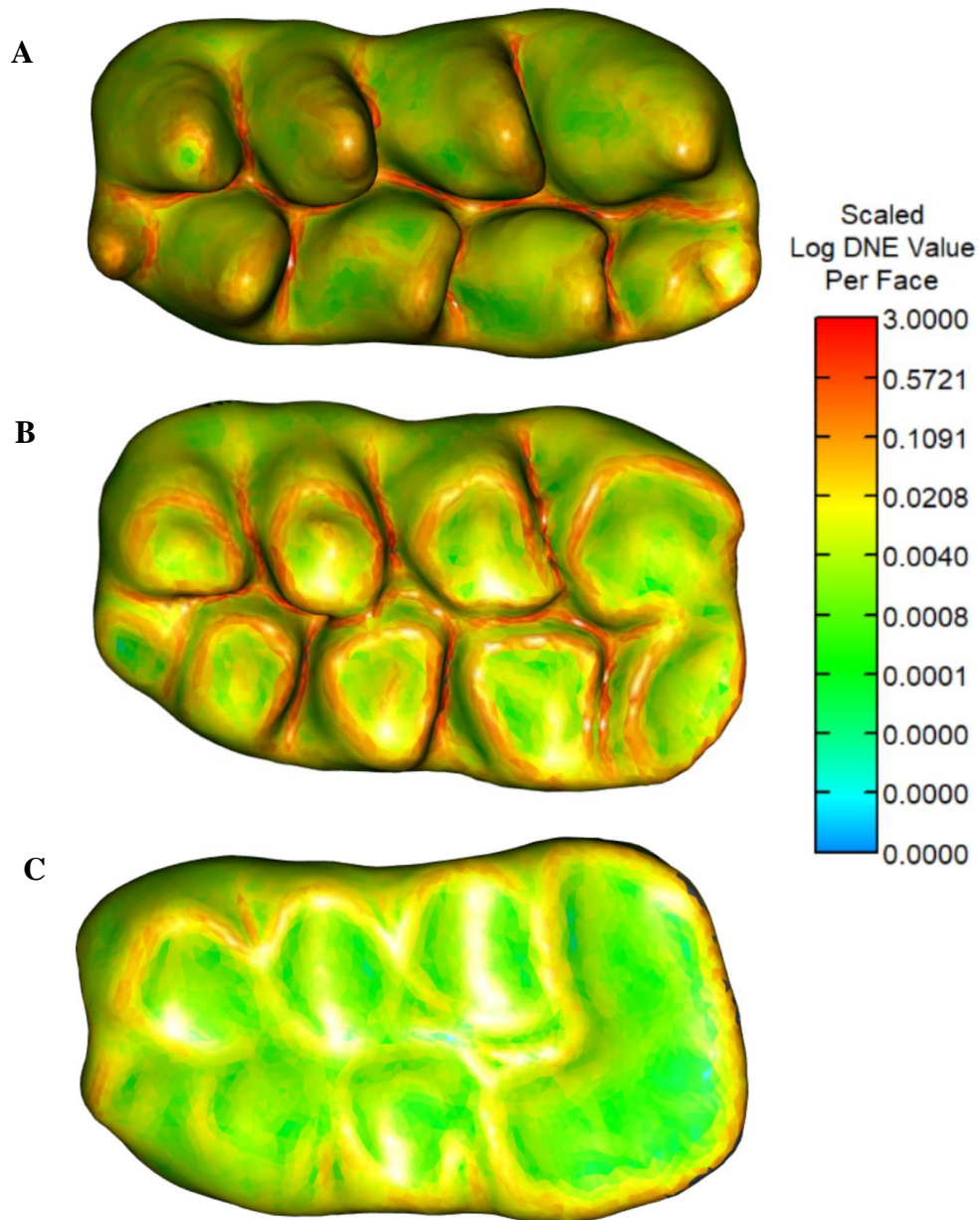
Figure I6. Examples of teeth used to calculate DNE. All teeth are *V. joyneri* left m1s. The teeth are coloured with heat maps that represent the distribution of log-scaled DNE values, with warmer colours representing higher values. A. Low wear (UALVP 28170) DNE = 427 B. Medium wear (UALVP 28178) DNE = 527 C. High wear (UALVP 7394) DNE = 126.

Given that there were no significant differences between low and medium wear for any of the topographic measures, I chose to combine the two wear stages in my analyses. I did not include high wear because there was a significant difference in RFI between the medium and high wear stage.

Table I1. Results for independent sample t-tests and Mann-Whitney-Wilcoxon tests used to compare wear stages. Bolded values are significant (p < 0.05).

	RFI	OPCR	DNE
Low-Medium	0.20	0.19	0.51
Medium-High	**0.04**	0.37	0.23
Low-High	0.06	0.11	0.27

Literature Cited

Berthaume, M. A., L. K. Delezene, and K. Kupczik. 2018. Dental topography and the diet of Homo naledi. Journal of Human Evolution 118:14–26.

Boyer, D. M. 2008. Relief index of second mandibular molars is a correlate of diet among prosimian primates and other euarchontan mammals. Journal of Human Evolution 55:1118–1137.

Bunn, J. M., and P. S. Ungar. 2009. Dental topography and diets of four old world monkey species. American Journal of Primatology 71:466–477.

M'Kirera, F., and P. S. Ungar. 2003. Occlusal relief changes with molar wear in *Pan troglodytes troglodytes* and *Gorilla gorilla gorilla*. American Journal of Primatology 60:31–41.

Pampush, J. D., J. M. Winchester, P. E. Morse, A. Q. Vining, D. M. Boyer, and R. F. Kay. 2016a. Introducing molaR: a New R Package for Quantitative Topographic Analysis of Teeth (and Other Topographic Surfaces). Journal of Mammalian Evolution 23:397–412.

Pampush, J. D., J. P. Spradley, P. E. Morse, A. R. Harrington, K. L. Allen, D. M. Boyer, and R. F. Kay. 2016b. Wear and its effects on dental topography measures in howling monkeys (*Alouatta palliata*). American Journal of Physical Anthropology 161:705–721.

R Core Team (2016). R: A language and environment for statistical computing. R Foundation for Statistical Computing, Vienna, Austria. https://www.R-project.org/.

Ungar, P., and M. Williamson. 2000. Exploring the effects of tooth wear on functional morphology: a preliminary study using dental topographic analysis. Palaeontologia Electronica 3:1–18.

Ungar, P. S., and F. M'Kirera. 2003. A solution to the worn tooth conundrum in primate functional anatomy. Proceedings of the National Academy of Sciences 100:3874–3877.

Wilson, G. P., A. R. Evans, I. J. Corfe, P. D. Smits, M. Fortelius, and J. Jernvall. 2012.

    Adaptive radiation of multituberculate mammals before the extinction of dinosaurs.

    Nature 483:457–460.

Table J1. OPCR values calculated with different parameters.

Institutional abbreviations: **NMMNH** – New Mexico Museum of Natural History and Science (Albuquerque, NM, USA); **ROM** – Royal Ontario Museum (Toronto, ON, Canada); **TMP** – Royal Tyrrell Museum of Palaeontology (Drumheller, AB, Canada); **UALVP** – University of Alberta Laboratory for Vertebrate Paleontology (Edmonton, AB, Canada); **UCM** – University of Colorado Museum of Natural History (Boulder, CO, USA); **UM** – University of Michigan Museum of Paleontology (Ann Arbor, MI, USA); **UW** – University of Wyoming Geological Museum (Laramie, WY, USA).

Table abbreviations: **SM** – SurferManipulator; **3p** – 3 patch minimum; **4p** – 4 patch minimum; **5p** – 5 patch minimum; **L** – low wear; **M** – medium wear; **H** – high wear.

Asterisks (*) denote values calculated with OPC instead of OPCR

Specimen	Taxon	Tooth	Wear	OPCR SM	3D-OPCR 3p	3D-OPCR 5p
TMP 2015.069.0174	Cf. *Acheronodon vossae*	Lm1	L	77.375	115.12	93
UCM 34136	*Catopsalis alexanderi*	Lp4-m2	M	198.125	361.25	253.12
UCM 34136	*Catopsalis alexanderi*	Lm1	M	85.5	142.75	103.25
UCM 34136	*Catopsalis alexanderi*	Lm2	M	64.75	127.25	87
UCM 34136	*Catopsalis alexanderi*	Lp4	M	19.375	22.38	19.62
UCM 34141	*Catopsalis alexanderi*	Lm1	L	81.25	148.75	114.62
UCM 34332	*Catopsalis alexanderi*	Rm1	L	75.75	127.38	98.38
TMP 2015.023.0001	*Catopsalis calgariensis*	Lm2	L	58.75	79.25	60.75
TMP 127	*Catopsalis calgariensis*	Rm2	M	77.625	120	86
UW 14051	*Catopsalis* cf. *calgariensis*	Rm2	L	66	102.25	78.5

UW 15100	*Catopsalis* cf. *calgariensis*	Rm1	L	92.375	161.25	123.5
UW 15102	*Catopsalis* cf. *calgariensis*	Rm2	H	75.375	136.5	91.38
UW 6387	*Catopsalis* cf. *calgariensis*	Lm2	M	92.875	161.88	108.62
UW 6387	*Catopsalis* cf. *calgariensis*	Rm1	M	89.25	189.75	135.75
UW 6388	*Catopsalis* cf. *calgariensis*	Lm2	M	56.25	85.25	62.88
UW 6388	*Catopsalis* cf. *calgariensis*	Rm1	L	85.75	156.12	122.62
NMMNH 8608	*Catopsalis fissidens*	Lp4-m2	M	234.875	375.25	266.62
NMMNH 8608	*Catopsalis fissidens*	Lm1	M	95	159.38	113
NMMNH 8608	*Catopsalis fissidens*	Lm2	M	85.75	112.62	75.88
NMMNH 8609	*Catopsalis fissidens*	Lm1-2	H	268.625	509.5	355.38
NMMNH 8609	*Catopsalis fissidens*	Lm1	H	134.75	324	225.5
NMMNH 8609	*Catopsalis fissidens*	Lm2	H	116.5	189.38	125.12
NMMNH 8613	*Catopsalis fissidens*	Rm1-2	L	167.625	246.38	187.75
NMMNH 8613	*Catopsalis fissidens*	Rm1	L	90	154.75	120
NMMNH 8613	*Catopsalis fissidens*	Rm2	L	57.25	80.38	61.75
UALVP 16058	*Catopsalis johnstoni*	Lm1	L	76	201.38	137
TMP 2009.133.0041	*Catopsalis kakwa*	Rm2	L	77.25	100	78.75
TMP 2009.133.0114	*Catopsalis kakwa*	Rm1	M	101.25	194.62	141
TMP 2010.097.0015	*Catopsalis kakwa*	Rm2	M	78.25	109.5	80.62
TMP 2010.097.0020	*Catopsalis kakwa*	Rm1	M	105	210.5	156.12
TMP 2015.071.0141	*Catopsalis kakwa*	Lp4	L	18	23.38	20
UALVP 57541	*Catopsalis kakwa*	Rp4	L	15.875	25*	21*
UM 90042	*Catopsalis waddleae*	Lm1	L	78.375	112.5	88.88
UALVP 1766	Cimolomyid 1	Rm1	L	86.125	173.62	128.5
UALVP 30096	Cimolomyid 1	Rm2	L	74	137.38	106.12
UALVP 30593	Cimolomyid 1	Rm1	L	83.125	191.5	136
UALVP 2141	*Cimolomys* sp.	Rm1	L	75	152	114.88
UALVP 30112	*Cimolomys* sp.	Lm1	L	75.125	139.62	111
UALVP 30605	*Cimolomys* sp.	Lm2	L	66.5	134.88	100
UALVP 709	*Cimolomys* sp.	Rm1	L	81.875	164.62	121.5

UALVP 15164	*Meniscoessus major*	Rm1	L	79.125	163.38	126.75
UALVP 15165	*Meniscoessus major*	Rm1	L	85.125	163.25	124.88
UALVP 15167	*Meniscoessus major*	Rm1	M	57.875	129.38	100.38
UALVP 15182	*Meniscoessus major*	Lp4-m2	M	130.25	341*	241*
UALVP 15182	*Meniscoessus major*	Lm1	M	59.625	152.25	111.25
UALVP 15182	*Meniscoessus major*	Lm2	M	71.125	118.12	89.5
UALVP 15182	*Meniscoessus major*	Lp4	M	12.5	44*	37*
UALVP 15187	*Meniscoessus major*	Rm2	M	70.625	113.88	85.12
UALVP B	*Meniscoessus major*	Rm2	L	81.875	159.25	125.38
ROM M	*Meniscoessus robustus*	Lm2	M	83.875	208.38	137
ROM B1	*Mesodma* sp.	Rm1	L	74.25	117.25	95.25
ROM T	*Mesodma* sp.	Rm1	L	74.625	109.5	91.12
ROM V	*Mesodma* sp.	Lm2	L	55	72.12	58.38
UALVP 7278	*Mesodma* sp.	Lm1	L	78.375	151.5	118.12
UALVP 7288	*Mesodma* sp.	Lm1	L	73.625	120.12	94.75
TMP 2009.132.0239	Neoplagiaulacid	Lm1	M	75.75	144.75	116.38
TMP 2010.097.0126	*Ptilodus wyomingensis*	Lm1	M	84.75	141.38	113.38
UALVP 6533	*Stygimys kuszmauli*	Rm1	L	76.25	205.12	154.25
NMMNH 2763	*Taeniolabis taoensis*	Lm2	L	84.75	114.88	80.38
NMMNH 42938	*Taeniolabis taoensis*	Rm2	H	105.25	204.88	145.88
NMMNH 42939	*Taeniolabis taoensis*	Lm2	H	125.75	196.62	142.38
NMMNH 44417	*Taeniolabis taoensis*	Rm1	M	98.75	216.38	158.75
NMMNH 47445	*Taeniolabis taoensis*	Rm1-2	H	204.5	404.5	283.75
NMMNH 47445	*Taeniolabis taoensis*	Rm1	H	90.625	229.12	158.88
NMMNH 47445	*Taeniolabis taoensis*	Rm2	H	99.75	204.38	141.38
NMMNH 47447	*Taeniolabis taoensis*	Rm2	H	91.25	161.75	117.62
NMMNH 8631	*Taeniolabis taoensis*	Rp4-m2	L	292.625	440.38	336.12
NMMNH 8631	*Taeniolabis taoensis*	Rm1	L	103.625	204.75	159.25
NMMNH 8631	*Taeniolabis taoensis*	Rm2	L	109.125	141.12	111
NMMNH 8631	*Taeniolabis taoensis*	Rp4	L	26.875	52	35.5

NMMNH 8632	*Taeniolabis taoensis*	Rp4-m2	M	333.5	495.75	365.12
NMMNH 8632	*Taeniolabis taoensis*	Rm1	M	89.25	198.62	148.75
NMMNH 8632	*Taeniolabis taoensis*	Rm2	M	137.75	193	146
NMMNH 8632	*Taeniolabis taoensis*	Rp4	M	42.25	65.75	42.38
ROM H	*Valenopsalis joyneri*	Lm2	H	71.5	148.88	106.38
ROM I	*Valenopsalis joyneri*	Lp4	L	26	32.75	27.12
UALVP 28167	*Valenopsalis joyneri*	Rm1	L	70.375	134.62	98.75
UALVP 28170	*Valenopsalis joyneri*	Lm1	L	65.5	112.88	88.88
UALVP 28172	*Valenopsalis joyneri*	Rm1	L	72.375	129.88	99.12
UALVP 28175	*Valenopsalis joyneri*	Rm1	L	80.75	151.12	117.75
UALVP 28178	*Valenopsalis joyneri*	Lm1	M	107.125	222.75	161.38
UALVP 28202	*Valenopsalis joyneri*	Lm2	L	57.125	109.62	81.62
UALVP 28203	*Valenopsalis joyneri*	Rm2	H	76.875	143.12	101
UALVP 28204	*Valenopsalis joyneri*	Lm2	L	53	93	70.25
UALVP 28205	*Valenopsalis joyneri*	Lm2	M	73.125	145.5	104.25
UALVP 28207	*Valenopsalis joyneri*	Rm2	L	52.5	126.62	84.25
UALVP 28211	*Valenopsalis joyneri*	Rp4	L	27.875	40.5	34.62
UALVP 6596	*Valenopsalis joyneri*	Rm1	L	71.625	129.25	94.75
UALVP 6608	*Valenopsalis joyneri*	Rm2	H	76.875	269.5	180.12
UALVP 6609	*Valenopsalis joyneri*	Rm2	H	67.5	136.12	99.12
UALVP 6610	*Valenopsalis joyneri*	Rm2	H	76.75	153.88	110.62
UALVP 7394	*Valenopsalis joyneri*	Lm1	H	63.5	133.88	101.62
UALVP 7395	*Valenopsalis joyneri*	Lp4	H	24.75	39.38	32.25
UALVP 7412	*Valenopsalis joyneri*	Lp4	L	24.125	46.75	38.25

Table J2. DNE values calculated with different parameters.

Institutional abbreviations: **NMMNH** – New Mexico Museum of Natural History and Science (Albuquerque, NM, USA); **ROM** – Royal Ontario Museum (Toronto, ON, Canada); **TMP** – Royal Tyrrell Museum of Palaeontology (Drumheller, AB, Canada); **UALVP** – University of Alberta Laboratory for Vertebrate Paleontology (Edmonton, AB, Canada); **UCM** – University of Colorado Museum of Natural History (Boulder, CO, USA); **UM** – University of Michigan Museum of Paleontology (Ann Arbor, MI, USA); **UW** – University of Wyoming Geological Museum (Laramie, WY, USA).

Table abbreviations: **LS** – Laplacian Smoothing; **30i** – 30 iterations of smoothing; **L** – low wear; **M** – medium wear; **H** – high wear. Percentages (%) indicate outlier exclusion threshold.

Specimen	Taxon	Tooth	Wear	DNE 0.1%	DNE 1.0%	DNE 5.0%	DNE LS	DNE LS 5.0%	DNE 30i	DNE 30i 5.0%
TMP 2015.069.0174	Cf. *Acheronodon vossae*	Lm1	L	459.5445	386.8034	279.5988	428.6025	248.1505	494.0553	301.2238
UCM 34136	*Catopsalis alexanderi*	Lp4-m2	M	1451.306	1123.91	606.0976	2770.891	505.7339	1527	671.6173
UCM 34136	*Catopsalis alexanderi*	Lm1	M	541.7408	411.7442	243.486	636.0421	199.2147	556.1823	390.9069
UCM 34136	*Catopsalis alexanderi*	Lm2	M	354.7214	282.6476	161.5373	500.5609	134.0425	363.2045	174.0842
UCM 34136	*Catopsalis alexanderi*	Lp4	M	67.78125	59.61614	44.15956	54.60609	36.2465	82.9765	54.65123
UCM 34141	*Catopsalis alexanderi*	Lm1	L	632.623	545.4622	360.8898	715.3202	314.6176	659.5783	278.7637
UCM 34332	*Catopsalis alexanderi*	Rm1	L	889.4622	679.059	378.185	2132.568	328.8068	877.4473	415.4804
TMP 2015.023.0001	*Catopsalis calgariensis*	Lm2	L	540.6683	413.7409	190.092	1529.222	168.9268	530.5134	205.7803
TMP 127	*Catopsalis calgariensis*	Rm2	M	238.5107	197.7812	135.3177	194.7115	101.5962	266.3749	151.0088
UW 14051	*Catopsalis* cf. *calgariensis*	Rm2	L	1702.566	746.9886	307.7877	5391.037	266.4968	1488.772	354.4881
UW 15100	*Catopsalis* cf. *calgariensis*	Rm1	L	1430.933	761.1249	395.2769	3819.473	310.9448	1617.024	463.5832
UW 15102	*Catopsalis* cf. *calgariensis*	Rm2	H	267.1236	192.5194	112.0877	378.5814	91.0398	300.0854	127.5167

UW 6387	*Catopsalis* cf. *calgariensis*	Lm2	M	1246.442	772.1375	364.2256	4275.403	308.615	1268.955	414.5445
UW 6387	*Catopsalis* cf. *calgariensis*	Rm1	M	854.5214	621.1258	344.0656	1114.798	256.8384	852.3266	392.7163
UW 6388	*Catopsalis* cf. *calgariensis*	Lm2	M	343.785	256.7592	151.5411	695.7116	128.3038	374.9041	176.4841
UW 6388	*Catopsalis* cf. *calgariensis*	Rm1	L	1414.825	1100.845	525.5	7252.849	440.1985	1362.261	583.2956
NMMNH 8608	*Catopsalis fissidens*	Lp4-m2	M	1140.397	1021.304	773.5707	1101.846	649.5795	1251.53	889.6289
NMMNH 8608	*Catopsalis fissidens*	Lm1	M	552.7633	501.0109	369.085	488.3061	312.2471	594.7177	431.4887
NMMNH 8608	*Catopsalis fissidens*	Lm2	M	288.3578	247.5212	184.5361	242.814	148.4653	334.2969	219.8837
NMMNH 8609	*Catopsalis fissidens*	Lm1-2	H	1102.597	981.1789	720.1495	1059.986	522.4534	1439.565	972.9299
NMMNH 8609	*Catopsalis fissidens*	Lm1	H	609.051	550.3048	414.1997	516.6808	281.2542	838.2076	585.0587
NMMNH 8609	*Catopsalis fissidens*	Lm2	H	422.443	358.2317	261.2062	614.2508	205.2723	487.5513	305.268
NMMNH 8613	*Catopsalis fissidens*	Rm1-2	L	815.9196	730.5026	552.6647	734.3396	471.2558	917.5956	640.3238
NMMNH 8613	*Catopsalis fissidens*	Rm1	L	548.9403	495.8896	384.4224	497.3231	337.1248	606.8592	440.3899
NMMNH 8613	*Catopsalis fissidens*	Rm2	L	185.8866	162.7213	126.148	144.0461	101.1477	212.3816	145.5866
UALVP 16058	*Catopsalis johnstoni*	Lm1	L	3816.921	2896.604	1430.718	18840.08	1789.057	3380.975	1466.55
TMP 2009.133.0041	*Catopsalis kakwa*	Rm2	L	530.4773	431.984	256.6008	921.021	226.2086	537.4111	277.7901
TMP 2009.133.0114	*Catopsalis kakwa*	Rm1	M	1057.937	885.5929	588.26	2097.196	543.6716	1045.146	616.7563
TMP 2010.097.0015	*Catopsalis kakwa*	Rm2	M	1251.058	850.5046	415.2518	5232.658	408.0335	1118.952	452.912
TMP 2010.097.0020	*Catopsalis kakwa*	Rm1	M	1615.717	1264.302	708.5982	6399.4	691.4078	1536.757	760.7056
TMP 2015.071.0141	*Catopsalis kakwa*	Lp4	L	109.0036	91.3443	65.16082	88.60738	55.06495	120.625	70.02987
UALVP 57541	*Catopsalis kakwa*	Rp4	L	98.85131	88.14438	62.35502	83.7897	54.61389	104.0286	64.37987
UM 90042	*Catopsalis waddleae*	Lm1	L	699.5744	559.3784	288.8077	1292.816	262.5572	700.7058	314.3356
UALVP 1766	Cimolomyid 1	Rm1	L	1339.619	1106.93	702.305	5105.114	626.1589	1224.296	760.1317
UALVP 30096	Cimolomyid 1	Rm2	L	1246.414	946.2098	461.1006	6709.425	398.7643	1146.465	523.7775
UALVP 30593	Cimolomyid 1	Rm1	L	1140.851	963.7779	669.9467	2594.128	621.8183	1102.132	694.3989
UALVP 2141	*Cimolomys* sp.	Rm1	L	711.3611	596.3361	389.2594	911.7982	343.5579	710.2374	417.896
UALVP 30112	*Cimolomys* sp.	Lm1	L	841.3788	711.4017	452.6207	1445.964	428.0345	803.1554	463.5919
UALVP 30605	*Cimolomys* sp.	Lm2	L	951.3683	773.5167	425.0067	3056.31	384.562	860.586	443.6819
UALVP 709	*Cimolomys* sp.	Rm1	L	800.4201	689.397	451.011	1394.411	405.2818	773.2418	475.616
UALVP 15164	*Meniscoessus major*	Rm1	L	708.3281	592.6202	445.2711	1188.417	353.3703	808.1897	536.7393
UALVP 15165	*Meniscoessus major*	Rm1	L	777.4714	686.1858	497.6583	810.2837	408.8926	853.8737	566.6434

245

UALVP 15167	*Meniscoessus major*	Rm1	M	359.6523	335.5572	267.5625	313.159	223.7436	390.4301	293.0396
UALVP 15182	*Meniscoessus major*	Lp4-m2	M	1983.389	1112.134	645.1882	6698.378	537.3465	2003.956	757.7959
UALVP 15182	*Meniscoessus major*	Lm1	M	489.5477	322.5466	244.5159	1360.616	198.3855	517.8153	289.8415
UALVP 15182	*Meniscoessus major*	Lm2	M	344.2204	289.6837	211.2739	309.3294	173.1437	416.1038	255.2606
UALVP 15182	*Meniscoessus major*	Lp4	M	142.2482	121.7349	64.85646	133.7574	61.06918	147.1877	65.15437
UALVP 15187	*Meniscoessus major*	Rm2	M	629.1821	538.591	357.3373	900.1207	316.9317	654.3038	392.6259
UALVP B	*Meniscoessus major*	Rm2	L	795.1089	716.0001	526.2372	1162.007	454.075	876.356	596.4515
ROM M	*Meniscoessus robustus*	Lm2	M	758.7587	653.3724	443.8451	1074.494	335.7605	896.3075	528.9734
ROM B1	*Mesodma* sp.	Rm1	L	359.0192	324.5997	259.371	306.2162	225.3741	377.897	273.6781
ROM T	*Mesodma* sp.	Rm1	L	340.0744	316.4683	256.4904	289.6525	223.9009	357.3593	271.4379
ROM V	*Mesodma* sp.	Lm2	L	253.7808	224.4787	177.4244	209.6717	152.2559	143.8378	110.6687
UALVP 7278	*Mesodma* sp.	Lm1	L	453.8035	429.0095	359.1565	386.4986	307.4858	484.8899	384.2197
UALVP 7288	*Mesodma* sp.	Lm1	L	306.173	287.1259	236.8731	254.6223	202.6214	326.0536	249.4141
TMP 2009.132.0239	Neoplagiaulacid	Lm1	M	496.0154	458.9304	363.2973	424.4578	310.0138	542.483	402.8481
TMP 2010.097.0126	*Ptilodus wyomingensis*	Lm1	M	403.3635	365.3884	280.7865	332.3983	230.1354	445.0997	317.7832
UALVP 6533	*Stygimys kuszmauli*	Rm1	L	771.2938	586.443	482.8296	1262.956	424.7215	749.71	498.0175
NMMNH 2763	*Taeniolabis taoensis*	Lm2	L	534.4268	412.1716	225.0892	728.804	186.0716	565.3749	257.5722
NMMNH 42938	*Taeniolabis taoensis*	Rm2	H	458.9073	374.4548	253.5315	439.962	192.0732	529.5024	332.5496
NMMNH 42939	*Taeniolabis taoensis*	Lm2	H	296.3237	258.1063	190.9072	225.3512	143.7808	383.9127	250.5281
NMMNH 44417	*Taeniolabis taoensis*	Rm1	M	1109.893	880.611	522.6082	2161.545	381.0757	1188.163	606.8667
NMMNH 47445	*Taeniolabis taoensis*	Rm1-2	H	606.5534	548.7041	409.8139	446.5158	301.4908	778.0693	527.0815
NMMNH 47445	*Taeniolabis taoensis*	Rm1	H	300.5912	277.5633	213.8553	202.1138	150.6874	420.189	292.8363
NMMNH 47445	*Taeniolabis taoensis*	Rm2	H	235.7604	214.6379	158.7814	198.1057	127.5113	294.2526	195.5329
NMMNH 47447	*Taeniolabis taoensis*	Rm2	H	209.7678	194.9267	146.471	164.8298	111.9332	274.576	188.9347
NMMNH 8631	*Taeniolabis taoensis*	Rp4-m2	L	1206.706	1073.671	823.4503	956.9986	651.6895	1418.735	986.5297
NMMNH 8631	*Taeniolabis taoensis*	Rm1	L	491.8675	451.9885	359.8685	383.1407	281.4932	584.7287	432.3253
NMMNH 8631	*Taeniolabis taoensis*	Rm2	L	342.6652	296.2675	221.2519	278.9545	168.5435	408.8277	277.3057
NMMNH 8631	*Taeniolabis taoensis*	Rp4	L	263.2658	153.0393	101.3421	286.5537	77.22643	308.6944	125.2349
NMMNH 8632	*Taeniolabis taoensis*	Rp4-m2	M	1133.28	1039.295	806.9857	873.1032	614.9828	1354.474	986.3679
NMMNH 8632	*Taeniolabis taoensis*	Rm1	M	402.9648	364.9155	286.1045	317.4846	208.715	498.6686	359.4269

NMMNH 8632	*Taeniolabis taoensis*	Rm2	M	386.8691	358.06	281.7162	282.5275	208.0903	474.6572	344.34
NMMNH 8632	*Taeniolabis taoensis*	Rp4	M	212.1823	154.5491	109.8274	249.8948	84.11438	255.8001	134.3157
ROM H	*Valenopsalis joyneri*	Lm2	H	853.3773	473.472	269.9516	2493.682	222.744	685.1985	304.6683
ROM I	*Valenopsalis joyneri*	Lp4	L	125.1672	109.6513	76.83998	108.9286	68.72993	130.923	79.82187
UALVP 28167	*Valenopsalis joyneri*	Rm1	L	1028.082	842.5237	475.0514	3240.761	439.6054	954.4831	488.382
UALVP 28170	*Valenopsalis joyneri*	Lm1	L	847.185	696.3564	419.9853	2200.788	408.289	787.2325	426.9067
UALVP 28172	*Valenopsalis joyneri*	Rm1	L	983.2767	784.5918	483.822	2103.643	461.7174	927.1404	500.7147
UALVP 28175	*Valenopsalis joyneri*	Rm1	L	1430.672	1042.825	589.5313	5163.311	528.5838	1345.563	643.244
UALVP 28178	*Valenopsalis joyneri*	Lm1	M	937.8408	746.7387	496.538	2432.055	406.2373	901.1805	527.2994
UALVP 28202	*Valenopsalis joyneri*	Lm2	L	1199.187	805.0538	399.7002	4903.402	367.9797	1154.863	424.0184
UALVP 28203	*Valenopsalis joyneri*	Rm2	H	341.7751	246.8702	168.8193	419.3768	134.8996	376.1477	190.3924
UALVP 28204	*Valenopsalis joyneri*	Lm2	L	1479.632	890.3221	380.1274	5719.237	363.6057	1235.539	395.4072
UALVP 28205	*Valenopsalis joyneri*	Lm2	M	487.5694	383.9457	252.456	870.1843	214.7834	499.8523	279.9391
UALVP 28207	*Valenopsalis joyneri*	Rm2	L	2004.4	1345.124	624.2631	6960.981	376.673	1825.798	649.0982
UALVP 28211	*Valenopsalis joyneri*	Rp4	L	194.8959	174.6767	132.7003	172.9499	118.8727	195.7061	134.52
UALVP 6596	*Valenopsalis joyneri*	Rm1	L	1021.341	817.7005	494.3043	2580.25	473.5975	977.8637	509.7648
UALVP 6608	*Valenopsalis joyneri*	Rm2	H	493.267	388.8435	248.8441	685.346	194.9344	537.72	283.3543
UALVP 6609	*Valenopsalis joyneri*	Rm2	H	362.8698	293.3079	192.9167	349.6882	153.694	410.6175	224.2338
UALVP 6610	*Valenopsalis joyneri*	Rm2	H	712.8138	506.9281	282.809	2536.046	238.4943	664.3069	305.5976
UALVP 7394	*Valenopsalis joyneri*	Lm1	H	172.0584	155.3537	113.9941	146.9197	94.89446	183.5118	125.6853
UALVP 7395	*Valenopsalis joyneri*	Lp4	H	169.7352	149.4437	109.5744	145.3963	96.57773	180.7833	113.2311
UALVP 7412	*Valenopsalis joyneri*	Lp4	L	175.0369	151.7923	114.463	152.5232	98.60178	181.8331	121.0196

Table J3. RFI values calculated with different parameters.

Institutional abbreviations: **NMMNH** – New Mexico Museum of Natural History and Science (Albuquerque, NM, USA); **ROM** – Royal Ontario Museum (Toronto, ON, Canada); **TMP** – Royal Tyrrell Museum of Palaeontology (Drumheller, AB, Canada); **UALVP** – University of Alberta Laboratory for Vertebrate Paleontology (Edmonton, AB, Canada); **UCM** – University of Colorado Museum of Natural History (Boulder, CO, USA); **UM** – University of Michigan Museum of Paleontology (Ann Arbor, MI, USA); **UW** – University of Wyoming Geological Museum (Laramie, WY, USA).

Table abbreviations: **L** – low wear; **M** – medium wear; **H** – high wear.

Specimen	Taxon	Tooth	Wear	RFI	3D Area	2D Area
TMP 2015.069.0174	Cf. *Acheronodon vossae*	Lm1	L	0.533091	5.981209	2.059455
UCM 34136	*Catopsalis alexanderi*	Lp4-m2	M	0.366023	149.0794	71.69583
UCM 34136	*Catopsalis alexanderi*	Lm1	M	0.319112	71.8741	37.96607
UCM 34136	*Catopsalis alexanderi*	Lm2	M	0.390397	55.94982	25.62736
UCM 34136	*Catopsalis alexanderi*	Lp4	M	0.484139	18.76404	7.125395
UCM 34141	*Catopsalis alexanderi*	Lm1	L	0.431218	92.30983	38.96702
UCM 34332	*Catopsalis alexanderi*	Rm1	L	0.533836	102.7019	35.30975
TMP 2015.023.0001	*Catopsalis calgariensis*	Lm2	L	0.464278	157.5591	62.2554
TMP 127	*Catopsalis calgariensis*	Rm2	M	0.374837	139.4646	65.89997
UW 14051	*Catopsalis* cf. *calgariensis*	Rm2	L	0.493412	221.8356	82.69121
UW 15100	*Catopsalis* cf. *calgariensis*	Rm1	L	0.580438	405.6319	127.0487
UW 15102	*Catopsalis* cf. *calgariensis*	Rm2	H	0.308945	159.4412	85.95165
UW 6387	*Catopsalis* cf. *calgariensis*	Lm2	M	0.524182	227.9979	79.91578
UW 6387	*Catopsalis* cf. *calgariensis*	Rm1	M	0.416969	263.347	114.381
UW 6388	*Catopsalis* cf. *calgariensis*	Lm2	M	0.408108	142.9304	63.18966
UW 6388	*Catopsalis* cf. *calgariensis*	Rm1	L	0.511456	332.0854	119.4001

NMMNH 8608	*Catopsalis fissidens*	Lp4-m2	M	0.411036	282.2739	125.2717
NMMNH 8608	*Catopsalis fissidens*	Lm1	M	0.417622	153.9299	66.76998
NMMNH 8608	*Catopsalis fissidens*	Lm2	M	0.406408	91.5157	40.59704
NMMNH 8609	*Catopsalis fissidens*	Lm1-2	H	0.357883	218.3546	106.7352
NMMNH 8609	*Catopsalis fissidens*	Lm1	H	0.335652	127.6549	65.23696
NMMNH 8609	*Catopsalis fissidens*	Lm2	H	0.39053	88.01476	40.30373
NMMNH 8613	*Catopsalis fissidens*	Rm1-2	L	0.426271	254.1288	108.3427
NMMNH 8613	*Catopsalis fissidens*	Rm1	L	0.444852	159.4032	65.47924
NMMNH 8613	*Catopsalis fissidens*	Rm2	L	0.381687	92.21435	42.9803
UALVP 16058	*Catopsalis johnstoni*	Lm1	L	0.542966	119.6992	40.40892
TMP 2009.133.0041	*Catopsalis kakwa*	Rm2	L	0.624415	41.58008	11.92684
TMP 2009.133.0114	*Catopsalis kakwa*	Rm1	M	0.595018	40.73493	12.39198
TMP 2010.097.0015	*Catopsalis kakwa*	Rm2	M	0.687862	44.47843	11.23776
TMP 2010.097.0020	*Catopsalis kakwa*	Rm1	M	0.574873	45.43418	14.38979
TMP 2015.071.0141	*Catopsalis kakwa*	Lp4	L	0.645052	7.956314	2.189911
UALVP 57541	*Catopsalis kakwa*	Rp4	L	0.675787	12.42721	3.216565
UM 90042	*Catopsalis waddleae*	Lm1	L	0.542604	362.4309	122.4406
UALVP 1766	Cimolomyid 1	Rm1	L	0.576754	21.36313	6.740665
UALVP 30096	Cimolomyid 1	Rm2	L	0.619658	16.97147	4.914636
UALVP 30593	Cimolomyid 1	Rm1	L	0.597392	20.68009	6.261303
UALVP 2141	*Cimolomys* sp.	Rm1	L	0.51771	11.70925	4.157685
UALVP 30112	*Cimolomys* sp.	Lm1	L	0.569749	11.18254	3.578189
UALVP 30605	*Cimolomys* sp.	Lm2	L	0.499506	9.925655	3.655057
UALVP 709	*Cimolomys* sp.	Rm1	L	0.520584	12.18964	4.303457
UALVP 15164	*Meniscoessus major*	Rm1	L	0.543491	44.76005	15.09455
UALVP 15165	*Meniscoessus major*	Rm1	L	0.516422	40.4714	14.40753
UALVP 15167	*Meniscoessus major*	Rm1	M	0.461497	37.72388	14.98875
UALVP 15182	*Meniscoessus major*	Lp4-m2	M	0.528349	103.1528	36.20831
UALVP 15182	*Meniscoessus major*	Lm1	M	0.42227	31.54275	13.55566
UALVP 15182	*Meniscoessus major*	Lm2	M	0.463506	30.94125	12.24451

249

UALVP 15182	*Meniscoessus major*	Lp4	M	0.689333	37.58699	9.468711
UALVP 15187	*Meniscoessus major*	Rm2	M	0.580683	36.08479	11.29663
UALVP B	*Meniscoessus major*	Rm2	L	0.614348	38.64369	11.31
ROM M	*Meniscoessus robustus*	Lm2	M	0.432228	60.18245	25.35371
ROM B1	*Mesodma* sp.	Rm1	L	0.473557	5.655045	2.193359
ROM T	*Mesodma* sp.	Rm1	L	0.474334	5.664211	2.193504
ROM V	*Mesodma* sp.	Lm2	L	0.537331	5.387989	1.83953
UALVP 7278	*Mesodma* sp.	Lm1	L	0.540915	8.516568	2.8869
UALVP 7288	*Mesodma* sp.	Lm1	L	0.396127	4.511086	2.042722
TMP 2009.132.0239	Neoplagiaulacid	Lm1	M	0.510964	11.09408	3.992761
TMP 2010.097.0126	*Ptilodus wyomingensis*	Lm1	M	0.493019	13.95166	5.204695
UALVP 6533	*Stygimys kuszmauli*	Rm1	L	0.531775	18.14367	6.26371
NMMNH 2763	*Taeniolabis taoensis*	Lm2	L	0.417117	320.4908	139.1595
NMMNH 42938	*Taeniolabis taoensis*	Rm2	H	0.317975	259.0871	137.1691
NMMNH 42939	*Taeniolabis taoensis*	Lm2	H	0.306372	253.8273	137.5395
NMMNH 44417	*Taeniolabis taoensis*	Rm1	M	0.374067	411.5502	194.7657
NMMNH 47445	*Taeniolabis taoensis*	Rm1-2	H	0.280906	499.8897	285.0254
NMMNH 47445	*Taeniolabis taoensis*	Rm1	H	0.295179	283.7421	157.2296
NMMNH 47445	*Taeniolabis taoensis*	Rm2	H	0.263936	206.5822	121.8544
NMMNH 47447	*Taeniolabis taoensis*	Rm2	H	0.361008	265.3337	128.8918
NMMNH 8631	*Taeniolabis taoensis*	Rp4-m2	L	0.405651	746.6094	331.7029
NMMNH 8631	*Taeniolabis taoensis*	Rm1	L	0.374779	382.0005	180.5241
NMMNH 8631	*Taeniolabis taoensis*	Rm2	L	0.382084	267.362	124.5162
NMMNH 8631	*Taeniolabis taoensis*	Rp4	L	0.524947	84.86376	29.7002
NMMNH 8632	*Taeniolabis taoensis*	Rp4-m2	M	0.388235	666.1451	306.8984
NMMNH 8632	*Taeniolabis taoensis*	Rm1	M	0.356965	350.5302	171.6602
NMMNH 8632	*Taeniolabis taoensis*	Rm2	M	0.35093	230.2921	114.1472
NMMNH 8632	*Taeniolabis taoensis*	Rp4	M	0.564576	70.4761	22.9947
ROM H	*Valenopsalis joyneri*	Lm2	H	0.46072	44.3231	17.63818
ROM I	*Valenopsalis joyneri*	Lp4	L	0.667826	20.80452	5.471306

UALVP 28167	*Valenopsalis joyneri*	Rm1	L	0.596026	70.63925	21.44589
UALVP 28170	*Valenopsalis joyneri*	Lm1	L	0.612831	62.47061	18.33909
UALVP 28172	*Valenopsalis joyneri*	Rm1	L	0.620423	77.29062	22.34776
UALVP 28175	*Valenopsalis joyneri*	Rm1	L	0.605027	65.79219	19.618
UALVP 28178	*Valenopsalis joyneri*	Lm1	M	0.437927	46.83326	19.50632
UALVP 28202	*Valenopsalis joyneri*	Lm2	L	0.592644	64.08608	19.58842
UALVP 28203	*Valenopsalis joyneri*	Rm2	H	0.423268	46.23375	19.82958
UALVP 28204	*Valenopsalis joyneri*	Lm2	L	0.577911	68.43108	21.54203
UALVP 28205	*Valenopsalis joyneri*	Lm2	M	0.509458	59.21324	21.37517
UALVP 28207	*Valenopsalis joyneri*	Rm2	L	0.614183	60.85744	17.81726
UALVP 28211	*Valenopsalis joyneri*	Rp4	L	0.683723	12.17235	3.10099
UALVP 6596	*Valenopsalis joyneri*	Rm1	L	0.567193	50.07456	16.10495
UALVP 6608	*Valenopsalis joyneri*	Rm2	H	0.489983	57.5652	21.60561
UALVP 6609	*Valenopsalis joyneri*	Rm2	H	0.409661	45.37918	19.99997
UALVP 6610	*Valenopsalis joyneri*	Rm2	H	0.425756	44.83117	19.13257
UALVP 7394	*Valenopsalis joyneri*	Lm1	H	0.398499	37.07351	16.70828
UALVP 7395	*Valenopsalis joyneri*	Lp4	H	0.649058	11.16598	3.048823
UALVP 7412	*Valenopsalis joyneri*	Lp4	L	0.610377	11.98827	3.53663